Stochastic Properties of Student-Lévy Processes with Applications

Dissertation

zur

Erlangung des Grades Dr. rer. pol.
der Wirtschaftswissenschaftlichen Fakultät
der Universität Duisburg-Essen

vorgelegt von
Till Philipp Georg Massing

Juli 2018

Datum der mündlichen Prüfung: 19.02.2019

Erstgutachter: Prof. Dr. Christoph Hanck
Zweitgutachter: Prof. Dr. Rüdiger Kiesel

Frequently used symbols and abbreviations:

$\mathbb{N}$	:	$\{1, 2, \ldots\}$
$\mathbb{R}$	:	set of real numbers
$\mathbb{C}$	:	set of complex numbers
i	:	imaginary unit, $\mathrm{i}^2 = -1$
$\mathrm{Re}(z)$	:	real part a of $z = a + b\mathrm{i} \in \mathbb{C}$
$\arg(z)$	:	the argument of a complex number z
A^{T}	:	transpose of a matrix $A \in \mathbb{R}^{m \times n}$
$\langle x, y \rangle$	:	$x^{\mathrm{T}} y$, for $x, y \in \mathbb{R}^n$
$\mathbb{1}_A$	:	indicator function $\mathbb{1}_A(x) = 1$, if $x \in A$; $\mathbb{1}_A(x) = 0$, if $x \notin A$
$\Gamma(x)$	:	gamma function for $x > 0$
$J_\lambda(x)$	:	Bessel function of the first kind
$Y_\lambda(x)$	:	Bessel function of the second kind
$K_\lambda(x)$	:	modified Bessel function of the second kind
$f(x) \sim g(x)$	:	$\lim_{x \to a} \frac{f(x)}{g(x)} = 1, a \in \mathbb{R} \cup \{\pm\infty\}$
$f(x) = \mathcal{O}(g(x))$	:	$\limsup_{x \to a} \frac{\lvert f(x) \rvert}{\lvert g(x) \rvert} < \infty, a \in \mathbb{R} \cup \{\pm\infty\}$
$X \sim \mu$	:	X has distribution μ
$\stackrel{\mathcal{L}}{=}$	:	equality in distribution
$\stackrel{\mathcal{L}}{\to}$	:	convergence in distribution
$X_n \stackrel{\mathcal{L}}{\sim} Y_n$	:	$X_n \stackrel{\mathcal{L}}{\to} X, Y_n \stackrel{\mathcal{L}}{\to} X$
$X_n = o_P(1)$	:	$X_n \to 0$ in probability for $n \to \infty$
a.s.	:	almost surely
i.i.d.	:	independent, identically distributed
$N(\mu, \sigma^2)$	:	normal distribution with mean μ and variance σ^2
$t(\nu, \mu, \sigma^2)$	:	Student t distribution with degree of freedom ν, location μ and scale σ
$t(\nu, \mu, \sigma^2, \beta)$	:	Skew Student t distribution with skewness parameter β
$R\Gamma(\alpha, \beta)$	:	inverse gamma distribution with shape parameter α and scale β
$Poi(\lambda)$	:	Poisson distribution with intensity parameter λ
$Exp(\lambda)$	:	Exponential distribution with rate λ
$\mathcal{U}_{[a,b]}$	:	Uniform distribution on $[a, b]$

Contents

Preface

The topic of this thesis goes back to two famous mathematicians. William S. Gosset, better known by his pseudonym Student (1908), is the origin of the name of the Student t distribution. Over time, the Student t distribution proved to be extremely useful in many statistical fields, both in theoretical foundations and applications.

Paul Lévy (1948) studied time-continuous stochastic processes with stationary and independent increments, a generalization of Brownian motion, which is based on the normal distribution. These processes, called Lévy processes, have become well known in stochastics as well as in many financial and physical applications. Any Lévy process has an underlying infinitely divisible distribution characterizing its behavior. Since the Student t distribution is infinitely divisible, there exist Lévy processes having Student t distributed increments, which we call Student-Lévy processes in this thesis. However, not every marginal of the Student-Lévy process is Student t distributed, in contrast to Brownian motion, where all marginals are normally distributed. There exists only one point in time where the Student-Lévy process is Student t distributed at $t = 1$. If $t \neq 1$, the distribution of the Student-Lévy process has no closed form. This may explain why the time-continuous Student-Lévy process has received little attention in the literature. Its complicated form in continuous time makes analytical derivations and numerical computations challenging. In this thesis, we contribute to the literature by developing new useful statistical techniques to make the Student-Lévy process accessible. The main goal is to work out an efficient estimation scheme for the t-increments with $t \neq 1$.

Heyde & Leonenko (2005) elaborated on the Student-Lévy process among other Student processes. Grigelionis (2012) gave a good overview and discussed some very useful results, such as its Lévy-Khintchine representation. Student-Lévy processes may be used in, e.g., finance, as one-day returns are not normally distributed but are often assumed to be Student t distributed due to their heavy tails (cf. Blattberg & Gonedes (1974) or Bouchaud & Potters (2003), among many others). Heyde & Leonenko (2005) proposed the Student-Lévy process as an alternative to Gaussian processes in asset return modeling. Additionally, Cufaro Petroni et al. (2005) discussed the Student-Lévy process in a physics context (for halos in accelerator beams).

The thesis consists of three parts. Due to the complicated nature of the Student-Lévy process standard simulation techniques are not applicable. Thus there is a need

for an appropriate simulation routine to generate quasi-time-continuous paths. Series representations according to Rosiński (2001) for Lévy processes play a prominent role in path generation. However, since the Lévy measure for the Student-Lévy process has a complicated form, series representations are not directly applicable. The first part of the thesis (Chapter 2) therefore proposes simulation algorithms based on series representations. Furthermore, we prove bounds for approximation errors.

The second part deals with maximum likelihood parameter estimation. If a Student-Lévy path is observed in high frequency, it is of interest to establish how this data can be used to estimate the unknown parameters. Again, due to the complicated form of the Student-Lévy process, there is no straightforward closed-form maximum likelihood estimator. Chapter 3 thus develops a numerical maximum likelihood estimation procedure. We then study its asymptotic properties and prove that it is asymptotically normal and asymptotically efficient.

The third part shows that the Student-Lévy process is of practical interest. In Chapter 4 we apply it to high-frequency financial data and observe that a model based on a Student-Lévy process is a reasonable alternative in finance if other models do not fit well.

In summary, this thesis covers simulation of the Student-Lévy process in Chapter 2, estimation in Chapter 3 and applications in Chapter 4. Chapters 2 and 3 are addressed to mathematically versed readers, while Chapter 4 has been written for financial practitioners and contains less mathematical detail. Although all chapters focus on the Student-Lévy process, they cover different aspects and may be read in a sequence. Readers will find that some details have been mentioned more than once to ensure that each chapter can be read independently. The exception is Chapter 1, which introduces the technical preliminaries including necessary definitions and theorems, and to which all the following chapters refer at various points. Finally, Chapter 5 concludes.

Acknowledgments

I wrote this thesis while being a member of the academic staff at the Chair for Econometrics at the University of Duisburg-Essen. The thesis was written under the supervision of Prof. Dr. Christoph Hanck. I owe him my deepest thanks for his supervision, especially for the freedom I was granted in my research and for his very valuable comments.

The present thesis relies heavily on numerical simulations. Christoph Hanck provided me with access to two(!) 80-core cluster servers, which reduced my computing time enormously. Without these, the thesis could not have been written in such a short time, or, without high additional costs.

I am very grateful to Prof. Dr. Rüdiger Kiesel for agreeing to be my second supervisor.

I thank Benjamin Ackermann of Thomson Reuters for providing me with access to the trial version of Thomson Reuters Eikon. I regret that I was not able to convince my department to purchase Eikon.

Thanks go to Dr. Yannick Hoga and Dr. Paul Navas Alban as well as anonymous reviewers for valuable comments which helped me to substantially improve this thesis. I thank our "Hiwis" for their excellent research assistance and Theresa Kemper for carefully reading my work.

I acknowledge the assistance of Graham Sutherland with the language of the thesis.

Till Massing

1 Technical preliminaries

This introductory chapter briefly presents definitions and theorems needed throughout the thesis. Section 1.1 defines the Student t and related distributions. Section 1.2 highlights important general properties of Lévy processes. Section 1.3 discusses the notion of stability. Section 1.4 defines the Student-Lévy process and gives an overview of useful results in the literature. Section 1.5 defines Bessel functions which are used throughout the thesis. However, this section is included primarily as a reference. It is not necessary for an understanding of the remainder of the thesis and may be omitted by the reader.

1.1 Student t and related distributions

In this section we mainly list the Student t and important related distributions and their connections. We start with the univariate Student t distribution.

Definition 1.1. We consider the *univariate Student t distribution* $t(\nu, \mu, \sigma^2)$ with $\nu > 0$ degrees of freedom, location parameter $\mu \in \mathbb{R}$ and scale parameter $\sigma > 0$ with density function

$$f^{St}_{\nu,\mu,\sigma^2}(x) = \frac{\Gamma\left(\frac{\nu+1}{2}\right)}{\Gamma\left(\frac{\nu}{2}\right)\sqrt{\pi\nu\sigma^2}}\left(1+\frac{1}{\nu}\left(\frac{x-\mu}{\sigma}\right)^2\right)^{-\frac{\nu+1}{2}}$$

and characteristic function

$$\varphi^{St}_{\nu,\mu,\sigma^2}(x) = \frac{2^{1-\frac{\nu}{2}}\nu^{\nu/4}\sigma^{\nu/2}e^{\mathrm{i}\mu x}\left|x\right|^{\nu/2}K_{\frac{\nu}{2}}\left(\sqrt{\nu}\sigma\left|x\right|\right)}{\Gamma\left(\frac{\nu}{2}\right)}, \tag{1.1}$$

where $\Gamma(x)$ denotes the gamma function of x and $K_\nu(x)$ denotes the modified Bessel function of the second kind. (See Section 1.5 for the definition of Bessel functions and some of their properties.) We denote by $t(\nu)$ the standard Student t distribution $t(\nu, 0, 1)$.

For $\nu = 1$ we have the special case of the *Cauchy distribution*. While the theoretical results in Chapters 2 and 3 and the empirical application in Chapter 4

are discussed in the one-dimensional case, the simulation routine (Chapter 2) is also available for the multivariate Student t distribution, defined below.

Definition 1.2. The *d-dimensional Student t distribution* $t_d(\nu, \mu, \Sigma)$ has density function

$$f^{St}_{\nu,\mu,\Sigma}(x) = \frac{\Gamma\left(\frac{\nu+d}{2}\right)}{\Gamma\left(\frac{\nu}{2}\right)(\pi\nu)^{\frac{d}{2}}\sqrt{|\Sigma|}}\left(1 + \frac{\left\langle (x-\mu)\Sigma^{-1}, (x-\mu)\right\rangle}{\nu}\right)^{-\frac{\nu+1}{2}}$$

for all $x \in \mathbb{R}^d$, where $\nu > 0$ is the degree of freedom, $\mu \in \mathbb{R}^d$ is the location vector and $\Sigma \in \mathbb{R}^{d\times d}$ is a symmetric and positive definite scaling matrix.

The Student t distribution is symmetric. For empirical applications where the data exhibits skewness, a skew version of the Student t distribution is helpful. We use Aas & Haff's (2006) skew Student t distribution.

Definition 1.3. The *one-dimensional skew Student t distribution* $t(\nu, \mu, \sigma^2, \beta)$ is defined by its density function

$$f^{SSt}_{\nu,\mu,\sigma^2,\beta}(x) = \frac{2^{\frac{1-\nu}{2}}\nu^{\nu/2}\sigma^\nu \exp\left(\beta(x-\mu)\right)}{\Gamma\left(\frac{\nu}{2}\right)\sqrt{\pi}}\left(\frac{\beta^2}{\nu\sigma^2 + (x-\mu)^2}\right)^{\frac{\nu+1}{4}} \cdot K_{\frac{\nu+1}{2}}\left(\sqrt{\beta^2\left(\nu\sigma^2 + (x-\mu)^2\right)}\right),$$

with $\nu > 0$ degrees of freedom, location parameter $\mu \in \mathbb{R}$, scale parameter $\sigma > 0$ and skewness parameter $\beta \in \mathbb{R}\backslash\{0\}$. The characteristic function (v. Hammerstein 2010) is given by

$$\varphi^{SSt}_{\nu,\mu,\sigma^2,\beta}(x) = \frac{K_{\nu/2}(\sqrt{\nu}\sigma\sqrt{u^2 - 2\mathrm{i}\beta u})(\sqrt{\nu}\sigma)^{\nu/2}(u^2 - 2\mathrm{i}\beta u)^{\nu/4}e^{\mathrm{i}\mu u}}{\Gamma\left(\frac{\nu}{2}\right)2^{\nu/2-1}}.$$

Note that there exist different skew Student t distributions, e.g., the version proposed by Azzalini & Capitanio (2003), which we do not consider here. The reason why we choose the version in Definition 1.3 is because it is a special case of the generalized hyperbolic distribution, which we also use for the application in Chapter 4.

Definition 1.4. The *one-dimensional generalized hyperbolic (GH) distribution*

$GH(\lambda, \alpha, \beta, \delta, \mu)$ is defined by its density function

$$f^{GH}_{\lambda,\alpha,\beta,\delta,\mu}(x) = \frac{(\alpha^2-\beta^2)^{\lambda/2} K_{\lambda-1/2}\left(\alpha\sqrt{\delta^2+(x-\mu)^2}\right)\exp(\beta(x-\mu))}{\sqrt{2\pi}\alpha^{\lambda-1/2}\delta^{\lambda}K_{\lambda}\left(\delta\sqrt{\alpha^2-\beta^2}\right)\left(|\delta|+(x-\mu)^2\right)^{1/2-\lambda}},$$

with shape parameter $\lambda \in \mathbb{R}$, shape parameter α, skewness parameter $\beta \in \mathbb{R}$, scale parameter δ, location parameter $\mu \in \mathbb{R}$ such that

$$\begin{aligned} &\delta \geq 0,\ 0 \leq |\beta| < \alpha \qquad \text{if } \lambda > 0,\\ &\delta > 0,\ 0 \leq |\beta| < \alpha \qquad \text{if } \lambda = 0,\\ &\delta > 0,\ 0 \leq |\beta| \leq \alpha \qquad \text{if } \lambda < 0. \end{aligned}$$

The Student t distribution is the weak limit of the GH distribution $f^{St}_{\nu,\mu,\sigma^2}(x) = \lim_{\alpha,\beta\to 0} f^{GH}_{\lambda,\alpha,\beta,\delta,\mu}(x)$ and the skew Student t is the weak limit $f^{SSt}_{\nu,\mu,\sigma^2,\alpha}(x) = \lim_{|\beta|\to\alpha>0} f^{GH}_{\lambda,\alpha,\beta,\delta,\mu}(x)$ for each $x \in \mathbb{R}$. Additionally, $f^{St}_{\nu,\mu,\sigma^2}(x) = \lim_{\beta\to 0} f^{SSt}_{\nu,\mu,\sigma^2,\beta}(x)$ for each $x \in \mathbb{R}$.

Student-Lévy processes can be constructed by subordination of Brownian motion, see Section 1.4. The inverse gamma distribution, which is the distribution of the reciprocal of a gamma distributed random variable, is crucial for this subordination. We define both distributions by their densities.

Definition 1.5. The *gamma distribution* $\Gamma(\alpha, \beta)$ on $(0, \infty)$ has density function

$$f^{\Gamma}_{\alpha,\beta}(x) = \frac{\beta^{\alpha}}{\Gamma(\alpha)} x^{\alpha-1}\exp(-\beta x),$$

with shape parameter $\alpha > 0$ and rate parameter $\beta > 0$.

Definition 1.6. The *inverse* (or *reciprocal*) *gamma distribution* $R\Gamma(\alpha, \beta)$ on $(0, \infty)$ has density function

$$f^{R\Gamma}_{\alpha,\beta}(x) = \frac{\beta^{\alpha}}{\Gamma(\alpha)} x^{-\alpha-1}\exp\left(-\frac{\beta}{x}\right),$$

with shape parameter $\alpha > 0$ and rate parameter $\beta > 0$.

The *Lévy distribution* $Lévy(\mu, \beta)$ is a special case of the inverse gamma distribution, $Lévy(0, \beta) = R\Gamma(1/2, \beta/2)$. The gamma and the inverse gamma distributions are special cases of the generalized inverse Gaussian (GIG) distribution. We do not use the GIG distribution extensively in this thesis but state it for completeness. Furthermore, the GH-Lévy process can be constructed by subordination of a Brownian motion with a GIG subordinator. (For the definition of subordination see Section 1.2 below).

Definition 1.7. The *generalized inverse Gaussian (GIG) distribution* $GIG(\lambda, \delta, \gamma)$ on $(0, \infty)$ has density function

$$f^{GIG}_{\lambda,\delta,\gamma}(x) = \left(\frac{\gamma}{\delta}\right)^{\lambda} \frac{x^{\lambda-1}}{2K_\lambda(\gamma\delta)} \exp\left(-\frac{1}{2}(\delta^2 x^{-1} + \gamma^2 x)\right),$$

with $\lambda \in \mathbb{R}$ and

$$\begin{aligned} &\delta \geq 0,\ \gamma > 0 \qquad \text{if } \lambda > 0, \\ &\delta > 0,\ \gamma > 0 \qquad \text{if } \lambda = 0, \\ &\delta > 0,\ \gamma \geq 0 \qquad \text{if } \lambda < 0. \end{aligned}$$

The inverse gamma distribution is the weak limit $f^{R\Gamma}_{\alpha,\beta}(x) = \lim_{\gamma\to 0} f^{GIG}_{\lambda,\delta,\gamma}(x)$ for each $x \in (0, \infty)$. The GH and the GIG distribution have many special and limiting cases which we do not discuss in detail. See Eberlein & v. Hammerstein (2004) and v. Hammerstein (2010) for a deeper discussion.

1.2 Lévy processes

In this section we define and discuss some of the properties of Lévy processes. Sato (1999) is a standard reference for theoretical results on Lévy processes. The definition of a Lévy process is as follows.

Definition 1.8. An $\mathbb{R}^d$-valued process $\{X_t : t \geq 0\}$ is called a *Lévy process* on $\mathbb{R}^d$ if the following conditions are satisfied:

1. $X_0 = 0$ a.s.
2. *Independent increments*: for any $0 \leq t_0 < t_1 < \cdots < t_n < \infty$, the random variables $X_{t_0}, X_{t_1} - X_{t_0}, X_{t_2} - X_{t_1}, \ldots, X_{t_n} - X_{t_{n-1}}$ are independent.
3. *Stationary increments*: for any $s > 0$, $X_{t+s} - X_t \stackrel{\mathcal{L}}{=} X_s$.
4. *Stochastic continuity:* for any $\varepsilon > 0$, $\lim_{s\to 0} P[|X_{t+s} - X_t| > \varepsilon] = 0$.
5. The path function $t \mapsto X_t(\omega)$ is right-continuous and has left limits (càdlàg) a.s.

There is a direct connection between Lévy processes and infinitely divisible distributions, to be defined now.

Definition 1.9. Let X be a random variable in $\mathbb{R}^d$ with distribution $\mathcal{L}(X)$. $\mathcal{L}(X)$ is

infinitely divisible if there exist i.i.d. random variables $Y_1^{(n)}, \dots, Y_n^{(n)}$ such that

$$X \stackrel{\mathcal{L}}{=} Y_1^{(n)} + \cdots + Y_n^{(n)},$$

for any choice of $n \in \mathbb{N}$.

The following theorem establishes the one-to-one correspondence between Lévy processes and infinitely divisible distributions.

Theorem 1.1. *If $\{X_t\}$ is a Lévy process on $\mathbb{R}^d$, then $\mathcal{L}(X_t)$ is infinitely divisible for any $t \geq 0$. On the other hand, if μ is an infinitely divisible distribution on $\mathbb{R}^d$, then there exists a Lévy process $\{X_t\}$, uniquely in law, such that $\mathcal{L}(X_1) = \mu$.*

The next theorem and corollary present the unique Lévy-Khintchine characterization of Lévy processes.

Theorem 1.2 (Lévy-Khintchine representation)**.** *A probability distribution μ_X on $\mathbb{R}^d$ of a random variable X is infinitely divisible if and only if there exists a unique triple (called Lévy triple) (γ, A, Π), such that*

$$E\left[e^{\mathrm{i}\langle z, X\rangle}\right] = \exp\left(\mathrm{i}\,\langle z, \gamma\rangle - \frac{1}{2}\,\langle z, Az\rangle + \int_{\mathbb{R}_0^d} \left(e^{\mathrm{i}\langle z, x\rangle} - 1 - \mathrm{i}\,\langle z, x\rangle\, \mathbb{1}_{\{|x|\leq 1\}}\right) \Pi(\mathrm{d}x)\right), \tag{1.2}$$

for all $z \in \mathbb{R}^d$, where $\gamma \in \mathbb{R}^d$, A is a symmetric non-negative definite $d \times d$ matrix and Π is a measure on $\mathbb{R}_0^d$ satisfying

$$\int_{\mathbb{R}_0^d} (|x|^2 \wedge 1)\Pi(\mathrm{d}x) < \infty,$$

which is to ensure that Π is σ-finite. We call $\psi(z) := -\log E\left[e^{\mathrm{i}\langle z, X\rangle}\right]$ the characteristic exponent*.*

Corollary 1.1. *Let $\{X_t\}$ be a Lévy process on $\mathbb{R}^d$ such that X_1 has characteristic function $\varphi(z) = E[e^{\mathrm{i}\langle z, X_1\rangle}]$ given in* (1.2)*. Then the law of X_t is uniquely characterized by its characteristic function*

$$E\left[e^{\mathrm{i}\langle z, X_t\rangle}\right] = \varphi(z)^t,$$

or, equivalently, by its characteristic exponent.

The *Lévy measure* Π is the key ingredient for path simulation in Chapter 2. The Lévy measure is zero if and only if the Lévy process is Gaussian (or deterministic if, moreover, $A = 0$) and has continuous paths a.s. On the other hand, if $\Pi \neq 0$ and

$A = 0$, the Lévy process is a pure jump process.

The Lévy-Itô decomposition splits any Lévy process into its continuous and pure jump parts.

Theorem 1.3 (Lévy-Itô decomposition)**.** *If $\{X_t\}$ is a Lévy process on $\mathbb{R}^d$ with triple (γ, A, Π), then there exists the decomposition*

$$X_t = \gamma t + G_t + \int_{|x|>1} x N_t(\mathrm{d}x) + \lim_{\varepsilon \searrow 0} \int_{\varepsilon<|x|\leq 1} x(N_t(\mathrm{d}x) - t\Pi(\mathrm{d}x)),$$

where $\{G_t\}$ is a Gaussian Lévy process with covariance matrix A and $\{N_t\}$ is an independent Poisson point process with intensity measure Π. All four summands are independent Lévy processes. The third summand is a compound Poisson process representing the "large" jumps and the fourth summand is a square integrable pure jump martingale representing the "small" jumps.

We use the Lévy-Itô decomposition implicitly for simulation in Chapter 2. The compound Poisson process (the large jumps) can be expressed via series representations, see Section 2.2. The very small jumps can either be neglected or approximated, see Section 2.3.3.

Subordinators are useful special cases of Lévy processes and some interesting Lévy processes (such as the Student-Lévy process, see Section 1.4) can be constructed by means of subordination. In subordination the subordinator represents the random time process.

Definition 1.10. A *subordinator* is a one-dimensional, (a.s.) non-decreasing Lévy process.

Lemma 1.1. *A Lévy process $\{Y_t\}$ is a subordinator if and only if its Lévy triple has the form $(\beta, 0, Q)$, such that $\beta_0 \geq 0$, where $\beta_0 = \beta - \int_{|u|\leq 1} uQ(\mathrm{d}u)$ and Q is a σ-finite measure on $(0, \infty)$ satisfying $\int_0^\infty (u \wedge 1)Q(\mathrm{d}u) < \infty$.*

It is therefore common practice to represent subordinators in terms of their *Laplace exponent*

$$\eta(z) := -\log \frac{1}{t} E\left[e^{-zY_t}\right] = \beta_0 z + \int_0^\infty \left(1 - e^{-zu}\right) Q(\mathrm{d}u), \quad z \geq 0$$

and call (β_0, Q) the *Laplace characteristics*. β_0 is called *drift* and Q *Lévy measure*.

The next theorem states the Lévy triple for subordinated processes. A proof can be found in Sato (1999).

Theorem 1.4. *Let $\{Y_t\}$ be a subordinator with Laplace characteristics (β_0, Q). Let*

$\{Z_t\}$ be a Lévy process on $\mathbb{R}^d$ with characteristic triple (γ, Σ, Π), independent of $\{Y_t\}$. Let $\mu^t(B) = P[Z_t \in B]$ with $B \in \mathcal{B}(\mathbb{R}^d)$, $t \geq 0$. Let

$$X_t := Z_{Y_t}, \quad t \geq 0$$

be the subordinated process. Then, $\{X_t\}$ is a Lévy process on $\mathbb{R}^d$ with characteristic triple $(\tilde{\gamma}, \tilde{\Sigma}, \tilde{\Pi})$, where

$$\begin{aligned}
\tilde{\gamma} &= \beta_0 \gamma + \int_{(0,\infty)} \int_{|x| \leq 1} x \mu^s(\mathrm{d}x) Q(\mathrm{d}s), \\
\tilde{\Sigma} &= \beta_0 \Sigma, \\
\tilde{\Pi}(B) &= \beta_0 \Pi(B) + \int_{(0,\infty)} \mu^s(B) Q(\mathrm{d}s), \quad B \in \mathcal{B}(\mathbb{R}^d).
\end{aligned}$$

1.3 Stability

We work with α-stable Lévy processes in Section 2.3.2 for simulation using the rejection method, in Section 3.2 to prove local asymptotic normality and in Section 4.2.3 for the application. Here we briefly present their definition and characterizing properties.

Definition 1.11. Let X be a random variable in $\mathbb{R}^d$ with distribution $\mathcal{L}(X)$ and characteristic function $\varphi_X(z)$. $\mathcal{L}(X)$ is called *stable* if for every $a > 0$ there exist $b > 0$ and $c \in \mathbb{R}^d$ such that

$$\varphi_X(z)^a = \varphi_X(bz) e^{\mathrm{i}\langle c, z \rangle}, \quad z \in \mathbb{R}^d.$$

It is called *strictly stable* if $c = 0$.

Furthermore, a Lévy process $\{X_t\}$ is called *(strictly) stable* if $\mathcal{L}(X_1)$ is (strictly) stable.

Definition 1.12. A (strictly) stable random variable X is called *(strictly) α-stable*, $\alpha \in (0, 2]$, if

$$\varphi_X(z)^a = \varphi_X(a^{1/\alpha} z) e^{\mathrm{i}\langle c, z \rangle}, \quad z \in \mathbb{R}^d$$

for all $a > 0$ and $c \in \mathbb{R}^d$. α is called the *index of stability*.

It can be shown that for every stable X there exists a unique constant $\alpha \in (0, 2]$ such that X is α-stable. Furthermore, α-stable Lévy processes are characterized by:

Proposition 1.1. *A Lévy process $\{X_t\}$ with characteristic triple (β, A, Π) is α-stable,*

$\alpha \in (0, 2]$, if and only if exactly one of the following holds:

(i) $\alpha = 2$ *and* $\Pi = 0$*, i.e., the Lévy process is Gaussian.*

(ii) $\alpha \in (0, 2)$*,* $A = 0$ *and*

$$\Pi(B) = \int_{S^{d-1}} \int_{(0,\infty)} \mathbb{1}_{\{r\xi \in B\}} \frac{\mathrm{d}r}{r^{1+\alpha}} \lambda(d\xi), \quad B \in \mathcal{B}(\mathbb{R}^d),$$

where λ *is a finite measure on the unit sphere* S^{d-1}*.*

It follows that for real-valued α-stable Lévy processes with index of stability $\alpha \in (0, 2)$ the Lévy measure can be written as

$$\Pi(\mathrm{d}x) = \left(c_+ x^{-1-\alpha} \mathbb{1}_{\{x>0\}} + c_- |x|^{-1-\alpha} \mathbb{1}_{\{x<0\}} \right) \mathrm{d}x,$$

for some $c_+, c_- \geq 0$.

1.4 The Student-Lévy process

This section discusses the Student-Lévy process. As stated in Theorem 1.1, infinite divisibility of a particular distribution is a necessary and sufficient condition for the existence of the associated Lévy process.

Proposition 1.2 (Grosswald (1976))**.** *The multivariate Student t distribution is infinitely divisible.*

Hence Lévy processes with Student t marginals do exist. However, only the 1-increments are Student t distributed since the Student t distribution is not closed under convolution.

Definition 1.13. A d-dimensional Lévy process $\{X_t\}$ on $[0, T]$, $T > 0$ is called a *Student-Lévy process* if

$$\mathcal{L}(X_1) = t_d(\nu, \mu, \Sigma).$$

This means the Student-Lévy process on $[0, T]$ has Student t margins for all increments with $\Delta t = 1$. Of course, the time unit corresponding to $\Delta t = 1$, for example one hour or one day, depends on the context in practice. Additionally, we define the skew Student-Lévy process in the same manner.

Definition 1.14. A one-dimensional Lévy process $\{X_t\}$ on $[0, T]$, $T > 0$ is called a *skew Student-Lévy process* if

$$\mathcal{L}(X_1) = t(\nu, \mu, \sigma^2, \beta).$$

Of course, there exists an extension to d dimensions which we omit here.

The next proposition ensures that inverse gamma Lévy processes exist.

Proposition 1.3 (Barndorff-Nielsen & Halgreen (1977))**.** *The inverse gamma distribution is infinitely divisible.*

Definition 1.15. A subordinator $\{Y_t\}$ is called an *inverse gamma subordinator* or an *inverse gamma Lévy process* if

$$\mathcal{L}(Y_1) = R\Gamma(\alpha, \beta).$$

Barndorff-Nielsen & Shephard (2001) computed the Laplace characteristics of the inverse gamma subordinator.

Proposition 1.4. *Let $\{Y_t\}$ be an inverse gamma subordinator with $\mathcal{L}(Y_1) = R\Gamma(\alpha, \beta)$. Its Laplace characteristics are given by $(0, Q)$ with Lévy measure*

$$Q(\mathrm{d}u) = \left(u^{-1} \int_0^\infty e^{-su} 2\beta g_{|\alpha|}(4\beta s) \mathrm{d}s \right) \mathrm{d}u,$$

where

$$g_{|\alpha|}(x) := 2 \left(\pi^2 x \left(J_{|\alpha|}^2 \left(\sqrt{x} \right) + Y_{|\alpha|}^2 \left(\sqrt{x} \right) \right) \right)^{-1}, \quad x > 0, \tag{1.3}$$

and J_α and Y_α are the Bessel functions of the first and second kind, respectively. (See Section 1.5 for the definition of Bessel functions and some of their properties.)

Using Theorem 1.4, Grigelionis (2012) computed the Lévy triple for the Student-Lévy process.

Theorem 1.5. *Let $\{Y_t\}$ be an inverse gamma subordinator such that $\mathcal{L}(Y_1) = R\Gamma(\nu/2, \nu/2)$ for $\nu > 1$. Let $\{G_t\}$ be a d-dimensional Gaussian Lévy process with Lévy triple $(0, \Sigma, 0)$ and independent of $\{Y_t\}$. Set*

$$X_t := G_{Y_t} + \mu t, \quad t \geq 0,$$

with $\mu \in \mathbb{R}^d$. Then, $\{X_t\}$ is the Student-Lévy process such that $\mathcal{L}(X_1) = t_d(\nu, \mu, \Sigma)$. $\{X_t\}$ has Lévy triple $(\gamma, 0, \Pi)$, where

$$\begin{aligned} \gamma &= \int_{\{|x| \leq 1\}} x\ell(x)\mathrm{d}x + \mu, \\ \Pi(\mathrm{d}x) &= \ell(x)\mathrm{d}x, \end{aligned}$$

and

$$\ell(x) = \frac{\nu 2^{\frac{d}{4}+1} \left(\left\langle x\Sigma^{-1}, x \right\rangle \right)^{-\frac{d}{4}}}{\sqrt{|\Sigma|}(2\pi)^{\frac{d}{2}}} \int_0^\infty s^{\frac{d}{4}} K_{\frac{d}{2}} \left(\left(2s \left\langle x\Sigma^{-1}, x \right\rangle \right)^{\frac{1}{2}} \right) g_{\frac{\nu}{2}}(2\nu s) \mathrm{d}s,$$

where K_λ is the modified Bessel function of the second kind and g_ν is defined in (1.3)*.*

If we replace the Gaussian process $\{G_t\}$ in Theorem 1.5 by a Brownian motion $\{B_t\}$ (i.e., $\Sigma = I$), and with $\mu = 0$, we have a Student-Lévy $\{X_t\}$ process with standard scaling.

Figure 1.1 shows a sample path of a one-dimensional Student-Lévy process with standard scaling ($\mu = 0$ and $\Sigma = 1$) and $\nu = 4$ using the simulation methods described in Chapter 2. Very small jumps occur frequently, while big jumps occur more rarely.

It is well-known that the standard normal distribution is the limiting case of the Student t distribution as $\nu \to \infty$. We can thus conclude that this carries over to Lévy processes because $\varphi(z) \to \exp\left(-\frac{1}{2}z^2\right)$ implies $\varphi(z)^t \to \exp\left(-\frac{1}{2}tz^2\right)$ for $\nu \to \infty$, where $\varphi(z)$ is the characteristic function of the Student t distribution. Hence the law of the Student-Lévy process converges weakly to the law of the Brownian motion for increasing degrees of freedom. Recall that sample paths of a Student-Lévy process are not continuous, whereas Brownian motion paths are, a.s.

We focus on the inverse gamma subordinator with marginals $\mathcal{L}(Y_1) = R\Gamma(\nu/2, \nu/2)$ for $\nu > 0$, since this subordinator induces the Student-Lévy process. In this case, the Lévy measure of the inverse gamma subordinator is given by

$$Q(\mathrm{d}u) := \rho(u)\mathrm{d}u := \left(u^{-1} \int_0^\infty e^{-su} \nu g_{\nu/2}(2\nu s) \mathrm{d}s \right) \mathrm{d}u,$$

with g_ν as in (1.3). The results concerning the inverse gamma subordinator in this thesis can easily be generalized to the $\mathcal{L}(Y_1) = R\Gamma(\alpha, \beta)$ situation with $\alpha, \beta > 0$ and $\alpha \neq \beta$ because if $Y_1 \sim R\Gamma(\alpha, \alpha)$, then $\frac{\beta}{\alpha} Y_1 \sim R\Gamma(\alpha, \beta)$.

1.5 Bessel functions

Here we briefly present an outline of Bessel functions based on Olver et al. (2010); see Watson (1995) for comprehensive information.

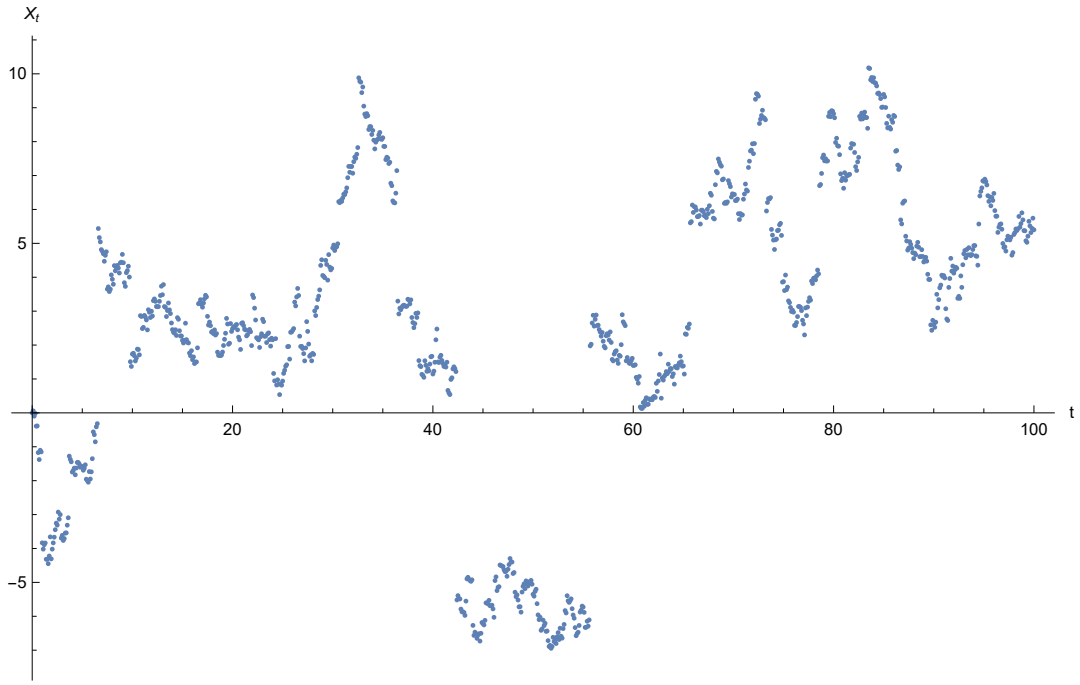

Figure 1.1: Path simulation of the Student-Lévy process with $\nu = 4$ and standard scaling using the inverse Lévy measure method; see Section 2.4.

Consider the differential equation called *Bessel's equation*,

$$x^2 \frac{\mathrm{d}^2 w}{\mathrm{d}x^2} + x \frac{\mathrm{d}w}{\mathrm{d}x} + (x^2 - \lambda^2) w = 0.$$

The *Bessel function of the first kind* $J_\lambda(x)$, the *Bessel function of the second kind* $Y_\lambda(x)$ and the *Bessel functions of the third kind* (also called *Hankel functions*) $H_\lambda^{(1)}(x)$, $H_\lambda^{(2)}(x)$ are solutions to Bessel's equation. The function $J_\lambda(x)$ can be represented as

$$J_\lambda(x) = \left(\frac{x}{2}\right)^\lambda \sum_{k=0}^{\infty} (-1)^k \frac{\left(\frac{x^2}{4}\right)^k}{k!\Gamma(\lambda + k + 1)},$$

for $x \in \mathbb{C}$, except for $x = 0$ if λ is negative and not an integer. The function $Y_\lambda(x)$ can be represented as

$$Y_\lambda(x) = \frac{J_\lambda(x)\cos(\lambda\pi) - J_{-\lambda}(x)}{\sin(\lambda\pi)},$$

where the right-hand side is replaced by its limiting value if λ is an integer. The Hankel functions can be written as

$$H_\lambda^{(1)}(x) = J_\lambda(x) + \mathrm{i}Y_\lambda(x),$$
$$H_\lambda^{(2)}(x) = J_\lambda(x) - \mathrm{i}Y_\lambda(x),$$

If we replace x by $\pm\mathrm{i}x$ in Bessel's equation, we obtain the *modified Bessel's equation*

$$x^2\frac{\mathrm{d}^2w}{\mathrm{d}x^2} + x\frac{\mathrm{d}w}{\mathrm{d}x} - (x^2+\lambda^2)w = 0. \tag{1.4}$$

The *modified Bessel function of the first kind* $I_\lambda(x)$ and the *modified Bessel function of the second kind* $K_\lambda(x)$ are solutions to (1.4). $I_\lambda(x)$ can be represented as

$$I_\lambda(x) = \left(\frac{x}{2}\right)^\lambda \sum_{k=0}^{\infty} \frac{\left(\frac{x^2}{4}\right)^k}{k!\Gamma(\lambda+k+1)},$$

for $x \in \mathbb{C}$, except for $x = 0$ if λ is negative and not an integer. $K_\lambda(x)$ can be represented as

$$K_\lambda(x) = \frac{\pi}{2}\frac{I_\lambda(x) - I_{-\lambda}(x)}{\sin(\lambda\pi),}$$

where the right-hand side is replaced by its limiting value if λ is an integer.

Some properties that we shall make repeated use of are

$$J_{-n}(x) = (-1)^n J_n(x),$$
$$Y_{-n}(x) = (-1)^n Y_n(x),$$
$$I_{-n}(x) = I_n(x),$$

for all $x \in \mathbb{C}$ and $n \in \mathbb{N}$ and

$$K_{-\lambda}(x) = K_\lambda(x),$$

for all $x \in \mathbb{C}\backslash\{0\}$ and $\lambda \in \mathbb{C}$.

The limiting behavior of $K_\lambda(x)$ is

$$K_\lambda(x) \sim \sqrt{\frac{\pi}{2x}}e^{-x},$$

as $x \to \infty$ in $|\arg(x)| < \frac{3}{2}\pi$ (which is always satisfied throughout the thesis). For

$\lambda = \frac{1}{2}$

$$K_{1/2}(x) = \sqrt{\frac{\pi}{2x}} e^{-x},$$

for all $x \in \mathbb{C}$.

Except for some special cases, Bessel functions are not available in closed forms and can only be represented in terms of series or integral representations. Common statistical packages approximate Bessel functions numerically.

2 Simulation of Student-Lévy processes using series representations

In this chapter we address path simulation for the Student-Lévy process. Although theoretically available, there is a lack of path simulation techniques in the literature due to its complicated form. We use series representations (Rosiński 2001) with the inverse Lévy measure method and the rejection method and prove upper bounds for the mean squared approximation error. Furthermore, we extend the numerical inverse Lévy measure method of Imai & Kawai (2013) to incorporate explosive Lévy tail measures. Monte Carlo studies verify the error bounds and the effectiveness of the simulation routine. As a side result we obtain series representations of the so-called inverse gamma subordinator which are used to generate paths in this model.

2.1 Introduction

We present simulation techniques for the time-continuous Student-Lévy process on $[0, T]$, $T > 0$, i.e., a Lévy process where the 1-increments are Student t distributed. Although theoretically available, there is a lack of path simulation techniques in the literature due to its complicated form. Namely, the $\Delta t \neq 1$ increments' density function and distribution function do not exist in closed form. In this chapter we perform path simulation by using the characterizing Lévy measure (of the Lévy-Khintchine representation, Theorem 1.2) for different series representations.

In a physics context (for halos in accelerator beams), Cufaro Petroni (2007) restricted the simulation to time one increments which are Student t distributed. This comes at the price that the increments $\Delta t < 1$ are not available. One solution is Hubalek's (2005) idea to sample from the characteristic function. More recently, Barth & Stein (2016) proposed another method based on sampling from the characteristic function.

Here, we discuss another approach using series representations of Lévy processes (Rosiński 2001). Series representations have been used widely in the literature, e.g., Todorov & Tauchen (2006) or Imai & Kawai (2011). Series representations were introduced by Bondesson (1982) for simulating random variables with infinitely

divisible distributions and next, due to the direct connection, for the simulation of paths of Lévy processes. Among existent methods, the inverse Lévy tail measure method (see Proposition 2.1) is a very popular one, with the drawback that in many applications the inverse Lévy measure does not exist in closed form. Recently, Imai & Kawai (2013) provided algorithms which compute the inverse Lévy measure efficiently.

This chapter contributes to the literature by proposing an inversion algorithm for explosive Lévy tail measures and by applying it to simulate paths of the inverse gamma Lévy process and, via subordination, of the Student-Lévy process. Moreover, we propose an alternative algorithm using the rejection method. For both methods we prove error bounds for the Student-Lévy process and the inverse gamma subordinator.

The organization of this chapter is as follows: Section 2.2 introduces the general theory of series representations. Section 2.3 presents our main results for the error estimates. Section 2.4 describes the numerical methods which are used for simulation. In Section 2.5 we perform Monte Carlo simulations to validate the theoretical results and illustrate the effectiveness of the numerical methods. The last section concludes.

2.2 Series representations

In this section we review some general theoretical results on series representations of Lévy processes. For instance, we consider different forms which may represent a Lévy process. We focus on the inverse Lévy measure method and the rejection method, treated in Proposition 2.1. In Section 2.3 we discuss the special cases of the Student-Lévy process and the inverse gamma subordinator and derive bounds for the approximation error using the introduced series representations. Numerical simulation techniques will be discussed in Section 2.4. Although we restrict the focus to the Student-Lévy process in the one-dimensional case in Section 2.3, we first discuss the general theory in d dimensions since the numerical algorithms also work for d dimensions.

Let $\{X_t\}$ be a d-dimensional Lévy process and $\{Y_t\}$ be a subordinator on the compact interval $[0,T]$, where $T>0$ is fixed. Let $\{E_i\}_{i\in\mathbb{N}}$ be a sequence of i.i.d. unit exponential random variables and let $\{\Gamma_i\}_{i\in\mathbb{N}}$ with $\Gamma_i=\sum_{j=1}^{i}E_i$ be standard Poisson arrival times. Furthermore, let $\{U_i\}_{i\in\mathbb{N}}$ denote a sequence of i.i.d. $\mathcal{U}_{[0,T]}$ random variables independent of $\{\Gamma_i\}$.

We now present some important results on series representations. This is motivated by the question of how to simulate Lévy processes with general characteristics (γ,A,Π). It turns out that this is easy if the density function $f_t(x)$ of X_t is known explicitly. If this is this case, e.g., if the Lévy process under consideration is a d-dimensional Gaussian Lévy process, we partition the domain $[0,T]$ into a discrete

subset $0 = t_0 < t_h < t_{2h} < \ldots < t_{nh} = T$ with sufficiently small precision $h > 0$ and simulate n i.i.d. random variables X_{j,t_h} from the density function $f_{t_h}(x)$. The Lévy process is built with $X_t = \sum_{j=0}^{\lfloor nt \rfloor} X_{j,t_h}$.

However, in many prominent cases, for instance the Student-Lévy process or the inverse gamma Lévy process, the density function at time $t \neq 1$ is not available in closed form. Hence, simulation turns out to be more difficult. One approach in the Student t case was considered by Hubalek (2005) by simulating from the characteristic function using the methods of Devroye (1981) which is based on Fourier inversion and the ratio-of-uniforms method. Barth & Stein (2016) sampled from the characteristic function using Fourier inversion and direct inversion. Our approach using series representations has the advantage that we do not need to fix the minimal step size Δt at the beginning and hold it fixed but simulate the series representation and evaluate the path afterwards at desired time points. Appendix 2.A compares our simulation approach with those of Hubalek (2005) and Barth & Stein (2016).

The idea of series representations is that infinitely divisible random variables (and hence Lévy processes) can be represented as an infinite sum of effects $H(\Gamma_i, V_i)$ of a *shot* V_i after Γ_i time units. These effects should be decreasing in time to make the series summable. Rosiński (2001) – based on Bondesson (1982) and Rosiński (1990) – derived the general shot noise theory and presented widely-used series representations.

We now state the theorem for general shot noise representations.

Theorem 2.1 (Rosiński (2001))**.** *Let $\{V_i\}_{i\geq 1}$ be an i.i.d. sequence of random variables in a measurable space S with distribution function F. Let $\{\Gamma_i\}_{i\geq 1}$ be a sequence of standard Poisson arrival times independent of $\{V_i\}$. Let $\{U_i\}_{i\geq 1}$ be a sequence of independent, $\mathcal{U}_{[0,T]}$ random variables independent of $\{V_i\}$ and $\{\Gamma_i\}$. Let*

$$H : (0, \infty) \times S \to \mathbb{R}^d$$

be a measurable function such that for each $v \in S$, $r \mapsto |H(r, v)|$ is non-increasing. Define measures on $\mathbb{R}^d$ by

$$\sigma(r, B) = P(H(r, V_i) \in B), \quad r > 0,\ B \in \mathcal{B}(\mathbb{R}^d),$$

and

$$\Pi(B) = \int_0^\infty \sigma(r, B)\mathrm{d}r, \quad B \in \mathcal{B}(\mathbb{R}^d).$$

Set

$$A(s) = \int_0^s \int_{|x|\leq 1} x\sigma(r, \mathrm{d}x)\mathrm{d}r, \quad s \geq 0.$$

(i) $\sum_{i=1}^{\infty} H(\frac{\Gamma_i}{T}, V_i)\mathbb{1}_{\{U_i \leq t\}}$ *converges almost surely and uniformly on* $[0,T]$ *to a Lévy process with characteristic function*

$$\phi_t(z) = \exp\left\{ t\left(\mathrm{i}\langle z, a\rangle + \int_{\mathbb{R}_0^d} (e^{\mathrm{i}\langle z,x\rangle} - 1 - \mathrm{i}\langle z, x\rangle \mathbb{1}_{\{|x|\leq 1\}})\Pi(\mathrm{d}x) \right) \right\}, \quad z \in \mathbb{R}^d,$$

if and only if

$$\int_{\mathbb{R}_0^d} (|x|^2 \wedge 1)\Pi(\mathrm{d}x) < \infty \tag{2.1}$$

and $a := \lim_{s\to\infty} A(s)$ *exists in* $\mathbb{R}^d$.

(ii) If only (2.1) *holds, then* $\sum_{i=1}^{\infty} H(\frac{\Gamma_i}{T}, V_i)\mathbb{1}_{\{U_i\leq t\}} - tc_i$, *where* c_i *are deterministic centering constants, given by* $c_i = A(i) - A(i-1)$, *converges a.s. and uniformly on* $[0,T]$ *to a Lévy process with triple* $(0,0,\Pi)$.

Unfortunately, this general theorem does not yield a unique representation for any Lévy process since $H(r,v)$ and the random variables V_i can have many different forms. For a specific Lévy process it may be complicated to find an appropriate representation or it may have several ones and the question arises as to which is the most useful. We later provide some common series representations but first discuss how to implement representations using Theorem 2.1. It is necessary to truncate the sum as we cannot simulate infinitely many summands. We will cut off if an effect of a shot noise becomes "too small". Of course, we can truncate the sums deterministically at $i = n_0$ for large n_0. We will consider this in Section 2.3.1 as a first step. A more sophisticated way for truncating the infinite sum is the following random cutoff:

Remark 2.1. Assume condition (i) of Theorem 2.1 is fulfilled and the Lévy process $\{X_t\}$ can be represented as $\sum_{i=1}^{\infty} H(\frac{\Gamma_i}{T}, V_i)\mathbb{1}_{\{U_i\leq t\}}$. Then, for a given level of truncation $\tau > 0$, the randomly truncated process

$$X_t^\tau := \sum_{\{i\in\mathbb{N}:\Gamma_i\leq\tau\}} H\left(\frac{\Gamma_i}{T}, V_i\right)\mathbb{1}_{\{U_i\leq t\}}$$

for $t \in [0,T]$ is a compound Poisson process (and hence a Lévy process) with characteristics $(0,0,\Pi^\tau)$, where

$$\Pi^\tau(B) = \int_0^\tau \sigma(r,B)\mathrm{d}r, \quad B \in \mathcal{B}(\mathbb{R}^d).$$

Hence, the key motivation for random truncation is that we replace the true Lévy process by another actual Lévy process.

Even if there exist series representations for general d-dimensional Lévy processes $\{X_t\}$, from now on we restrict ourselves to one-dimensional subordinators $\{Y_t\}$. We do so because many interesting Lévy processes can be constructed by subordination, such as the Student-Lévy process (possibly d-dimensional). Simulation of subordinators together with Corollary 2.2 below provides a reasonable simulation method for $\{X_t\}$ without having to bother with more complicated series representations of $\{X_t\}$. First note

Corollary 2.1. *If $\{Y_t\}$ is a subordinator with zero drift and Lévy measure $Q(B) = \int_0^\infty \sigma(r, B)\mathrm{d}r$ for $B \in \mathcal{B}((0,\infty))$ then the conditions of part (i) of Theorem 2.1 are fulfilled and $Y_t = \sum_{i=1}^\infty H(\frac{\Gamma_i}{T}, V_i)\mathbb{1}_{\{U_i \le t\}}$ a.s.*

The next theorem provides important series representations for subordinators. There exist more standard forms which we do not discuss here, because they are not applicable for the inverse gamma subordinator.

Proposition 2.1. *Let $\{Y_t\}$ be a subordinator with zero drift and Lévy measure $Q(B)$. Then we have the following series representations:*

(i) (Inverse Lévy measure method, Ferguson & Klass (1972)) *Let $Q^{\leftarrow}(y) = \inf\{x > 0 : Q([x,\infty)) < y\}$ be the inverse Lévy tail measure for $y > 0$. Then*

$$Y_t \overset{\mathcal{L}}{=} \sum_{i=1}^{\infty} Q^{\leftarrow}\left(\frac{\Gamma_i}{T}\right)\mathbb{1}_{\{U_i \le t\}}, \quad t \in [0,T].$$

(ii) (Rejection method, Rosiński (2001)) *Let $\{Y_t^{(0)}\}$ be a subordinator with Laplace characteristics $(0, Q_0)$ such that $\frac{\mathrm{d}Q}{\mathrm{d}Q_0} \le 1$. Let $\{W_i\}_{i\ge1}$ be a sequence of i.i.d. random variables uniform on $[0,1]$ which are independent of $\{\Gamma_i\}_{i\ge1}$ and $\{U_i\}_{i\ge1}$. Then*

$$Y_t \overset{\mathcal{L}}{=} \sum_{i=1}^{\infty} Q_0^{\leftarrow}\left(\frac{\Gamma_i}{T}\right)\mathbb{1}\left(\left\{\frac{\mathrm{d}Q}{\mathrm{d}Q_0}\left(Q_0^{\leftarrow}\left(\frac{\Gamma_i}{T}\right)\right) \ge W_i\right\}\right)\mathbb{1}_{\{U_i \le t\}}, \quad t \in [0,T]. \tag{2.2}$$

(iii) (Thinning method, Rosiński (1990)) *Let F be any probability distribution on $(0,\infty)$ such that Q is absolutely continuous with respect to F. Let $\{V_i\}_{i\ge1}$ be an independent F-distributed sequence, which is independent of $\{\Gamma_i\}_{i\ge1}$ and $\{U_i\}_{i\ge1}$. Then*

$$Y_t \overset{\mathcal{L}}{=} \sum_{i=1}^{\infty} V_i\mathbb{1}\left(\left\{\frac{\mathrm{d}Q}{\mathrm{d}F}(V_i) \ge \frac{\Gamma_i}{T}\right\}\right)\mathbb{1}_{\{U_i \le t\}}, \quad t \in [0,T].$$

We discuss both the inverse Lévy measure and the rejection methods in detail for the Student-Lévy process and inverse gamma subordinator in this chapter. The thinning method is, although technically available, computationally burdensome, as briefly discussed in Remark 2.3 and therefore only introduced for completeness here. The general problem, as for the inverse gamma subordinator, is that the inverse Lévy measure often is not available in closed form. In these cases we may use another series representation or numerical methods as in Section 2.4.

In the next example the inverse Lévy measure is known explicitly. We use this example in Subsection 2.3.2.

Example 2.1. Consider an α-stable subordinator $\{Y_0(t)\}_{t\in[0,T]}$ for $\alpha \in (0,2)$ with zero drift and Lévy measure

$$Q_0(\mathrm{d}u) = c_+ u^{-1-\alpha} \mathbb{1}_{\{u>0\}}.$$

Then the inverse tail measure is given by

$$Q_0^{\leftarrow}(y) = \left(\frac{\alpha}{c_+}\right)^{-1/\alpha} y^{-1/\alpha}$$

and $Y_0(t)$ can be represented as

$$\left(\frac{\alpha}{c_+}\right)^{-1/\alpha} \sum_{i=1}^{\infty} \left(\frac{\Gamma_i}{T}\right)^{-1/\alpha} \mathbb{1}_{\{U_i \le t\}},$$

for $t \in [0,T]$.

The next corollary (cf. Tankov & Cont (2015)) closes the gap between the simulation of a subordinator (via Proposition 2.1) and the desired simulation of Gaussian subordination, e.g., the Student-Lévy process (see Theorem 1.5). Here we state it for the inverse Lévy measure method. The series representations using the rejection or the thinning method can be formulated analogously.

Corollary 2.2. *Let Y_t be a subordinator with zero drift and Lévy measure $Q(B)$. Let $Q^{\leftarrow}(y)$ be defined as in Proposition 2.1. Let $\{V_i\}_{i\ge1}$ be a sequence of d-dimensional i.i.d. standard normal vectors, independent both of $\{\Gamma_i\}$ and $\{U_i\}$. Then we have the following series representation for $\{X_t\}$, where $X_t = B_{Y_t}$ and $\{B_t\}$ is a d-dimensional Brownian motion independent of $\{Y_t\}$:*

$$X_t \overset{\mathcal{L}}{=} \sum_{i=1}^{\infty} \sqrt{Q^{\leftarrow}\left(\frac{\Gamma_i}{T}\right)} V_i \mathbb{1}_{\{U_i \le t\}}, \quad t \in [0,T].$$

From now on, we focus on the inverse gamma subordinator with marginals $\mathcal{L}(Y_1) = R\Gamma(\nu/2, \nu/2)$ for $\nu > 1$, since this subordinator induces the Student-Lévy process. For $\nu = 1$ the Student-Lévy process is a Cauchy-Lévy process. The Cauchy-Lévy process is much easier to simulate since the Cauchy distribution is closed under convolution and thus not considered here. For $0 < \nu < 1$ we can still use the numerical algorithms proposed in Section 2.4 but the theoretical results within the next subsections do not hold. Furthermore, we consider the case of a Student-Lévy process with standard scaling ($\mu = 0, \Sigma = I$) for the simulation purpose throughout because the general case is an easy consequence using the transformation $AX_t + \mu t$, where $\Sigma = AA^{\mathrm{T}}$.

2.3 Mean squared error bounds

2.3.1 Inverse Lévy measure method

In this section we discuss mean squared approximation errors for the inverse gamma subordinator and the Student-Lévy process simulation. All theoretical results within this section are discussed for the one-dimensional Student-Lévy process $\{X_t\}$ while the simulation routine in Section 2.4 also works well for d dimensions.

Recall that the Lévy measure of the inverse gamma subordinator $\{Y_t\}$ with $Y_1 \sim R\Gamma(\nu/2, \nu/2)$ has the rather complex form

$$Q(\mathrm{d}u) := \rho(u)\mathrm{d}u := \left(u^{-1} \int_0^\infty e^{-su} \nu g_{\nu/2}(2\nu s) \mathrm{d}s \right) \mathrm{d}u, \tag{2.3}$$

with

$$g_{|\alpha|}(x) := 2 \left(\pi^2 x \left(J_{|\alpha|}^2 \left(\sqrt{x} \right) + Y_{|\alpha|}^2 \left(\sqrt{x} \right) \right) \right)^{-1}, \quad x > 0,$$

and J_α and Y_α are the Bessel functions of the first and the second kind, respectively. There exists no closed-form solution for the inverse Lévy tail measure. Hence, the inverse Lévy measure series representation is non-trivial. For now, assume that it is possible to find $Q^{\leftarrow}(y)$, at least numerically. Section 2.4 provides a justification. Figure 2.1 shows numerically computed inverse Lévy measures for different degrees of freedom. The inverse Lévy measure is higher for smaller degrees of freedom close to the origin and lower in the tail. Let $\{\Gamma_i\}$ be a process of Poisson arrival times. Then $Q^{\leftarrow}(\Gamma_i/T)$ is larger for $\nu = 4$ than for higher ν in case of small values of Γ_i/T (the big jumps). On the other hand, for a given large Γ_i/T the jump $Q^{\leftarrow}(\Gamma_i/T)$ is smaller for $\nu = 4$. In practice, this means that for a truncated series representation we cut off the very small jumps earlier for high ν. Hence, the truncated representation for

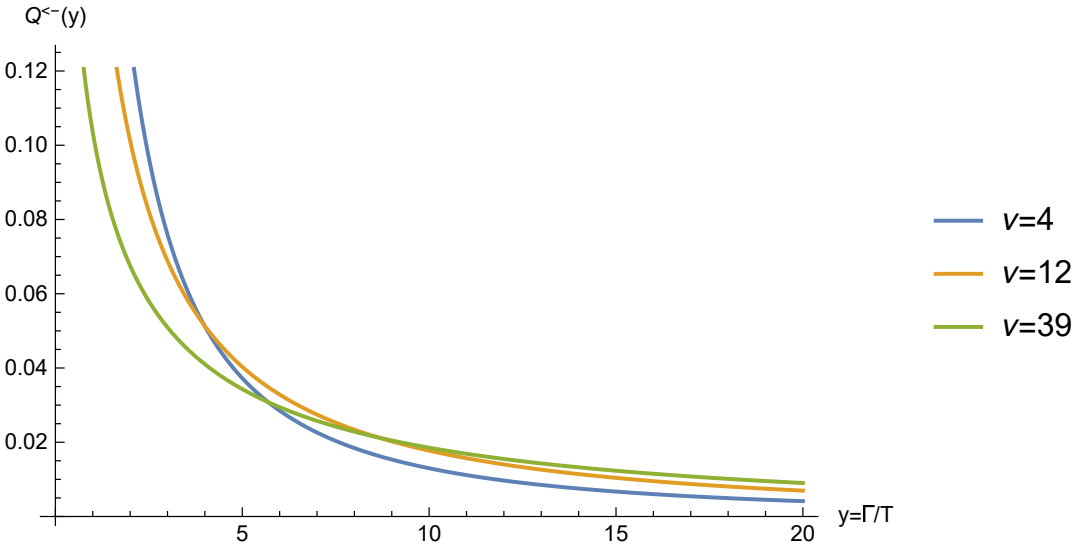

Figure 2.1: Comparison of the inverse Lévy measures for the inverse gamma subordinator (computed via Algorithms 1 and 2 for $y = \frac{\Gamma_i}{T} \in (0, \infty)$). Note that the inverse Lévy measure is higher for smaller degrees of freedom close to the origin and lower in the tail.

$\nu = 4$ contains more big jumps and more very small jumps. Figure 2.2 also illustrates this pattern.

The aim of this subsection is to find an upper bound for the mean squared error (MSE) of the approximation. For this purpose we now bound the Lévy measure and the inverse tail measure (see Figure 2.3). This is also helpful for the rejection method in Subsection 2.3.2.

Lemma 2.1. *Let $\{Y_t\}$ be the inverse gamma subordinator with $\mathcal{L}(Y_1) = R\Gamma(\nu/2, \nu/2)$ and let $\nu > 1$. Let $Q(\mathrm{d}u)$ defined in (2.3) be its Lévy measure and $Q^{\leftarrow}(y)$ be its inverse tail measure. Then*

$$Q(\mathrm{d}u) < \sqrt{\frac{\nu}{2\pi u^3}}\mathrm{d}u \tag{2.4}$$

and

$$Q^{\leftarrow}(y) < \frac{2\nu}{\pi y^2}. \tag{2.5}$$

Proof. Recall that

$$Q(\mathrm{d}u) = u^{-1} \int_0^\infty e^{-su} \nu 2 \left[\pi^2 2\nu s \left(J^2_{\frac{\nu}{2}}(\sqrt{2\nu s}) + Y^2_{\frac{\nu}{2}}(\sqrt{2\nu s})\right)\right]^{-1} \mathrm{d}s\mathrm{d}u.$$

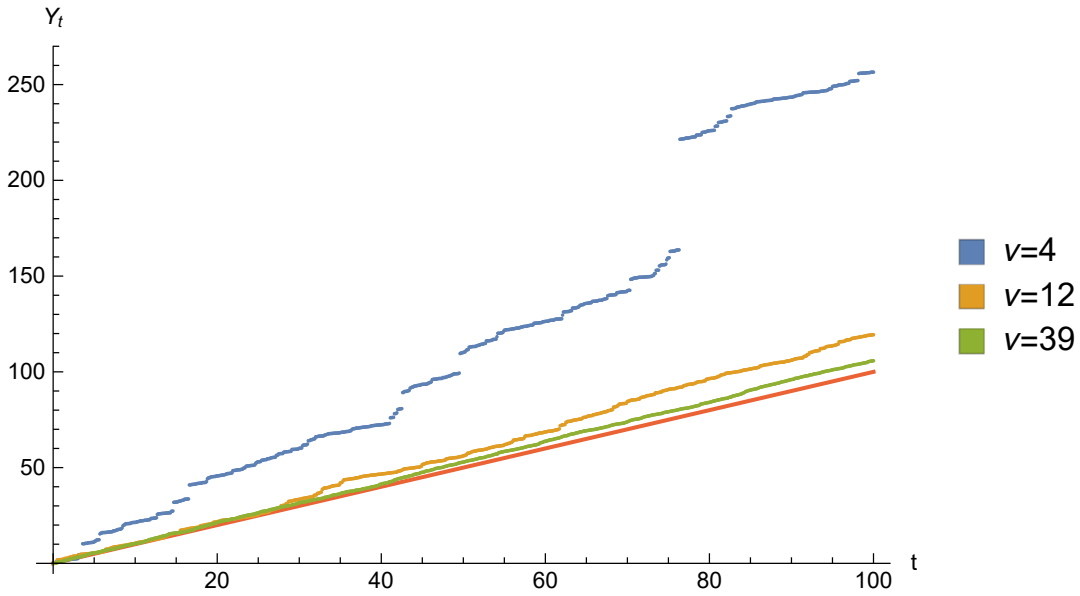

Figure 2.2: Simulation of sample paths of the inverse gamma subordinator with $Y_1 \sim R\Gamma(\nu/2, \nu/2)$ for various degrees of freedom. The red line maps $t \mapsto t$ for comparison using the standard time process in Brownian motion (no subordination). For $\nu = 4$ note the characteristic big jumps. For $\nu = 39$ and even for $\nu = 12$ there are no big jumps and the trajectories are close to the $t \mapsto t$ line.

We use the inequality

$$J_\nu^2(x) + Y_\nu^2(x) > \frac{2}{\pi x},$$

first derived by Schafheitlin (1906); an elegant proof can be found in Watson (1995). Hence,

$$\nu g_{\frac{\nu}{2}}(2\nu s) = \nu \left[\pi^2 \nu s \left(J_{\frac{\nu}{2}}^2(\sqrt{2\nu s}) + Y_{\frac{\nu}{2}}^2(\sqrt{2\nu s})\right)\right]^{-1} < \sqrt{\frac{\nu}{2\pi^2 s}}.$$

By standard integration,

$$Q(\mathrm{d}u) < u^{-1} \int_0^\infty e^{-su} \sqrt{\frac{\nu}{2\pi^2 s}} \mathrm{d}s\mathrm{d}u = \sqrt{\frac{\nu}{2\pi u^3}} \mathrm{d}u$$

such that (2.4) follows. To derive (2.5), the tail mass function is bounded by

$$Q([z, \infty)) = \int_z^\infty Q(\mathrm{d}u) < \int_z^\infty \sqrt{\frac{\nu}{2\pi u^3}} \mathrm{d}u = \sqrt{\frac{2\nu}{\pi z}}.$$

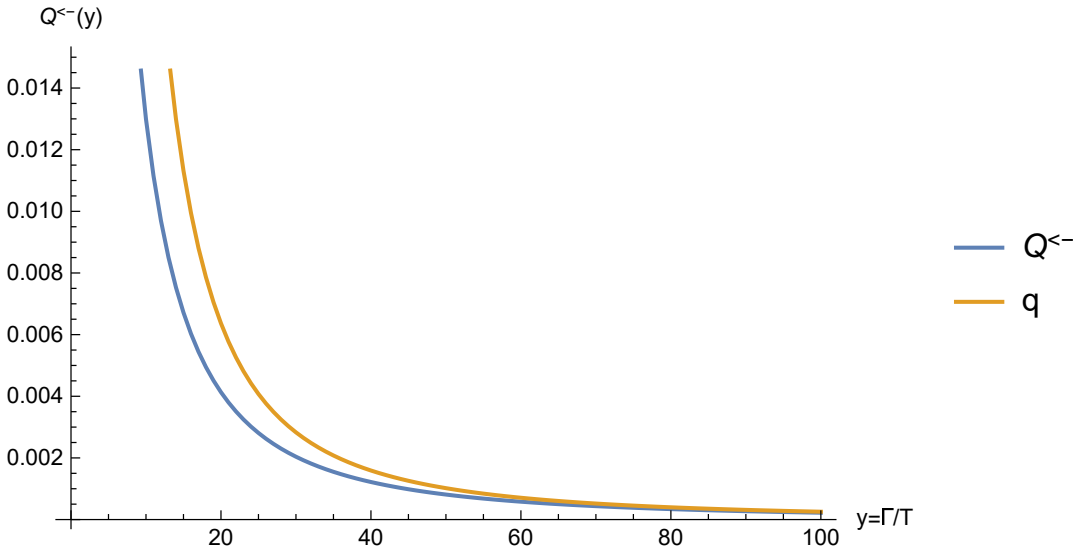

Figure 2.3: The inverse Lévy measure $Q^{\leftarrow}(y)$ for the inverse gamma subordinator with $Y_1 \sim R\Gamma(\nu/2, \nu/2)$ and its bound $q(y) := \frac{2\nu}{\pi y^2}$ with $\nu = 4$. Note that the bound converges to the true inverse Lévy measure for increasing y.

Since $Q([z, \infty))$ is strictly decreasing and continuous, $Q^{\leftarrow}(y)$ is the true inverse and

$$\begin{aligned} Q^{\leftarrow}(y) &= \inf\{z > 0 : Q([z, \infty)) < y\} \\ &< \inf\{z > 0 : \sqrt{\frac{2\nu}{\pi z}} < y\} \\ &= \frac{2\nu}{\pi y^2}, \end{aligned}$$

which completes the proof. □

We next derive the bound for the mean square error approximation for the inverse gamma subordinator. Remark 2.1 discusses the random truncation of the series where we cut off all summands for which $\Gamma_i > \tau$ for a given τ. For the next results it is however convenient to consider a deterministic truncation first where we cut off all summands $i > n$. Corollary 2.3 discusses how to deduce the approximation error for the random truncation.

Theorem 2.2. *Let $\{Y_t\}$ be the inverse gamma subordinator, with $\mathcal{L}(Y_1) = R\Gamma(\nu/2, \nu/2)$,*

$\nu > 1$, represented with the inverse Lévy measure method:

$$Y_t = \sum_{i=1}^{\infty} Q^{\leftarrow}\left(\frac{\Gamma_i}{T}\right) \mathbb{1}_{\{U_i \leq t\}}, \quad t \in [0,T].$$

Let

$$Y_t^{(n)} := \sum_{i=1}^{n} Q^{\leftarrow}\left(\frac{\Gamma_i}{T}\right) \mathbb{1}_{\{U_i \leq t\}}, \quad t \in [0,T],$$

be the deterministically truncated process. Assume that $n \geq 4$. Then

$$E[Y_t - Y_t^{(n)}] < \frac{2\nu}{\pi} \frac{T}{n-1} t, \tag{2.6}$$

and the mean squared error is bounded by

$$E[(Y_t - Y_t^{(n)})^2] < \frac{4\nu^2 T^3}{\pi^2} t \left(\frac{1}{n-2.5} + \frac{1}{(n-3)^2}\right)^2, \tag{2.7}$$

for $t \in [0,T]$.

Remark 2.2. The bound (2.6) depends on t, n, T and ν. While the former two seem reasonable, the dependence on T might be puzzling at first sight. However, if T is large, we expect more big jumps in this longer time interval. The reason for this is that small values of Γ_i/T correspond to large jumps, see the plot of $Q^{\leftarrow}(\Gamma_i/T)$ in Figure 2.1. Hence, the presence (or absence) of large jumps causes a higher error. This effect is even higher for the mean squared error, which is proportional to T^3.

The second interesting fact is that (2.6) and (2.7) increase in ν. In other words, it is more difficult to simulate inverse gamma subordinators with high degrees of freedom. To understand this, recall that the paths of the inverse gamma subordinator converge to the path process $t \mapsto t$ for $\nu \to \infty$ (Figure 2.2). But this limiting case is the constant drift subordinator with Lévy measure zero, which hence has no inverse Lévy measure.

Proof of Theorem 2.2. Note that

$$\begin{aligned} Y_t - Y_t^{(n)} &= \sum_{i=1}^{\infty} Q^{\leftarrow}\left(\frac{\Gamma_i}{T}\right) \mathbb{1}_{\{U_i \leq t\}} - \sum_{i=1}^{n} Q^{\leftarrow}\left(\frac{\Gamma_i}{T}\right) \mathbb{1}_{\{U_i \leq t\}} \\ &= \sum_{i=n+1}^{\infty} Q^{\leftarrow}\left(\frac{\Gamma_i}{T}\right) \mathbb{1}_{\{U_i \leq t\}} \end{aligned}$$

Denote by $q(y) := \frac{2\nu}{\pi y^2}$ the bound for $Q^{\leftarrow}$ derived in Lemma 2.1. We start by proving

(2.6). Taking expectations to obtain

$$E\left[\sum_{i=n+1}^{\infty} Q^{\leftarrow}\left(\frac{\Gamma_i}{T}\right)\mathbb{1}_{\{U_i\leq t\}}\right] = \sum_{i=n+1}^{\infty} E\left[Q^{\leftarrow}\left(\frac{\Gamma_i}{T}\right)\right] E\left[\mathbb{1}_{\{U_i\leq t\}}\right]$$
$$< \frac{t}{T}\sum_{i=n+1}^{\infty} E\left[q\left(\frac{\Gamma_i}{T}\right)\right], \tag{2.8}$$

where we have used the monotonicity of the expected value. Since the Γ_is are $\Gamma(i,1)$ distributed (with density function denoted by $\gamma_i(x)$), (2.8) is equal to

$$\frac{t}{T}\sum_{i=n+1}^{\infty}\int_0^{\infty} q(x/T)\gamma_i(x)\mathrm{d}x = \frac{t}{T}\sum_{i=n+1}^{\infty}\frac{2\nu}{\pi}\frac{T^2}{(i-1)(i-2)}$$
$$= \frac{2\nu}{\pi}\frac{T}{n-1}t.$$

It remains to prove (2.7). Using the monotone convergence theorem

$$E\left[\left(\sum_{i=n+1}^{\infty} Q^{\leftarrow}\left(\frac{\Gamma_i}{T}\right)\mathbb{1}_{\{U_i\leq t\}}\right)^2\right]$$
$$= \sum_{i=n+1}^{\infty}\sum_{j=n+1}^{\infty} E\left[Q^{\leftarrow}\left(\frac{\Gamma_i}{T}\right)\mathbb{1}_{\{U_i\leq t\}}Q^{\leftarrow}\left(\frac{\Gamma_j}{T}\right)\mathbb{1}_{\{U_j\leq t\}}\right],$$

since $Q^{\leftarrow}\left(\frac{\Gamma_i}{T}\right)\mathbb{1}_{\{U_i\leq t\}} \geq 0$ for all i. Next, by the Cauchy-Schwarz inequality

$$\sum_{i=n+1}^{\infty}\sum_{j=n+1}^{\infty} E\left[Q^{\leftarrow}\left(\frac{\Gamma_i}{T}\right)\mathbb{1}_{\{U_i\leq t\}}Q^{\leftarrow}\left(\frac{\Gamma_j}{T}\right)\mathbb{1}_{\{U_j\leq t\}}\right]$$
$$\leq \sum_{i=n+1}^{\infty}\sum_{j=n+1}^{\infty}\sqrt{E\left[Q^{\leftarrow}\left(\frac{\Gamma_i}{T}\right)^2\mathbb{1}_{\{U_j\leq t\}}\right]E\left[Q^{\leftarrow}\left(\frac{\Gamma_j}{T}\right)^2\mathbb{1}_{\{U_j\leq t\}}\right]}$$
$$< \sum_{i=n+1}^{\infty}\sum_{j=n+1}^{\infty}\sqrt{\frac{t^2}{T^2}E\left[q\left(\frac{\Gamma_i}{T}\right)^2\right]E\left[q\left(\frac{\Gamma_j}{T}\right)^2\right]}$$
$$= \frac{t}{T}\sum_{i=n+1}^{\infty}\sum_{j=n+1}^{\infty}\sqrt{\int_0^{\infty} q(x/T)^2\gamma_i(x)\mathrm{d}x\cdot\int_0^{\infty} q(x/T)^2\gamma_j(x)\mathrm{d}x}$$

$$=\frac{t}{T}\frac{4\nu^2}{\pi^2}\sum_{i=n+1}^{\infty}\sum_{j=n+1}^{\infty}\sqrt{\frac{T^4}{(i-1)(i-2)(i-3)(i-4)}\frac{T^4}{(j-1)(j-2)(j-3)(j-4)}} \tag{2.9}$$

Since $i, j \geq n+1 \geq 5$, we can bound (2.9) using $(i-1)(i-2)(i-3)(i-4) \geq (i-4)^4$ by

$$\frac{t}{T}\frac{4\nu^2}{\pi^2}\left(\sum_{i=n+1}^{\infty}\frac{T^2}{(i-4)^2}\right)^2 = \frac{4\nu^2T^3}{\pi^2}t\psi'(n-3)^2, \tag{2.10}$$

where $\psi'(x)$ denotes the first derivative of the digamma function $\psi(x) := \frac{\Gamma'(x)}{\Gamma(x)}$ (also called polygamma function of order 1). Guo et al. (2015) provided a sharp bound for polygamma functions. The inequality for $\psi'(x)$ is

$$|\psi'(x)| < \frac{1}{x+\frac{1}{2}} + \frac{1}{x^2}. \tag{2.11}$$

Applying (2.11) to (2.10) we obtain the bound

$$E\left[\left(\sum_{i=n+1}^{\infty} Q^{\leftarrow}\left(\frac{\Gamma_i}{T}\right)\mathbb{1}_{\{U_i\leq t\}}\right)^2\right] < \frac{4\nu^2T^3}{\pi^2}t\left(\frac{1}{n-2.5}+\frac{1}{(n-3)^2}\right)^2.$$

□

With Theorem 2.2 we can also derive mean squared error bounds for the Student-Lévy process using Corollary 2.2.

Theorem 2.3. *Let $\{Y_t\}$ be the inverse gamma subordinator with $\mathcal{L}(Y_1) = R\Gamma(\nu/2, \nu/2)$ and Laplace characteristics $(0, Q)$, $\nu > 1$, and let $\{B_t\}_{t\in[0,T]}$ be a Brownian motion independent of $\{Y_t\}$. Let $X_t := B_{Y_t}$ be the subordinated Student-Lévy process, represented with the inverse Lévy measure for subordination (see Corollary 2.2)*

$$X_t = \sum_{i=1}^{\infty}\sqrt{Q^{\leftarrow}\left(\frac{\Gamma_i}{T}\right)}V_i\mathbb{1}_{\{U_i\leq t\}}, \quad t\in[0,T],$$

where V_i are i.i.d. $N(0,1)$. Let

$$X_t^{(n)} := \sum_{i=1}^{n}\sqrt{Q^{\leftarrow}\left(\frac{\Gamma_i}{T}\right)}V_i\mathbb{1}_{\{U_i\leq t\}}, \quad t\in[0,T]$$

be the deterministically truncated process. Assume that $n \geq 2$. Then, $E[X_t - X_t^{(n)}] = 0$

and the mean squared error is bounded by

$$E[(X_t - X_t^{(n)})^2] < \frac{2\nu}{\pi}\frac{T}{n-1}t, \tag{2.12}$$

for $t \in [0,T]$.

Proof. Again,

$$X_t - X_t^{(n)} = \sum_{i=n+1}^{\infty} \sqrt{Q^{\leftarrow}\left(\frac{\Gamma_i}{T}\right)} V_i \mathbb{1}_{\{U_i \leq t\}}.$$

Note that $E[V_i] = 0$ and that V_i is independent of $Q^{\leftarrow}\left(\frac{\Gamma_i}{T}\right)$ and U_i. Hence, by Fubini's theorem,

$$E\left[\sum_{i=n+1}^{\infty} \sqrt{Q^{\leftarrow}\left(\frac{\Gamma_i}{T}\right)} V_i \mathbb{1}_{\{U_i \leq t\}}\right] = 0.$$

Furthermore, analogously to Theorem 2.2,

$$\begin{aligned}
&E\left[\left(\sum_{i=n+1}^{\infty} \sqrt{Q^{\leftarrow}\left(\frac{\Gamma_i}{T}\right)} V_i \mathbb{1}_{\{U_i \leq t\}}\right)^2\right] \\
&= \sum_{i=n+1}^{\infty}\sum_{j=n+1}^{\infty} E\left[\sqrt{Q^{\leftarrow}\left(\frac{\Gamma_i}{T}\right)} V_i \mathbb{1}_{\{U_i \leq t\}} \sqrt{Q^{\leftarrow}\left(\frac{\Gamma_j}{T}\right)} V_j \mathbb{1}_{\{U_j \leq t\}}\right] \\
&= \sum_{i=n+1}^{\infty}\sum_{j=n+1}^{\infty} E\left[\sqrt{Q^{\leftarrow}\left(\frac{\Gamma_i}{T}\right)} \sqrt{Q^{\leftarrow}\left(\frac{\Gamma_j}{T}\right)} \mathbb{1}_{\{U_i \leq t\}} \mathbb{1}_{\{U_j \leq t\}}\right] E\left[V_i V_j\right]. \qquad (2.13)
\end{aligned}$$

Since $E[V_i V_j] = \delta_{i,j}$, (2.13) equals

$$\sum_{i=n+1}^{\infty} E\left[Q^{\leftarrow}\left(\frac{\Gamma_i}{T}\right) \mathbb{1}_{\{U_i \leq t\}}\right] < \frac{t}{T}\sum_{i=n+1}^{\infty} E\left[q\left(\frac{\Gamma_i}{T}\right)\right] = \frac{2\nu}{\pi}\frac{T}{n-1}t$$

as in the proof of Theorem 2.2. □

If $\nu > 2$ the variance of X_t is finite and equal to $\frac{\nu t}{\nu-2}$. In this case the error bound (2.12) has the share $\frac{2(\nu-2)T}{\pi(n-1)}$ of the variance of X_t. This means that if the time horizon or the degrees of freedom increase the truncation level n has to increase proportionally to hold this share constant. If the level of truncation is large enough

(e.g., one hundred times higher than T) this share will be about a few percentages for small ν. Section 2.5.1 presents detailed information on the size of the bounds above and those below with a Monte Carlo verification.

Next, we return to the case of the random truncation for X_t, cf. Remark 2.1. This is done by replacing $\sum_i^n$ with $\sum_i^{N_\tau}$ with a unit rate Poisson process N_t. We then make use of the law of iterated expectation. Here, we skip this for the inverse gamma subordinator Y_t as the derivation of the expression becomes very tedious. The numerical values are very close anyway.

Corollary 2.3. *Let $\{Y_t\}$ and $\{X_t\}$ be defined as in Theorems 2.2 and 2.3. Let τ be a large positive number and define $N_\tau := \#\{i \in \mathbb{N} : \Gamma_i \leq \tau\}$. Given the randomly truncated series representations*

$$Y_t^\tau := \sum_{\{i\in\mathbb{N}:\Gamma_i\leq\tau\}} Q^{\leftarrow}\left(\frac{\Gamma_i}{T}\right)\mathbb{1}_{\{U_i\leq t\}}$$

and

$$X_t^\tau := \sum_{\{i\in\mathbb{N}:\Gamma_i\leq\tau\}} \sqrt{Q^{\leftarrow}\left(\frac{\Gamma_i}{T}\right)}V_i\mathbb{1}_{\{U_i\leq t\}},$$

the conditional mean squared error for the Student-Lévy process is bounded by

$$E[(X_t - X_t^\tau)^2|\Gamma_2 \leq \tau] < \frac{2\nu T t}{\pi}\frac{\tau + 1 - e^\tau - \tau\gamma + \tau Ei(\tau) - \tau\log(\tau)}{e^\tau}\frac{1}{1-\Gamma(3,\tau)/2}, \tag{2.14}$$

with $\gamma = 0.577216\ldots$ the Euler-Mascheroni constant, $Ei(x) = -\int_{-x}^{\infty}\frac{e^{-t}}{t}\mathrm{d}t$ the exponential integral and $\Gamma(s,x) = \int_s^\infty t^{s-1}e^{-t}\mathrm{d}t$ the incomplete gamma function.

Proof. Since $N_\tau = \#\{i \in \mathbb{N} : \Gamma_i \leq \tau\}$ and the Γ_i are unit Poisson arrival times, $N_\tau \sim Poi(\tau)$. We now use the law of iterated expectation.

$$\begin{aligned} E[(X_t - X_t^\tau)^2|\Gamma_2 \leq \tau] &= E\left[E[(X_t - X_t^\tau)^2|N_\tau, \Gamma_2 \leq \tau]|\Gamma_2 \leq \tau\right] \\ &< E\left[\frac{2\nu}{\pi}\frac{Tt}{N_\tau - 1}\middle|\Gamma_2 \leq \tau\right], \end{aligned}$$

by Theorem 2.3. The conditional expected value $E\left[\frac{1}{N_\tau-1}|\Gamma_2 \leq \tau\right]$ exists and $N_\tau|\Gamma_2 \leq \tau$ follows a truncated Poisson distributed with density function

$$P[N_\tau = k|N_\tau \geq 2] = \frac{e^{-\tau}\tau^k}{k!(1-P[N_\tau \leq 2])} = \frac{e^{-\tau}\tau^k}{k!(1-\Gamma(3,\tau)/2)}.$$

Hence, the conditional expectation is

$$E\left[\frac{1}{N_\tau - 1}\Big|\Gamma_2 \le \tau\right] = \sum_{k=2}^{\infty} \frac{1}{k-1}\frac{e^{-\tau}\tau^k}{k!(1-\Gamma(3,\tau)/2)}$$
$$= \frac{e^{-\tau}}{(1-\Gamma(3,\tau)/2)}\left(\tau + 1 - e^{\tau} - \tau\gamma + \tau Ei(\tau) - \tau\log(\tau)\right),$$

which completes the proof. □

The bounds are only valid under the condition $\Gamma_2 \le \tau$. However, this condition is extremely likely to hold for reasonably high τ. The reason for this condition is to ensure that $N_\tau \ge 2$. This is necessary for $E(\frac{1}{N_\tau - 1})$ to exist.

2.3.2 Rejection method

The rejection method (2.2) provides another approach for the series representation. The advantage is that we do not need to perform numerical inversions of $Q([u,\infty))$. The rejection method works with another subordinator $Y_0(t)$ which has a closed form inverse tail measure such that the measure Q is absolutely continuous with respect to Q_0 and the corresponding density is bounded by 1. We simulate the subordinator $Y_0(t)$ and accept summands $Q_0^{\leftarrow}(\Gamma_i/T)$ with probability $\frac{\mathrm{d}Q}{\mathrm{d}Q_0}(Q_0^{\leftarrow}(\Gamma_i/T))$.

The following result establishes the same upper bound for the rejection method as for the inverse tail measure method.

Corollary 2.4. *Let $\{Y_t\}$ be the inverse gamma subordinator with $\mathcal{L}(Y_1) = R\Gamma(\nu/2, \nu/2)$ and Laplace characteristics $(0, Q)$ with Q defined in (2.3), $\nu > 1$, and let $\{B_t\}$ be a Brownian Motion independent of $\{Y_t\}$. Consider a Lévy process $\{Y_0(t)\}$ with zero drift and Lévy measure $Q_0(\mathrm{d}u) = \sqrt{\frac{\nu}{2\pi u^3}}\mathrm{d}u$. Let $X_t := B_{Y_t}$ be the subordinated Student-Lévy process, represented with the rejection method for subordination*

$$X_t = \sum_{i=1}^{\infty} \sqrt{Q_0^{\leftarrow}\left(\frac{\Gamma_i}{T}\right)} V_i \mathbb{1}\left(\left\{\frac{\mathrm{d}Q}{\mathrm{d}Q_0}\left(Q_0^{\leftarrow}\left(\frac{\Gamma_i}{T}\right)\right) \ge W_i\right\}\right)\mathbb{1}_{\{U_i \le t\}}, \quad t \in [0,T],$$

where V_i are i.i.d. standard normal and W_i are i.i.d. uniform on $[0,T]$. Then, both the deterministically truncated series representation $X_t^{(n)}$ (for $n \ge 2$) and the randomly truncated representation X_t^{τ} have the same mean squared error bounds (2.12) and (2.14) as in Theorem 2.3 and Corollary 2.3 as the inverse Lévy measure method.

Proof. We only prove the claim for the deterministic truncation; the random trunca-

tion bound follows as in Corollary 2.3. Note that Lemma 2.1 implies that $\frac{\mathrm{d}Q}{\mathrm{d}Q_0} \leq 1$ and that the tail inverse $Q_0^{\leftarrow}(y) = \frac{2\nu}{\pi y^2}$ exists in closed form. Let us start with the mean squared error

$$E\left[\left(\sum_{i=n+1}^{\infty}\sqrt{Q_0^{\leftarrow}\left(\frac{\Gamma_i}{T}\right)}V_i\mathbb{1}\left(\left\{\frac{\mathrm{d}Q}{\mathrm{d}Q_0}\left(Q_0^{\leftarrow}\left(\frac{\Gamma_i}{T}\right)\right) \geq W_i\right\}\right)\mathbb{1}_{\{U_i\leq t\}}\right)^2\right]$$
$$= \sum_{i=n+1}^{\infty} E\left[Q_0^{\leftarrow}\left(\frac{\Gamma_i}{T}\right)\mathbb{1}\left(\left\{\frac{\mathrm{d}Q}{\mathrm{d}Q_0}\left(Q_0^{\leftarrow}\left(\frac{\Gamma_i}{T}\right)\right) \geq W_i\right\}\right)\mathbb{1}_{\{U_i\leq t\}}\right],$$

analogously as in the proof of Theorem 2.3, since $E[V_iV_j] = \delta_{i,j}$. By the law of iterated expectation, this is equal to

$$\sum_{i=n+1}^{\infty} E\left[E\left[Q_0^{\leftarrow}\left(\frac{\Gamma_i}{T}\right)\mathbb{1}\left(\left\{\frac{\mathrm{d}Q}{\mathrm{d}Q_0}\left(Q_0^{\leftarrow}\left(\frac{\Gamma_i}{T}\right)\right) \geq W_i\right\}\right)\middle|\,\Gamma_i\right]\right] E\left[\mathbb{1}_{\{U_i\leq t\}}\right]$$
$$= \sum_{i=n+1}^{\infty} E\left[Q_0^{\leftarrow}\left(\frac{\Gamma_i}{T}\right) P\left[\frac{\mathrm{d}Q}{\mathrm{d}Q_0}\left(Q_0^{\leftarrow}\left(\frac{\Gamma_i}{T}\right)\right) \geq W_i\middle|\,\Gamma_i\right]\right] E\left[\mathbb{1}_{\{U_i\leq t\}}\right]$$
$$= \sum_{i=n+1}^{\infty} E\left[Q_0^{\leftarrow}\left(\frac{\Gamma_i}{T}\right)\frac{\mathrm{d}Q}{\mathrm{d}Q_0}\left(Q_0^{\leftarrow}\left(\frac{\Gamma_i}{T}\right)\right)\right] E\left[\mathbb{1}_{\{U_i\leq t\}}\right]$$
$$\leq \sum_{i=n+1}^{\infty} E\left[Q_0^{\leftarrow}\left(\frac{\Gamma_i}{T}\right)\right] E\left[\mathbb{1}_{\{U_i\leq t\}}\right],$$

because $\frac{\mathrm{d}Q}{\mathrm{d}Q_0} \leq 1$. The rest of the proof follows as in the proof of Theorem 2.3 since $Q_0^{\leftarrow} \equiv q$. □

A key term is the probability of acceptance. This should not be too small, so as not to simulate many random numbers which are not used. For the inverse gamma subordinator there is no closed formula for this probability. Nevertheless, we can simplify the expression to numerically evaluate it. As in the proof of Corollary 2.4,

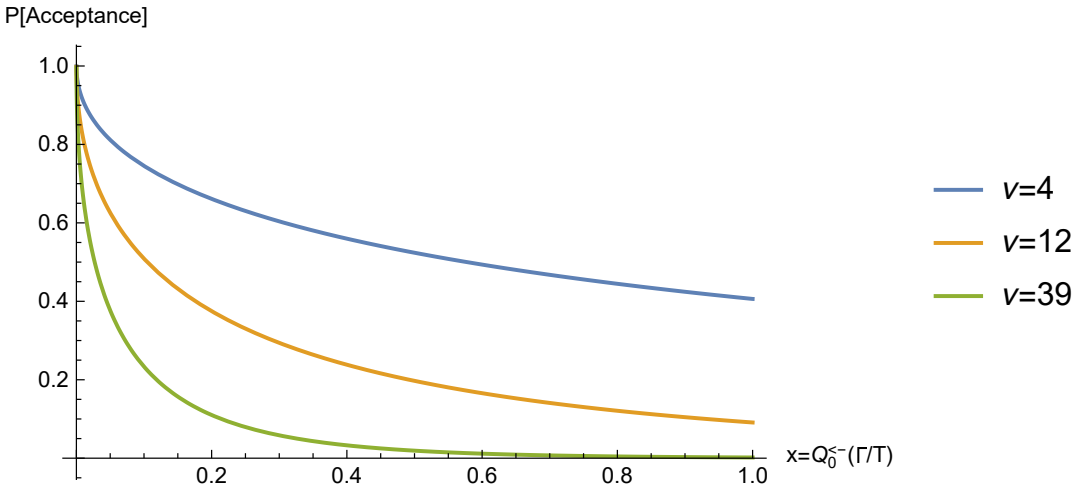

Figure 2.4: Plots of the acceptance probabilities $\frac{\mathrm{d}Q}{\mathrm{d}Q_0}(x)$ for the inverse gamma subordinator for different degrees of freedom. For $\nu = 39$ big jumps are accepted with a very small probability.

$$
\begin{aligned}
P\left[\frac{\mathrm{d}Q}{\mathrm{d}Q_0}\left(Q_0^{\leftarrow}\left(\frac{\Gamma_i}{T}\right)\right) \geq W_i\right] &= E\left[P\left[\frac{\mathrm{d}Q}{\mathrm{d}Q_0}\left(Q_0^{\leftarrow}\left(\frac{\Gamma_i}{T}\right)\right) \geq W_i \middle| \Gamma_i\right]\right] \\
&= E\left[\frac{\mathrm{d}Q}{\mathrm{d}Q_0}\left(Q_0^{\leftarrow}\left(\frac{\Gamma_i}{T}\right)\right)\right] \\
&= \int_0^{\infty} \frac{\mathrm{d}Q}{\mathrm{d}Q_0}\left(Q_0^{\leftarrow}\left(\frac{x}{T}\right)\right) \gamma_i(x)\mathrm{d}x,
\end{aligned}
$$

where $\gamma_i(x)$ is the density function of the $\Gamma(i,1)$ distribution, $Q_0^{\leftarrow}(y) = \frac{2\nu}{\pi y^2}$ and $\frac{\mathrm{d}Q}{\mathrm{d}Q_0}(u) = \rho(u)/\sqrt{\frac{\nu}{2\pi u^3}}$, ρ being given in (2.3). Figure 2.4 plots the acceptance probability $\frac{\mathrm{d}Q}{\mathrm{d}Q_0}(x)$ for various ν. Note that $x = Q_0^{\leftarrow}(\Gamma_i/T)$ decreases to zero for increasing i. This means that it is crucial to know how fast $\frac{\mathrm{d}Q}{\mathrm{d}Q_0}(x)$ converges to 1 for $x \searrow 0$. The rejection method works better for small ν than for large ν.

Note that for both the inverse Lévy measure method and the rejection method it is not possible to compute the mean squared error directly. Since the upper bounds coincide, it is natural to ask whether or not the mean squared errors are equal. Imai & Kawai (2013) provided an answer:

Proposition 2.2. *Consider the setting of Corollary 2.2 and let $Y_0(t)$ be a subordinator with Lévy measure Q_0 such that $\frac{\mathrm{d}Q}{\mathrm{d}Q_0}(Q_0^{\leftarrow}(\Gamma_i/T)) \leq 1$. Define the approximating series representations*

$$X_t^{\tau,1} := \sum_{\{i\in\mathbb{N}:\Gamma_i\leq\tau\}} \sqrt{Q^{\leftarrow}\left(\frac{\Gamma_i}{T}\right)} V_i \mathbb{1}_{\{U_i\leq t\}},$$

$$X_t^{\tau,2} := \sum_{\{i\in\mathbb{N}:\Gamma_i\leq\tau\}} \sqrt{Q_0^{\leftarrow}\left(\frac{\Gamma_i}{T}\right)} V_i \mathbb{1}\left(\left\{\frac{\mathrm{d}Q}{\mathrm{d}Q_0}\left(Q_0^{\leftarrow}\left(\frac{\Gamma_i}{T}\right)\right) \geq W_i\right\}\right) \mathbb{1}_{\{U_i\leq t\}},$$

for $t \in [0,T]$. Then

$$E[(X_t - X_t^{\tau,1})^2] < E[(X_t - X_t^{\tau,2})^2].$$

Imai & Kawai (2013) proved a more general version of Theorem 2.2. They also show that the inverse Lévy measure method is better at simulating the tails of the Lévy measure than the rejection method (and further methods), which instead performs better near the origin.

Since both methods have reasonably small approximation errors for sufficiently large τ, we evaluate their numerical advantages and disadvantages in Section 2.5.2.

Remark 2.3 (Thinning method)**.** Although we discussed that the thinning method is theoretically valid (see Proposition 2.1), it is not useful to simulate Lévy processes in general. While the technique may be fine for just one infinitely divisible random variable, we now argue why it cannot easily simulate a (quasi-)time-continuous process.

Consider any subordinator with Lévy measure Q and any distribution function F on $(0,\infty)$ such that Q is absolutely continuous with respect to F. Recall that the thinning series representation is given by

$$\sum_{i=1}^{\infty} V_i \mathbb{1}\left(\left\{\frac{\mathrm{d}Q}{\mathrm{d}F}(V_i) \geq \frac{\Gamma_i}{T}\right\}\right) \mathbb{1}_{\{U_i\leq t\}}, \quad t \in [0,T],$$

where $V_i \sim F$ i.i.d. We are interested in the number of accepted V_is in the representation, i.e., in the probability

$$\begin{aligned} P\left[\frac{\mathrm{d}Q}{\mathrm{d}F}(V_i) \geq \frac{\Gamma_i}{T}\right] &= E\left[P\left[\frac{\mathrm{d}Q}{\mathrm{d}F}(V_i) \geq \frac{\Gamma_i}{T}\middle| V_i\right]\right] \\ &= E\left[G_i\left(T\frac{\mathrm{d}Q}{\mathrm{d}F}(V_i)\right)\right], \end{aligned} \tag{2.15}$$

where G_i denotes the cumulative distribution function of the $\Gamma(i,1)$ distribution. Since $G_i(x) = \frac{\gamma(i,x)}{\Gamma(i)}$, with $\gamma(i,x) = \int_0^x t^{i-1}e^{-t}\mathrm{d}t$, is a strictly decreasing function in $i \in \mathbb{N}$, it follows that $G_i(x)$ converges to zero for increasing i. Hence the probability (2.15) converges to zero (recall that the acceptance probability for the inverse gamma subordinator converges to one using the rejection method).

This is not a problem from a theoretical point of view. However, for computational purposes a shrinking acceptance probability means that for a pure jump Lévy process with infinitely many jumps we have to draw many simulations to obtain enough accepted jumps. Even for the gamma subordinator (see, e.g., Rosiński 2001) our simulations suggest a very low acceptance rate.

2.3.3 Gaussian approximation

Instead of just discarding the small jumps, we now show that there is an appropriate refinement in the case of the one-dimensional Student-Lévy process and the inverse gamma subordinator. Asmussen & Rosiński (2001) (and, for multivariate series representations, Cohen & Rosiński (2007)) proposed a Gaussian approximation of the small jumps, which are truncated in the series representation. To this end, decompose a Lévy process $\{X_t\}$ with characteristics (γ, A, Π) into two Lévy processes

$$X(t) = X^{\varepsilon}(t) + X_{\varepsilon}(t),$$

where $X^{\varepsilon}(t) = \sum_{\{i\in\mathbb{N}:H(\Gamma_i/T,V_i)>\varepsilon\}} H\left(\frac{\Gamma_i}{T}, V_i\right)\mathbb{1}_{\{U_i\leq t\}}$, with $\varepsilon > 0$, is a truncated series representation with Lévy measure denoted by Π^{ε}. $X_{\varepsilon}(t)$ is the corresponding remainder with Lévy measure $\Pi_{\varepsilon} = \Pi - \Pi^{\varepsilon}$. Under some conditions (see (2.16)) on the error variance

$$\sigma_{\varepsilon}^2 = \int_{\mathbb{R}} x^2 \Pi_{\varepsilon}(\mathrm{d}x),$$

we can replace $X_{\varepsilon}(t)$ by an approximation

$$\mu_{\varepsilon} t + \sigma_{\varepsilon} W_t,$$

with $\mu_{\varepsilon} = \int_{\mathbb{R}} x\Pi_{\varepsilon}(\mathrm{d}x)$, and where W_t is a Brownian motion.

The next two propositions show that the Gaussian approximation is valid for the inverse Gamma subordinator and the Student-Lévy process. This approximation can be used to improve the goodness of fit of the simulated paths; see Section 2.5.3. For brevity we only discuss the inverse Lévy measure case here. Eberlein & v. Hammerstein (2004) provided a proof for the GH and GIG processes. The Gaussian approximation for Student-Lévy process and the inverse gamma subordinator can then be proven by a limiting argument. We here prove it directly.

Proposition 2.3. *Consider the error of the truncated series representation*

$$Y_\varepsilon(t) = \sum_{\{i\in\mathbb{N}:Q^{\leftarrow}(\Gamma_i/T)<\varepsilon\}} Q^{\leftarrow}\left(\frac{\Gamma_i}{T}\right)\mathbb{1}_{\{U_i\leq t\}},$$

for the inverse gamma subordinator. Then

$$\sigma_\varepsilon^{-1}(Y_\varepsilon(t)-\mu_\varepsilon t) \xrightarrow{\mathcal{L}} W_t, \quad \text{in } \mathcal{D}[0,T]$$

for $\varepsilon\to 0$, with $\mu_\varepsilon = \int_0^\varepsilon uQ(\mathrm{d}u)$ and $\sigma_\varepsilon^2 = \int_0^\varepsilon u^2Q(\mathrm{d}u)$, where Q defined in (2.3) denotes the Lévy measure of the inverse gamma subordinator and W_t is a Brownian motion.

Proof. Asmussen & Rosiński (2001) showed that the distributional convergence is implied by

$$\lim_{\varepsilon\to 0}\frac{\sigma_\varepsilon}{\varepsilon} = +\infty. \tag{2.16}$$

We show that $\lim_{\varepsilon\to 0}\frac{\sigma_\varepsilon^2}{\varepsilon^2} = +\infty$. Recall that

$$\lim_{\varepsilon\to 0}\frac{\sigma_\varepsilon^2}{\varepsilon^2} = \lim_{\varepsilon\to 0}\frac{\int_0^\varepsilon u^2\int_0^\infty u^{-1}e^{-su}\nu g_{\frac{\nu}{2}}(2\nu s)\mathrm{d}s\mathrm{d}u}{\varepsilon^2}. \tag{2.17}$$

Using l'Hôspital's rule, (2.17) is equal to

$$\lim_{\varepsilon\to 0}\frac{\varepsilon^2\int_0^\infty \varepsilon^{-1}e^{-s\varepsilon}\nu g_{\frac{\nu}{2}}(2\nu s)\mathrm{d}s}{2\varepsilon} = \lim_{\varepsilon\to 0}\frac{1}{2}\int_0^\infty e^{-s\varepsilon}g_{\frac{\nu}{2}}(2\nu s)\mathrm{d}s.$$

The monotone convergence theorem can be applied to (2.17) and thus

$$\frac{1}{2}\int_0^\infty \lim_{\varepsilon\to 0} e^{-s\varepsilon}\nu g_{\frac{\nu}{2}}(2\nu s)\mathrm{d}s = \frac{1}{2}\int_0^\infty \nu g_{\frac{\nu}{2}}(2\nu s)\mathrm{d}s = \infty.$$

□

Proposition 2.4. *Consider the error of the truncated series representation*

$$X_\varepsilon(t) = \sum_{\{i\in\mathbb{N}:Q^{\leftarrow}(\Gamma_i/T)<\varepsilon\}} Q^{\leftarrow}\left(\frac{\Gamma_i}{T}\right)V_i\mathbb{1}_{\{U_i\leq t\}},$$

for the Student-Lévy process. Then

$$\sigma_\varepsilon^{-1}X_\varepsilon(t) \xrightarrow{\mathcal{L}} W(t), \quad \text{in } \mathcal{D}[0,T]$$

for $\varepsilon \to 0$, with $\sigma_\varepsilon^2 = \int_{-\varepsilon}^{\varepsilon} x^2 \Pi(\mathrm{d}x)$, where Π denotes the Lévy measure of the Student-Lévy process (see Theorem 1.5) and W_t is a Brownian motion.

Proof. Note that in the non-finite variation case μ_ε has to be zero (Sato 1999). Recall the Lévy measure for the univariate Student-Lévy process (with no drift and standard scaling) is given by

$$\Pi(\mathrm{d}x) = \frac{\nu 2^{\frac{3}{4}} |x|^{-\frac{1}{2}}}{\pi^{\frac{1}{2}}} \int_0^\infty s^{\frac{1}{4}} K_{\frac{1}{2}} \left(\sqrt{2s}|x| \right) g_{\frac{\nu}{2}}(2\nu s) \mathrm{d}s \mathrm{d}x.$$

In the following we use the identity

$$K_{\frac{1}{2}}(z) = \sqrt{\frac{\pi}{2}} e^{-z} z^{-\frac{1}{2}}$$

for $z > 0$. As Π is a symmetric measure,

$$\sigma_\varepsilon^2 = \int_{-\varepsilon}^{\varepsilon} x^2 \Pi(\mathrm{d}x) = 2 \int_0^{\varepsilon} x^2 \Pi(\mathrm{d}x).$$

Again using l'Hôspital's rule, for some constant $C > 0$ that may change from line to line

$$\begin{aligned}
\lim_{\varepsilon \to 0} \frac{\sigma_\varepsilon^2}{\varepsilon^2} &= \lim_{\varepsilon \to 0} \frac{C \int_0^\varepsilon x^2 |x|^{-\frac{1}{2}} \int_0^\infty s^{\frac{1}{4}} K_{\frac{1}{2}} \left(\sqrt{2s}|x| \right) g_{\frac{\nu}{2}}(2\nu s) \mathrm{d}s \mathrm{d}x}{\varepsilon^2} \\
&= \lim_{\varepsilon \to 0} C \frac{\varepsilon^2 \varepsilon^{-\frac{1}{2}} \int_0^\infty s^{\frac{1}{4}} e^{-\sqrt{2s}\varepsilon} \left(\sqrt{2s} \right)^{-\frac{1}{2}} \varepsilon^{-\frac{1}{2}} g_{\frac{\nu}{2}}(2\nu s) \mathrm{d}s}{\varepsilon} \\
&= \lim_{\varepsilon \to 0} C \int_0^\infty e^{-\sqrt{2s}\varepsilon} g_{\frac{\nu}{2}}(2\nu s) \mathrm{d}s \\
&= C \int_0^\infty g_{\frac{\nu}{2}}(2\nu s) \mathrm{d}s \\
&= \infty.
\end{aligned}$$

The second-to-last last step uses the monotone convergence theorem. □

2.4 Numerical methods

This section presents numerical methods for generating Lévy processes using series representations, with a focus on the inverse Lévy measure method. Unfortunately, there exists no closed form inverse, due to the complicated form of the Lévy measure

(2.3) for the inverse gamma subordinator. Furthermore, since finding its tail measure requires double integration, numerical root finding is very slow and, for a large number of jumps, highly inefficient. Thus, we need a numerical procedure which approximates roots in reasonable time.

Derflinger et al. (2010) proposed an inversion method for random variate generation if only the density is known. Imai & Kawai (2013) applied these ideas to the inversion of the Lévy tail measure. They – as we do here – considered a compact interval $[x_{\min}, x_{\max}] \subset (0, \infty)$ on which the inversion is performed. If we set $q_{\min} := Q([x_{\min}, \infty))$ and $q_{\max} := Q([x_{\max}, \infty))$, we can define a probability distribution function $F(x) := \frac{q_{\min} - Q([x,\infty))}{q_{\min} - q_{\max}} \mathbb{1}_{[x_{\min}, x_{\max}]}(x) + \mathbb{1}_{(x_{\max}, \infty)}(x)$ and accordingly its density function $f(x) := \frac{\rho(x)}{q_{\min} - q_{\max}} \mathbb{1}_{[x_{\min}, x_{\max}]}(x)$ and then apply the algorithms of Derflinger et al. (2010).

Imai & Kawai (2013) point out that the algorithms behave nicely in many applications, but that it can be problematic for explosive behavior near the origin, as it is the case for tail measures of α-stable processes. In fact (by Corollary 2.4) the inverse Gamma subordinator's explosive tail measure is close to an α-stable subordinator and their algorithm does not terminate, meaning that the desired accuracy is never achieved. Thus, the algorithm gets stuck in an infinite loop. Here we do not transform to a probability function and consider the Lévy tail measure directly. This implies some changes to their approach, which we discuss now.

The following algorithms work well with inverse gamma subordinators, for which we explain the algorithms. Inverse gamma subordinators can be replaced with other subordinators having a strictly decreasing Lévy tail measure.

Consider a compact interval $[x_{\min}, x_{\max}] \subset (0, \infty)$ with a sufficiently small $x_{\min}$. The idea is not to find the root by root finding algorithms, but first to find appropriate points $\{x_i\}$ in the support and the corresponding $Q_i = Q([x_i, \infty))$ using numerical integration. Then, second, we perform an interpolation between $\{Q_i, x_i\}$. If we then evaluate the interpolated function at a value y, we want the result to be as close as possible to the true value $Q^{\leftarrow}(y)$.

We split (as in the original proposal by Derflinger et al. (2010)) the algorithm into an initialization where a proper set $\{x_i, Q_i\}$ is found and the numerical inversion routine, which is applied to y to estimate $Q^{\leftarrow}(y)$. The key advantage is that, while generating the setup may take some time, the actual inversion is very fast. We present Algorithm 1 for the setup in pseudo code and discuss it in detail.

We fix a number $\varepsilon_{\text{tol}} > 0$ as a tolerance level for the maximal relative error. We start a loop by setting the current subinterval $[x_{\text{L}}, x_{\text{R}}]$ of length Δ. This subinterval is again partitioned into six further subintervals $[x_{\text{int}}[j-1], x_{\text{int}}[j]]$ for $j = 1, \ldots, 6$. Next, we compute the corresponding tail measures in line 21 using the adaptive

Algorithm 1 Numerical Inversion Setup

Input: $Q([x,\infty))$; ▷Tail measure.
$\rho(x)$; ▷Lévy density.
$[x_{\min}, x_{\max}] \subset (0,\infty)$; ▷Compact domain on which the inverse is computed.
$\varepsilon_{\text{tol}} > 0$; ▷Maximal tolerated relative error.
Output: $\{x[i]\}_{i\in\mathbb{N}_0}$;
$\{Q[i]\}_{i\in\mathbb{N}_0}$;

$\Delta \leftarrow (x_{\max} - x_{\min})/32$; ▷Initial step size.
$x[0] \leftarrow x_{\min}$; $Q[0] \leftarrow Q([x_{\min},\infty))$;
$i \leftarrow 0$; ▷Index of subintervals.
while $x[i] < x_{\max}$ **do** ▷Loop for all subintervals.
  $x_{\text{L}} \leftarrow x[i]$; ▷Set left boundary for current subinterval $[x_{\text{L}}, x_{\text{R}}]$.
  repeat ▷Repeat refinement until error is small enough.
    if $x_{\text{L}} + \Delta < x_{\max}$ **then** ▷Set right boundary of current subinterval.
      $x_{\text{R}} \leftarrow x_{\text{L}} + \Delta$;
    else
      $x_{\text{R}} \leftarrow x_{\max}$;
    end if
    $x_{\text{int}}[0] \leftarrow x_{\text{L}}$; ▷Set seven interpolation points in $[x_{\text{L}}, x_{\text{R}}]$.
    $x_{\text{int}}[1] \leftarrow \frac{x_{\text{L}}+x_{\text{R}}}{2} - \sqrt{\frac{2}{3}}\frac{x_{\text{R}}-x_{\text{L}}}{2}$;
    $x_{\text{int}}[2] \leftarrow \frac{x_{\text{L}}+x_{\text{R}}}{2} - \sqrt{\frac{1}{5}}\frac{x_{\text{R}}-x_{\text{L}}}{2}$;
    $x_{\text{int}}[3] \leftarrow \frac{x_{\text{L}}+x_{\text{R}}}{2}$;
    $x_{\text{int}}[4] \leftarrow \frac{x_{\text{L}}+x_{\text{R}}}{2} + \sqrt{\frac{1}{5}}\frac{x_{\text{R}}-x_{\text{L}}}{2}$;
    $x_{\text{int}}[5] \leftarrow \frac{x_{\text{L}}+x_{\text{R}}}{2} + \sqrt{\frac{2}{3}}\frac{x_{\text{R}}-x_{\text{L}}}{2}$;
    $x_{\text{int}}[6] \leftarrow x_{\text{R}}$;
    $Q_{\text{int}}[0] \leftarrow Q[i]$; ▷Compute the corresponding seven $Q([x[i],\infty))$.
    for $j = 1$ **to** 6 **do**
      $Q_{\text{int}}[j] \leftarrow \texttt{GaussQuadrature}(\rho(x); x_{\text{int}}[j], \infty)$;
        ▷Global adaptive Gauss-Kronrod rule for Lévy density $\rho(x)$.
    end for
    $\varepsilon_{\max} \leftarrow 0$; ▷Maximal relative error.
    decr $\leftarrow$ **true**; ▷Boolean variable for monotonic decrease.
    for $j = 0$ **to** 5 **do**
      $x_{\text{mid}} \leftarrow \frac{x_{\text{int}}[j]+x_{\text{int}}[j+1]}{2}$;
        ▷Set midpoint of consecutive interpolation points.
      $Q_{\text{mid}} \leftarrow \texttt{GaussQuadrature}(\rho(x); x_{\text{mid}}, \infty)$;
        ▷Compute the corresponding Q midpoints.
      $x_{\text{inv}} \leftarrow \texttt{NewtonInterpolation}(\{Q_{\text{int}}\}, \{x_{\text{int}}\}; Q_{\text{mid}})$;
        ▷Newton Interpolation $\{(Q_{\text{int}}[j], x_{\text{int}}[j])\}_{j=0,\dots,6}$. Find x_{inv} for Q_{mid}.
      $\varepsilon \leftarrow \left|\frac{x_{\text{inv}}-x_{\text{mid}}}{x_{\text{mid}}}\right|$;
        ▷Relative error between interpolated value and true midpoint.

Algorithm 1 Numerical Inversion Setup – ctd.

30: $\varepsilon_{\max} \leftarrow \texttt{Max}(\varepsilon, \varepsilon_{\max})$; ▷Reset maximal error
31: **if** $x_{\text{inv}} < x_{\text{int}}[j]$ **or** $x_{\text{inv}} > x_{\text{int}}[j+1]$ **then**
32: decr $\leftarrow$ **false**;
33: **end if** ▷Check if monotonicity fails.
34: **if** $\varepsilon_{\max} > \varepsilon_{\text{tol}}$ **or** decr = **false then**
35: $\Delta \leftarrow \Delta/2$ **and**
36: **exit for**
▷If error is too large: refine step size, exit for loop, go back to line 7.
37: **end if**
38: **end for**
39: **until** $\varepsilon_{\max} < \varepsilon_{\text{tol}}$ **and** decr = **true**
40: **for** $k = 1$ **to** 6 **do** ▷If error is small enough save current subinterval.
41: $x[i+k] \leftarrow x_{\text{int}}[k]$;
42: $Q[i+k] \leftarrow Q_{\text{int}}[k]$;
43: **end for**
44: $\Delta \leftarrow 2\Delta$; ▷Resize step size.
45: $i \leftarrow i + 6$; ▷Proceed to next subinterval, go back to line 5.
46: **end while**
47: $i_{\max} \leftarrow i$;
48: **return** $\{x[i]\}_{i=0,\dots i_{\max}}$ and $\{Q[i]\}_{i=0,\dots i_{\max}}$.

Gauss-Kronrod rule (cf. Piessens & Branders (1974)). A simple but useful trick for the gamma subordinator's tail measure is not to perform two one-dimensional numerical integrations but rather use an adaptive quadrature rule for two-dimensional integration over the domain $[x, \infty) \times (0, \infty)$.

Let $\varepsilon_{\max}$ denote the maximal relative error which is obtained for this refinement of the current subinterval. We will reject the subinterval and try another refinement in case $\varepsilon_{\max}$ exceeds the tolerated error. The for-loop beginning in line 26 has the following goal: compute the midpoint x_{mid} for the subinterval $[x_{\text{int}}[j-1], x_{\text{int}}[j]]$ and the corresponding $Q([x_{\text{mid}}, \infty))$. Next, perform a Newton interpolation with the set $\{Q_{\text{int}}[j], x_{\text{int}}[j]\}$ and evaluate the interpolated function at $Q([x_{\text{mid}}, \infty))$ to find the approximate inverse (say, x_{inv}). Now, compute the relative error between this approximation and the true inverse x_{mid}. If the maximum of the relative errors for each subinterval $[x_{\text{int}}[j-1], x_{\text{int}}[j]]$ is greater than the tolerance level, halve Δ and go back to the beginning of the repeat loop (line 7) to work with a smaller subinterval.

Line 34 gives another important condition. Since the tail measure of an inverse gamma process is strictly decreasing, so is its inverse. We check whether the interpolated function (which shall approximate the inverse) is decreasing. In case this fails

we, again, halve Δ and go back to line 7.

We thus eventually find a small subinterval which fulfills the properties that all six relative errors between the approximation and the true midpoint are small enough. Then, we store the current points $\{x_{\text{int}}[j], Q_{\text{int}}[j]\}$ in the table and proceed to the next subinterval. We compute relative errors rather than absolute errors because for large values of $x = Q^{\leftarrow}(y)$ absolute errors would be unnecessarily restrictive while for very small values of x, which represent the many small jumps in the series, they would be not sufficiently precise.

In the end, we obtain a table with points which are used to execute the numerical inversion in Algorithm 2.

Algorithm 2 Numerical Inversion

Input: $\{x[i]\}_{i=0,\dots i_{\max}}$; ▷Coordinates generated in Algorithm 1.
$\{Q[i]\}_{i=0,\dots i_{\max}}$;
Output: $u = Q^{\leftarrow}(y)$; ▷Inverted value in $[x_{\min}, x_{\max}]$.

1: Find minimal index k such that $Q[k] \leq y$ through BinarySearch;
2: **if** $k < 3$ **then**
3: $k \leftarrow 3$
4: **end if**
5: **if** $k > i_{\max} - 3$ **then**
6: $k \leftarrow i_{\max} - 3$
7: **end if**
8: $u \leftarrow$ NewtonInterpolation$(\{Q[k-3], \dots, Q[k+3]\}, \{x[k-3], \dots, x[k+3]\}; y)$;
▷ Compute the Newton interpolation as approximation for the inverse.
9: **if** $u < x[k-3]$ **or** $u > x[k+3]$ **then**
▷ In case decreasingness fails, use linear interpolation instead.
10: $u \leftarrow$ `LinearInterpolation`$(\{Q[k-1], Q[k]\}, \{x[k-1], x[k]\}; y)$;
11: **if** $u < x[k-1]$ **or** $u > x[k]$ **then** ▷ If monotonicity still fails, exit.
12: print ERROR and **exit**;
13: **else**
14: **return** u;
15: **end if**
16: **else**
17: **return** u;
18: **end if**

The numerical inversion in Algorithm 2 is, using the table $\{x[i], Q[i]\}$ of Algorithm 1, easy and efficient. If y is given, we compute $Q^{\leftarrow}(y)$ by finding the minimal index k such that $Q[k] \leq y$, using an iterative binary search algorithm which is faster for ordered points than an ordinary sequential search (Hörmann et al. 2004). Next, we

use the Newton Interpolation for the seven points $\{Q[j], x[j]\}$ for $j = k-3, \ldots, k+3$ to find the inverse $Q^{\leftarrow}(y)$. As discussed in Derflinger et al. (2010) and Imai & Kawai (2013), it is advisable to have an alternative if the Newton polynomial is not strictly decreasing. Although we did not observe such behavior for the inverse gamma subordinator's simulation, we still recommend employing linear interpolation in case this apparently rare event occurs.

The path generation with the rejection method is easy to implement but more time-consuming due to the numerical integration required for the rejection probability. We discuss the computing times of the algorithms in Section 2.5.2.

2.5 Monte Carlo study

We now test the algorithms of Section 2.4. Although simulation of d-dimensional Student-Lévy paths is possible we for simplicity consider one-dimensional paths. We discuss three cases: a small degree of freedom $\nu = 4$, an intermediate $\nu = 12$ and a higher degree of freedom $\nu = 39$ whose Student t density comes close to the Gaussian density. We consider, unless stated otherwise, a fixed time domain $[0, T]$ with $T = 100$. In the case of the inverse Lévy measure method, Algorithm 1 requires a compact interval $Q^{\leftarrow}(y) \in [x_{\min}, x_{\max}]$. For each ν we choose $x_{\min} = 10^{-9}$, but the upper bound can differ because for higher ν there are rarely big jumps in the inverse gamma subordinator. Here, let $x_{\max} = 10^4$ for $\nu = 4$, $x_{\max} = 10^2$ for $\nu = 12$ and $x_{\max} = 10$ for $\nu = 39$. Of course it is possible to choose higher $x_{\max}$. However, higher jumps than the chosen $x_{\max}$ are very unlikely and hence not considered to reduce computational time. We set $\varepsilon_{\text{tol}} = 10^{-6}$. The error determines the execution time of the setup and should be selected with care. For instance, for higher ν and a lower tolerated error it can take much longer to run Algorithm 1 than discussed below. We feel that our particular choice is sufficient even if it implies that for big jumps the absolute error increases. To justify our choice we test the setup points by computing absolute and relative errors

$$\varepsilon_{\text{a}}(x) := |x - Q_*^{\leftarrow}(Q([x, \infty)))|$$

and

$$\varepsilon_{\text{r}}(x) := \frac{|x - Q_*^{\leftarrow}(Q([x, \infty)))|}{x},$$

where $Q_*^{\leftarrow}$ is the approximate inverse from Algorithm 2 of the Lévy tail measure $Q([x, \infty))$ of the inverse gamma subordinator. Its Lévy measure is given in (2.3) and is numerically computed with the Gauss-Kronrod rule. For any subinterval $(10^r, 10^{r+1}]$ for $r \in \{-9, -8, \ldots, \log_{10}(x_{\max})\}$ we take equidistant test points $x_{rk} = \frac{k}{1000} 10^{r+1}$, for $k = 1, \ldots, 1000$. (Exclude the last point $x_{\max}$.) Imai & Kawai (2013) instead

(a): Relative errors $\varepsilon_{\mathrm{r}}(x)$

$/\nu$	4	12	39
Min	$4.9 \cdot 10^{-14}$	$4.06 \cdot 10^{-15}$	≈ 0
25%	$4.62 \cdot 10^{-9}$	$4.31 \cdot 10^{-9}$	$4.04 \cdot 10^{-9}$
Median	$1.89 \cdot 10^{-8}$	$1.79 \cdot 10^{-8}$	$1.91 \cdot 10^{-8}$
Mean	$7.94 \cdot 10^{-8}$	$1.18 \cdot 10^{-7}$	$9.19 \cdot 10^{-8}$
75%	$6.81 \cdot 10^{-8}$	$7.01 \cdot 10^{-8}$	$6.97 \cdot 10^{-8}$
Max	$1.63 \cdot 10^{-4}$	$7.9 \cdot 10^{-4}$	$1.63 \cdot 10^{-4}$
$P[\varepsilon_{\mathrm{r}}(x) < 10^{-6}]$	0.9963	0.9905	0.9933

(b): Absolute errors $\varepsilon_{\mathrm{a}}(x)$

Min	$3.75 \cdot 10^{-21}$	$1.94 \cdot 10^{-21}$	≈ 0
25%	$4.45 \cdot 10^{-14}$	$1.86 \cdot 10^{-14}$	$5.16 \cdot 10^{-15}$
Median	$9.09 \cdot 10^{-11}$	$6.91 \cdot 10^{-12}$	$8.52 \cdot 10^{-13}$
Mean	$2.81 \cdot 10^{-5}$	$2.15 \cdot 10^{-7}$	$2 \cdot 10^{-9}$
75%	$1.24 \cdot 10^{-7}$	$3.75 \cdot 10^{-9}$	$8.63 \cdot 10^{-11}$
Max	0.22	$3.72 \cdot 10^{-4}$	$9.14 \cdot 10^{-7}$

Table 2.1: Panel (a) displays the quartiles and the mean of the relative errors. The last line in panel (a) is the relative frequency of errors smaller than 10^{-6}. Panel (b) for the absolute errors. The statistics on the errors are computed for the $1000 \cdot (10 + \log_{10}(x_{\max}))$ number of test points x_{rk}.

controlled the error $\varepsilon(y) = |y - Q([Q^{\leftarrow}(y), \infty))|$ in their approach. However, we think that errors based on the x-axis are preferable, because we are interested in the distance between the approximate inversion and the true inversion.

Table 2.1 presents some statistics on the numerical errors. For both types we compute the sample mean and the five quartiles of $\varepsilon_{\mathrm{a}}(x_{rk})$ and $\varepsilon_{\mathrm{r}}(x_{rk})$. Furthermore, in rare cases the observed empirical errors exceed the maximal tolerated error $\varepsilon_{\mathrm{tol}} = 10^{-6}$. Since this happens in less than 1% of all test points, we do not consider this to be an issue. The relative errors are very similar for the three different degrees of freedom which suggests that our method is robust. On the other hand, the absolute error is smaller for higher degrees of freedom, since the inverse Lévy measure is not that extreme around the origin.

2.5.1 Mean squared error simulation

In this subsection we illustrate by simulation the theoretical mean squared error bounds for the inverse gamma subordinator and the Student-Lévy process derived in Section 2.3.1. In order to compare with simulated MSE bounds we first compute the theoretical counterparts. The theoretical MSE is defined as expected quadratic deviation between the series representation and the truncated series, $E((X_t - X_t^\tau)^2)$. The empirical counterpart is given by $\frac{1}{B}\sum_{b=1}^{B}(X_{t,b}-X_{t,b}^\tau)^2$ for $b = 1, \dots, B$ replications. Tables 2.2 and 2.3 show the theoretical upper bounds for the MSE computed with the formulas (2.7) and (2.14), respectively, for various ν and T with $t = T$ and different levels of truncation τ. It is obvious that we need a higher level of truncation for a larger domain $[0, T]$ since a larger domain requires more jumps. In the case of the inverse gamma subordinator Table 2.2 shows that a ten times larger interval approximately requires a hundred times larger truncation level, (compare one entry with one to the right, two down). This is because the error in (2.7) (for deterministic truncation) is of order T^4 (at the end point) and $1/n^2$ (or $1/\tau^2$ for random truncation, respectively). The same is true for the Student-Lévy process where (2.14) (or easier to see for the deterministic determination in (2.12)) is of order T^2 and $1/\tau$. The relationship between the degree of freedom and the level of truncation is linear for both processes, since (2.7) is of order ν^2 and (2.12) is of order ν. In summary, it is important to choose the truncation level high enough because the error bounds can be very large for large T.

Now, we discuss how to replicate the mean squared error bounds of Theorem 2.2 and Theorem 2.3 (Corollary 2.3) empirically. Consider the truncated jumps over $\{i \in \mathbb{N} : \Gamma_i > \tau\}$. Recall that the errors are given by

$$Y_t - Y_t^\tau = \sum_{\{i\in\mathbb{N}:\Gamma_i>\tau\}} Q^{\leftarrow}\left(\frac{\Gamma_i}{T}\right)\mathbb{1}_{\{U_i\le t\}}$$

and

$$X_t - X_t^\tau = \sum_{\{i\in\mathbb{N}:\Gamma_i>\tau\}} \sqrt{Q^{\leftarrow}\left(\frac{\Gamma_i}{T}\right)V_i}\mathbb{1}_{\{U_i\le t\}}.$$

Since we do not know $Q^{\leftarrow}$ explicitly, we have to compute it numerically with the algorithms of Section 2.4. Recall that the inversion is only available on the compact interval $[x_{\min}, x_{\max}]$, which means that we truncate all $Q^{\leftarrow}\left(\frac{\Gamma_i}{T}\right)$ which are smaller than the left boundary $x_{\min}$. For all $i \in \mathbb{N}$ such that $\Gamma_i > \tau$ we replace $Q^{\leftarrow}(y)$ by its

(a): $\nu = 4$

τ / T	0.1	1	10	100
10	$1.53 \cdot 10^{-5}$	0.153	$1.53 \cdot 10^{4}$	$1.53 \cdot 10^{7}$
100	$6.96 \cdot 10^{-8}$	$6.96 \cdot 10^{-4}$	6.96	$6.96 \cdot 10^{4}$
1000	$6.53 \cdot 10^{-10}$	$6.53 \cdot 10^{-6}$	$6.53 \cdot 10^{-2}$	$6.53 \cdot 10^{2}$
10000	$6.49 \cdot 10^{-12}$	$6.49 \cdot 10^{-8}$	$6.49 \cdot 10^{-4}$	6.49
100000	$6.49 \cdot 10^{-14}$	$6.49 \cdot 10^{-10}$	$6.49 \cdot 10^{-6}$	$6.49 \cdot 10^{-2}$
1000000	$6.48 \cdot 10^{-16}$	$6.48 \cdot 10^{-12}$	$6.48 \cdot 10^{-8}$	$6.48 \cdot 10^{-4}$

(b): $\nu = 12$

10	$1.38 \cdot 10^{-4}$	1.38	$1.38 \cdot 10^{4}$	$1.38 \cdot 10^{8}$
100	$6.27 \cdot 10^{-7}$	$6.27 \cdot 10^{-3}$	62.67	$6.27 \cdot 10^{5}$
1000	$5.88 \cdot 10^{-9}$	$5.88 \cdot 10^{-5}$	0.588	$5.88 \cdot 10^{3}$
10000	$5.84 \cdot 10^{-11}$	$5.84 \cdot 10^{-7}$	$5.84 \cdot 10^{-3}$	58.4
100000	$5.84 \cdot 10^{-13}$	$5.84 \cdot 10^{-9}$	$5.84 \cdot 10^{-5}$	0.584
1000000	$5.84 \cdot 10^{-15}$	$5.84 \cdot 10^{-11}$	$5.84 \cdot 10^{-7}$	$5.84 \cdot 10^{-3}$

(c): $\nu = 39$

10	$1.46 \cdot 10^{-3}$	14.6	$1.46 \cdot 10^{5}$	$1.46 \cdot 10^{9}$
100	$6.62 \cdot 10^{-6}$	$6.62 \cdot 10^{-2}$	$6.62 \cdot 10^{2}$	$6.62 \cdot 10^{6}$
1000	$6.21 \cdot 10^{-8}$	$6.21 \cdot 10^{-4}$	6.21	$6.21 \cdot 10^{4}$
10000	$6.17 \cdot 10^{-10}$	$6.17 \cdot 10^{-6}$	$6.17 \cdot 10^{-2}$	$6.17 \cdot 10^{2}$
100000	$6.16 \cdot 10^{-12}$	$6.16 \cdot 10^{-8}$	$6.16 \cdot 10^{-4}$	6.16
1000000	$6.16 \cdot 10^{-14}$	$6.16 \cdot 10^{-10}$	$6.16 \cdot 10^{-6}$	$6.16 \cdot 10^{-2}$

Table 2.2: Theoretical MSE bounds for the inverse gamma subordinator's series representation for different degree of freedom ν, time horizon T and level of truncation τ. The formula (2.7) for the deterministic truncation here gives very similar numbers as for the random truncation.

upper bound $q(y) = \frac{2\nu}{\pi y^2}$. We then simulate the mean squared error with

$$\sum_{i=N_\tau}^{\infty} \sqrt{q\left(\frac{\Gamma_i}{T}\right)} V_i \mathbb{1}_{\{U_i \leq t\}}$$

(or alternatively the version for the inverse gamma subordinator), by choosing an

(a): $\nu = 4$

τ / T	0.1	1	10	100
10	$2.83 \cdot 10^{-3}$	0.283	28.3	$2.82 \cdot 10^{3}$
100	$2.57 \cdot 10^{-4}$	$2.57 \cdot 10^{-2}$	2.57	$2.57 \cdot 10^{2}$
1000	$2.55 \cdot 10^{-5}$	$2.55 \cdot 10^{-3}$	0.255	25.5
10000	$2.55 \cdot 10^{-6}$	$2.55 \cdot 10^{-4}$	$2.55 \cdot 10^{-2}$	2.55
100000	$2.55 \cdot 10^{-7}$	$2.55 \cdot 10^{-5}$	$2.55 \cdot 10^{-3}$	0.255
1000000	$2.55 \cdot 10^{-8}$	$2.55 \cdot 10^{-6}$	$2.55 \cdot 10^{-4}$	$2.55 \cdot 10^{-2}$

(b): $\nu = 12$

10	$8.49 \cdot 10^{-3}$	0.849	84.9	$8.49 \cdot 10^{3}$
100	$7.72 \cdot 10^{-4}$	$7.72 \cdot 10^{-2}$	7.72	$7.72 \cdot 10^{2}$
1000	$7.65 \cdot 10^{-5}$	$7.65 \cdot 10^{-3}$	0.765	76.5
10000	$7.64 \cdot 10^{-6}$	$7.64 \cdot 10^{-4}$	$7.64 \cdot 10^{-2}$	7.64
100000	$7.64 \cdot 10^{-7}$	$7.64 \cdot 10^{-5}$	$7.64 \cdot 10^{-3}$	0.764
1000000	$7.64 \cdot 10^{-8}$	$7.64 \cdot 10^{-6}$	$7.64 \cdot 10^{-4}$	$7.64 \cdot 10^{-2}$

(c): $\nu = 39$

10	$2.76 \cdot 10^{-2}$	2.76	$2.76 \cdot 10^{2}$	$2.76 \cdot 10^{4}$
100	$2.51 \cdot 10^{-3}$	0.251	25.1	$2.51 \cdot 10^{3}$
1000	$2.49 \cdot 10^{-4}$	$2.49 \cdot 10^{-2}$	2.49	$2.49 \cdot 10^{2}$
10000	$2.48 \cdot 10^{-5}$	$2.48 \cdot 10^{-3}$	0.248	24.8
100000	$2.48 \cdot 10^{-6}$	$2.48 \cdot 10^{-4}$	$2.48 \cdot 10^{-2}$	2.48
1000000	$2.48 \cdot 10^{-7}$	$2.48 \cdot 10^{-5}$	$2.48 \cdot 10^{-3}$	0.248

Table 2.3: Theoretical MSE bounds for the Student-Lévy process' series representation for different degree of freedom ν, time horizon T and level of truncation τ. The formula (2.12) for the deterministic truncation gives very similar numbers as for the random truncation (2.14) here.

extremely high cutoff point, e.g., if we replace ∞ by $m = 10^8$.

For the rest of this subsection we fix $T = 100$. Table 2.4 shows the empirical MSE bounds for the inverse gamma subordinator and Table 2.5 for the Student-Lévy process for $B = 10,000$ replications. The empirical MSE values are very close to the theoretical ones. Of course, the empirical MSE values are a bit smaller due to the truncation, which has to be applied at some point. Again, for Y_t the MSE

τ/ν	4	12	39
10	$6.73 \cdot 10^6$	$6.05 \cdot 10^7$	$6.39 \cdot 10^8$
100	$6.5 \cdot 10^4$	$5.86 \cdot 10^5$	$6.19 \cdot 10^6$
1000	$6.49 \cdot 10^2$	$5.84 \cdot 10^3$	$6.16 \cdot 10^4$
10000	6.48	58.4	$6.16 \cdot 10^2$
100000	$6.47 \cdot 10^{-2}$	0.58	6.15
1000000	$6.36 \cdot 10^{-4}$	$5.72 \cdot 10^{-2}$	0.06

Table 2.4: Empirical mean squared errors for the inverse gamma subordinator with various degree of freedom ν and level of truncation τ and fixed time horizon $T = 100$.

τ/ν	4	12	39
10	$2.52 \cdot 10^3$	$7.55 \cdot 10^3$	$2.45 \cdot 10^4$
100	$2.55 \cdot 10^2$	$7.66 \cdot 10^2$	$2.49 \cdot 10^3$
1000	25.8	77.3	$2.51 \cdot 10^2$
10000	2.53	7.6	24.7
100000	0.254	0.763	2.48
1000000	$2.5 \cdot 10^{-2}$	$7.5 \cdot 10^{-2}$	0.244

Table 2.5: Empirical mean squared errors for the Student-Lévy process with various degree of freedom ν and level of truncation τ and fixed time horizon $T = 100$.

depends quadratically on ν and linearly for X_t. Hence, if we consider simulating an inverse gamma subordinator we should take this into account by carefully choosing an appropriately high value of τ.

2.5.2 Comparison between methods

This subsection compares the inverse Lévy measure method with the rejection method. For simplicity we consider Student t distributed X_1 increments for different degrees of freedom ($\nu = 4, 12$ and 39). We simulate 10,000 random variates according to both methods. Figure 2.5 shows QQ-plots to check if the empirical distribution is approximately Student t. We additionally compare it with the standard acceptance-rejection method for simulating Student t random variates (in the first column of Figure 2.5). The second column corresponds to the inverse Lévy measure method and the third to the rejection method. The latter two are generated with a truncation

τ / ν	4	12	39
10	0.647	0.271	0.016
100	0.931	0.81	0.564
1000	0.99	0.968	0.914
10000	0.999	0.996	0.987

Table 2.6: The average probabilities of acceptance in the rejection method for various ν and τ. The average is taken over all jumps in the truncated series representation and over all of the 10000 realizations.

level $\tau = 10,000$. The comparison suggests that both methods work equally well as the standard method for generating Student t random variates. Moreover, since the level of truncation is very high, there is no visible difference for higher degrees of freedom in the bottom panels.

Figures 2.6 (inverse Lévy measure method) and 2.7 (rejection method) also show QQ-plots each for a given method of random variate generation. In both figures the panels' rows correspond to the degrees of freedom $\nu = 4, 12$ and 39. The columns correspond to different levels of truncation $\tau = 10, 100$ and 1000. Obviously, the truncation at $\tau = 10$ is not sufficient. For the rejection method, this level yields many paths exclusively with rejections. This causes the odd behavior of the QQ-line being zero. To see this, Table 2.6 shows the average acceptance probabilities $\frac{1}{10000}\sum_{j=1}^{10000} r_j$ with each r_j the average of a realization of $\frac{1}{N_\tau}\sum_{i=1}^{N_\tau} P[\frac{\mathrm{d}Q}{\mathrm{d}Q_0}(Q_0^{\leftarrow}(\Gamma_i/T)) \geq W_i]$. The values imply that for large τ the acceptance probability is high enough, meaning that most simulated jumps are accepted. This holds true for each ν. For $\tau = 10$ and especially for large degrees of freedom we have a very low average acceptance probability. This means that there is a high probability that no jump is accepted for some realizations.

On the other hand, $\tau = 100$ seems fine as there is no visible difference to even higher τ. However, we strongly recommend not to choose τ too small. Our experiments demonstrate that for smaller increments $X_{\Delta t}$ with $\Delta t < 1$, choosing τ too small does not ensure that $\{X_{\Delta t}\}$ is empirically distributed as the Δt law of the Student-Lévy process. Hence, to simulate values in between intervals of size 1, we should adjust τ.

Next, we discuss execution times of the algorithms. All algorithms are written in Mathematica and run on a Windows 10 personal computer using one kernel with 3.2 GHz. The numerical inversion setup, which has to run only once for each degree of freedom, needs 1961.7 seconds for $\nu = 4$, 2605.2 sec. for $\nu = 12$ and 1118.3 sec. for $\nu = 39$. We test the algorithm for some other degree of freedoms and find no typical

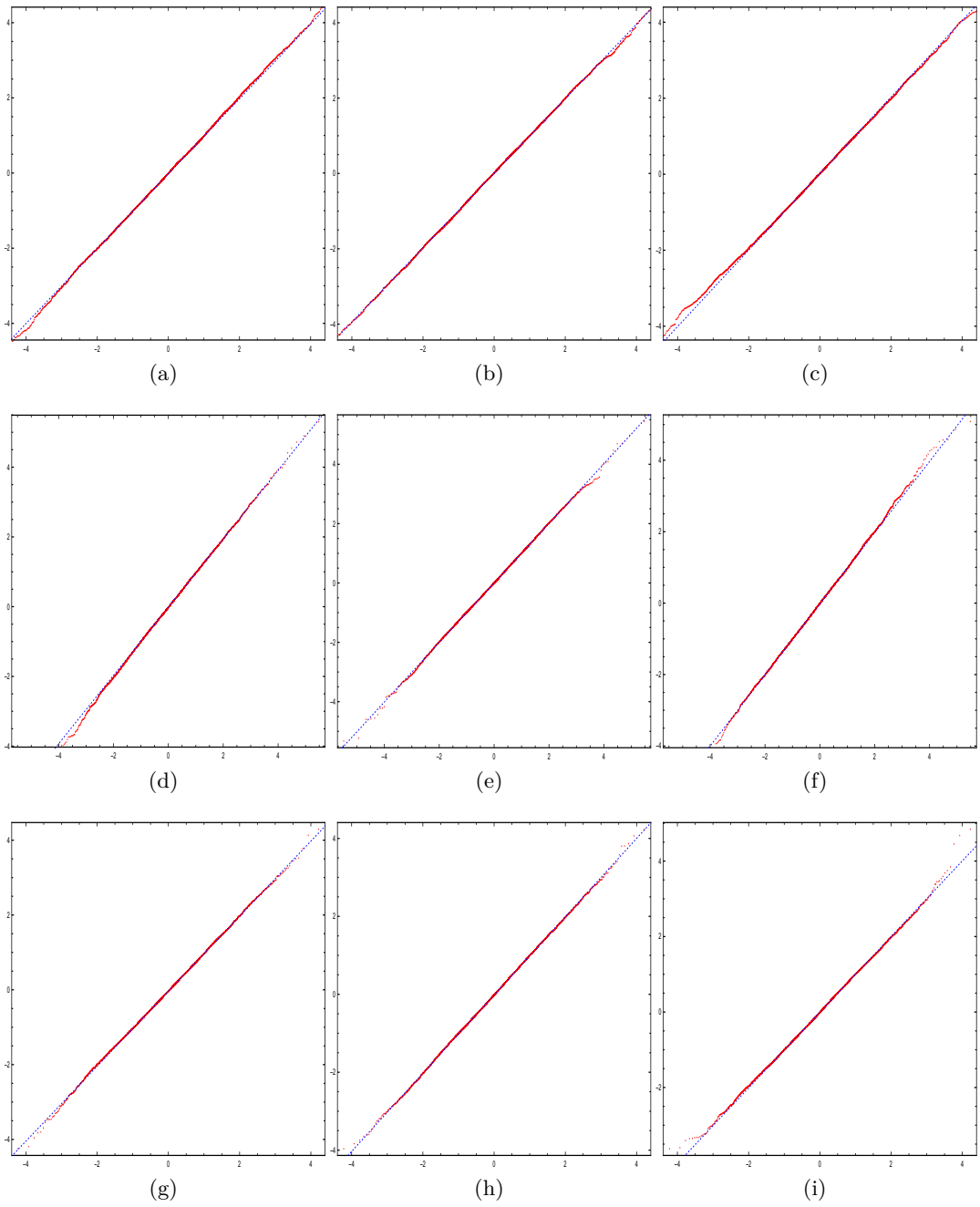

Figure 2.5: QQ-Plot of empirical quantiles from different simulation methods versus the theoretical quantiles for the Student-Lévy process, reference line in blue, dotted. For panels (a)-(c) $\nu = 4$, for panels (d)-(f) $\nu = 12$, for panels (g)-(i) $\nu = 39$. The first column (panels (a), (d), (g)) rv's are simulated with standard acceptance-rejection. The second column is simulated with the inverse Lévy measure method, the third with the rejection method. For both $\tau = 10000$.

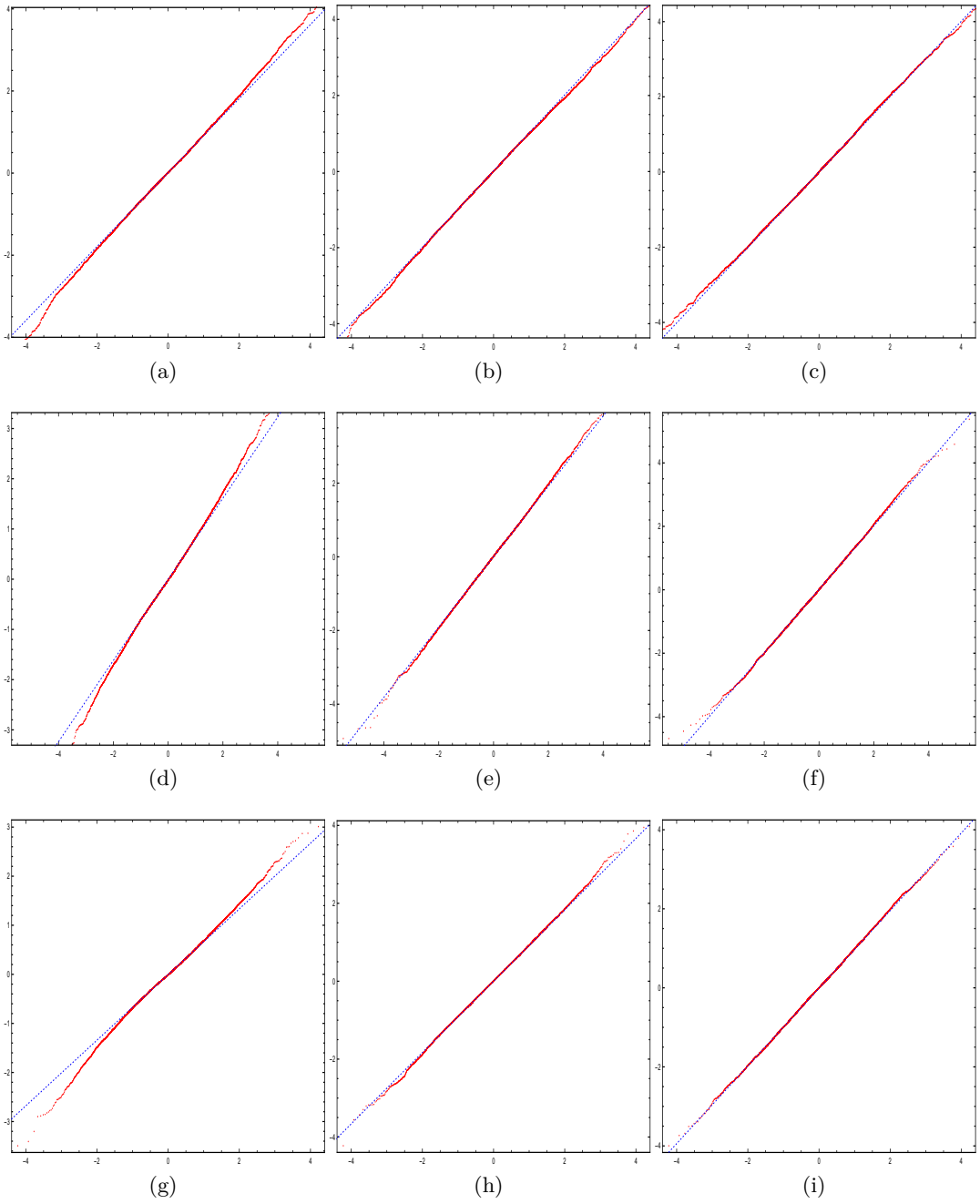

Figure 2.6: QQ-Plot of empirical quantiles from different simulation methods versus the theoretical quantiles for the Student-Lévy process, reference line in blue, dotted. For panels (a)-(c) $\nu = 4$, for panels (d)-(f) $\nu = 12$, for panels (g)-(i) $\nu = 39$. In all we use the inverse Lévy measure method with different levels of truncation. First column $\tau = 10$, second column $\tau = 100$ and third column $\tau = 1000$.

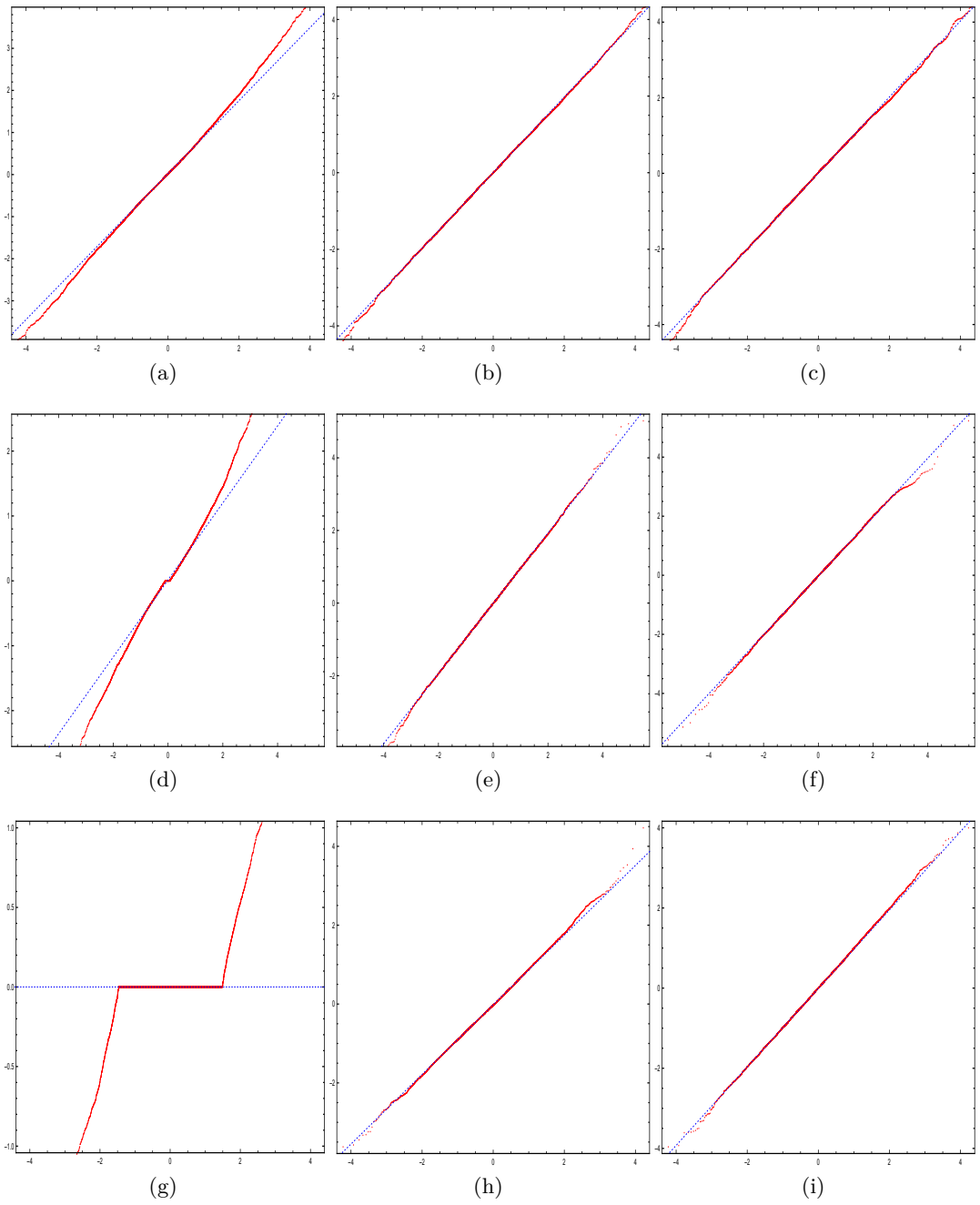

Figure 2.7: QQ-Plot of empirical quantiles from different simulation methods versus the theoretical quantiles for the Student-Lévy process, reference line in blue, dotted. For panels (a)-(c) $\nu = 4$, for panels (d)-(f) $\nu = 12$, for panels (g)-(i) $\nu = 39$. In all we use the rejection method with different levels of truncation. First column $\tau = 10$, second column $\tau = 100$ and third column $\tau = 1000$.

Method	τ / ν	4	12	39
Standard		$4 \cdot 10^{-5}$	$4 \cdot 10^{-5}$	$4 \cdot 10^{-5}$
Inverse Lévy measure	10	10^{-3}	10^{-3}	10^{-3}
Inverse Lévy measure	100	10^{-2}	10^{-2}	10^{-2}
Inverse Lévy measure	1000	0.09	0.08	0.09
Inverse Lévy measure	10000	0.81	0.79	0.82
Rejection	10	0.28	0.09	0.07
Rejection	100	4.7	2	0.79
Rejection	1000	81.3	23.8	11
Rejection	10000	880	254.8	121.8

Table 2.7: Computing time in seconds to generate one Student t random number for the standard (acceptance-rejection) method, the numerical inversion (Algorithm 2) and the rejection method. The latter two for different τ.

pattern for the runtime, except that odd degree of freedoms mostly run a bit shorter. Table 2.7 compares the runtime of the different methods to generate one Student t distributed random number and Table 2.8 the computing time to generate one path of a Student-Lévy process with $\nu = 4$ on $[0, T]$ for a varying level of truncation τ (which also is the number of observable jumps, if accepted). The rejection method is considerably slower than the inverse Lévy measure method due to the numerical integration. The inverse Lévy measure method quickly generates random numbers and random paths even for a high accuracy, cf. Table 2.3 for MSE bounds. There is no difference in computing time in ν for the inverse Lévy measure method. However, the rejection method is a bit faster for higher ν because the numerical integrations perform faster.

To conclude, we briefly summarize the relative merits of the methods. The inverse Lévy measure method is, if implemented as in Section 2.4, very fast and robust. That said, the inverse function is not exact and exhibits numerical errors as discussed at the beginning of that section. The present Monte Carlo evidence suggests that this is a minor problem, however. On the other hand, the rejection method is numerically more precise but the repeated computation of the integral in $\rho(x)$ is time-consuming. We therefore prefer the inverse Lévy measure method, due to its lower MSE (see Proposition 2.2) and its fast computation.

2.5.3 Goodness of fit

In this subsection we only use the inverse Lévy measure method to simulate paths of the Student-Lévy process and investigate whether the simulated trajectories obey the

Method	τ	Runtime
Inverse Lévy measure	10^3	0.14
Inverse Lévy measure	10^4	0.87
Inverse Lévy measure	10^5	8.2
Inverse Lévy measure	10^6	83.3
Rejection	10^3	29.2
Rejection	10^4	526.6
Rejection	10^5	8692.6
Rejection	10^6	109891.5

Table 2.8: Computing time in seconds to generate one Student-Lévy path on $[0, T]$ with $\nu = 4$ with the numerical inversion (Algorithm 2) and the rejection method for different level of truncation τ.

Student-Lévy law. For this purpose we apply the Kolmogorov-Smirnov distance and test to some points of the simulated paths.

Definition 2.1. Let

$$F_k(x) = \frac{1}{k} \sum_{i=1}^{k} \mathbb{1}_{(-\infty,x]}(x_i)$$

be the empirical distribution function. The *Kolmogorov-Smirnov statistic* for a given cumulative distribution function is

$$D_k = \sup_{x \in \mathbb{R}} |F_k(x) - F(x)|.$$

For the hypothesis $H_0 : F = F_0$ versus $H_1 : F \neq F_0$ it is true that $D_k \to 0$ a.s. for $k \to \infty$ if and only if H_0 is true. Moreover, Kolmogorov (1933) proved

Lemma 2.2. *For $x > 0$,*

$$\lim_{k \to \infty} P[\sqrt{k} D_k \leq x] = 1 - 2 \sum_{j=1}^{\infty} (-1)^{j-1} e^{-2j^2 x^2}.$$

For simplicity, we compute the p-value from the asymptotic ($k \to \infty$) distribution.

Let $F_t(x)$ denote the cumulative distribution function of the Student-Lévy process. Since F_t is not known explicitly, except for $t = 1$, we use the following inversion theorem (Gil-Pelaez 1951):

Lemma 2.3. *Let X be a continuous random variable in $\mathbb{R}$. Let $F(x)$ be its cumulative*

(a): Standard

Δt / ν	4	12	39	"∞"
0.1	-	-	-	0.0272783
				(0.0521)
1	0.0849081	0.0852336	0.0849289	0.0850967
	(0.045)	(0.0407)	(0.0428)	(0.0436)

(b): Inverse Lévy measure

0.1	0.0274064	0.0271817	0.0272413	-
	(0.0506)	(0.0452)	(0.0455)	
1	0.0853521	0.0852608	0.0851765	-
	(0.0463)	(0.0428)	(0.0434)	

Table 2.9: Mean Kolmogorov-Smirnov statistics and empirical sizes (in parentheses). The "∞" column stands for simulated Brownian motions.

distribution function and $\varphi(z)$ *its corresponding characteristic function. Then,*

$$F(x) = \frac{1}{2} - \frac{1}{\pi}\int_0^\infty \mathrm{Re}\left[\frac{e^{-\mathrm{i}zx}\varphi(z)}{\mathrm{i}z}\right]\mathrm{d}z, \tag{2.18}$$

where $\mathrm{Re}(y)$ *denotes the real part of* $y \in \mathbb{C}$.

However, we can only compute $F_t(x)$ for $t \neq 1$ numerically, again, by using the adaptive Gauss-Kronrod rule.

The procedure is the following: we simulate a path of length $T = 100$ and look at the 1-increments and the 0.1-increments. We estimate the empirical distribution function, the Kolmogorov-Smirnov statistic and test the null $F = F_t$ for $t = 1$ and for $t = 0.1$. We perform two additional comparisons. First, as in Subsection 2.5.2, we simulate 100 Student t random variates using acceptance-rejection. Second, we simulate paths of a Brownian motion and perform the Kolmogorov-Smirnov test for the increments. We repeat this 10,000 times for each configuration.

Table 2.9 shows the average Kolmogorov-Smirnov statistic of this Monte Carlo study. The values of the standard method and the inverse Lévy measure method are indeed very similar for 1-increments. For the 0.1-increments there is no standard method of generation. Hence, we compare it with the Brownian motion where the mean KS statistic is also of the same magnitude. The statistics for 0.1-increments

are smaller because we have 1000 instead of 100 sampling points in $[0, 1]$.

We also computed other statistical distance measures as the Hellinger distance but as the results were qualitatively the same, we omit these here.

Table 2.9 also presents the empirical sizes if we apply the Kolmogorov-Smirnov test to the increments with a nominal level 5%. We use (2.18) to compute the p-values, although for small sample sizes exact formulas are available. Thus, the number of rejections is slightly too small.

Additionally, Figure 2.8 shows histograms of the Kolmogorov-Smirnov statistics for $\nu = 4$ (for other ν it looks very similar). If we compare the generated paths using the inverse Lévy measure (panels (b) and (d) for 1- and 0.1-increments, resp.) with the corresponding Brownian motion generation there is no visible difference. This suggests that our proposed method works very well.

Furthermore, we tested the Gaussian approximation for small jumps (see Subsection 2.3.3). We skip the discussion of the results, as these were very similar to those above without Gaussian approximation. One issue is that we do not know $\int_{-\varepsilon}^{\varepsilon} x^2 \Pi(\mathrm{d}x)$ exactly and have to approximate it. Positively speaking, this means that the series representation works well even without additional Gaussian approximation.

2.6 Conclusion and future work

This chapter analyzes the Student-Lévy process and the inverse gamma subordinator, their series representations and (conditional) MSE bounds. We furthermore propose a numerically feasible path generation method. A simulation study confirms the validity of our results.

In future work we aim to extend the results to multidimensional Student-Lévy processes. The simulation can be generalized in a straightforward way (we only need to incorporate the inverse gamma's inverse Lévy measure and use Corollary 2.2 with d-dimensional V_i). We shall investigate how the d dimensions influence the accuracy of the simulation, e.g., whether there is a "curse of dimensionality". Simulations of generalizations of the Student-Lévy process such as the generalized hyperbolic Lévy process will also be considered.

The tools developed here prove useful in the context of parameter estimation for the Student-Lévy process and stochastic differential equations driven by Student-Lévy processes. This will be discussed in the next chapter and illustrated with empirical applications in Chapter 4.

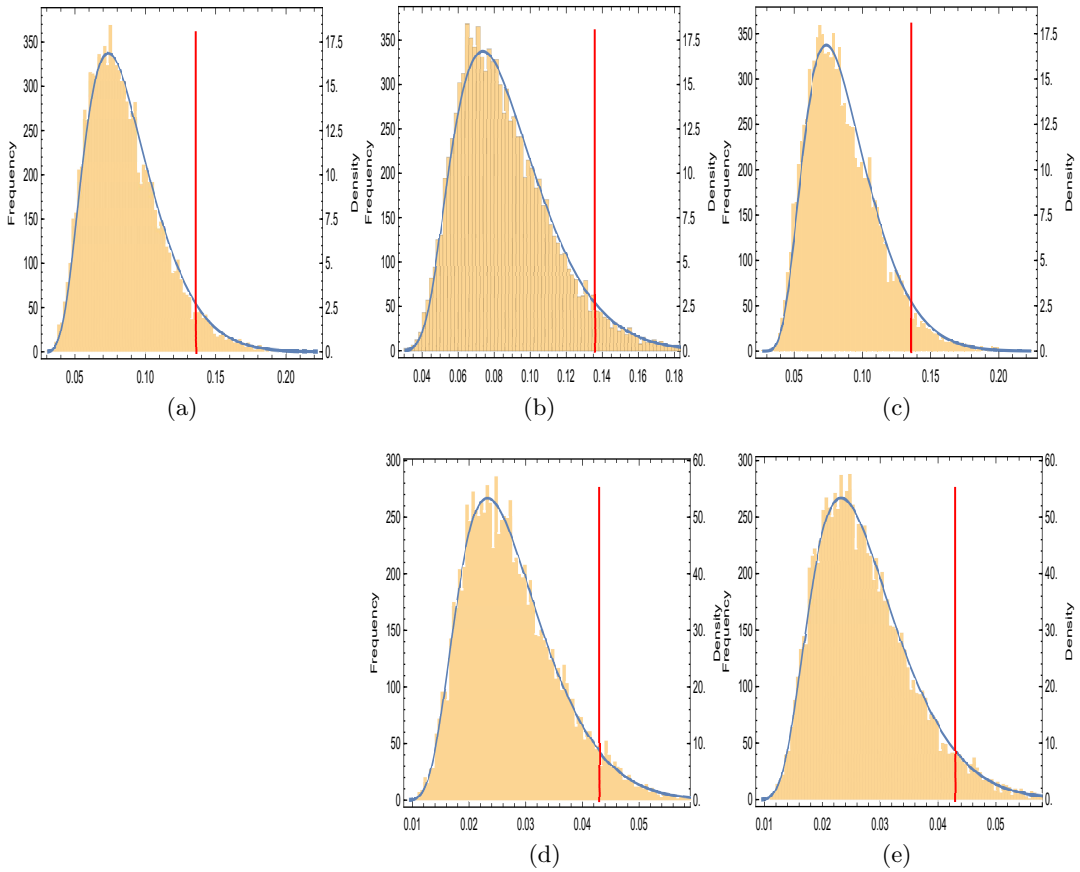

Figure 2.8: Histogram of the Kolmogorov-Smirnov statistics. Panel (a) for standard Student t random variates. Panel (b) for 1-increments of the Student-Lévy process. Panel (c) for 1-increments of the Brownian motion. Panel (d) for 0.1-increments of the Student-Lévy process. Panel (e) for 0.1-increments of the Brownian motion, red line indicating the 5% critical value, blue line the theoretical Kolmogorov-Smirnov density.

2.A Other simulation methods

We compare the simulation method introduced in Chapter 2 with other methods in the literature. Hubalek (2005) proposed sampling from the characteristic function (1.1) using Devroye (1981), which is based on the ratio-of-uniforms method. The details are as follows. Let $\varphi(u)$ denote the characteristic function (1.1) and $\psi(u)$ the characteristic exponent for the Student t distribution with standard scaling $t(\nu)$ and

let $\varphi(u;t) = e^{\psi(u)t}$ be the characteristic function of X_t for a Student-Lévy process $\{X_t\}$ with standard scaling. Then,

$$\varphi''(u;t) = \varphi(u;t)(\psi''(u)t + \varphi'(u)^2 t^2).$$

In a preprocessing step numerically evaluate

$$c = \frac{1}{2\pi}\int_{-\infty}^{\infty} |\varphi(u;t)|\mathrm{d}u,$$
$$k = \frac{1}{2\pi}\int_{-\infty}^{\infty} |\varphi''(u;t)|\mathrm{d}u.$$

Set $A = 4\sqrt{kc}$ and

$$g(x) = \min\left(c, \frac{k}{x^2}\right).$$

The algorithm generates a sample of $\{X_t\}$ with density $A^{-1}g(x)$ by the ratio-of-uniforms method and accepts iff $g(X) < f_t(X)$, where $f_t(x)$ denotes the density of X_t and has to be evaluated numerically using the following Fourier inversion

$$f_t(x) = \frac{1}{\pi}\int_0^{\infty} \cos(xu)\varphi(u;t)\mathrm{d}u.$$

Then the algorithm is

Algorithm 3 Hubalek (2005)

Input: Numbers k, c, function $g(x)$ depending on ν and t;
Output: Random variate Y with density function $f_t(x)$.

1: **repeat**
2: Sample $V_1 \leftarrow \mathcal{U}_{(-1,1)}$,
3: Sample $V_2 \leftarrow \mathcal{U}_{(-1,1)}$,
4: Sample $U \leftarrow \mathcal{U}_{(0,1)}$,
5: $X \leftarrow \sqrt{\frac{k}{c}}\frac{V_1}{V_2}$,
6: $Y \leftarrow g(X) \cdot U$,
7: **until** $Y \leq f(X)$.

Note that the average number of repetitions until acceptance is given by A (Devroye 1981).

More recently, Barth & Stein (2016) discussed a slightly different approach based on the direct inversion method. Let $F_t(x)$ denote the cumulative distribution function

of X_t, which can be evaluated numerically using

$$F_t(x) = \frac{1}{2} - \frac{1}{\pi} \int_0^\infty \operatorname{Re}\left[\frac{e^{-\mathrm{i}ux}\varphi(u)}{\mathrm{i}u}\right] \mathrm{d}u,$$

see Gil-Pelaez (1951). Then the algorithm is

Algorithm 4 Barth & Stein (2016)

Input: ν and t;
Output: Random variate Y with distribution function $F_t(x)$.
1: Sample $U \leftarrow \mathcal{U}_{(0,1)}$,
2: Find root $Y \leftarrow \inf\{x \in \mathbb{R} | F_t(x) = U\}$.

We compare both with the inverse Lévy measure method of Chapter 2. For each method we simulate a Student-Lévy path on $[0, 100]$ with a frequency $\Delta t = 0.1$. Actually, this means we simulate 1,000 random variables with distribution function $F_{0.1}(x)$. Figure 2.9 shows QQ-plots comparing the empirical quantiles with the theoretical quantiles. The three methods appear to work qualitatively equally well.

Additionally, we compare the execution times of the three methods. In this experiment Hubalek's (2005) algorithm takes about 67 seconds and Barth & Stein's (2016) algorithm 74 seconds. The numerical Fourier inversion is crucial for the execution time. Depending on the method used, this may shorten or lengthen the runtime.

Recall Table 2.8 on page 52 for the runtime of the inverse Lévy measure method. For a high level of truncation $\tau = 10^6$ (which we choose here) it takes about 83 seconds to run the inverse Lévy measure method. Note that for $\tau = 10^2$, with a runtime of about 8 seconds, the QQ-plot in this case looks very similar. This means that a "good" path can be simulated in an even shorter time.

An additional advantage of the inverse Lévy measure method is that after the series is simulated it can be evaluated extremely fast at desired times t. This means that we do not need to fix the frequency a priori as for Algorithms 3 & 4. If we choose a different frequency for these, we have to simulate new paths.

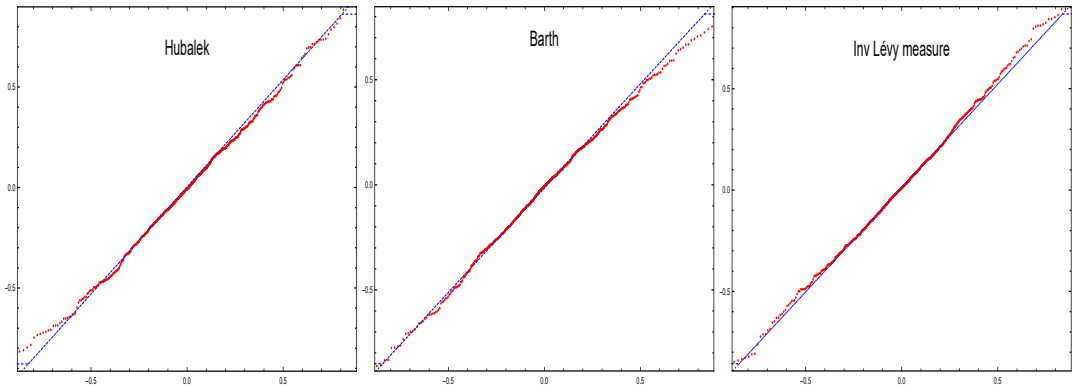

(a) (b) (c)

Figure 2.9: QQ-plots comparing the empirical distribution of simulated increments using different methods with the model distribution $F_{0.1}(x)$.

3 Local asymptotic normality for Student-Lévy processes under high-frequency sampling

There is considerable interest in parameter estimation in Lévy models. The maximum likelihood estimator is widely used because under certain conditions it enjoys asymptotic efficiency properties. The toolkit for Lévy processes is the local asymptotic normality which guarantees these conditions. Although the likelihood function is not known explicitly, we prove local asymptotic normality for the parameters of the Student-Lévy process assuming high-frequency data for location and scale parameter (μ, σ). In addition, we propose a numerical method to make maximum likelihood estimates feasible based on the Monte Carlo expectation-maximization algorithm. A simulation study verifies the theoretical results.

3.1 Introduction

There is considerable interest in Lévy processes and parameter estimation in Lévy models, see, e.g., Masuda (2015) and the references therein. However, estimation is difficult because the transition density often is not available in closed form. This chapter deals with parameter estimation for the Student-Lévy process $\{X_t\}_{t\geq 0}$ such that $X_1 \sim t(\nu, \mu, \sigma^2)$ given a sample path. Throughout we are interested in estimating the unknown $\theta = (\mu, \sigma)$, while we assume $\nu > 1$ to be known. The reason for this assumption is discussed in Section 3.5. The additional estimation of ν is left for future research.

As the crude method of moment estimator has poor asymptotic efficiency properties, we focus on maximum likelihood (ML) estimation. The maximum likelihood estimator (MLE) requires the density function (or likelihood function) to be known. In the case of the Student-Lévy process, however, we only know the transition density for the 1-increments. For $t \neq 1$, X_t has no closed-form transition density. Thus, maximum likelihood estimation is difficult both theoretically and practically.

The purpose of this chapter is, first, to develop asymptotic theory for the MLE

in the Student-Lévy model even though the likelihood function is not given explicitly. Second, we propose a time-efficient numerical method in order to make ML estimation feasible.

Let us introduce some notation. Let $(\Omega, \mathcal{F}, P)$ be a probability space and let $\{X_t\}_{t\geq 0}$ be a real-valued Student-Lévy process with $\mathcal{L}(X_1) = t(\nu, \mu, \sigma^2)$. Let ν be the known degree of freedom and $\theta = (\mu, \sigma) \in \Theta$, where Θ is a bounded convex domain such that its closure $\overline{\Theta} \subset \mathbb{R} \times (0, \infty)$. Importantly, this implies that $\sigma \in (a, b)$ with $0 < a < b < \infty$ to exclude the limiting case $\sigma \to 0$. Let $(P_\theta; \theta \in \Theta)$ be the family of distributions of $\{X_t\}$ dependent on the unknown parameter θ. The Radon-Nikodym derivative $\frac{dP_{\theta'}}{dP_\theta}$ denotes the likelihood ratio (which in the case of the Student-Lévy process is well-defined). By $p_t(x|\theta)$ we denote the Lebesgue density of X_t, which is always positive, and by $\ell_n(\theta)$ the log-likelihood function. Since the Student-Lévy process is a pure jump process we denote by $\Delta X_t := X_t - \lim_{s\uparrow t} X_s$ the jump size at time t.

A useful concept for studying asymptotics is the local asymptotic normality (LAN) of a family of probability measures, which means that the logarithm of the likelihood ratio behaves asymptotically as a normal random variable. More precisely, we have

Definition 3.1. A sequence of parametric statistical models $(P_\theta^n, \theta \in \Theta, n \in \mathbb{N})$ is said to be *locally asymptotic normal (LAN)* with rate A_n and Fisher information matrix $\mathscr{I}(\theta)$, if for each $u \in \mathbb{R}^p$ and $\theta_n := \theta + A_n u \in \Theta$

$$\log \frac{dP_{\theta_n}^n}{dP_\theta^n} = \ell_n(\theta_n) - \ell_n(\theta) = u^{\mathrm{T}} A_n \nabla \ell_n(\theta) - \frac{1}{2} u^{\mathrm{T}} \mathscr{I}(\theta) u + o_{P_\theta}(1) \tag{3.1}$$

holds true under P_θ, where $A_n \nabla \ell_n(\theta) \xrightarrow{\mathcal{L}} N_p(0, \mathscr{I}(\theta))$.

The LAN concept implies many useful properties, including the asymptotic normality and asymptotic efficiency of likelihood-based estimation. It was introduced by Le Cam (1960) and since then has been applied in various statistical models. Le Cam & Lo Yang (1990) provided a concise introduction to the topic. Because Lévy processes have a diverse structure, a universal LAN theory is lacking: the very different forms of the likelihood function make analysis difficult, for instance, if the likelihood function $p_t(x|\theta)$ does not exist in closed form (as is the case for the Student-Lévy process). However, there are some specific cases for which the LAN does exist. Examples for special Lévy models include Masuda (2009*b*) for the gamma subordinator and the inverse Gaussian subordinator, Kawai & Masuda (2011) for the Meixner Lévy process, and Kawai & Masuda (2013) for the normal inverse Gaussian Lévy process, Kawai (2015) for the variance gamma Lévy process.

Aït-Sahalia & Jacod (2008) and Masuda (2009*a*) derived LAN results for non-Gaussian stable Lévy processes (recall Definition 1.11 for stability). More recently Ivanenko et al. (2015) investigated locally stable Lévy processes, i.e., $\mathcal{L}(h^{-1}X_h)$ weakly tends to an α-stable distribution as $h \to 0$, which contain the Student-Lévy process as a special case. For more comments on locally stable processes, see below. Masuda (2015) provided an excellent detailed overview and summarized many of the results to be found in the literature.

For the purposes of estimating θ, it is important to clarify the structure of the available data and the meaning of large sample theory. There are three different senses in which we may sample a path of $\{X_t\}_{t\geq 0}$ (see Masuda 2015).

- Sampling the path $\{X_t\}_{t\in[0,T]}$ in *continuous-time*. This means that we observe the whole path for any time $t \in [0,T]$. Here asymptotic theory assumes $T \to \infty$. In this setting, some parameters may be estimated without error.
- Sampling $\{X_t\}$ at discrete and *low-frequency* time points $\{t_k^n\}_{k=0,\dots,n} \subseteq [0,\infty)$ such that
$$0 = t_0^n < t_1^n < \cdots < t_n^n =: T_n$$
for each $n \in \mathbb{N}$ and the sampling intervals $\Delta_k^n t := t_k^n - t_{k-1}^n$ satisfy
$$\liminf_{n\to\infty} \min_{1\leq k\leq n} \Delta_k^n t > 0,$$
which requires that $T_n \to \infty$.
- Sampling $\{X_t\}$ at discrete time points $\{t_k^n\}_{k=0,\dots,n}$ but with *high-frequency*, i.e.,
$$h_n := \max_{1\leq k\leq n} \Delta_k^n t \to 0,$$
as $n \to \infty$. Here T_n does not need to tend to infinity and, moreover, may even be fixed as $T \equiv T_n$. We mainly consider the case where the step sizes are of equal length $h_n \equiv \Delta_k^n t$ for each $1 \leq k \leq n$.

The main difference between high-frequency and low-frequency sampling is that in the former case the differences between the observation times h_n become arbitrarily small. For the latter, this is not the case. Here, the endpoint T_n must tend to infinity. A simple example of sampling at low-frequency is given by the scheme $t_k^n = k$. This means we sample the 1-increments of the path, which in the case of the Student-Lévy process are Student t distributed. As $T_n \to \infty$ we obtain classic asymptotic theory for the estimation of Student t random variables. For any other low-frequency sampling scheme, the theory becomes more involved; see Remark 3.4. Most references above mainly under low-frequency sampling (and some under high-frequency sampling) in certain special cases.

This chapter also mainly focuses on high-frequency sampling. The contribution to the literature is to derive the LAN property for (μ, σ) for high-frequency sampling in the Student-Lévy model. Moreover, we discuss why there is no such LAN result for the skew Student-Lévy process. Results for the other schemes are relegated to the end of Section 3.2.

The second contribution of this chapter is more practical. As is the case even for the plain Student t distribution, there is no closed-form solution for the MLE in the Student-Lévy model. For the Student t distribution ML estimation becomes numerically feasible using the Expectation-Maximization (EM) algorithm introduced by Dempster et al. (1977). Since Rubin (1983) (see also Little & Rubin (2014)) applied the EM algorithm to the Student t distribution, many extensions have been developed. For example, Liu & Rubin (1995) described ML estimation of the unknown ν by Expectation-Conditional Maximization Either (ECME; see Liu & Rubin (1994)). Nadarajah & Kotz (2008) summarized some of the most important methods for the Student t distribution. McLachlan & Krishnan (2007) is a standard reference for the EM algorithm.

Returning to the Student-Lévy process, we here propose a Monte Carlo EM (MCEM) algorithm. The MCEM algorithm was initially developed by Wei & Tanner (1990) and replaces one or both of the E- and the M-steps with a Monte Carlo variant. Details are discussed in Section 3.3 below. We aim to estimate (μ, σ) given a sample with density $p_t(x|\theta)$ where $t \neq 1$ and possibly is smaller.

In this chapter as already mentioned, we consider ν to be known. Possible extensions are discussed in Section 3.5.

The remainder of this chapter is organized as follows: Section 3.2 states and proves the LAN result for the Student-Lévy process. Numerical methods such as the MCEM algorithm are discussed in Section 3.3. In Section 3.4 we test these methods in Monte Carlo experiments. Section 3.5 concludes.

3.2 Main results

Under the high-frequency sampling scheme with observation times $\{t_k^n\}$ and observed points $\{X_{t_k^n}\}$ we define the k-th increments of $\{X_t\}$ as

$$\Delta_k^n X := X_{t_k^n} - X_{t_{k-1}^n}, \quad k = 1, \ldots, n.$$

$\Delta_k^n X$ are i.i.d. with density function $p_{h_n}(x|\theta)$. We define the log-likelihood function by

$$\ell_n(\theta) := \sum_{k=1}^{n} \log p_{h_n}(\Delta_k^n X|\theta).$$

We write

$$g_{nk}(\theta) := \nabla \log p_{h_n}(\Delta_k^n X|\theta) = \left(\frac{\partial}{\partial \mu} p_{h_n}(\Delta_k^n X|\theta), \frac{\partial}{\partial \sigma} p_{h_n}(\Delta_k^n X|\theta) \right)^{\mathrm{T}}.$$

We now state the main result.

Theorem 3.1. *Let $\{X_t\}$ be a Student-Lévy process such that $\mathcal{L}(X_1) = t(\nu, \mu, \sigma^2)$ (with known $\nu > 1$). Consider a sample $(X_{kh_n})_{1 \le k \le n}$ with a sequence $\{h_n\}_{n \in \mathbb{N}}$ of positive step sizes. If $h_n \to 0$ as $n \to \infty$, the LAN property* (3.1) *holds true for each $\theta = (\mu, \sigma) \in \Theta$ with rate*

$$A_n := \operatorname{diag}\left(\frac{1}{\sqrt{n}}, \frac{1}{\sqrt{n}} \right) \tag{3.2}$$

and Fisher information

$$\mathscr{I}(\theta) := \begin{pmatrix} \frac{1}{2\nu\sigma^2} & 0 \\ 0 & \frac{1}{2\sigma^2} \end{pmatrix}. \tag{3.3}$$

In particular, $\mathscr{I}(\theta)$ is positive definite for each $\theta \in \Theta$ and, moreover, the maximum likelihood estimator $\hat{\theta}$ exists and is asymptotically normal:

$$A_n^{-1}(\hat{\theta} - \theta) \xrightarrow{\mathcal{L}} N_2(0, \mathscr{I}(\theta)^{-1}) \quad \text{as } n \to \infty.$$

The positive definiteness of $\mathscr{I}(\theta)$ implies that $\mathscr{I}(\theta)^{-1}$ exists. $\hat{\theta}$ is asymptotically efficient because it attains the Cramér-Rao bound asymptotically.

Theorem 3.1 is actually a special case of Theorem 2.1 is Ivanenko et al. (2015) since the Student-Lévy process is locally stable, as we prove in Lemma 3.2. However, we present a different proof here because we can use these methods for the skew Student-Lévy process in Proposition 3.1, which was not treated in Ivanenko et al. (2015). Furthermore, the ideas in our version of the proof will turn out to be constructive in Section 3.3 for deriving a numerical procedure to compute the MLE.

Before we turn to the details of the proof, we make some additional comments.

Remark 3.1. The time horizon T_n does not need to tend to infinity. It may possibly be fixed as $T \equiv T_n$. This is in contrast to, e.g., Gaussian Lévy processes, where the maximum likelihood estimator for μ is not even consistent if T_n does not tend to

infinity. This can easily be visualized by a short simulation. The LAN for Gaussian Lévy processes has rate $(\sqrt{T_n}, \sqrt{n})$ for (μ, σ) (see, e.g., Kawai 2013).

Remark 3.2. Although the Student-Lévy process is clearly not stable, it has the same asymptotic Fisher information as a stable Cauchy-Lévy process. (In fact, the Cauchy-Lévy process is a special case of the Student-Lévy process with $\nu = 1$. As all increments are Cauchy distributed, ML estimation is reduced to the standard i.i.d. Cauchy case (Haas 1969), which we do not consider here.) Masuda (2009*a*) derived the LAN property for symmetric stable Lévy processes. A Lévy process whose 1-increments are Cauchy$(\mu, \sqrt{\nu}\sigma)$ distributed fulfills the LAN with Fisher information (3.3) and rate (3.2).

Kawai & Masuda (2013) showed that the following conditions of Lemma 3.1 are sufficient for the LAN to hold true. In the proof of Theorem 3.1 we will verify that conditions (i) – (iii) are satisfied under the assumptions of Theorem 3.1.

Lemma 3.1. *Assume the following conditions hold true as* $n \to \infty$*:*

(i) $nE_\theta \left[A_n g_{n1}(\theta) g_{n1}(\theta)^{\mathrm{T}} A_n \right] \to \mathscr{I}(\theta)$,

(ii) $n|E_\theta[A_n g_{n1}(\theta)]|^2 \to 0$,

(iii) $n \left(\sup_{\theta \in \Theta} E_\theta \left[|A_n \nabla (g_{n1}(\theta)^{\mathrm{T}}) A_n|^2 + |A_n g_{n1}(\theta)|^4 \right] \right) \to 0$.

Then the LAN (3.1) *holds true.*

Assumption (iii) implies the Lindeberg condition

$$\sum_{k=1}^{n} E_\theta \left[|A_n g_{nk}(\theta)|^2 ; |A_n g_{nk}(\theta)| \geq \varepsilon \right] \to 0$$

for every $\varepsilon > 0$. This allows us to apply the central limit theorem.

The following lemmas are needed in order to prove Theorem 3.1. The first two show the locally stable behavior of Student-Lévy increments as well as inverse gamma subordinator's increments. The third gives a bound for the density function of the inverse gamma subordinator's increments.

Lemma 3.2. *Let* $\{X_t\}$ *be a Student-Lévy process such that* $\mathcal{L}(X_1) = t(\nu, \mu, \sigma^2)$*. As* $n \to \infty$

$$\frac{X_{h_n} - h_n \mu}{h_n \sigma} \xrightarrow{\mathcal{L}} \mathit{Cauchy}(0, \sqrt{\nu}),$$

i.e., the Cauchy distribution with density function

$$\frac{1}{\pi\sqrt{\nu}\left(1+\frac{x^2}{\nu}\right)}, \quad x \in \mathbb{R}.$$

Proof. We use the convergence of the characteristic function to prove the claim. Recall that the characteristic function for X_t is given in (1.1) by

$$\left(\frac{K_{\nu/2}(\sqrt{\nu}\sigma|u|)(\sqrt{\nu}\sigma|u|)^{\nu/2}e^{\mathrm{i}\mu u}}{\Gamma\left(\frac{\nu}{2}\right)2^{\nu/2-1}}\right)^t,$$

where $K_\nu(x)$ is the modified Bessel function of the second kind. Hence $\frac{X_{kh_n}-h_n\mu}{h_n\sigma}$ has the characteristic function

$$\left(\frac{K_{\nu/2}\left(\sqrt{\nu}\sigma\left|\frac{u}{h_n\sigma}\right|\right)\left(\sqrt{\nu}\sigma\left|\frac{u}{h_n\sigma}\right|\right)^{\nu/2}}{\Gamma\left(\frac{\nu}{2}\right)2^{\nu/2-1}}\right)^{h_n}. \tag{3.4}$$

Using

$$K_{\nu/2}(z) \sim \sqrt{\frac{\pi}{2z}}e^{-z}$$

for $z \to \infty$, we have for $h_n \to 0$ as $n \to \infty$

$$K_{\nu/2}\left(\sqrt{\nu}\left|\frac{u}{h_n}\right|\right)^{h_n} \sim \left(\sqrt{\frac{\pi h_n}{2\sqrt{\nu}|u|}}\right)^{h_n} e^{-\sqrt{\nu}\frac{|u|}{h_n}h_n} \to e^{-\sqrt{\nu}|u|},$$

since all other terms of (3.4) converge to 1. Of course, $e^{-\sqrt{\nu}|u|}$ is the characteristic function of the Cauchy$(0,\sqrt{\nu})$ distribution. □

Lemma 3.3. *Let $\{Y_t\}$ be an inverse gamma subordinator such that $\mathcal{L}(Y_1) = R\Gamma(\nu/2,\nu/2)$. As $n \to \infty$*

$$\frac{Y_{h_n}}{h_n^2} \xrightarrow{\mathcal{L}} \textit{Lévy}(0,\nu),$$

i.e., the Lévy distribution with density function

$$\sqrt{\frac{\nu}{2\pi}}\ \frac{e^{-\frac{\nu}{2x}}}{x^{3/2}}, \quad x \in \mathbb{R}.$$

Proof. Again, as in the proof of Lemma 3.2, we use convergence of the characteristic function. The characteristic function of Y_t is given by

$$\left(\frac{2\left(-\mathrm{i}\frac{\nu}{2}u\right)^{\nu/4}}{\Gamma\left(\frac{\nu}{2}\right)} K_{\nu/2}\left(\sqrt{-2\mathrm{i}\nu u}\right) \right)^t$$

Hence $\frac{Y_{h_n}}{h_n^2}$ has the characteristic function

$$\left(\frac{2\left(-\mathrm{i}\frac{\nu}{2}\frac{u}{h_n^2}\right)^{\nu/4}}{\Gamma\left(\frac{\nu}{2}\right)} \right)^{h_n} K_{\nu/2}\left(\sqrt{-2\mathrm{i}\nu\frac{u}{h_n^2}}\right)^{h_n}.$$

Similarly, as in the proof of Lemma 3.2,

$$K_{\nu/2}\left(\sqrt{-2\mathrm{i}\nu\frac{u}{h_n^2}}\right)^{h_n} \sim h_n^{h_n} e^{-\sqrt{-2\mathrm{i}\nu\frac{u}{h_n^2}}h_n} \to e^{-\sqrt{-2\mathrm{i}\nu u}}$$

for $n \to \infty$. Of course, $e^{-\sqrt{-2\mathrm{i}\nu u}}$ is the characteristic function of the Lévy$(0,\nu)$ distribution. □

Lemma 3.4. *Let $R\Gamma(y|\alpha,\beta)$ denote the density function for the $R\Gamma(\alpha,\beta)$ distribution and let $R\Gamma^{*t}(y|\alpha,\beta)$ denote its t-fold convolution. Then for $\nu > 1$ and any $t > 0$ there exists a $K > 0$ such that for all $0 < y < K$,*

$$R\Gamma^{*t}\left(y\left|\frac{\nu}{2},\frac{\nu}{2}\right.\right) > R\Gamma\left(y\left|\frac{\nu}{2},t^2\frac{\nu}{2}\right.\right), \qquad t > 1,$$
$$R\Gamma^{*t}\left(y\left|\frac{\nu}{2},\frac{\nu}{2}\right.\right) < R\Gamma\left(y\left|\frac{\nu}{2},t^2\frac{\nu}{2}\right.\right), \qquad t < 1.$$

Proof. Girón & del Castillo (2001) showed that

$$R\Gamma^{*2}\left(y\left|\frac{\nu}{2},\frac{\nu}{2}\right.\right) = \sum_{i=0}^{\frac{\nu-1}{2}} w_i R\Gamma\left(y\left|\frac{\nu}{2}+i,2^2\frac{\nu}{2}\right.\right)$$

for odd $\nu > 1$ with $w_i \geq 0$ and $\sum_i w_i = 1$. The cumbersome formulas for w_i can be

found in Girón & del Castillo (2001). For small y it holds true that

$$\sum_{i=0}^{\frac{\nu-1}{2}} w_i R\Gamma\left(y\left|\frac{\nu}{2}+i, 2^2\frac{\nu}{2}\right.\right) > R\Gamma\left(y\left|\frac{\nu}{2}, 2^2\frac{\nu}{2}\right.\right),$$

since $R\Gamma\left(y\left|\frac{\nu}{2}+i, 2^2\frac{\nu}{2}\right.\right) > R\Gamma\left(y\left|\frac{\nu}{2}, 2^2\frac{\nu}{2}\right.\right)$ for all $i \geq 1$. The difference $R\Gamma^{*2}\left(y\left|\frac{\nu}{2}, \frac{\nu}{2}\right.\right) - R\Gamma\left(y\left|\frac{\nu}{2}, 2^2\frac{\nu}{2}\right.\right)$ increases in ν. Hence, by continuity in ν,

$$R\Gamma^{*2}\left(y\left|\frac{\nu}{2}, \frac{\nu}{2}\right.\right) > R\Gamma\left(y\left|\frac{\nu}{2}, 2^2\frac{\nu}{2}\right.\right),$$

for all $\nu > 1$ and small y. By induction,

$$R\Gamma^{*m}\left(y\left|\frac{\nu}{2}, \frac{\nu}{2}\right.\right) > R\Gamma\left(y\left|\frac{\nu}{2}, m^2\frac{\nu}{2}\right.\right), \tag{3.5}$$

for all integers $m \geq 2$, for y small enough.

Obviously, $(R\Gamma^{*\frac{1}{m}})^{*m}\left(y\left|\frac{\nu}{2}, \frac{\nu}{2}\right.\right) \equiv R\Gamma\left(y\left|\frac{\nu}{2}, \frac{\nu}{2}\right.\right)$. By (3.5),

$$R\Gamma^{*m}\left(y\left|\frac{\nu}{2}, \frac{1}{m^2}\frac{\nu}{2}\right.\right) > R\Gamma\left(y\left|\frac{\nu}{2}, \frac{\nu}{2}\right.\right) = (R\Gamma^{*\frac{1}{m}})^{*m}\left(y\left|\frac{\nu}{2}, \frac{\nu}{2}\right.\right),$$

which implies

$$R\Gamma^{*\frac{1}{m}}\left(y\left|\frac{\nu}{2}, \frac{\nu}{2}\right.\right) < R\Gamma\left(y\left|\frac{\nu}{2}, \frac{1}{m^2}\frac{\nu}{2}\right.\right), \tag{3.6}$$

for all integer $m \geq 2$, for y small enough. (3.5) and (3.6) together with the infinite divisibility of the inverse gamma distribution imply the claim for all $t > 0$. □

The next lemma clarifies the asymptotic behavior of the density of Student-Lévy increments.

Lemma 3.5 (Berg & Vignat (2008))**.** *Let $p_t(x|\nu,\theta)$ be the transition density of X_t, where $\{X_t\}$ is the Student-Lévy process. Then for any $t > 0$, $\nu > 0$ and $\theta \in \mathbb{R}\times(0,\infty)$,*

$$p_t(x|\nu,\theta) \sim \frac{C_\nu t}{\sigma\left|\frac{x-h_n\mu}{\sigma}\right|^{\nu+1}},$$

as $|x| \to \infty$, where C_ν is a constant only depending on ν.

Berg & Vignat (2008) actually proved the statement for $p_t(x|\nu,0,1) \sim \frac{C_\nu t}{|x|^{\nu+1}}$. We generalize this using $p_t(x|\nu,\theta) = \frac{1}{\sigma} p_t(\frac{x-h_n\mu}{\sigma}|\nu,0,1)$.

Using these lemmas we now prove Theorem 3.1. There are two main ideas in the proof. First, we use the fact that the Student-Lévy process is a subordinated Gaussian process. Second, we apply Monte Carlo integration techniques to treat complicated integrals.

Proof of Theorem 3.1. We prove the theorem by checking the assumptions of Lemma 3.1. Before that, we prove boundedness in order to be able to apply the bounded convergence theorem. Note that $p_{h_n}(x|\theta) > 0$ for any $x \in \mathbb{R}, h_n > 0, \theta \in \Theta, \nu > 0$. We start with the first entry of $\nabla \log p_{h_n}(X_{h_n}|\theta)$

$$E_\theta \left[\left(\frac{\partial}{\partial \mu} \log p_{h_n}(X_{h_n}|\theta) \right)^2 \right] = \int_{-\infty}^{\infty} \left(\frac{\frac{\partial}{\partial \mu} p_{h_n}(x|\theta)}{p_{h_n}(x|\theta)} \right)^2 p_{h_n}(x|\theta) \mathrm{d}x.$$

Observe that

$$p_{h_n}(x|\theta) = \int_0^\infty p_{h_n}(x,y|\theta) \mathrm{d}y,$$

where $p_{h_n}(x,y|\theta)$ is the joint density of $G_{Y_{h_n}} + h_n\mu$, where $\{G_t\}$ is a Gaussian Lévy process such that $G_t \sim N(0,\sigma^2 t)$ (see Theorem 1.5). Thus,

$$p_{h_n}(x|\theta) = \int_0^\infty p_{h_n}(x,y|\theta) \mathrm{d}y = \int_0^\infty N(x|h_n\mu, \sigma^2 y) p_{h_n}(y) \mathrm{d}y, \tag{3.7}$$

where $N(x|h_n\mu,\sigma^2 y)$ denotes the density of the $N(h_n\mu,\sigma^2 y)$-distribution and $p_{h_n}(y) := R\Gamma^{*h_n}\left(y \middle| \frac{\nu}{2}, \frac{\nu}{2}\right)$, the density of the (unobserved) subordinator Y_{h_n}. Next,

$$\frac{\partial}{\partial \mu} \int_0^\infty N(x|h_n\mu,\sigma^2 y) p_{h_n}(y) \mathrm{d}y = \int_0^\infty \frac{\partial}{\partial \mu} N(x|h_n\mu,\sigma^2 y) p_{h_n}(y) \mathrm{d}y, \tag{3.8}$$

since $\left| \frac{\partial}{\partial \mu} N(x|h_n\mu,\sigma^2 y) \right| \leq C \frac{h_n}{y}$ for a constant C independent of y and θ. But $\int_0^\infty \frac{1}{y} p_{h_n}(y) \mathrm{d}y < \infty$ is implied by the uniform integrability, which we show below. (3.8) can be proven analogously for $\frac{\partial}{\partial \sigma}$ using the fact that $\overline{\Theta}$ is a compact set.

We now show that $\left|\frac{\frac{\partial}{\partial\mu}p_{h_n}(x|\theta)}{p_{h_n}(x|\theta)}\right|$ is uniformly bounded in x and h_n. This implies

$$\lim_{n\to\infty} E_\theta\left[\left(\frac{\partial}{\partial\mu}\log p_{h_n}(X_{h_n}|\theta)\right)^2\right] = E_\theta\left[\lim_{n\to\infty}\left(\frac{\partial}{\partial\mu}\log p_{h_n}(X_{h_n}|\theta)\right)^2\right].$$

Note that $p_{h_n}(x|\theta) \sim \frac{C_\nu h_n}{\sigma\left(\frac{x-h_n\mu}{\sigma}\right)^{\nu+1}}$ as $x \to +\infty$ (see Lemma 3.5). This straightforwardly leads to $\frac{\partial}{\partial\mu}p_{h_n}(x|\theta) \sim \frac{\partial}{\partial\mu}\frac{C_\nu h_n}{\sigma\left(\frac{x-h_n\mu}{\sigma}\right)^{\nu+1}}$ by applying (3.8) in the proof of Theorem 2 in Berg & Vignat (2008). Hence it holds true that

$$\frac{\frac{\partial}{\partial\mu}p_{h_n}(x|\theta)}{p_{h_n}(x|\theta)} \sim \frac{\frac{\partial}{\partial\mu}\frac{C_\nu h_n}{\sigma\left(\frac{x-h_n\mu}{\sigma}\right)^{\nu+1}}}{\frac{C_\nu h_n}{\sigma\left(\frac{x-h_n\mu}{\sigma}\right)^{\nu+1}}} \to 0,$$

as $x \to +\infty$, and analogously for $x \to -\infty$ which implies that $\left|\frac{\frac{\partial}{\partial\mu}p_{h_n}(x|\theta)}{p_{h_n}(x|\theta)}\right|$ is bounded in x.

Furthermore,

$$\frac{\frac{\partial}{\partial\mu}p_{h_n}(x|\theta)}{p_{h_n}(x|\theta)} \sim \frac{2\frac{x-h_n\mu}{h_n\sigma}}{\sigma\left(\nu+\left(\frac{x-h_n\mu}{h_n\sigma}\right)^2\right)} =: C_n(x) \to 0$$

as $n \to \infty$, for any x, see (i) below. Moreover, $\sup_x |C_n(x)| = \frac{1}{\sqrt{\nu}\sigma}$ implies uniform convergence. By the continuity of $\frac{\frac{\partial}{\partial\mu}p_{h_n}(x|\theta)}{p_{h_n}(x|\theta)}$ in (x, h_n) there exists a constant $C > 0$ such that

$$\left|\frac{\frac{\partial}{\partial\mu}p_{h_n}(x|\theta)}{p_{h_n}(x|\theta)}\right| < C < \infty,$$

for all $x \in \mathbb{R}$, and all $h_n \in (0, \infty)$. The proof of the boundedness of $\frac{\partial}{\partial\sigma}\log p_{h_n}(x|\theta)$ functions in a very similar fashion.

Next, we prove that $h_n N(x|h_n\mu, \sigma^2 Y_{h_n})$, $h_n\frac{\partial}{\partial\mu}N(x|h_n\mu, \sigma^2 Y_{h_n})$ and $h_n\frac{\partial}{\partial\sigma}N(x|h_n\mu, \sigma^2 Y_{h_n})$ are uniformly integrable for $n \in \mathbb{N}$. This implies that

$$\lim_{n\to\infty}\int_0^\infty h_n N(X_{h_n}|h_n\mu, \sigma^2 y)p_{h_n}(y)\mathrm{d}y = \int_0^\infty \lim_{n\to\infty} h_n N(X_{h_n}|h_n\mu, \sigma^2 y)p_{h_n}(y)\mathrm{d}y,$$

or, if replacing integrals with its Monte Carlo estimators,

$$\lim_{n\to\infty}\lim_{B\to\infty}\frac{1}{B}\sum_{b=1}^{B}h_nN(X_{h_n}|h_n\mu,\sigma^2Y_{h_nb})=\lim_{B\to\infty}\frac{1}{B}\sum_{b=1}^{B}\lim_{n\to\infty}h_nN(X_{h_n}|h_n\mu,\sigma^2Y_{h_nb}),$$

and analogously for the integrals containing $\frac{\partial}{\partial\mu}$ and $\frac{\partial}{\partial\sigma}$. Uniform integrability can be proven using uniform integrability test functions (Doob 2012). If for a $\varphi:[0,\infty)\to[0,\infty)$ with $\lim_{z\to\infty}\frac{\varphi(z)}{z}=\infty$ it holds true that $\sup_{n\in\mathbb{N}}E_\theta[\varphi(|h_nN(X_{h_n}(\omega)|h_n\mu,\sigma^2Y_{h_n})|)]<\infty$, then we have uniform integrability. We choose $\varphi(z)=z^2$. Since $p_{h_n}(y)$ is not available in closed form, we use two approximations. The first approximation $p^*_{h_n}(y):=R\Gamma(y|\nu/2,h_n^2\nu/2)$ is motivated by the fact that for $\nu=1$, $p_{h_n}(y)=p^*_{h_n}(y)$ for all $y>0,h_n>0$. Additionally, the approximation $p^*_{h_n}(y)$ is chosen because $p_{h_n}(y)<p^*_{h_n}(y)$ for small $y>0$ and $h_n<1$ (Lemma 3.4). The second approximation makes use of Lemma 2.1 in Chapter 2, which states that the Lévy measure of the inverse gamma subordinator is bounded from above by the explosive Lévy measure of the 1/2-stable Lévy subordinator with density function $\tilde{p}_{h_n}(y):=R\Gamma(y|1/2,h_n^2\nu/2)$ for every h_n if $\nu>1$. This implies that $p_{h_n}(y)<\tilde{p}_{h_n}(y)$ for large values of y. Hence for all n there exist $K_n^{(1)},K_n^{(2)}>0$ such that

$$\begin{aligned}
&\int_0^\infty h_n^2N(X_{h_n}|h_n\mu,\sigma^2y)^2p_{h_n}(y)\mathrm{d}y\\
=&\int_0^{K_n^{(1)}}h_n^2N(X_{h_n}|h_n\mu,\sigma^2y)^2p_{h_n}(y)\mathrm{d}y+\int_{K_n^{(1)}}^{K_n^{(2)}}h_n^2N(X_{h_n}|h_n\mu,\sigma^2y)^2p_{h_n}(y)\mathrm{d}y\\
&+\int_{K_n^{(2)}}^\infty h_n^2N(X_{h_n}|h_n\mu,\sigma^2y)^2p_{h_n}(y)\mathrm{d}y\\
\leq&C\left(\int_0^{K_n^{(1)}}\frac{h_n^2}{y}p^*_{h_n}(y)\mathrm{d}y+\int_{K_n^{(1)}}^{K_n^{(2)}}\frac{h_n^2}{y}p_{h_n}(y)\mathrm{d}y+\int_{K_n^{(2)}}^\infty\frac{h_n^2}{y}\tilde{p}_{h_n}(y)\mathrm{d}y\right)\\
\leq&C\left(\int_0^\infty\frac{h_n^2}{y}p^*_{h_n}(y)\mathrm{d}y+(K_n^{(2)}-K_n^{(1)})\frac{h_n^2}{K_n^{(1)}}p_{h_n}(K_n^{(1)})+\int_0^\infty\frac{h_n^2}{y}\tilde{p}_{h_n}(y)\mathrm{d}y\right)\\
=&C\left(1+(K_n^{(2)}-K_n^{(1)})\frac{h_n^2}{K_n^{(1)}}p_{h_n}(K_n^{(1)})+\frac{1}{\nu}\right),
\end{aligned}$$

where $C>0$ is a finite constant independent of y and n, which may vary from line to line. $(K_n^{(2)}-K_n^{(1)})\frac{h_n^2}{K_n^{(1)}}p_{h_n}(K_n^{(1)})$ converges to zero for $n\to\infty$ since $K_n^{(1)},K_n^{(2)}\to0$ and $\frac{h_n^2}{K_n^{(1)}}=\mathcal{O}(1)$. This implies uniform integrability for $h_nN(X_{h_n}|h_n\mu,\sigma^2Y_{h_n})$.

We also show uniform integrability for $\frac{\partial}{\partial\mu}h_nN(X_{h_n}|h_n\mu,\sigma^2y)$ by

$$\begin{aligned}
&\int_0^\infty h_n^2\left(\frac{\partial}{\partial\mu}N(X_{h_n}|h_n\mu,\sigma^2y)\right)^2 p_{h_n}(y)\mathrm{d}y\\
\leq& C\left(\int_0^\infty \frac{h_n^2(h_n(X_{h_n}-h_n\mu))^2}{y^3}p^*_{h_n}(y)\mathrm{d}y + (K_n^{(2)}-K_n^{(1)})\frac{h_n^2(h_n(X_{h_n}-h_n\mu))^2}{(K_n^{(1)})^3}p_{h_n}(K_n^{(1)})\right.\\
&\left.+\int_0^\infty \frac{h_n^2(h_n(X_{h_n}-h_n\mu))^2}{y^3}\tilde{p}_{h_n}(y)\mathrm{d}y\right)\\
\leq& C\left(\frac{(X_{h_n}-h_n\mu)^2}{h^2} + (K_n^{(2)}-K_n^{(1)})\frac{h_n^2(h_n(X_{h_n}-h_n\mu))^2}{(K_n^{(1)})^3}p_{h_n}(K_n^{(1)}) + \frac{(X_{h_n}-h_n\mu)^2}{h^2}\right),
\end{aligned}$$

and by Lemma 3.2 $\frac{(X_{h_n}-h_n\mu)^2}{h^2}\xrightarrow{\mathcal{L}}\tilde{X}^2$, $\tilde{X}\sim\text{Cauchy}(0,\sqrt{\nu})$ and $\tilde{X}^2$ is a.s. finite. Uniform integrability for $\frac{\partial}{\partial\sigma}h_nN(X_{h_n}|h_n\mu,\sigma^2y)$ can be proven analogously.

We are now able to check the assumptions (i)–(iii) of Lemma 3.1.

(i) We here derive the limiting form (3.3) of the Fisher information matrix. The expression (3.7) is crucial and is used multiple times subsequently. We begin with the first entry $\mathscr{I}^{(11)}(\theta)$.

$$\begin{aligned}
\lim_{n\to\infty} nE_\theta\left[\left(A_n^{(11)}g_{n1}^{(1)}(\theta)\right)^2\right] &= \lim_{n\to\infty} E_\theta\left[\left(\frac{\partial}{\partial\mu}\log p_{h_n}(\Delta_1^nX|\theta)\right)^2\right]\\
&= \lim_{n\to\infty} E_\theta\left[\left(\frac{\frac{\partial}{\partial\mu}p_{h_n}(X_{h_n}|\theta)}{p_{h_n}(X_{h_n}|\theta)}\right)^2\right]. \qquad (3.9)
\end{aligned}$$

We again make use of the fact that the Student-Lévy density can be expressed as (3.7). Hence, we can write (3.9) as

$$\begin{aligned}
&\lim_{n\to\infty} E_\theta\left[\frac{\left(\frac{\partial}{\partial\mu}\int_0^\infty N(X_{h_n}|h_n\mu,\sigma^2y)p_{h_n}(y)\mathrm{d}y\right)^2}{\left(\int_0^\infty N(X_{h_n}|h_n\mu,\sigma^2y)p_{h_n}(y)\mathrm{d}y\right)^2}\right]\\
=&\lim_{n\to\infty} E_\theta\left[\frac{\left(\int_0^\infty \frac{\partial}{\partial\mu}N(X_{h_n}|h_n\mu,\sigma^2y)p_{h_n}(y)\mathrm{d}y\right)^2}{\left(\int_0^\infty N(X_{h_n}|h_n\mu,\sigma^2y)p_{h_n}(y)\mathrm{d}y\right)^2}\right]. \qquad (3.10)
\end{aligned}$$

The bounded convergence theorem implies that (3.10) equals

$$E_\theta\left[\lim_{n\to\infty}\frac{h_n^2\left(\int_0^\infty \frac{\partial}{\partial\mu}N(X_{h_n}|h_n\mu,\sigma^2 y)p_{h_n}(y)\mathrm{d}y\right)^2}{h_n^2\left(\int_0^\infty N(X_{h_n}|h_n\mu,\sigma^2 y)p_{h_n}(y)\mathrm{d}y\right)^2}\right]$$
$$=E_\theta\left[\frac{\left(\lim_{n\to\infty} h_n\int_0^\infty \frac{\partial}{\partial\mu}N(X_{h_n}|h_n\mu,\sigma^2 y)p_{h_n}(y)\mathrm{d}y\right)^2}{\left(\lim_{n\to\infty} h_n\int_0^\infty N(X_{h_n}|h_n\mu,\sigma^2 y)p_{h_n}(y)\mathrm{d}y\right)^2}\right]. \tag{3.11}$$

Since the density $p_{h_n}(y)$ of Y_{h_n} is unknown, we cannot compute the inner integrals of (3.11) directly. Therefore, we use the approach of Monte Carlo integration. Let $\{Y_{h_n1}\},\ldots,\{Y_{h_nB}\}$ be independent inverse gamma subordinators, each independent of $(X_{kh_n})_{1\le k\le n}$, such that Y_{h_nb} has density function $p_{h_n}(y)$. (See Chapter 2 for more information on simulation of the inverse gamma subordinator.) Then, a.s.,

$$\lim_{n\to\infty}\int_0^\infty \frac{\partial}{\partial\mu}h_nN(X_{h_n}|h_n\mu,\sigma^2 y)p_{h_n}(y)\mathrm{d}y$$
$$=\lim_{n\to\infty}\lim_{B\to\infty}\frac{1}{B}\sum_{b=1}^{B}\frac{\partial}{\partial\mu}h_nN(X_{h_n}|h_n\mu,\sigma^2 Y_{h_nb})$$

and

$$\lim_{n\to\infty}\int_0^\infty h_nN(X_{h_n}|h_n\mu,\sigma^2 y)p_{h_n}(y)\mathrm{d}y$$
$$=\lim_{n\to\infty}\lim_{B\to\infty}\frac{1}{B}\sum_{b=1}^{B}h_nN(X_{h_n}|h_n\mu,\sigma^2 Y_{h_nb}).$$

By uniform integrability of $h_nN(X_{h_n}|h_n\mu,\sigma^2 y)$ and $\frac{\partial}{\partial\mu}h_nN(X_{h_n}|h_n\mu,\sigma^2 y)$ in y and n, (3.11) is equal to

$$E_\theta\left[\frac{\left(\lim_{B\to\infty}\frac{1}{B}\sum_{b=1}^{B}\lim_{n\to\infty}\frac{\partial}{\partial\mu}h_nN(X_{h_n}|h_n\mu,\sigma^2 Y_{h_nb})\right)^2}{\left(\lim_{B\to\infty}\frac{1}{B}\sum_{b=1}^{B}\lim_{n\to\infty}h_nN(X_{h_n}|h_n\mu,\sigma^2 Y_{h_nb})\right)^2}\right]. \tag{3.12}$$

Now,

$$N(X_{h_n}|h_n\mu,\sigma^2 Y_{h_nb}) = \frac{1}{\sqrt{2\pi\sigma^2 Y_{h_nb}}}\exp\left(-\frac{(X_{h_n}-h_n\mu)^2}{2\sigma^2 Y_{h_nb}}\right)$$
$$= \frac{1}{h_n}\frac{1}{\sqrt{2\pi\sigma^2\frac{Y_{h_nb}}{h_n^2}}}\exp\left(-\frac{(X_{h_n}-h_n\mu)^2}{2\sigma^2 h_n^2\frac{Y_{h_nb}}{h_n^2}}\right).$$

By Lemmas 3.2 and 3.3 we know that $\frac{X_{h_n}-h_n\mu}{h_n\sigma} \xrightarrow{\mathcal{L}} \tilde{X} \sim \text{Cauchy}(0,\sqrt{\nu})$ and $\frac{Y_{h_nb}}{h_n^2} \xrightarrow{\mathcal{L}} \tilde{Y}_b \sim \text{Lévy}(0,\nu)$ for any b. Then,

$$\frac{1}{\sqrt{2\pi\sigma^2\frac{Y_{h_nb}}{h_n^2}}}\exp\left(-\frac{(X_{h_n}-h_n\mu)^2}{2\sigma^2 h_n^2\frac{Y_{h_nb}}{h_n^2}}\right) \xrightarrow{\mathcal{L}} \frac{1}{\sqrt{2\pi\sigma^2\tilde{Y}_b}}\exp\left(-\frac{\tilde{X}^2}{2\tilde{Y}_b}\right),$$

as $n\to\infty$. Analogously,

$$\frac{\partial}{\partial\mu}N(X_{h_n}|h_n\mu,\sigma^2 Y_{h_nb}) = \frac{1}{\sqrt{2\pi\sigma^2 Y_{h_nb}}}\exp\left(-\frac{(X_{h_n}-h_n\mu)^2}{2\sigma^2 Y_{h_nb}}\right)h_n\frac{X_{h_n}-h_n\mu}{\sigma^2 Y_{h_nb}}$$
$$= \frac{1}{h_n}\frac{1}{\sqrt{2\pi\sigma^2\frac{Y_{h_nb}}{h_n^2}}}\exp\left(-\frac{(X_{h_n}-h_n\mu)^2}{2\sigma^2 h_n^2\frac{Y_{h_nb}}{h_n^2}}\right)\frac{1}{\sigma}\frac{X_{h_n}-h_n\mu}{\sigma h_n\frac{Y_{h_nb}}{h_n^2}},$$

and

$$\frac{1}{\sqrt{2\pi\sigma^2\frac{Y_{h_nb}}{h_n^2}}}\exp\left(-\frac{(X_{h_n}-h_n\mu)^2}{2\sigma^2 h_n^2\frac{Y_{h_nb}}{h_n^2}}\right)\frac{1}{\sigma}\frac{X_{h_n}-h_n\mu}{\sigma h_n\frac{Y_{h_nb}}{h_n^2}} \xrightarrow{\mathcal{L}} \frac{1}{\sqrt{2\pi\sigma^2\tilde{Y}_b}}\exp\left(-\frac{\tilde{X}^2}{2\tilde{Y}_b}\right)\frac{\tilde{X}}{\sigma\tilde{Y}_b}.$$

Using this expression in (3.12) (note that the $1/h_n$ factors cancel each other out), (3.12) equals

$$E_\theta\left[\frac{\left(\lim_{B\to\infty}\frac{1}{B}\sum_{b=1}^{B}\lim_{n\to\infty}\frac{\partial}{\partial\mu}h_nN(X_{h_n}|h_n\mu,\sigma^2Y_{h_nb})\right)^2}{\left(\lim_{B\to\infty}\frac{1}{B}\sum_{b=1}^{B}\lim_{n\to\infty}h_nN(X_{h_n}|h_n\mu,\sigma^2Y_{h_nb})\right)^2}\right]$$

$$= E_\theta \left[\frac{\left(\lim_{B\to\infty} \frac{1}{B} \sum_{b=1}^{B} \frac{1}{\sqrt{2\pi\sigma^2 \tilde{Y}_b}} \exp\left(-\frac{\tilde{X}^2}{2\tilde{Y}_b}\right) \frac{\tilde{X}}{\sigma \tilde{Y}_b} \right)^2}{\left(\lim_{B\to\infty} \frac{1}{B} \sum_{b=1}^{B} \frac{1}{\sqrt{2\pi\sigma^2 \tilde{Y}_b}} \exp\left(-\frac{\tilde{X}^2}{2\tilde{Y}_b}\right) \right)^2} \right]$$

$$= E_\theta \left[\frac{\left(\int_0^\infty \frac{1}{\sqrt{2\pi\sigma^2 y}} \exp\left(-\frac{\tilde{X}^2}{2y}\right) \frac{\tilde{X}}{\sigma y} p_{\tilde{Y}}(y) \mathrm{d}y \right)^2}{\left(\int_0^\infty \frac{1}{\sqrt{2\pi\sigma^2 y}} \exp\left(-\frac{\tilde{X}^2}{2y}\right) p_{\tilde{Y}}(y) \mathrm{d}y \right)^2} \right], \tag{3.13}$$

by reversing the Monte Carlo integration argument. $p_{\tilde{Y}}(y)$ denotes the density function of $\tilde{Y} \sim \text{Lévy}(0, \nu)$. The inner integrals of (3.13) can be computed explicitly, that is

$$E_\theta \left[\frac{\left(\frac{2\sqrt{\nu}\tilde{X}}{\pi\sigma^2(\tilde{X}^2+\nu)^2} \right)^2}{\left(\frac{\sqrt{\nu}}{\pi\sigma(\tilde{X}^2+\nu)} \right)^2} \right] = \int_{-\infty}^{\infty} \frac{4x^2}{\sigma^2(x^2+\nu)^2} p_{\tilde{X}}(x) \mathrm{d}x = \frac{1}{2\nu\sigma^2},$$

where $p_{\tilde{X}}(x)$ is the density function of the Cauchy$(0, \sqrt{\nu})$ distribution.

We continue with the computation of $\mathscr{I}^{(22)}(\theta)$. Analogously to the computation above,

$$\begin{aligned}
&\lim_{n\to\infty} n E_\theta \left[\left(A_n^{(22)} g_{n1}^{(2)}(\theta) \right)^2 \right] \\
=& \lim_{n\to\infty} E_\theta \left[\left(\frac{\frac{\partial}{\partial\sigma} p_{h_n}(X_{h_n}|\theta)}{p_{h_n}(X_{h_n}|\theta)} \right)^2 \right] \\
=& E_\theta \left[\frac{\left(\lim_{B\to\infty} \frac{1}{B} \sum_{b=1}^{B} \lim_{n\to\infty} h_n \frac{\partial}{\partial\sigma} N(X_{h_n}|h_n\mu, \sigma^2 Y_{h_n b}) \right)^2}{\left(\lim_{B\to\infty} \frac{1}{B} \sum_{b=1}^{B} \lim_{n\to\infty} h_n N(X_{h_n}|h_n\mu, \sigma^2 Y_{h_n b}) \right)^2} \right].
\end{aligned} \tag{3.14}$$

Then,

$$\begin{aligned}
&\frac{\partial}{\partial\sigma} N(X_{h_n}|h_n\mu, \sigma^2 Y_{h_n b}) \\
=& \frac{1}{\sqrt{2\pi\sigma^2 Y_{h_n b}}} \exp\left(-\frac{(X_{h_n}-h_n\mu)^2}{2\sigma^2 Y_{h_n b}}\right) \frac{1}{\sigma^2} \frac{(X_{h_n}-h_n\mu)^2}{\sigma^2 Y_{h_n b}}
\end{aligned}$$

$$
\begin{aligned}
&- \frac{1}{\sqrt{2\pi\sigma^2 Y_{h_n b}}} \exp\left(-\frac{(X_{h_n} - h_n\mu)^2}{2\sigma^2 Y_{h_n b}}\right) \frac{1}{\sigma^2} \\
=&\frac{1}{h_n}\frac{1}{\sigma^2}\frac{1}{\sqrt{2\pi\sigma^2 \frac{Y_{h_n b}}{h_n^2}}} \exp\left(-\frac{(X_{h_n} - h_n\mu)^2}{2\sigma^2 h_n^2 \frac{Y_{h_n b}}{h_n^2}}\right)\left(\frac{(X_{h_n} - h_n\mu)^2}{\sigma^2 h_n^2 \frac{Y_{h_n b}}{h_n^2}} - 1\right),
\end{aligned}
$$

and

$$
\begin{aligned}
&\frac{1}{\sigma^2}\frac{1}{\sqrt{2\pi\sigma^2 \frac{Y_{h_n b}}{h_n^2}}} \exp\left(-\frac{(X_{h_n} - h_n\mu)^2}{2\sigma^2 h_n^2 \frac{Y_{h_n b}}{h_n^2}}\right)\left(\frac{(X_{h_n} - h_n\mu)^2}{\sigma^2 h_n^2 \frac{Y_{h_n b}}{h_n^2}} - 1\right) \\
\xrightarrow{\mathcal{L}} &\frac{1}{\sigma^2}\frac{1}{\sqrt{2\pi\tilde{Y}_b}} \exp\left(-\frac{\tilde{X}^2}{2\tilde{Y}_b}\right)\left(\frac{\tilde{X}^2}{\tilde{Y}_b} - 1\right)
\end{aligned}
$$

as $n \to \infty$. Therefore, (3.14) equals

$$
\begin{aligned}
&E_\theta\left[\frac{\left(\int_0^\infty \frac{1}{\sigma^2}\frac{1}{\sqrt{2\pi y}} \exp\left(-\frac{\tilde{X}^2}{2y}\right)\left(\frac{\tilde{X}^2}{y} - 1\right) p_{\tilde{Y}}(y)\mathrm{d}y\right)^2}{\left(\int_0^\infty \frac{1}{\sqrt{2\pi\sigma^2 y}} \exp\left(-\frac{\tilde{X}^2}{2y}\right) p_{\tilde{Y}}(y)\mathrm{d}y\right)^2}\right] \\
&= E_\theta\left[\frac{\left(\frac{(\tilde{X}^2-\nu)\sqrt{\nu}}{\pi\sigma^2(\tilde{X}^2+\nu)^2}\right)^2}{\left(\frac{\sqrt{\nu}}{\pi\sigma(\tilde{X}^2+\nu)}\right)^2}\right] \\
&= \frac{1}{2\sigma^2}.
\end{aligned}
$$

For the off-diagonal elements $\mathscr{I}^{(12)}(\theta) = \mathscr{I}^{(21)}(\theta)$ observe that

$$
\begin{aligned}
&\lim_{n\to\infty} nE_\theta\left[\left(A_n^{(11)} g_{n1}^{(1)}(\theta)\right)\left(A_n^{(22)} g_{n1}^{(2)}(\theta)\right)\right] \\
=&E_\theta\left[\frac{\left(\frac{2\sqrt{\nu}\tilde{X}}{\pi\sigma^2(\tilde{X}^2+\nu)^2}\right)\left(\frac{(\tilde{X}^2-\nu)\sqrt{\nu}}{\pi\sigma^2(\tilde{X}^2+\nu)^2}\right)}{\left(\frac{\sqrt{\nu}}{\pi\sigma(\tilde{X}^2+\nu)}\right)^2}\right] = 0.
\end{aligned}
$$

(ii) Use

$$\lim_{n\to\infty} E_\theta\left[\frac{\frac{\partial}{\partial\mu}p_{h_n}(X_{h_n}|\theta)}{p_{h_n}(X_{h_n}|\theta)}\right] = E_\theta\left[\frac{2\tilde{X}}{\sigma(\tilde{X}^2+\nu)}\right] = 0,$$

and

$$\lim_{n\to\infty} E_\theta\left[\frac{\frac{\partial}{\partial\sigma}p_{h_n}(X_{h_n}|\theta)}{p_{h_n}(X_{h_n}|\theta)}\right] = E_\theta\left[\frac{\tilde{X}^2-\nu}{\sigma(\tilde{X}^2+\nu)}\right] = 0,$$

which implies (ii).

(iii) We continue by verifying the Lindeberg condition. First,

$$nE_\theta\left[\left(A_n^{(11)}g_{n1}^{(1)}(\theta)\right)^4\right] \sim \frac{1}{n}E_\theta\left[\frac{16\tilde{X}^4}{\sigma^4(\tilde{X}+\nu)^4}\right] = \frac{1}{n}\frac{3}{8\nu^2\sigma^4},$$
$$nE_\theta\left[\left(A_n^{(22)}g_{n1}^{(2)}(\theta)\right)^4\right] \sim \frac{1}{n}E_\theta\left[\frac{(\tilde{X}-\nu)^4}{\sigma^4(\tilde{X}^2+\nu)^4}\right] = \frac{1}{n}\frac{3}{8\sigma^4},$$

which both converge to zero for $n\to\infty$. The compactness of $\overline{\Theta}$ implies that

$$\lim_{n\to\infty}\sup_{\theta\in\Theta} nE_\theta\left[|A_n g_{n1}(\theta)|^4\right] = 0.$$

Second, we look at the entries of the Hessian matrix $\nabla(g_{n1}(\theta)^{\mathrm{T}})$. Note that $h_n\frac{\partial^2}{\partial\mu^2}N(X_{h_n}|h_n\mu,\sigma^2Y_{h_nb})$, $h_n\frac{\partial^2}{\partial\sigma^2}N(X_{h_n}|h_n\mu,\sigma^2Y_{h_nb})$ and $h_n\frac{\partial^2}{\partial\mu\partial\sigma}N(X_{h_n}|h_n\mu,\sigma^2Y_{h_nb})$ are uniformly integrable, analogously to the terms above. Thus

$$h_n\frac{\partial^2}{\partial\mu^2}N(X_{h_n}|h_n\mu,\sigma^2Y_{h_nb})$$
$$\xrightarrow{\mathcal{L}}\left(\frac{1}{\sqrt{2\pi\sigma^2\tilde{Y}_b}}\exp\left(-\frac{\tilde{X}^2}{2\tilde{Y}_b}\right)\right)\left(\frac{\tilde{X}^2}{\sigma^2\tilde{Y}_b^2}-\frac{1}{\sigma^2\tilde{Y}_b}\right),$$

and

$$h_n\frac{\partial^2}{\partial\sigma^2}N(X_{h_n}|h_n\mu,\sigma^2Y_{h_nb})$$
$$\xrightarrow{\mathcal{L}}\left(\frac{1}{\sqrt{2\pi\sigma^2\tilde{Y}_b}}\exp\left(-\frac{\tilde{X}^2}{2\tilde{Y}_b}\right)\right)\left(-\frac{2\tilde{X}^2}{\sigma^2\tilde{Y}_b}+\frac{2}{\sigma^2}+\frac{\tilde{X}^4}{\sigma^2\tilde{Y}_b^2}-\frac{3\tilde{X}^2}{\sigma^2\tilde{Y}_b}\right),$$

and cross partial derivative

$$\begin{aligned}
&h_n \frac{\partial^2}{\partial\mu\partial\sigma} N(X_{h_n}|h_n\mu, \sigma^2 Y_{h_n b}) \\
\xrightarrow{\mathcal{L}} &\left(\frac{1}{\sqrt{2\pi\sigma^2\tilde{Y}_b}} \exp\left(-\frac{\tilde{X}^2}{2\tilde{Y}_b}\right)\right)\left(\frac{\tilde{X}^3}{\sigma^2\tilde{Y}_b^2} - \frac{3\tilde{X}}{\sigma^2\tilde{Y}_b}\right).
\end{aligned}$$

Hence, by repeating the Monte Carlo integration argument,

$$\begin{aligned}
&nE_\theta\left[\left(A_n^{(11)}\frac{\partial^2}{\partial\mu^2}\log p_{h_n}(X_{h_n}|\theta)A_n^{(11)}\right)^2\right] \\
=&\frac{1}{n}E_\theta\left[\left(\frac{\frac{\partial^2}{\partial\mu^2}p_{h_n}(X_{h_n}|\theta)}{p_{h_n}(X_{h_n}|\theta)} - \left(\frac{\frac{\partial}{\partial\mu}p_{h_n}(X_{h_n}|\theta)}{p_{h_n}(X_{h_n}|\theta)}\right)^2\right)^2\right] \\
\sim&\frac{1}{n}E_\theta\left[\left(\frac{-\frac{2\nu(-3\tilde{X}^2+\nu)}{\pi\sigma^3(\tilde{X}^2+\nu)^3}}{\frac{\sqrt{\nu}}{\pi\sigma(\tilde{X}^2\nu)}} - \left(\frac{4\tilde{X}^2}{\sigma^2(\tilde{X}^2+\nu)^2}\right)^2\right)^2\right] \\
=&\frac{1}{n}\frac{7}{8\nu^2\sigma^4},
\end{aligned}$$

and

$$\begin{aligned}
&nE_\theta\left[\left(A_n^{(22)}\frac{\partial^2}{\partial\sigma^2}\log p_{h_n}(X_{h_n}|\theta)A_n^{(22)}\right)^2\right] \\
=&\frac{1}{n}E_\theta\left[\left(\frac{\frac{\partial^2}{\partial\sigma^2}p_{h_n}(X_{h_n}|\theta)}{p_{h_n}(X_{h_n}|\theta)} - \left(\frac{\frac{\partial}{\partial\sigma}p_{h_n}(X_{h_n}|\theta)}{p_{h_n}(X_{h_n}|\theta)}\right)^2\right)^2\right] \\
\sim&\frac{1}{n}E_\theta\left[\left(\frac{\frac{2\nu^{3/2}(-3\tilde{X}^2+\nu)}{\pi\sigma^3(\tilde{X}^2+\nu)^3}}{\frac{\sqrt{\nu}}{\pi\sigma(\tilde{X}^2\nu)}} - \left(\frac{(\tilde{X}^2-\nu)^2}{\sigma^2(\tilde{X}^2+\nu)^2}\right)^2\right)^2\right] \\
=&\frac{1}{n}\frac{7}{8\sigma^4},
\end{aligned}$$

and

$$
\begin{aligned}
& nE_\theta\left[\left(A_n^{(11)}\frac{\partial^2}{\partial\mu\partial\sigma}\log p_{h_n}(X_{h_n}|\theta)A_n^{(22)}\right)^2\right] \\
=&\frac{1}{n}E_\theta\left[\left(\frac{\frac{\partial^2}{\partial\mu\partial\sigma}p_{h_n}(X_{h_n}|\theta)}{p_{h_n}(X_{h_n}|\theta)}-\frac{\frac{\partial}{\partial\mu}p_{h_n}(X_{h_n}|\theta)\frac{\partial}{\partial\sigma}p_{h_n}(X_{h_n}|\theta)}{p_{h_n}(X_{h_n}|\theta)^2}\right)^2\right] \\
\sim&\frac{1}{n}E_\theta\left[\left(\frac{\frac{2\sqrt{\nu}\tilde{X}(\tilde{X}^2-3\nu)}{\pi\sigma^3(\tilde{X}^2+\nu)^3}}{\frac{\sqrt{\nu}}{\pi\sigma(\tilde{X}^2\nu)}}-\frac{\left(\frac{2\sqrt{\nu}\tilde{X}}{\pi\sigma^2(\tilde{X}^2+\nu)^2}\right)\left(\frac{(\tilde{X}^2-\nu)\sqrt{\nu}}{\pi\sigma^2(\tilde{X}^2+\nu)^2}\right)}{\left(\frac{\sqrt{\nu}}{\pi\sigma(\tilde{X}^2+\nu)}\right)^2}\right)^2\right] \\
=&\frac{1}{n}\frac{5}{8\nu\sigma^4},
\end{aligned}
$$

as $n\to\infty$. This implies

$$\lim_{n\to\infty}\sup_{\theta\in\Theta}nE_\theta\left[|A_n\nabla(g_{n1}(\theta)^{\mathrm{T}})A_n|^2\right]=0,$$

since the matrix norm is the Frobenius norm and $\overline{\Theta}$ is compact. This completes the proof.

□

Having obtained the result for the non-skew Student-Lévy process, it is natural to ask if it can be extended to the skew Student-Lévy process. The answer is no.

Proposition 3.1. *Let $\{X_t\}$ be the skew Student-Lévy process (Definition 1.3) such that $\mathcal{L}(X_1)=t(\nu,\mu,\sigma^2,\beta)$ (with known ν). The LAN (3.1) property for $\theta=(\mu,\sigma,\beta)\in\Theta$ with Θ bounded and convex such that $\overline{\Theta}\subset\mathbb{R}\times(0,\infty)\times(\mathbb{R}\backslash\{0\})$ does not hold true, since the Fisher information $\mathscr{I}(\theta)$ does not exist for $A_n=\mathrm{diag}(\sqrt{n},\sqrt{n},\sqrt{n}h_n)^{-1}$ converging to zero as $n\to\infty$, i.e., $\sqrt{n}h_n\to\infty$ as $n\to\infty$.*

The proposition requires that $\sqrt{nh_n^2}=\sqrt{T_nh_n}\to\infty$ as $n\to\infty$, implying that the upper boundary of the sampling interval T_n has to tend to infinity. If this is not given (e.g., if $T\equiv T_n$) we also have no LAN result because in this case A_n is divergent.

Proof of Proposition 3.1. Consider a sample $(X_{kh_n})_{1\le k\le n}$. First, similarly to the proof of Lemma 3.2, we check the local stability of the skew Student-Lévy process.

Recall Definition 1.3 and that $X_1 \sim t(\nu, \mu, \sigma^2, \beta)$ has the characteristic function

$$\frac{K_{\nu/2}(\sqrt{\nu}\sigma\sqrt{u^2 - 2\mathrm{i}\beta u})(\sqrt{\nu}\sigma)^{\nu/2}(u^2 - 2\mathrm{i}\beta u)^{\nu/4}e^{\mathrm{i}\mu u}}{\Gamma\left(\frac{\nu}{2}\right)2^{\nu/2-1}}.$$

Then $\frac{X_{kh_n} - h_n\mu}{h_n\sigma}$ has the characteristic function

$$\left(\frac{K_{\nu/2}\left(\sqrt{\nu}\sigma\sqrt{\frac{u^2}{h_n^2\sigma^2} - 2\mathrm{i}\beta\frac{u}{h_n\sigma}}\right)\left(\sqrt{\nu}\sigma\right)^{\nu/2}\left(\frac{u^2}{h_n^2\sigma^2} - 2\mathrm{i}\beta\frac{u}{h_n\sigma}\right)^{\nu/4}}{\Gamma\left(\frac{\nu}{2}\right)2^{\nu/2-1}}\right)^{h_n}.$$

All terms, except the one with the Bessel function, tend to unity as $n \to \infty$. As above we have

$$\begin{aligned}
K_{\nu/2}\left(\sqrt{\nu}\sqrt{\frac{u^2}{h_n^2} - 2\mathrm{i}\beta\sigma\frac{u}{h_n}}\right)^{h_n} &\sim \sqrt{\frac{\pi}{2\sqrt{\nu}\sqrt{\frac{u^2}{h_n^2} - 2\mathrm{i}\beta\sigma\frac{u}{h_n}}}}^{h_n} \exp\left(-\sqrt{\nu}\sqrt{\frac{u^2}{h_n^2} - 2\mathrm{i}\beta\sigma\frac{u}{h_n}}\right)^{h_n} \\
&\sim \exp\left(-\sqrt{\nu}\sqrt{u^2 - 2\mathrm{i}\beta\sigma u h_n}\right) \\
&\to \exp\left(-\sqrt{\nu}|u|\right),
\end{aligned}$$

for $h_n \to 0$, which is the characteristic function of $\tilde{X} \sim \text{Cauchy}(0, \sqrt{\nu})$.

Second, we focus on $\frac{\partial}{\partial\beta}p_{h_n}(X_{h_n}|\theta)$. The skew Student-Lévy process $\{X_t\}$ can be constructed by $X_t = \sigma B_{Y_t} + \beta\sigma^2 Y_t + \mu t$ with an inverse gamma subordinator $\{Y_t\}$ such that $Y_1 \sim R\Gamma(\nu/2, \nu/2)$ and with a Brownian motion $\{B_t\}$. Then $X_t|Y_t \sim N(\mu t + \beta\sigma^2 Y_t, \sigma^2 Y_t)$. Thus,

$$\begin{aligned}
&\frac{\partial}{\partial\beta}N(X_{h_n}|h_n\mu + \beta\sigma^2 Y_{h_n b}, \sigma^2 Y_{h_n b}) \\
&= \exp\left(-\frac{(X_{h_n} - h_n\mu - \beta\sigma^2 Y_{h_n b})^2}{2\sigma^2 Y_{h_n b}}\right)\frac{X_{h_n} - h_n\mu - \beta\sigma^2 Y_{h_n b}}{\sqrt{2\pi\sigma^2 Y_{h_n b}}} \\
&\xrightarrow{\mathcal{L}} \exp\left(-\frac{\tilde{X}^2}{2\tilde{Y}_b}\right)\frac{\tilde{X}}{\sqrt{2\pi\tilde{Y}_b}}.
\end{aligned}$$

This is because $\frac{X_{h_n}-h_n\mu-\beta\sigma^2 Y_{h_nb}}{h_n\sigma} \overset{\mathcal{L}}{\sim} \frac{X_{h_n}-h_n\mu}{h_n\sigma}$ as $\frac{Y_{h_nb}}{h_n} \xrightarrow{p} 0$. Using

$$\int_0^\infty \exp\left(-\frac{\tilde{X}^2}{2y}\right)\frac{\tilde{X}}{\sqrt{2\pi y}}p_{\tilde{Y}}(y)\mathrm{d}y = \frac{\sqrt{\nu}\tilde{X}}{\pi(\tilde{X}^2+\nu)}$$

yields

$$\frac{1}{h_n^2}\left(\frac{\frac{\partial}{\partial\beta}p_{h_n}(X_{h_n}|\theta)}{p_{h_n}(X_{h_n}|\theta)}\right)^2 \xrightarrow{\mathcal{L}} \left(\frac{\frac{\sqrt{\nu}\tilde{X}}{\pi(\tilde{X}^2+\nu)}}{\frac{\sqrt{\nu}}{\pi\sigma(\tilde{X}^2+\nu)}}\right)^2 = \sigma^2\tilde{X}^2.$$

This means that for rate $A_n^{(33)} = \frac{1}{\sqrt{n}h_n}$ we have

$$E_\theta\left[\sigma^2\tilde{X}^2\right] = \infty,$$

implying that, by Fatou's Lemma, the LAN property does not hold true. □

The issue of having no LAN result cannot be solved by simply choosing another rate $A_n^{(33)}$. For example, if $A_n^{(33)} = (nh_n)^{-1}$, this would cause a singular Fisher information matrix and thus make the LAN result not meaningful (see, Masuda 2015).

This means that joint asymptotic normality (and optimality) for the MLE is not available. Fortunately, the result of Theorem 3.1 remains valid if we treat the non-zero skewness parameter β as known.

Corollary 3.1. *Let $\{X_t\}$ be the skew Student-Lévy process such that $\mathcal{L}(X_1) = t(\nu,\mu,\sigma^2,\beta)$ (with known ν and β). The LAN holds true for $\theta = (\mu,\sigma)$ with Fisher information* (3.3) *and rate* (3.2) *of Theorem 3.1.*

Proof. The proof is analogous to the proof of Theorem 3.1 but using the local Cauchy property of Proposition 3.1. Note that $N(X_{h_n}|h_n\mu+\beta\sigma^2Y_{h_nb},\sigma^2Y_{h_nb})$, $\frac{\partial}{\partial\mu}N(X_{h_n}|h_n\mu+\beta\sigma^2Y_{h_nb},\sigma^2Y_{h_nb})$, and $\frac{\partial}{\partial\sigma}N(X_{h_n}|h_n\mu+\beta\sigma^2Y_{h_nb},\sigma^2Y_{h_nb})$ have the same limiting behavior as for $\beta=0$ because $\frac{X_{h_n}-h_n\mu-\beta Y_{h_nb}}{h_n\sigma} \overset{\mathcal{L}}{\sim} \frac{X_{h_n}-h_n\mu}{h_n\sigma}$. Moreover, for the computation of $\mathscr{I}^{(22)}(\theta)$ and $\mathscr{I}^{(12)}(\theta)$, we use $(X_{h_n}-h_n\mu-Y_{h_n,b}\beta\sigma^2) \xrightarrow{p} 0$. □

Remark 3.3. We here find a special case of the generalized hyperbolic (GH) Lévy process for which the LAN does not hold. This means that it cannot be true for all parameter constellations of the GH process. More research is needed to find the conditions under which the LAN property holds.

We end the discussion of discretely sampled Student-Lévy processes with a short remark concerning low-frequency sampling.

Remark 3.4. Lemma 3.1 is also valid for low-frequency sampling with the difference that $h_n \to h$ for $n \to \infty$ implying that $p_h(x|\theta)$ is the h transition density of the X_h of the Student-Lévy process and is not available in closed form. This carries over to the Fisher information and is therefore omitted here. There is one exception, namely if $h = 1$. Then the transition density and the Fisher information are known explicitly, but we refer to Lange et al. (1989) for this standard case.

3.2.1 Continuous sampling

We now take a little detour and discuss the case of continuous data where the full path $\{X_t\}_{t\in[0,T]}$ is observed. We are interested in the estimation of parameters and the asymptotics when $T \to \infty$. Although this setting is unrealistic, it is interesting to spell out the differences to high-frequency sampling. It may be the case that some parameters can be estimated without error when we observe the whole path. To identify these parameters Raible (2000) (see also Masuda (2015) and Sato (1999)) proved the following proposition, which provides a criterion for when the likelihood ratio $\frac{P_{\theta_1}|_{\mathcal{F}_T}}{P_{\theta_2}|_{\mathcal{F}_T}}$ for parameters θ_1 and θ_2 is well-defined, where $P_\theta|_{\mathcal{F}_T}$ denotes the restriction of P_θ to the natural filtration $\mathcal{F}_T$ generated by $\{X_t\}_{t\leq T}$.

Proposition 3.2. *Let $\{X_t\}$ be a (one-dimensional) Lévy process with characteristics $(\gamma(\theta), A(\theta), \Pi(\mathrm{d}x;\theta))$ for $\theta \in \Theta \subset \mathbb{R}^p$. Let $T > 0$ and $\theta_1, \theta_2 \in \Theta$. Then the measures $P_{\theta_1}|_{\mathcal{F}_T}$ and $P_{\theta_2}|_{\mathcal{F}_T}$ are equivalent iff the following conditions hold true.*

(i) $\Pi(\mathrm{d}x;\theta_2) = k(x;\theta_1,\theta_2)\Pi(\mathrm{d}x;\theta_2)$ *for some Borel function* $k(\cdot;\theta_1,\theta_2) : \mathbb{R} \to (0,\infty)$,

(ii) $\gamma(\theta_2) = \gamma(\theta_1) + \int_{\mathbb{R}} x(k(x;\theta_1,\theta_2) - 1)\Pi(\mathrm{d}x;\theta_1) + \sqrt{A(\theta_1)}b$ *for some* b,

(iii) $A(\theta_2) = A(\theta_1)$,

(iv) $\int_{\mathbb{R}} \left(1 - \sqrt{k(x;\theta_1,\theta_2)}\right)^2 \Pi(\mathrm{d}x;\theta) < \infty$.

Using this criterion we obtain the following

Corollary 3.2. *Let $T > 0$ and let P_{θ_k}, $k = 1, 2$ denote the distribution of the Student-Lévy process with parameters $\theta_k = (\nu_k, \mu_k, \sigma_k, \beta_k)$. Then $P_{\theta_1}|_{\mathcal{F}_T}$ and $P_{\theta_2}|_{\mathcal{F}_T}$ are equivalent iff $\mu_1 = \mu_2$ and $\sqrt{\nu_1}\sigma_1 = \sqrt{\nu_2}\sigma_2$.*

Proof. Raible (2000) proved this for the more general GH process with 1-increments distributed as $GH(\lambda_k, \alpha_k, \beta_k, \delta_k, \mu_k)$. The measures are equivalent iff $\delta_1 = \delta_2$ and $\mu_1 = \mu_2$. The Student t distribution $t(\nu_k, \mu_k, \sigma_k^2, \beta_k)$ is the limiting case of the GH distribution $GH(-\frac{\nu_k}{2}, |\beta_k|, \beta_k, \sqrt{\nu_k}\sigma_k, \mu_k)$. □

Where ν is known, this reduces to $\sigma_1 = \sigma_2$. This means we can find (μ, σ) by observing the path. Raible (2000) proved that the statistics

$$\hat{\sigma}_{T,n} := \frac{\pi}{\sqrt{\nu} n T} \#\{t \leq T : \Delta X_t \geq 1/n\}, \tag{3.15}$$

$$\hat{\mu}_{T,n} = \frac{1}{T} \left(X_T - \sum_{0<t\leq T} \Delta X_t \mathbb{1}_{[1/n,\infty)}(|\Delta X_t|) \right) \tag{3.16}$$

are strongly consistent estimators of σ and μ, as $n \to \infty$. If we observe the path in continuous time we can compute $\sigma \overset{a.s.}{=} \lim_{n\to\infty} \hat{\sigma}_{T,n}$ and $\mu \overset{a.s.}{=} \lim_{n\to\infty} \hat{\mu}_{T,n}$. Section 3.4 compares these estimators (where the data is obviously available not continuously but in high-frequency) with the high-frequency MLE.

3.3 Numerical methods

Of course, the theory from the previous section is not directly informative about how to actually compute the MLE. As is the case for the Student t distribution (i.e., the Student-Lévy process observing 1-increments) the MLE does not exist in closed form. This carries over to the Student-Lévy process when observing $\Delta_k^n X$ with $h_n \neq 1$. Moreover, the density function of $\Delta_k^n X$ is not given explicitly. We discuss two approaches to tackling this issue. First, we numerically maximize the Fourier inversion of the characteristic function. Second, we use a Monte Carlo Expectation-Maximization (MCEM) algorithm. The first approach is less elegant and substantially slower to execute than the second one but involves no randomness.

Let $\varphi_{X_1} = \varphi_{\nu,\mu,\sigma^2}$ be the characteristic function of the 1-increment, i.e., the characteristic function of $t(\nu, \mu, \sigma^2)$. Then, the transition density of $\Delta_k^n X$ can be numerically found via

$$p_{h_n}(\Delta_k^n X|\theta) = \frac{1}{2\pi} \int \exp(-\mathrm{i}u\Delta_k^n X)\varphi_{X_1}(u)^{h_n} \mathrm{d}u. \tag{3.17}$$

There are multiple ways to numerically compute this integral. For example, by a suitable discretization and subsequent application of the Fast Fourier Transform algorithm; see Walker (1996) among many others. Instead, we here use a global adaptive Gauss-Kronrod quadrature rule (Piessens & Branders 1974). The log-likelihood function $\ell(\theta)$ can be numerically maximized in θ by the Nelder & Mead (1965) method. One issue with this method is that Fourier inversion needs to be executed extensively, which is highly time-consuming. Thus, we will use this approach only for comparison. We call it the *Characteristic Function–Maximum Likelihood Estimator* (CF-MLE).

As an alternative, we discuss an MCEM approach. The EM algorithm was developed by Dempster et al. (1977) and a Monte Carlo extension was proposed by Wei & Tanner (1990). We first sketch the details of how the EM algorithm works. Then we apply it to the present Student-Lévy scenario and explain why the MC extension is used. The resulting ML estimation routine is summarized in Algorithm 5.

We follow McLachlan & Krishnan (2007) for the details of the EM algorithm. The idea behind EM is to assume that besides the observed data $\boldsymbol{x}$ with density function $p(\boldsymbol{x}|\theta)$, there are missing values $\boldsymbol{y}$ which we cannot observe. If we could observe them, ML estimation using the joint density $p(\boldsymbol{x}, \boldsymbol{y}|\theta)$ would be easy.

Denote by $\ell(\theta|\boldsymbol{x})$ the incomplete log-likelihood and by $\ell(\theta|\boldsymbol{x}, \boldsymbol{y})$ the complete log-likelihood. Take some initial value θ_0. The following E- and M-steps are repeated alternately. On the $(j+1)$-th iteration we have:

- **E-Step.** Calculate

$$Q(\theta|\theta_j) := E_{\theta_j}[\ell(\theta|\boldsymbol{x}, \boldsymbol{y})|\boldsymbol{x}] = \int \log p(\boldsymbol{x}, \boldsymbol{y}|\theta) p(\boldsymbol{y}|\boldsymbol{x}, \theta_j) \mathrm{d}\boldsymbol{y}.$$

- **M-Step.** Find a value θ_{j+1} that maximizes $Q(\theta|\theta_j)$:

$$\theta_{j+1} = \arg\max Q(\theta|\theta_j).$$

In practice, we repeat the E- and M-steps until the sequence $\{\theta_j\}$ converges. We omit here the proof that the EM algorithm indeed finds the MLE and refer to Dempster et al. (1977) or McLachlan & Krishnan (2007), but note that the M-step implies that the incomplete-data log-likelihood function is non-decreasing, i.e.

$$\ell(\theta_{j+1}|\boldsymbol{x}) \geq \ell(\theta_j|\boldsymbol{x})$$

for any $j = 0, 1, \ldots$.

If the E-step is difficult to compute, i.e., the expectation has no closed form, as in the present Student-Lévy case, we replace the E-step with the following MCE-step. Assume that the missing data $\boldsymbol{y}$ can be sampled from the posterior latent distribution $p(y|\boldsymbol{x}, \theta_j)$. Then we have

- **MCE-Step.**

$$\hat{Q}(\theta|\theta_j) := \frac{1}{B} \sum_{b=1}^{B} \log p(\boldsymbol{x}, \boldsymbol{y}_b|\theta) \to Q(\theta|\theta_j),$$

  a.s., for $\boldsymbol{y}_b \sim p(\boldsymbol{y}|\boldsymbol{x}, \theta_j)$, $b = 1, \ldots, B$, i.i.d., as $B \to \infty$.

Next, we apply the MCEM algorithm to sample paths of the Student-Lévy process. The procedure is similar to the standard Student t distribution (McLachlan & Krishnan 2007), but differs in some of the details. Let

$$\boldsymbol{x} = \{\Delta_k^n X\}_{k=1,\dots,n}, \quad \boldsymbol{y} = \{\Delta_k^n Y\}_{k=1,\dots,n}, \quad \theta = \{\mu, \sigma\},$$

where $\{X_t\}$ denotes a Student-Lévy process of which we observe a sample path and $\{Y_t\}$ is the corresponding unobserved inverse gamma subordinator. $p_{h_n}(x|\theta)$ denotes the density of X_{h_n} and $p_{h_n}(y)$ denotes the density of Y_{h_n}, which is independent of θ. Then the joint density is given by

$$p_{h_n}(x, y|\theta) = p_{h_n}(x|y, \theta)p_{h_n}(y) = N(x|h_n\mu, \sigma^2 y)p_{h_n}(y).$$

The complete log-likelihood function is given by

$$\begin{aligned}
&\ell(\theta|\{\Delta_k^n X\}, \{\Delta_k^n Y\}) \\
&= \sum_{k=1}^{n} \log N(\Delta_k^n X|h_n\mu, \sigma^2\Delta_k^n Y) + \log p_{h_n}(\Delta_k^n Y) \\
&= \sum_{k=1}^{n} -\frac{1}{2}\log(2\pi) - \frac{1}{2}\log\sigma^2 - \frac{1}{2}\log\Delta_k^n Y - \frac{(\Delta_k^n X - h_n\mu)^2}{2\sigma^2\Delta_k^n Y} + \log p_{h_n}(\Delta_k^n Y).
\end{aligned}$$

The density $p_{h_n}(y)$ of the inverse gamma subordinator has no closed form. However, since it only depends on ν, which we assume to be known, it is irrelevant for maximization in (μ, σ). The normal part of the complete likelihood is independent of ν. This is indeed the reason why we assume ν to be fixed. As we do not explicitly know $p_{h_n}(\Delta_k^n Y)$, except that it depends solely on ν, we cannot perform likelihood-based estimation.

Next, we seek the posterior of the latent subordinator in order to take the expectation w.r.t. this posterior. In the case of the Student t distribution, the latent variables are inverse gamma distributed and therefore the posterior is also inverse gamma distributed because it is a conjugate prior for the normal distribution. This is not the case for the inverse gamma subordinator and general $h_n \neq 1$. By Bayes' law,

$$p_{h_n}(y|\Delta_k^n X, \theta) = \frac{p_{h_n}(\Delta_k^n X|y, \theta)p_{h_n}(y)}{p_{h_n}(\Delta_k^n X|\theta)} = \frac{N(\Delta_k^n X|h_n\mu, \sigma^2 y)p_{h_n}(y)}{p_{h_n}(\Delta_k^n X|\theta)}. \tag{3.18}$$

To find $Q(\theta|\theta_j)$ we integrate the log-likelihood with respect to this posterior.

$$Q(\theta|\theta_j) = \qquad E_{\theta_j}[\ell(\theta|\{\Delta_k^n X\}, \{\Delta_k^n Y\})|\{\Delta_k^n X\}]$$

$$= \sum_{k=1}^{n} -\frac{1}{2}\log(2\pi) - \frac{1}{2}\log\sigma^2 - \frac{1}{2}E_{\theta_j}[\log \Delta_k^n Y | \Delta_k^n X] - \frac{(\Delta_k^n X - h_n\mu)^2}{2\sigma^2} E_{\theta_j}\left[\frac{1}{\Delta_k^n Y}\middle| \Delta_k^n X\right] + E_{\theta_j}[\log p_{h_n}(\Delta_k^n Y)|\Delta_k^n X].$$

We do not need to find $E_{\theta_j}[\log \Delta_k^n Y|\Delta_k^n X]$ and $E_{\theta_j}[\log p_{h_n}(\Delta_k^n Y)|\Delta_k^n X]$ because when we take the derivative w.r.t. μ or σ these terms vanish. It only remains to find $E_{\theta_j}\left[\frac{1}{\Delta_k^n Y}\middle| \Delta_k^n X\right]$. By (3.18),

$$E_{\theta_j}\left[\frac{1}{\Delta_k^n Y}\middle| \Delta_k^n X\right] = \int_0^\infty \frac{1}{y}\frac{N(\Delta_k^n X|h_n\mu, \sigma^2 y)}{p_{h_n}(\Delta_k^n X|\theta)} p_{h_n}(y)\mathrm{d}y. \tag{3.19}$$

At this point, Monte Carlo integration is useful. We approximate (3.19) by

$$\hat{E}_{\theta_j}\left[\frac{1}{\Delta_k^n Y}\middle| \Delta_k^n X\right] := \frac{1}{B}\sum_{b=1}^{B}\frac{1}{Y_{h_n b}}\frac{N(\Delta_k^n X|h_n\mu, \sigma^2 Y_{h_n b})}{p_{h_n}(\Delta_k^n X|\theta)},$$

where $Y_{h_n b}$, $b = 1, \ldots, B$, are i.i.d. draws from $p_{h_n}(y)$. They are simulated with the algorithms from Chapter 2. Then $\hat{E}_{\theta_j}\left[\frac{1}{\Delta_k^n Y}\middle| \Delta_k^n X\right] \to E_{\theta_j}\left[\frac{1}{\Delta_k^n Y}\middle| \Delta_k^n X\right]$ a.s. for $B \to \infty$. Note that we have to use the Fourier inversion (3.17) to compute $p_{h_n}(\Delta_k^n X|\theta)$. Although this is the most time-consuming step in the proposed MCEM algorithm, it is still much faster than the Nelder-Mead approach mentioned above.

We conclude the $(j+1)$-th **MCE-Step.**

$$\hat{Q}(\theta|\theta_j) = \sum_{k=1}^{n} -\frac{1}{2}\log(2\pi) - \frac{1}{2}\log\sigma^2 - \frac{(\Delta_k^n X - h_n\mu)^2}{2\sigma^2}\hat{E}_{\theta_j}\left[\frac{1}{\Delta_k^n Y}\middle| \Delta_k^n X\right] + C, \tag{3.20}$$

where we collect the terms vanishing during maximization in the constant C.

In order to maximize (3.20), we set $\frac{\partial Q}{\partial \mu} = 0$ and $\frac{\partial Q}{\partial \sigma} = 0$. We obtain the $(j+1)$-th **M-Step.**

$$\mu_{j+1} = \frac{\sum_{k=1}^{n}\hat{E}_{\theta_j}\left[\frac{1}{\Delta_k^n Y}\middle| \Delta_k^n X\right]\Delta_k^n X}{h_n\sum_{k=1}^{n}\hat{E}_{\theta_j}\left[\frac{1}{\Delta_k^n Y}\middle| \Delta_k^n X\right]}$$

and

$$\sigma_{j+1}^2 = \frac{1}{n}\sum_{k=1}^{n}(\Delta_k^n X - h_n\mu_{j+1})^2 \hat{E}_{\theta_j}\left[\frac{1}{\Delta_k^n Y}\middle|\Delta_k^n X\right].$$

Note that we need to find μ_{j+1} first, since it is needed to update σ_{j+1}. The MCE-step and the M-step are repeated iteratively until we observe convergence of (μ_j, σ_j). To speed up the MCEM, we draw $Y_{h_n b}$, $b = 1, \ldots, B$, only once and reuse them in any MCE-step as recommended by Levine & Casella (2001). For the initial (μ_0, σ_0) we take the raw moment estimates if $\nu > 2$. For $1 < \nu \leq 2$ we take some other initial values. The whole MCEM routine is summarized in compact form in Algorithm 5.

Algorithm 5 MCEM Algorithm for the Student-Lévy process with known ν

Input: Sample path observed at $(X_{kh_n})_{1\leq k\leq n}$, such that $\Delta_k^n X \sim p_{h_n}(x|\theta)$;
Output: Maximum likelihood estimates $\hat{\mu}$ and $\hat{\sigma}^2$.

1: $\mu_0 \leftarrow \frac{1}{h_n n}\sum_{k=1}^{n}\Delta_k^n X$;
   $\sigma_0^2 \leftarrow \frac{\nu-2}{\nu}\frac{1}{h_n n}\sum_{k=1}^{n}(\Delta_k^n X)^2 - \frac{\nu-2}{\nu}h_n\mu_0^2$; ▷ Start with moment estimation.
2: Draw B i.i.d. random variates $Y_{h_n 1}, \ldots, Y_{h_n B} \sim p_{h_n}(y)$;
3: $j \leftarrow 0$;
4: **repeat**
5: **MCE step:**
6: **for** $k = 1$ **to** n **do**
7: $\hat{E}_{\theta_j}\left[\frac{1}{\Delta_k^n Y}\middle|\Delta_k^n X\right] \leftarrow \frac{1}{B}\sum_{b=1}^{B}\frac{1}{Y_{h_n b}}\frac{N(\Delta_k^n X|h_n\mu_j, \sigma^2 Y_{h_n b})}{p_{h_n}(\Delta_k^n X|\theta_j)}$;
8: **end for**
9: **M step:**
10: **for** $k = 1$ **to** n **do**
11: $\mu_{j+1} \leftarrow \frac{\sum_{k=1}^{n}\hat{E}_{\theta_j}\left[\frac{1}{\Delta_k^n Y}|\Delta_k^n X\right]\Delta_k^n X}{h_n\sum_{k=1}^{n}\hat{E}_{\theta_j}\left[\frac{1}{\Delta_k^n Y}|\Delta_k^n X\right]}$;
12: $\sigma_{j+1}^2 \leftarrow \frac{1}{n}\sum_{k=1}^{n}(\Delta_k^n X - h_n\mu_{j+1})^2\hat{E}_{\theta_j}\left[\frac{1}{\Delta_k^n Y}\middle|\Delta_k^n X\right]$;
13: **end for**
14: **until** convergence.

3.4 Monte Carlo study

In this section we briefly present some experimental evidence for the above methods. The section is split into three experiments. First, we test the MCEM algorithm and

verify that a higher frequency leads to a better estimation result. A second experiment compares the MCEM algorithm with the Nelder-Mead maximization of the Fourier inversion. Third, we investigate the estimators $\hat{\mu}_{T,n}$ and $\hat{\sigma}_{T,n}$ for continuous sampling.

The first experiment tests the MCEM algorithm. We sample Student-Lévy paths for different degrees of freedom $\nu = 4, 12, 39$ with $h_n = 0.01, 0.1, 0.5, 1$ increments until $T \equiv T_n = 100$. We consider 5 constellations for $\theta = (\mu, \sigma)$. For each sampled path and each h_n we compute the ML estimate $(\hat{\mu}_{ML}, \hat{\sigma}_{ML})$ with the MCEM algorithm and the method of moments (MoM) estimate $(\hat{\mu}_{MoM}, \hat{\sigma}_{MoM})$. We repeat this 10,000 times for each constellation and compute the empirical bias and the empirical root mean squared error (RMSE). Tables 3.1, 3.2 and 3.3 report the results. In order to reduce computing time we only estimate the parameters for $h_n = 0.01$ in the setting $\theta = (0, 1)$.

Unsurprisingly, the estimates are closer to the true parameters for smaller step sizes in all constellations. In almost all setups, the ML estimates are better than the MoM estimates. Moreover, this pattern is more clearly visible for smaller degrees of freedom. This is due to the fact that, for high degrees of freedom, the increments are approximately normally distributed and the MoM estimator and the MLE coincide for Gaussian increments. Thus, the MLE performs better for low degrees of freedom.

Further, the bias for the scaling parameter is typically negative while the bias for the location parameter is positive in some cases. Next, the RMSEs for the ML estimates of both parameters only depend on the true σ (and not on μ). This is supported by Theorem 3.1, as the Fisher information matrix does not depend on μ. As ν increases, the differences in RMSEs for μ tend to vanish along h_n. Again, this is reasonable as the MLE and the MoM estimator are numerically close for high degrees of freedom. Although the Fisher information for σ does not depend on ν, there are some small differences in RMSEs of $\hat{\sigma}_{ML}$ for different ν in finite samples. Additionally, for $\nu = 4$, the RMSE of $\hat{\sigma}_{ML}$ is decisively smaller than that of $\hat{\sigma}_{MoM}$ throughout, whereas for $\nu = 39$ there are (if at all) only small differences.

Note that the moment estimator for μ is numerically equal to any digit among different times h_n since the moment estimator is not consistent if $T_n \nrightarrow \infty$.

Figures 3.1, 3.2 and 3.3 show kernel density estimates of the realizations of $\sqrt{n}\frac{(\hat{\mu}_{ML}-\mu)}{\sqrt{2\nu\sigma^2}}$ (panel (a)) and $\sqrt{n}\frac{(\hat{\sigma}_{ML}-\sigma)}{\sqrt{2\sigma^2}}$ (panel (b)) for different h_n compared with the theoretical standard normal density. Figure 3.1 considers $\nu = 4$, Figure 3.2 is for $\nu = 12$ and Figure 3.3 for $\nu = 39$. All figures share the same true parameter setup $(\mu, \sigma) = (0, 1)$.

Figure 3.1 illustrates asymptotic normality for both estimators, and the density estimates for $h_n = 0.01$ are not too far from the standard normal density. Figure 3.2 and 3.3 show that this is now less valid for large ν. In Figure 3.3 (b) all kernel density

True θ	h_n	$\hat{\mu}_{ML}$	$\hat{\sigma}_{ML}$	$\hat{\mu}_{MoM}$	$\hat{\sigma}_{MoM}$
$(0, 1)$	1	$-1.3 \cdot 10^{-3}$	$-5.5 \cdot 10^{-3}$	-10^{-3}	$-.019$
		(.118)	(.094)	(.141)	(.162)
	0.5	$-9.1 \cdot 10^{-4}$	$-3.2 \cdot 10^{-3}$	-10^{-3}	$-.016$
		(.106)	(.07)	(.141)	(.156)
	0.1	$5 \cdot 10^{-5}$	$-1.5 \cdot 10^{-4}$	-10^{-3}	$-.013$
		(.069)	(.037)	(.141)	(.149)
	0.01	$1.9 \cdot 10^{-4}$	$-3.2 \cdot 10^{-4}$	-10^{-3}	$-.012$
		(.027)	(.013)	(.141)	(.148)
$(0, 3)$	1	$-9 \cdot 10^{-3}$	$-1.7 \cdot 10^{-2}$	$-8.6 \cdot 10^{-3}$	$-.066$
		(.361)	(.278)	(.428)	(.459)
	0.5	$-7.2 \cdot 10^{-3}$	$-9.9 \cdot 10^{-3}$	$-8.6 \cdot 10^{-3}$	$-.056$
		(.324)	(.211)	(.428)	(.435)
	0.1	$-2 \cdot 10^{-3}$	$-3.1 \cdot 10^{-3}$	$-8.6 \cdot 10^{-3}$	$-.046$
		(.211)	(.111)	(.428)	(.416)
$(0, 0.1)$	1	$4.4 \cdot 10^{-5}$	$-5.9 \cdot 10^{-4}$	$2.4 \cdot 10^{-5}$	$-1.9 \cdot 10^{-3}$
		(.0118)	(.0094)	(.0142)	(.0179)
	0.5	$3.7 \cdot 10^{-5}$	$-4.1 \cdot 10^{-4}$	$2.4 \cdot 10^{-5}$	$-1.5 \cdot 10^{-3}$
		(.0106)	(.007)	(.0142)	(.0172)
	0.1	$3.3 \cdot 10^{-5}$	$-1.5 \cdot 10^{-4}$	$2.4 \cdot 10^{-5}$	$-1.1 \cdot 10^{-3}$
		(.0069)	(.0036)	(.0142)	(.0166)
$(2, 1)$	1	$-8 \cdot 10^{-4}$	$-4.7 \cdot 10^{-3}$	$-2.1 \cdot 10^{-3}$	$-.019$
		(.118)	(.093)	(.141)	(.16)
	0.5	$-9.9 \cdot 10^{-5}$	$-1.9 \cdot 10^{-3}$	$-2.1 \cdot 10^{-3}$	$-.015$
		(.106)	(.07)	(.141)	(.152)
	0.1	$-1.3 \cdot 10^{-3}$	$-8.7 \cdot 10^{-4}$	$-2.1 \cdot 10^{-3}$	$-.013$
		(.07)	(.036)	(.141)	(.147)
$(-0.5, 1)$	1	$-6.8 \cdot 10^{-4}$	$-3.7 \cdot 10^{-3}$	$-1.7 \cdot 10^{-3}$	$-.016$
		(.118)	(.094)	(.142)	(.166)
	0.5	$-1.3 \cdot 10^{-3}$	$-1.8 \cdot 10^{-4}$	$-1.7 \cdot 10^{-3}$	$-.013$
		(.106)	(.07)	(.142)	(.158)
	0.1	$-1.2 \cdot 10^{-3}$	$-3.3 \cdot 10^{-4}$	$-1.7 \cdot 10^{-3}$	$-.01$
		(.07)	(.036)	(.142)	(.152)

Table 3.1: Empirical bias and RMSE (in parentheses) for $\nu = 4$ comparing the MLE and the MoM estimator for different true θ and step size h_n.

True θ	h_n	$\hat{\mu}_{ML}$	$\hat{\sigma}_{ML}$	$\hat{\mu}_{MoM}$	$\hat{\sigma}_{MoM}$
$(0, 1)$	1	$5.7 \cdot 10^{-4}$	$-6.3 \cdot 10^{-3}$	$4 \cdot 10^{-4}$	$-9 \cdot 10^{-3}$
		(.106)	(0.08)	(.108)	(0.082)
	0.5	$8.9 \cdot 10^{-4}$	$-3.4 \cdot 10^{-3}$	$4 \cdot 10^{-4}$	$-5.7 \cdot 10^{-3}$
		(.102)	(.059)	(.108)	(.065)
	0.1	10^{-3}	$-1.3 \cdot 10^{-3}$	$4 \cdot 10^{-4}$	$-2.1 \cdot 10^{-3}$
		(.086)	(.031)	(.108)	(.048)
	0.01	$3.5 \cdot 10^{-5}$	$-3.2 \cdot 10^{-3}$	$4 \cdot 10^{-4}$	$-1.4 \cdot 10^{-3}$
		(.042)	(.013)	(.108)	(.043)
$(0, 3)$	1	$-6.8 \cdot 10^{-4}$	$-.023$	$-6.6 \cdot 10^{-4}$	$-.029$
		(.319)	(.24)	(.326)	(.25)
	0.5	$-2.5 \cdot 10^{-4}$	$-.013$	$-6.6 \cdot 10^{-4}$	$-.019$
		(.31)	(.179)	(.326)	(.2)
	0.1	$-7.1 \cdot 10^{-5}$	$-4.9 \cdot 10^{-3}$	$-6.6 \cdot 10^{-4}$	$-8.5 \cdot 10^{-3}$
		(.259)	(.093)	(.326)	(.145)
$(0, 0.1)$	1	$1.2 \cdot 10^{-4}$	$-6.1 \cdot 10^{-4}$	$1.4 \cdot 10^{-4}$	$-8.1 \cdot 10^{-4}$
		(.0108)	(.008)	(.0111)	(.0083)
	0.5	$1.4 \cdot 10^{-4}$	$-3.2 \cdot 10^{-4}$	$1.4 \cdot 10^{-4}$	$-4.7 \cdot 10^{-4}$
		(.0106)	(.006)	(.0111)	(.0066)
	0.1	$5.4 \cdot 10^{-5}$	$-9.8 \cdot 10^{-5}$	$1.4 \cdot 10^{-4}$	$-1.4 \cdot 10^{-4}$
		(.0088)	(.0031)	(.0111)	(.0049)
$(2, 1)$	1	$-1.8 \cdot 10^{-3}$	$-7.3 \cdot 10^{-3}$	$-1.8 \cdot 10^{-3}$	$-9.3 \cdot 10^{-3}$
		(.107)	(.079)	(.109)	(.082)
	0.5	$-1.8 \cdot 10^{-3}$	$-4.1 \cdot 10^{-3}$	$-1.8 \cdot 10^{-3}$	$-5.5 \cdot 10^{-3}$
		(.104)	(.059)	(.109)	(.065)
	0.1	$-7.2 \cdot 10^{-4}$	$-9.4 \cdot 10^{-4}$	$-1.8 \cdot 10^{-3}$	$-1.8 \cdot 10^{-3}$
		(.087)	(.031)	(.109)	(.048)
$(-0.5, 1)$	1	$1.3 \cdot 10^{-4}$	$-7.4 \cdot 10^{3}$	$5 \cdot 10^{-4}$	$-9.5 \cdot 10^{3}$
		(.108)	(.08)	(.11)	(.083)
	0.5	$1.9 \cdot 10^{-4}$	$-3.1 \cdot 10^{3}$	$5 \cdot 10^{-4}$	$-5 \cdot 10^{3}$
		(.105)	(.059)	(.11)	(.066)
	0.1	$8.6 \cdot 10^{-4}$	$-1.1 \cdot 10^{3}$	$5 \cdot 10^{-4}$	$-2 \cdot 10^{3}$
		(.087)	(.031)	(.11)	(.048)

Table 3.2: Empirical bias and RMSE (in parentheses) for $\nu = 12$ comparing the MLE and the MoM estimator for different true θ and step size h_n.

True θ	h_n	$\hat{\mu}_{ML}$	$\hat{\sigma}_{ML}$	$\hat{\mu}_{MoM}$	$\hat{\sigma}_{MoM}$
$(0, 1)$	1	$-1.1 \cdot 10^{-3}$	$-8.1 \cdot 10^{-3}$	-10^{-3}	$-8.7 \cdot 10^{-3}$
		(.103)	(.074)	(.103)	(.074)
	0.5	$-9.2 \cdot 10^{-4}$	$-4.6 \cdot 10^{-3}$	-10^{-3}	$-5.2 \cdot 10^{-3}$
		(.102)	(.054)	(.103)	(.054)
	0.1	$-7.3 \cdot 10^{-4}$	$-1.9 \cdot 10^{-3}$	-10^{-3}	$-2.3 \cdot 10^{-3}$
		(.097)	(.027)	(.103)	(.031)
	0.01	$3.6 \cdot 10^{-4}$	$-3.9 \cdot 10^{-3}$	-10^{-3}	$-1.7 \cdot 10^{-3}$
		(.065)	(.019)	(.103)	(.022)
$(0, 3)$	1	$-7.7 \cdot 10^{-4}$	$-2.8 \cdot 10^{-2}$	$-7.7 \cdot 10^{-4}$	$-3 \cdot 10^{-2}$
		(.308)	(.221)	(.309)	(.222)
	0.5	$-1.1 \cdot 10^{-3}$	$-1.4 \cdot 10^{-2}$	$-7.7 \cdot 10^{-4}$	$-1.6 \cdot 10^{-2}$
		(.307)	(.159)	(.309)	(.161)
	0.1	$5.3 \cdot 10^{-4}$	$-6.6 \cdot 10^{-3}$	$-7.2 \cdot 10^{-4}$	$-7.8 \cdot 10^{-3}$
		(.292)	(.081)	(.309)	(.091)
$(0, 0.1)$	1	$9.5 \cdot 10^{-5}$	$-6.9 \cdot 10^{-4}$	$9.5 \cdot 10^{-5}$	$-2.5 \cdot 10^{-4}$
		(.0103)	(.0073)	(.0103)	(.0074)
	0.5	10^{-5}	$-3.6 \cdot 10^{-4}$	$9.5 \cdot 10^{-5}$	$-1.7 \cdot 10^{-4}$
		(.0103)	(.0053)	(.0103)	(.0054)
	0.1	$9.6 \cdot 10^{-5}$	$-1.7 \cdot 10^{-4}$	$9.5 \cdot 10^{-5}$	$-1.4 \cdot 10^{-4}$
		(.0097)	(.0027)	(.0103)	(.003)
$(2, 1)$	1	$2.7 \cdot 10^{-4}$	$-7.9 \cdot 10^{-3}$	$2.6 \cdot 10^{-4}$	$-8.6 \cdot 10^{-3}$
		(.101)	(.074)	(.101)	(.075)
	0.5	$2.7 \cdot 10^{-4}$	$-4.5 \cdot 10^{-3}$	$2.6 \cdot 10^{-4}$	$-5 \cdot 10^{-3}$
		(.101)	(.054)	(.101)	(.055)
	0.1	-10^{-5}	$-1.7 \cdot 10^{-3}$	$2.6 \cdot 10^{-4}$	$-1.9 \cdot 10^{-3}$
		(.096)	(.027)	(.101)	(.031)
$(-0.5, 1)$	1	$-1.3 \cdot 10^{-3}$	$-8.5 \cdot 10^{-3}$	$-1.3 \cdot 10^{-3}$	$-9.1 \cdot 10^{-3}$
		(.104)	(.074)	(.104)	(.075)
	0.5	$-1.1 \cdot 10^{-3}$	$-4.8 \cdot 10^{-3}$	$-1.3 \cdot 10^{-3}$	$-5.3 \cdot 10^{-3}$
		(.103)	(.053)	(.104)	(.054)
	0.1	$-1.1 \cdot 10^{-3}$	$-2 \cdot 10^{-3}$	$-1.3 \cdot 10^{-3}$	$-2.1 \cdot 10^{-3}$
		(.097)	(.027)	(.104)	(.03)

Table 3.3: Empirical bias and RMSE (in parentheses) for $\nu = 39$ comparing the MLE and the MoM estimator for different true θ and step size h_n.

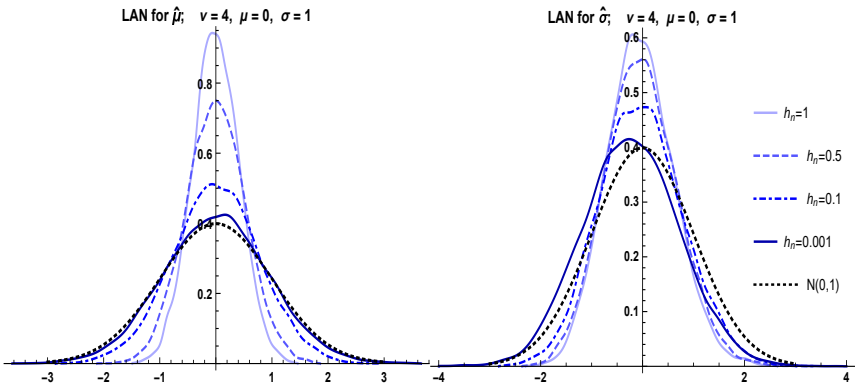

(a) (b)

Figure 3.1: Panel (a) compares kernel density estimates of $\sqrt{n}\frac{(\hat{\mu}_{ML}-\mu)}{\sqrt{2\nu\sigma^2}}$ for different h_n with the standard normal density. Analogously, panel (b) for $\sqrt{n}\frac{(\hat{\sigma}_{ML}-\sigma)}{\sqrt{2\sigma^2}}$.

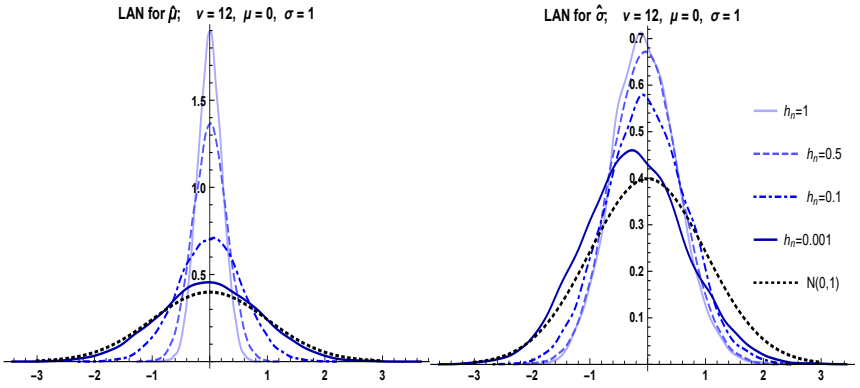

(a) (b)

Figure 3.2: Panel (a) compares kernel density estimates of $\sqrt{n}\frac{(\hat{\mu}_{ML}-\mu)}{\sqrt{2\nu\sigma^2}}$ for different h_n with the standard normal density. Analogously, panel (b) for $\sqrt{n}\frac{(\hat{\sigma}_{ML}-\sigma)}{\sqrt{2\sigma^2}}$.

estimates are closer to each other and obviously not standard normal. This is because Student-Lévy increments for high degrees of freedom are approximately normal. However, for Brownian motions the LAN holds true, but with Fisher information $\mathscr{I}^{(22)} = \frac{2}{\sigma^2}$ (Kawai 2013) instead of $\frac{1}{2\sigma^2}$ for Student-Lévy processes (yet with the same rate). If we do not interpret the high degrees of freedom as approximately normal but follow the Student-Lévy LAN theory, the asymptotic normality hence "occurs later".

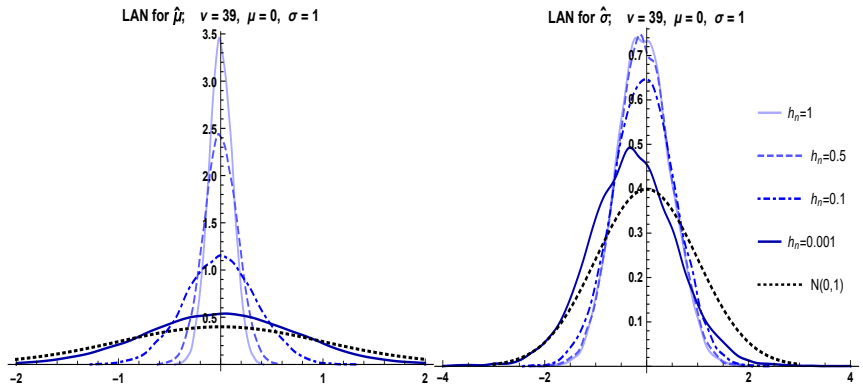

(a) (b)

Figure 3.3: Panel (a) compares kernel density estimates of $\sqrt{n}\frac{(\hat{\mu}_{ML}-\mu)}{\sqrt{2\nu\sigma^2}}$ for different h_n with the standard normal density. Analogously, panel (b) for $\sqrt{n}\frac{(\hat{\sigma}_{ML}-\sigma)}{\sqrt{2\sigma^2}}$.

3.4.1 Robustness

We perform a robustness simulation mainly to encourage future work on estimating ν. We now simulate paths with $\nu \in \{3, 5\}$ but still assume $\nu = 4$ for estimation. Table 3.4 reports the empirical biases and RMSEs. For a better comparison we again include the case in which we also simulate paths with $\nu = 4$.

Comparing $\nu = 4$ with $\nu = 5$ we see that the bias and RMSE are almost equal for $\hat{\mu}_{ML}$. The same is true for RMSEs of $\hat{\sigma}_{ML}$ while the biases are larger. For $\nu = 3$ we again see that the biases and RMSEs of $\hat{\mu}_{ML}$ are of the same size as for $\nu = 4$. The biases and RMSEs of $\hat{\sigma}_{ML}$ are slightly larger if the true $\nu = 3$. However, for both $\nu = 3, 5$ and both parameters a higher frequency decreases the RMSE.

3.4.2 Comparison between ML methods

The second experiment aims to specify the numerical error between the two different methods, MCEM-MLE and CF-MLE. We again test $\nu = 4, 12, 39$ and $h_n = 0.1, 0.5, 1$ but restrict ourselves to the setting $\mu = 0, \sigma = 1$. Since the execution time of CF-ML is too long, we only perform 100 iterations instead of 10,000 as before. In each iteration we simulate a Student-Lévy path and estimate parameters for h_n-increments both with MCEM and CF-ML. We then estimate the root mean squared deviance between both: $\left(\frac{1}{100}\sum_j(\mu^{(j)}_{n,\text{MCEM}} - \mu^{(j)}_{n,\text{CF-ML}})^2\right)^{1/2}$. For $h_n = 1$ (Student t random numbers) we also compare each with the standard EM-MLE. Table 3.5 shows the

True ν	h_n	$\hat{\mu}_{ML}$	$\hat{\sigma}_{ML}$	$\hat{\mu}_{MoM}$	$\hat{\sigma}_{MoM}$
3	1	$4.1 \cdot 10^{-4}$	.067	$-7.6 \cdot 10^{-4}$	.169
		(.124)	(.126)	(.175)	(.407)
	0.5	$3.8 \cdot 10^{-4}$	.035	$-7.6 \cdot 10^{-4}$	.173
		(.106)	(.085)	(.175)	(.406)
	0.1	$2.7 \cdot 10^{-4}$	-.037	$-7.6 \cdot 10^{-4}$	.176
		(.065)	(.052)	(.175)	(.405)
4	1	$-1.3 \cdot 10^{-3}$	$-5.5 \cdot 10^{-3}$	-10^{-3}	$-.019$
		(.118)	(.094)	(.141)	(.162)
	0.5	$-9.1 \cdot 10^{-4}$	$-3.2 \cdot 10^{-3}$	-10^{-3}	$-.016$
		(.106)	(.07)	(.141)	(.156)
	0.1	$5 \cdot 10^{-5}$	$-1.5 \cdot 10^{-4}$	-10^{-3}	$-.013$
		(.069)	(.037)	(.141)	(.149)
5	1	$2 \cdot 10^{-4}$	$-4.3 \cdot 10^{-2}$	$-1.1 \cdot 10^{-4}$	$-.099$
		(.117)	(.096)	(.129)	(.15)
	0.5	$6.6 \cdot 10^{-4}$	$-2.2 \cdot 10^{-2}$	$-1.1 \cdot 10^{-4}$	$-.096$
		(.107)	(.07)	(.129)	(.142)
	0.1	$7.3 \cdot 10^{-4}$	$2.8 \cdot 10^{-2}$	$-1.1 \cdot 10^{-4}$	$-.093$
		(.074)	(.046)	(.129)	(.134)

Table 3.4: Empirical bias and RMSE (in parentheses) assuming $\nu = 4$ for estimation comparing the MLE and the MoM estimator for different true ν and step size h_n.

results.

Apparently, the randomness caused by the Monte Carlo integration has little impact on the estimation results. This seems to be true for all degrees of freedom considered. There are some exceptions for the CF-ML, viz. the Nelder-Mead maximization occasionally fails to find the optimum. These outliers have been excluded in the table.

3.4.3 Continuous sampling

Finally, we discuss the estimators (3.15) and (3.16) for the continuous sampling scheme. Of course, continuous sampling is physically impossible. However, if a path is generated by a series representation (Chapter 2), we expect a sufficient number of

Comparison	h_n		$\hat{\mu}$			$\hat{\sigma}$		
		$\nu =$	4	12	39	4	12	39
MCEM vs CF-ML	1		$2.4 \cdot 10^{-4}$	$1.6 \cdot 10^{-4}$	$7.8 \cdot 10^{-5^*}$	$8 \cdot 10^{-4}$	$3.5 \cdot 10^{-4}$	$8.8 \cdot 10^{-5^*}$
	0.5		$3.2 \cdot 10^{-4}$	$7.7 \cdot 10^{-5^*}$	$1.6 \cdot 10^{-4^*}$	$5.4 \cdot 10^{-4}$	$1.5 \cdot 10^{-4^*}$	$1.7 \cdot 10^{-4^*}$
	0.1		$5 \cdot 10^{-5}$	$1.7 \cdot 10^{-4^*}$	$1.5 \cdot 10^{-4}$	$2.7 \cdot 10^{-4}$	$3.9 \cdot 10^{-4^*}$	$1.6 \cdot 10^{-4}$
MCEM vs EM	1		$2.4 \cdot 10^{-4}$	$1.6 \cdot 10^{-4}$	$7.8 \cdot 10^{-5}$	$8 \cdot 10^{-4}$	$3.4 \cdot 10^{-4}$	$8.8 \cdot 10^{-5^*}$
CF-ML vs EM	1		$6.1 \cdot 10^{-7}$	$2.8 \cdot 10^{-7}$	$6.8 \cdot 10^{-8^*}$	$2.4 \cdot 10^{-6}$	$7.3 \cdot 10^{-7}$	$1.4 \cdot 10^{-7^*}$

Table 3.5: Empirical root mean squared deviances between the different ML estimation approaches for different h_n and ν. Exceptions occur where Nelder-Mead does not work. These outliers have been excluded from analysis. The cases are highlighted with $*$.

jumps for estimation. See also Raible (2000) for the normal inverse Gaussian Lévy process.

Let $T = 1$, $\theta = (0, 1)$ and let $\tau = 50,400;\ 87,300;\ 157,300$ for $\nu = 4, 12, 39$, respectively, be the truncation levels for the random truncated series representation. The different levels of truncation are chosen such that the series contain all jumps up to size 10^{-9} for each ν. For each ν we generate 10,000 paths and compute the continuous sampling estimators $\hat{\mu}_{T,n}$ and $\hat{\sigma}_{T,n}$ for various n. Figure 3.4 plots the sample mean of the estimates versus $\log_{10} n$, both for $\hat{\mu}_{T,n}$ (panel (a)) and $\hat{\sigma}_{T,n}$ (panel (b)). The results illustrate the strong consistency of $\hat{\mu}_{T,n}$ for μ. However, there is evidently a problem for $\hat{\sigma}_{T,n}$ causing the decay. This is due to the fact that on average there are τ jumps in each path (due to the random truncation). This bounds $\#\{t \leq T : \Delta X_t \geq 1/n\}$ and, eventually, $\hat{\sigma}_{T,n} \to 0$ a.s. for $n \to \infty$.

If we pick $n = 10,000$ such that $\hat{\sigma}_{T,n}$ attains its maximum value, we find the RMSEs given in Table 3.6 outperforming the MCEM-MLE (see Tables 3.1 to 3.3, lines 1 to 3, values in parentheses). In practice, the series representation is not available but these estimators may be an alternative if a very high number of jumps is observed.

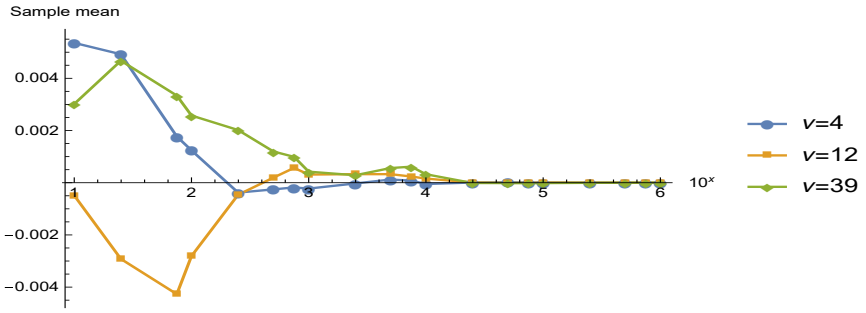

(a)

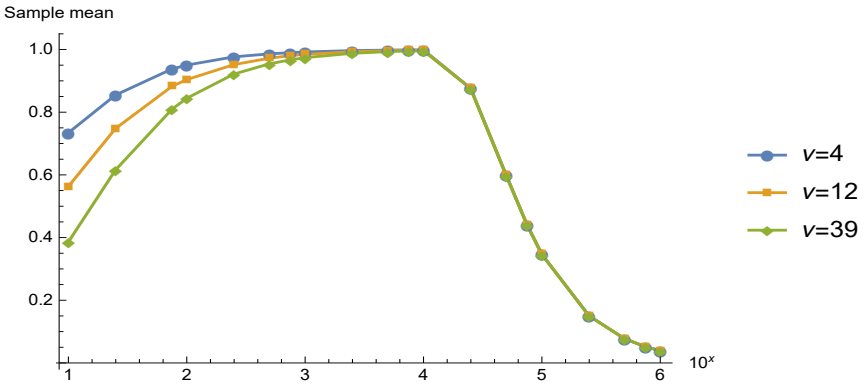

(b)

Figure 3.4: Empirical means of estimates of 10,000 trajectories using (3.15) and (3.16) for different ν and $\theta = (0, 1)$.

ν	$\hat{\mu}_{T,10^4}$	$\hat{\mu}_{T,10^6}$	$\hat{\sigma}_{T,10^4}$
4	$8.7 \cdot 10^{-3}$	$1.5 \cdot 10^{-5}$	$1.3 \cdot 10^{-2}$
12	$1.2 \cdot 10^{-2}$	$1.9 \cdot 10^{-5}$	$9.8 \cdot 10^{-3}$
39	$1.5 \cdot 10^{-2}$	$2.6 \cdot 10^{-5}$	$8.2 \cdot 10^{-3}$

Table 3.6: RMSEs for estimators (3.15) and (3.16) for different ν and $\theta = (0, 1)$.

3.5 Conclusion and future work

In this chapter we discuss and prove local asymptotic normality for the Student-Lévy process for high-frequency sampling. We find the rate of convergence and the Fisher information matrix. The LAN implies asymptotic normality and asymptotic efficiency for the maximum likelihood estimator. Additionally, we find that the LAN fails to

hold for the skew Student-Lévy process. We propose and test in simulations a Monte Carlo EM approach for numerical computations, which seems to work well.

In our future research we intend to further investigate estimation of GH Lévy processes. This involves classifying all special cases where a LAN does or does not hold. Furthermore, we aim to estimate the parameter ν, since this is also possible for Student t random numbers. Unfortunately, the density of $Y_t, t \neq 1$ is not available. In order to tackle this issue we plan to use appropriate approximations, e.g., Approximate Bayesian Computation.

In the next chapter we apply the procedures discussed above to real-world data, e.g., high-frequency financial data and compare how the resulting approach competes with existing ones.

4 What is the best Lévy model for stock indices? A comparative study with a view to time consistency

Lévy models are frequently used for asset log-returns. The crucial criterion here is the distributional assumption on the increments. Candidates include the generalized hyperbolic, the normal inverse Gaussian and the (skew) Student-Lévy process. We perform a comprehensive comparative study for multiple equity indices and competing Lévy models. We fit Lévy models to daily and also to hourly log-returns. In order to do so, we investigate Eberlein & Özkan's (2003) notion of time consistency. This means that we analyze whether a Lévy model for daily returns also fits well for hourly returns and vice versa. We conclude that the best fits for each index and sampling scheme are not necessarily from the same model family.

4.1 Introduction

This chapter investigates which distribution is the best distributional fit for asset log-returns in a large class of parametric models. Asset price modeling goes back to Bachelier (1900), who proposed the normal distribution for the log-returns. The distributional assumption is crucial, especially for option pricing. The famous Black & Scholes (1973) formula relies on the log-normality assumption. However, it is now well known that the normal distribution yields a poor fit for heavy-tailed returns. Several authors have proposed other more appropriate distributions. Among them, Mandelbrot (1961) recommended stable non-normal distributions. Praetz (1972) suggested the Student t distribution because it allows a finite variance for a degree of freedom higher than two. Other suggestions include the variance gamma distribution (Madan & Seneta 1990), the hyperbolic distribution (Eberlein et al. 1995), the normal inverse Gaussian distribution (Barndorff-Nielsen 1997), the Meixner distribution (Schoutens 2001), the generalized hyperbolic distribution (Eberlein & Prause 2002), and the skew Student t distribution (Aas & Haff 2006).

Since the distributional assumption is crucial for option pricing, there is considerable interest in the choice of distribution. Many studies have already investigated this

question. For example, Gray & French (1990), Peiró (1994) and Aparicio & Estrada (2001) compared different distributions for the daily log-returns of equity indices in different countries; see Corlu et al. (2016) or Göncü et al. (2016) for more recent studies. Corlu & Corlu (2015) and Nadarajah et al. (2015) investigated foreign exchange rate returns. The results of the studies cited differ depending on the countries and time periods considered. These recent studies often favor the normal inverse Gaussian or the variance gamma distribution.

Typically, financial data such as returns can only be observed in discrete frequency. The above comparative studies mostly considered daily returns. However, the log-return process is often modeled with a time-continuous Lévy process. The price process of an asset then is a so-called exponential Lévy model (see Section 4.2). Except for the Brownian motion (or, for the price process, the geometric Brownian motion) the Lévy models are pure jump processes. For a review of Lévy processes in finance and their relative advantages see Tankov & Cont (2015).

However, less attention has been paid to the question of whether these Lévy models for daily returns also fit well at higher frequencies, i.e., intraday returns. Eberlein & Özkan (2003) called this the "time consistency of Lévy processes". (For a precise definition see Section 4.5.) They fitted a hyperbolic Lévy model to daily DAX returns and compared the implied distribution for one hour according to the Lévy model with the empirical distribution of hourly returns. They found that this distance is approximately minimal if the hypothetical time t of the Lévy model is equal to the physical time of the market, i.e., the model time corresponds to the real time of the market. For example, if $t = 1$ represents one trading day with four tradings hours, then the distance of the implied distribution of one hour is minimal for approximately $t = 0.25$. Figueroa-López et al. (2011) revisited this topic for American equities using the normal inverse Gaussian and the variance gamma models. They found that these Lévy models can be time consistent for hourly log-returns. For very high frequencies, e.g., returns for every minute, there are perturbing microstructure effects in the market.

This chapter makes the following contributions. First, we analyze data for the multiple equity indices of different countries using different Lévy models to determine which is the best fit. To do this, we use the Kolmogorov-Smirnov statistic, the Anderson-Darling statistic and the Bayesian information criterion as goodness of fit measures. Second, we investigate hourly log-returns for the indices to establish the best model in terms of time consistency. Our key finding is that there are time inconsistencies. This means that some models which fit well for daily returns, e.g., the variance gamma model, fit poorly for hourly returns. We find that the Student-Lévy process is a more appropriate alternative.

The chapter is organized as follows: Section 4.2 introduces the different models

and highlights some of their important properties and differences. Section 4.3 gives a brief overview of the data. Section 4.4 presents the goodness of fit results. Section 4.5 formally introduces the notion of time consistency and investigates which Lévy model is the "most" time consistent. The last section concludes.

4.2 The models

In this section we introduce various competing Lévy models for asset returns. Let $\{S_t\}$ denote a price process for an asset. It is commonly assumed that the price process can be written as

$$S_t = S_0 \exp(X_t),$$

where $S_0 > 0$, and $\{X_t\}$, the log-return process, is a Lévy process. Daily log-returns are defined as $R_{t-1,t} = X_t - X_{t-1}$, i.e., the one-increments of the Lévy process $\{X_t\}$. This means we assume the daily returns to be independent and stationary. Throughout, we present models which are frequently used in the literature. Lévy models are induced by infinitely divisible distributions. If X_1 is distributed according to an infinitely divisible distribution, denoted $ID(\theta)$, this determines the whole Lévy process $\{X_t\}$, written $ID(\theta)$-Lévy process. We therefore fix the distribution for daily returns, and the corresponding exponential Lévy process models the price process. Although more models are possible, e.g., mixtures of the following, we focus on the basic ones.

4.2.1 The generalized hyperbolic model

The *generalized hyperbolic (GH) distribution* $GH(\lambda, \alpha, \beta, \delta, \mu)$ is one of the most flexible distributions used to model asset returns. It contains many other models as special or limiting cases. Its density function is

$$f^{GH}_{\lambda,\alpha,\beta,\delta,\mu}(x) = \frac{(\alpha^2 - \beta^2)^{\lambda/2} K_{\lambda-1/2}\left(\alpha\sqrt{\delta^2 + (x-\mu)^2}\right) \exp(\beta(x-\mu))}{\sqrt{2\pi}\alpha^{\lambda-1/2}\delta^{\lambda} K_{\lambda}\left(\delta\sqrt{\alpha^2-\beta^2}\right)\left(|\delta| + (x-\mu)^2\right)^{1/2-\lambda}},$$

with $K_\nu(x)$ the modified Bessel function of the second kind, shape parameters $\lambda \in \mathbb{R}$, $\alpha \in \mathbb{R}_0^+$, skewness parameter $\beta \in \mathbb{R}$, scale parameter δ, location parameter $\mu \in \mathbb{R}$ such that

$$\begin{aligned} &\delta \geq 0,\ 0 \leq |\beta| < \alpha && \text{if } \lambda > 0, \\ &\delta > 0,\ 0 \leq |\beta| < \alpha && \text{if } \lambda = 0, \\ &\delta > 0,\ 0 \leq |\beta| \leq \alpha && \text{if } \lambda < 0. \end{aligned}$$

Barndorff-Nielsen (1977) introduced the GH distribution (as a model for sand movement) and Barndorff-Nielsen & Halgreen (1977) proved its infinite divisibility. Eberlein & Prause (2002) proposed using the GH distribution for asset price returns. Eberlein & v. Hammerstein (2004) discussed the special and limiting cases of the GH distribution which we introduce below. Except for some special cases, the GH distribution is not closed under convolution. Hence, a GH Lévy process $\{X_t\}$ such that $X_1 \sim GH$ has no known distribution for X_t for $t \neq 1$. For $t = 1$, the GH distribution is fitted to data using numerical maximum likelihood (ML) estimation. Unfortunately, there exists no closed-form maximum likelihood estimator (MLE) and the likelihood function has a very complicated form and depends on five parameters. Thus, ML estimation may only find a local maximum. To address this issue, we use the numerical ML estimation algorithm of Breymann & Lüthi (2013) and our own Nelder-Mead-based approach for numerical maximization. Since, as already mentioned, there exists no likelihood function for X_t if $t \neq 1$ in closed form, we only perform ML estimation for $t = 1$ (one-day returns). GH distributions are *semi-heavy-tailed*, i.e., the tails are thinner than any power law but heavier than any normal law. For a rigorous definition, see Omey et al. (2017). An important consequence is that $E(e^X) < \infty$ if X follows a semi-heavy-tailed distribution. The GH distribution contains the following special cases.

The normal model

Bachelier (1900) proposed Brownian motion as a model for log-returns. Although numerous authors have stressed that asset returns are too heavy-tailed to be normal, the assumption features prominently in the frequently used Black & Scholes (1973) model for option pricing. Although there is overwhelming evidence against this model, we use it for the purposes of comparison. The normal distribution is the weak limit of the GH distribution $f^N_{\mu,\sigma^2}(x) = \lim f^{GH}_{\lambda,\alpha,\beta,\delta,\mu}(x)$ as $\alpha, \delta \to \infty$ and $\delta/\alpha \to \sigma^2$ for each $x \in \mathbb{R}$.

The Student model

Praetz (1972) and Blattberg & Gonedes (1974) were among the first to propose the *Student t distribution* $t(\nu, \mu, \sigma^2)$ for asset price returns. The Student t distribution has density function

$$f^{St}_{\nu,\mu,\sigma^2}(x) = \frac{\Gamma\left(\frac{\nu+1}{2}\right)}{\Gamma\left(\frac{\nu}{2}\right)\sqrt{\pi\nu\sigma^2}}\left(1 + \frac{1}{\nu}\left(\frac{x-\mu}{\sigma}\right)^2\right)^{-\frac{\nu+1}{2}},$$

with $\nu > 0$ degrees of freedom, location parameter $\mu \in \mathbb{R}$ and scale parameter $\sigma > 0$. Heyde & Leonenko (2005) proposed the Student-Lévy process as an alternative to Gaussian processes in asset return modeling. Grothe & Schmidt (2010) considered a different approach, rescaling the Student t distribution as an approximation of the Student-Lévy process. Cassidy et al. (2010) and Cassidy (2011) used this for option pricing. The Student t distribution is not closed under convolution. In other words, the Student-Lévy process $\{X_t\}$ only has a closed-form density for X_1. For X_t, $t \neq 1$, no density is known. ML estimation for Student t random variables can be performed by using an Expectation-Conditional Maximization Either (ECME) algorithm (Liu & Rubin 1994). ML estimation for a sample of $X_t, t \neq 1$ was developed in Chapter 3. The Student t distribution is heavy-tailed, meaning that $E(e^X)$ is infinite. The tails for small ν are heavier than for large ν. The Student t distribution is the weak limit of the GH distribution $f^{St}_{\nu,\mu,\sigma^2}(x) = \lim_{\alpha,\beta\to 0} f^{GH}_{\lambda,\alpha,\beta,\delta,\mu}(x)$ for each $x \in \mathbb{R}$.

The skew Student model

The Student t model mentioned above has the disadvantage that it can not capture skewness. As financial data often exhibit skewness, Aas & Haff (2006) suggested the use of the *skew Student t distribution* $t(\nu, \mu, \sigma^2, \beta)$. It has density function

$$f^{SSt}_{\nu,\mu,\sigma^2,\beta}(x) = \frac{2^{\frac{1-\nu}{2}}\nu^{\nu/2}\sigma^{\nu}\exp\left(\beta(x-\mu)\right)}{\Gamma\left(\frac{\nu}{2}\right)\sqrt{\pi}} \left(\frac{\beta^2}{\nu\sigma^2 + (x-\mu)^2}\right)^{\frac{\nu+1}{4}} \cdot K_{\frac{\nu+1}{2}}\left(\sqrt{\beta^2\left(\nu\sigma^2 + (x-\mu)^2\right)}\right),$$

with $\nu > 0$, $\mu \in \mathbb{R}$, $\sigma > 0$ and $\beta \in \mathbb{R}\backslash\{0\}$. The symmetric Student t distribution is the weak limit if $\beta \to 0$. Like the non-skew Student t distribution it is not closed under convolution. However, there is no likelihood estimation method for t-increments with $t \neq 1$. Hence we restrict ourselves to one-day returns and do not investigate time-consistency. An ML estimation algorithm for $t \neq 1$ is left for future research. The skew Student t distribution has a right (left) heavy tail and a left (right) semi-heavy tail if $\beta > 0$ ($\beta < 0$). It is the weak limit of the GH distribution $f^{SSt}_{\nu,\mu,\sigma^2,\beta}(x) = \lim_{|\beta|\to\alpha>0} f^{GH}_{\lambda,\alpha,\beta,\delta,\mu}(x)$ for each $x \in \mathbb{R}$.

The variance gamma model

Madan & Seneta (1990) introduced the *variance gamma distribution* $V\Gamma(\lambda, \alpha, \beta, \mu)$ to model market returns. It has density function

$$f^{V\Gamma}_{\lambda,\alpha,\beta,\mu}(x) = \frac{(\alpha^2-\beta^2)^\lambda |x-\mu|^{\lambda-1/2} K_{\lambda-1/2}(\alpha|x-\mu|)\exp(\beta(x-\mu))}{\sqrt{\pi}\Gamma(\lambda)(2\alpha)^{\lambda-1/2}},$$

with $\alpha, \lambda > 0$, $\beta \in \mathbb{R}$ such that $-\alpha < \beta < \alpha$ and $\mu \in \mathbb{R}$. It takes its name from the normal mean-variance mixture with a gamma distributed variable. The variance gamma distribution is the weak limit of the GH distribution $f^{V\Gamma}_{\lambda,\alpha,\beta,\mu}(x) = \lim_{\delta\downarrow 0} f^{GH}_{\lambda,\alpha,\beta,\delta,\mu}(x)$ for each $x \in \mathbb{R}$. The variance gamma distribution is closed under convolution, i.e., a variance gamma Lévy process $\{X_t\}$ fulfills $X_t \sim V\Gamma(t\lambda, \alpha, \beta, t\mu)$. The variance gamma distribution has two semi-heavy tails.

The normal inverse Gaussian model

Barndorff-Nielsen (1977) introduced the *normal inverse Gaussian (NIG) distribution* $NIG(\alpha, \beta, \delta, \mu)$. It has density function

$$f^{NIG}_{\alpha,\beta,\delta,\mu}(x) = \frac{\alpha\delta K_1\left(\alpha\sqrt{\delta^2+(x-\mu)^2}\right)}{\pi\sqrt{\delta^2(x-\mu)^2}} \exp\left(\delta\sqrt{\alpha^2-\beta^2}+\beta(x-\mu)\right),$$

with $\alpha, \delta > 0$ and $\beta, \mu \in \mathbb{R}$. Barndorff-Nielsen (1997) used the NIG distribution in the context of asset returns. The NIG distribution is a special case of the GH distribution $NIG(\alpha, \beta, \delta, \mu) = GH(-1/2, \alpha, \beta, \delta, \mu)$. The NIG distribution is closed under convolution, i.e., for a NIG Lévy process it holds true that $X_t \sim NIG(\alpha, \beta, t\delta, t\mu)$. The NIG distribution is semi-heavy-tailed.

The hyperbolic model

The *hyperbolic distribution* $H(\alpha, \beta, \delta, \mu)$ has density function

$$f^{H}_{\alpha,\beta,\delta,\mu}(x) = \frac{\sqrt{\alpha^2-\beta^2}}{2\alpha\delta K_1(\delta\sqrt{\alpha^2-\beta^2})} \exp\left(-\alpha\sqrt{\delta^2+(x-\mu)^2}+\beta(x-\mu)\right),$$

with $\alpha > 0$, $\beta \in \mathbb{R}$, $\delta \geq 0$ and $\mu \in \mathbb{R}$. Eberlein et al. (1995) introduced the hyperbolic distribution for asset price returns. The hyperbolic distribution is a special case of the GH distribution $H(\alpha, \beta, \delta, \mu) = GH(1, \alpha, \beta, \delta, \mu)$. The hyperbolic distribution is not closed under convolution and has semi-heavy tails.

4.2.2 The Meixner model

The *Meixner distribution* $M(\alpha, \beta, \mu, \delta)$ is not included in the GH family. Schoutens & Teugels (1998), Schoutens (2001) introduced the distribution for asset price returns as an alternative to the hyperbolic family. (It is named for Josef Meixner (1908-1994) to honor his work on so-called Meixner polynomials.) It has density function

$$f^M_{\alpha,\beta,\mu,\delta}(x) = \frac{(2\cos(\beta/2))^{2\delta}}{2\alpha\pi\Gamma(2\delta)} \exp\left(\frac{\beta(x-\mu)}{\alpha}\right) \left|\Gamma\left(\delta + \frac{\mathrm{i}(x-\mu)}{\alpha}\right)\right|,$$

with scale parameter $\alpha > 0$, shape parameter $\delta > 0$, skewness parameter $-\pi < \beta < \pi$ and location parameter $\mu \in \mathbb{R}$. The Meixner distribution is closed under convolution, i.e., for a Meixner-Lévy process $\{X_t\}$ it holds that $X_t \sim M(\alpha, \beta, t\delta, t\mu)$. Furthermore, the Meixner distribution is semi-heavy-tailed. The MLE can be found numerically using Newton methods since the derivative of the log-likelihood is explicitly available.

4.2.3 The stable model

Mandelbrot (1961, 1967) proposed *stable distributions* $S_\alpha(\beta, \mu, \sigma)$ as a model for returns. The stable distribution has no closed-form density (except in a few special cases) and is defined by its characteristic function

$$\varphi^S_{\alpha,\beta,\mu,\sigma}(u) = \begin{cases} \exp\left(\mathrm{i}\mu u - \sigma|u|\left(1 + \frac{2\mathrm{i}\beta}{\pi}\mathrm{sign}(u)\log|u|\right)\right), & \alpha = 1, \\ \exp\left(\mathrm{i}\mu u - \sigma^\alpha|u|^\alpha\left(1 - \mathrm{i}\beta\mathrm{sign}(u)\tan\frac{\alpha\pi}{2}\right)\right), & \alpha \neq 1, \end{cases}$$

with index of stability $\alpha \in (0, 2]$, skewness parameter $\beta \in [-1, 1]$, location parameter $\mu \in \mathbb{R}$ and scale parameter $\sigma > 0$. Important special cases of the stable family are the normal ($\alpha = 2$), the Cauchy ($\alpha = 1$) and "the" Lévy distribution ($\alpha = 1/2$). Since the index of stability is unknown we consider estimation only using the characteristic function. ML estimation is performed using Fourier inversion methods (Nolan 2001). The stable distribution has one heavy tail for $\alpha < 1$ and $\beta = \pm 1$, one light and one heavy tail for $\alpha \geq 1$ and $\beta = \pm 1$, two light tails for $\alpha = 2$ (Gaussian case), and two heavy tails for all other cases. For more properties of stable distributions see Nolan (2018). All stable distributions are closed under convolution. An α-stable Lévy process $\{X_t\}$ has marginals $X_t \sim S_\alpha(\beta, t\mu, t^{1/\alpha}\sigma)$.

4.3 Data

This section gives a brief overview of the data which we use study that follows. Data are provided by the *Thomson Reuters Eikon* database. We consider the 78 equity indices from 70 countries for which hourly data is available. We observe daily closing prices from 01/02/1997 until 11/02/2017 (or a shorter for some countries depending on availability). We compute daily log-returns for trading days. Furthermore, we observe hourly closing prices from 11/02/2016 12pm until 11/02/2017 12pm and compute hourly log-returns for trading hours. In other words, for the goodness of fit analysis of daily log-returns we can use a long sample of almost twenty years, while the analysis of time consistency is restricted to one year. We compute all statistics for daily returns in this and the next section both for the full period and for the one year period.

Figure 4.1 compares the logarithm of fitted densities of the above models to the daily log-returns of the S&P 500 index. The figure also contains the kernel density estimate of the returns. It visualizes the heavy tails of the stable, the Student and the skew Student distributions. The other distributions have semi-heavy tails. The normal distribution is omitted since its light tails are a very poor fit. The empirical density makes it hard to say which of the models fits the tail behavior best. We discuss this further in Section 4.4.

Table 4.1 reports on the countries and indices considered, the number of daily returns for the long period, as well as empirical mean, standard deviation, skewness, kurtosis and minimal and maximal values. The index returns typically have a mean close to and usually larger than zero. There is some skewness in the data. The empirical kurtosis is greater than three, indicating heavy tails. We group the countries into three segments: developed markets (top), emerging markets (middle) and frontier markets (bottom) and apply alphabetical ordering in each group.

Table 4.2 reports statistics for daily returns restricted to the last year of the period. Empirical kurtosis is lower than in Table 4.1 since fewer extreme events occur in this short period. Table 4.3 presents statistics for hourly returns.

Figure 4.2 (a) shows the daily S&P 500, panel (b) shows the daily log-returns. Figure 4.3 (a) shows the one-year hourly S&P 500, panel (b) shows hourly log returns. While the hourly log-returns appear to be stationary, the daily log-returns have different phases, e.g., the financial crisis.

Figure 4.4 shows dot plots of daily log-returns for some indices (entire sampling period). The red box indicates the interquartile range and the white line the median. This illustrates the heavy-tailed nature of the returns. The middle 50 percent of the daily log-returns are compressed into a small band, while the data outside the

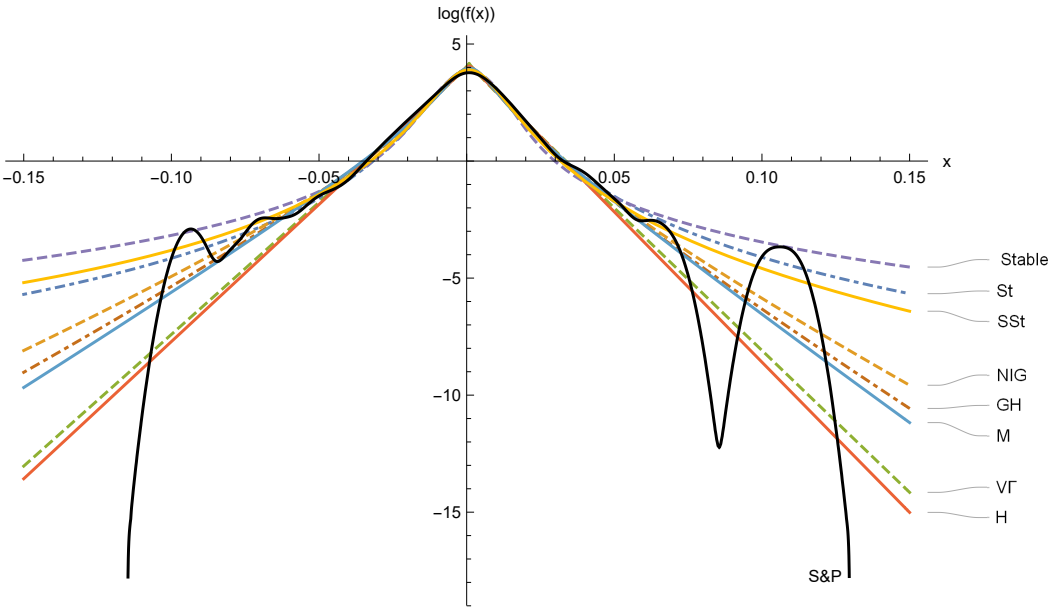

Figure 4.1: Logarithm of densities of fitted distributions to daily log-returns of the S&P 500 index, see Section 4.3. The kernel density estimator (oversmoothed) is given in black.

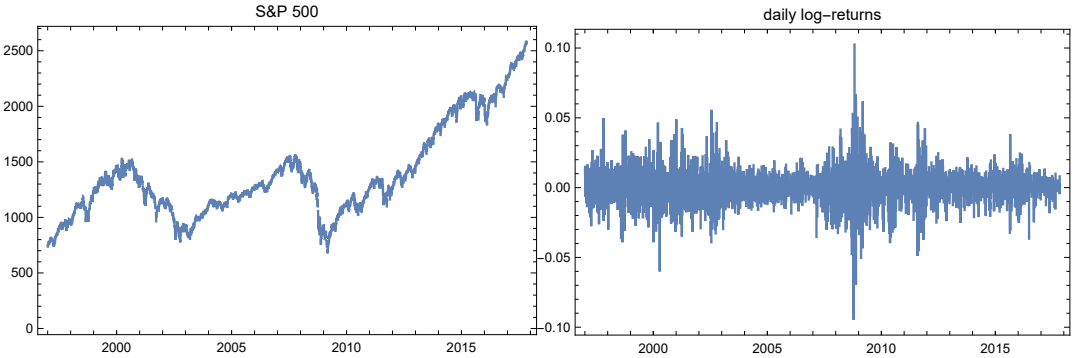

(a) (b)

Figure 4.2: Panel (a) shows the daily S&P 500 from 01/02/1997 until 11/02/2017. Panel (b) shows daily log-returns.

Countries	Index	n	Mean	Sd	Skewness	Kurtosis	Min	Max
Australia	ASX 200	5269	1.75E-04	0.0099	-0.4696	8.6670	-0.0870	0.0572
Australia	All Ordinaries	5268	1.75E-04	0.0096	-0.5483	8.9961	-0.0855	0.0574
Austria	ATX	5156	2.15E-04	0.0142	-0.4011	9.8215	-0.1025	0.1202
Belgium	BEL 20	5313	1.48E-04	0.0124	-0.0295	8.5770	-0.0832	0.0933
Canada	TSX 60	4727	1.95E-04	0.0118	-0.6155	12.4482	-0.1033	0.0983
Canada	TSX Composite	5235	1.91E-04	0.0110	-0.6830	12.0902	-0.0979	0.0937
EuroStoxx	EuroStoxx 50	5334	1.04E-04	0.0132	-0.0525	8.4418	-0.0900	0.1022
Finland	OMXH25	5229	2.62E-04	0.0181	-0.3584	10.2951	-0.1742	0.1456
France	CAC 40	5313	1.68E-04	0.0146	-0.0587	7.4755	-0.0947	0.1059
Germany	DAX	5288	2.95E-04	0.0152	-0.0917	6.9610	-0.0887	0.1080
Hong Kong	Hang Seng	5138	1.50E-04	0.0165	0.0958	13.1446	-0.1473	0.1725
Ireland	ISEQ Overall	5262	1.79E-04	0.0135	-0.6705	11.1581	-0.1396	0.0973
Israel	TA 35	5099	3.66E-04	0.0124	-0.2893	7.3446	-0.0988	0.0923
Italy	FTSE MIB	5034	-1.07E-05	0.0157	-0.1984	7.4934	-0.1333	0.1087
Japan	Topix	5117	3.75E-05	0.0139	-0.2921	8.5004	-0.1001	0.1286
Luxembourg	LuxX Index	4745	1.04E-04	0.0130	-0.3420	9.5255	-0.1116	0.0910
Netherlands	AEX	5317	1.23E-04	0.0145	-0.1441	8.6006	-0.0959	0.1003
New Zealand	NZX 50 Index	4232	3.72E-04	0.0069	-0.5181	8.4709	-0.0525	0.0581
Norway	OBX Index	4555	3.82E-04	0.0153	-0.5362	9.6656	-0.1127	0.1102
Portugal	PSI 20	5286	1.10E-05	0.0123	-0.3426	9.1062	-0.1038	0.1020
Singapore	STI Index	4563	9.56E-05	0.0115	-0.2637	8.3753	-0.0870	0.0753
South Korea	KOSPI	5236	2.60E-04	0.0173	-0.3124	7.8089	-0.1280	0.1128
Spain	IBEX 35	5272	1.40E-04	0.0151	-0.1365	8.3046	-0.1319	0.1348
Sweden	OMXS30	5230	2.45E-04	0.0152	0.0412	6.7460	-0.0880	0.1102
Switzerland	SMI	5241	1.63E-04	0.0121	-0.1909	8.9135	-0.0907	0.1079
UK	FTSE 100	5262	1.16E-04	0.0119	-0.1503	8.5470	-0.0927	0.0938
USA	DowJones 30	5241	2.46E-04	0.0114	-0.1522	10.8003	-0.0820	0.1051
USA	S&P 500	5241	2.39E-04	0.0122	-0.2360	10.9494	-0.0947	0.1096
USA	Nasdaq	5241	3.89E-04	0.0183	0.0952	8.8485	-0.1111	0.1720
Brazil	Bovespa	5158	4.58E-04	0.0206	0.2873	16.2452	-0.1721	0.2883
Chile	IPSA	5191	3.51E-04	0.0106	0.1155	11.4702	-0.0766	0.1180
China	CSI 300	3056	4.52E-04	0.0180	-0.5398	6.6949	-0.0969	0.0893
China	SSE	5045	2.58E-04	0.0163	-0.4007	7.8492	-0.0933	0.0940
Colombia	IGBC	3967	5.99E-04	0.0127	-0.1743	15.7878	-0.1105	0.1469
Czech Republic	PX	5209	1.30E-04	0.0138	-0.4608	14.7225	-0.1619	0.1236
Egypt	EGX 30	4838	5.50E-04	0.0171	-0.3222	11.6822	-0.1799	0.1837
Greece	Athex	5172	-4.19E-05	0.0195	-0.2864	8.3305	-0.1771	0.1343
Hungary	Budapest SE	5202	4.30E-04	0.0170	-0.6040	14.0900	-0.1803	0.1362
India	Nifty 50	5180	4.65E-04	0.0153	-0.2153	10.6826	-0.1305	0.1633
India	BSE Sensex	5180	4.50E-04	0.0154	-0.1664	9.3714	-0.1181	0.1599
Indonesia	IDX Composite	5078	4.42E-04	0.0158	-0.2011	11.0806	-0.1273	0.1313
Malaysia	KLCI	5128	6.77E-05	0.0130	0.5065	65.7219	-0.2415	0.2082
Mexico	IPC	5240	5.09E-04	0.0142	0.0175	11.0234	-0.1431	0.1215
Peru	Lima General	5201	5.06E-04	0.0136	-0.4256	14.0243	-0.1329	0.1282
Philippines	PSEi	5119	1.94E-04	0.0143	0.1849	14.2994	-0.1309	0.1618
Poland	WIG	5218	2.87E-04	0.0137	-0.3973	7.1969	-0.1029	0.0789
Qatar	QE 20 Index	4877	3.73E-04	0.0241	-0.5530	642.7196	-0.8581	0.8442
Russia	MICEX	5010	6.05E-04	0.0260	0.1227	19.3443	-0.2334	0.2750
Russia	RTSI	3154	-8.78E-05	0.0199	-0.7041	32.3405	-0.2596	0.2211
Saudi Arabia	TASI	5061	3.02E-04	0.0141	-0.8853	13.5072	-0.1033	0.0939
South Africa	JSE	5203	4.38E-04	0.0124	-0.4518	8.8747	-0.1263	0.0727
Taiwan	TWII	5261	8.72E-05	0.0139	-0.1695	5.6809	-0.0691	0.0652
Thailand	SET	5094	1.47E-04	0.0156	0.0528	10.9759	-0.1606	0.1135
Turkey	BIST 100	5206	9.11E-04	0.0239	-0.0405	9.5974	-0.1998	0.1777
Un Arab Em	DFM	3587	3.59E-04	0.0175	-0.0353	9.1104	-0.1216	0.1220
Un Arab Em	Abu Dhabi	4236	3.49E-04	0.0110	-0.0855	11.5268	-0.0868	0.0763
Argentina	MERVAL	5121	7.38E-04	0.0217	-0.3015	7.8039	-0.1476	0.1612
Bahrain	All Share	3643	5.70E-05	0.0056	-0.3859	9.3284	-0.0492	0.0361
Bulgaria	SOFIX	4188	4.53E-04	0.0152	-0.6017	37.1980	-0.2090	0.2107
Croatia	CROBEX	4844	1.35E-04	0.0145	0.1982	19.1451	-0.1109	0.1747
Cyprus	CYMAIN	3219	-9.46E-04	0.0266	0.0335	9.4221	-0.1670	0.1749
Estonia	OMXT	5092	3.96E-04	0.0150	-1.0884	28.4849	-0.2158	0.1287
Kazakhstan	KASE Index	4131	7.35E-04	0.0267	0.6189	67.2996	-0.4864	0.4876
Kuwait	Kuwait 15	1352	-2.38E-05	0.0076	-0.0227	7.8663	-0.0499	0.0506
Latvia	OMXR	4411	5.18E-04	0.0142	-0.3801	19.7370	-0.1471	0.1160
Lithuania	OMXV	4396	4.28E-04	0.0102	-0.5168	24.1855	-0.1194	0.1100
Mauritius	SEMDEX	5097	3.58E-04	0.0062	0.3365	26.8623	-0.0638	0.0765
Morocco	MASI	3950	3.07E-04	0.0076	-0.4295	9.7235	-0.0682	0.0446
Namibia	NSX Overall	3773	3.06E-04	0.0156	-0.4181	8.0880	-0.1483	0.0870
Oman	MSM 30	5083	1.82E-04	0.0138	0.5548	444.2203	-0.4398	0.4542
Pakistan	KSE 100	5093	6.67E-04	0.0151	-0.3510	9.2609	-0.1321	0.1276
Romania	BET 10	5024	4.11E-04	0.0165	-0.3589	10.7408	-0.1312	0.1056
Serbia	BELEX	3042	-1.04E-04	0.0126	0.1317	18.9038	-0.1086	0.1216
Sri Lanka	CSE All-Share	4969	4.81E-04	0.0111	0.2593	35.4884	-0.1389	0.1829
Tunesia	Tunindex	4878	3.71E-04	0.0078	-0.4186	561.8742	-0.2669	0.2654
Venezuela	IBC	4768	2.42E-03	0.0201	1.0871	19.0283	-0.2066	0.2006
Vietnam	HNX 30	2967	1.13E-05	0.0199	0.0106	7.2570	-0.1286	0.0973
Zambia	All Share	3919	1.00E-03	0.0207	1.2196	36.1472	-0.2086	0.3112

Table 4.1: Countries with equity indices, number of non-zero daily log-returns from 01/03/1997 until 11/02/2017 (if available), mean, standard deviation, skewness, kurtosis, minimal and maximal log-return.

Countries	Index	n	Mean	Sd	Skewness	Kurtosis	Min	Max
Australia	ASX 200	253	4.98E-04	0.00661	0.2122	4.9154	-0.0194	0.0329
Australia	All Ordinaries	253	4.84E-04	0.00630	0.2116	5.1678	-0.0196	0.0320
Austria	ATX	249	1.39E-03	0.00788	0.1120	3.3902	-0.0231	0.0304
Belgium	BEL 20	257	6.81E-04	0.00631	0.4721	4.7953	-0.0142	0.0307
Canada	TSX 60	250	3.96E-04	0.00503	-0.4571	3.8445	-0.0187	0.0124
Canada	TSX Composite	250	3.75E-04	0.00489	-0.4619	3.9177	-0.0175	0.0129
EuroStoxx	EuroStoxx 50	258	6.25E-04	0.00560	0.3087	3.6652	-0.0140	0.0202
Finland	OMXH25	253	6.91E-04	0.00660	-0.0460	3.4182	-0.0211	0.0199
France	CAC 40	257	8.63E-04	0.00677	0.8036	7.3632	-0.0189	0.0406
Germany	DAX	254	1.02E-03	0.00675	0.5890	5.3229	-0.0184	0.0332
Hong Kong	Hang Seng	247	9.04E-04	0.00717	-0.2403	3.6133	-0.0218	0.0222
Ireland	ISEQ Overall	254	6.65E-04	0.00755	0.3766	3.8261	-0.0179	0.0303
Israel	TA 35	244	1.43E-04	0.00527	0.1122	3.6891	-0.0154	0.0164
Italy	FTSE MIB	256	1.32E-03	0.00973	0.5764	5.5315	-0.0299	0.0466
Japan	Topix	247	1.10E-03	0.00824	0.4504	14.6809	-0.0468	0.0562
Luxembourg	LuxX Index	257	1.59E-04	0.01072	0.1878	3.8062	-0.0340	0.0367
Netherlands	AEX	256	8.69E-04	0.00576	0.1247	3.6523	-0.0153	0.0223
New Zealand	NZX 50 Index	251	6.57E-04	0.00521	-0.9906	11.5728	-0.0340	0.0241
Norway	OBX Index	252	1.14E-03	0.00746	-0.2402	3.0805	-0.0230	0.0224
Portugal	PSI 20	257	7.12E-04	0.00742	0.3931	4.8158	-0.0283	0.0273
Singapore	STI Index	251	7.40E-04	0.00535	-0.0616	3.1034	-0.0142	0.0159
South Korea	KOSPI	245	1.03E-03	0.00600	0.0437	5.3061	-0.0227	0.0227
Spain	IBEX 35	257	6.58E-04	0.00844	0.4616	4.6395	-0.0289	0.0369
Sweden	OMXS30	253	6.50E-04	0.00644	0.1710	3.3660	-0.0197	0.0226
Switzerland	SMI	253	7.31E-04	0.00613	0.2383	3.7790	-0.0151	0.0197
UK	FTSE 100	253	3.55E-04	0.00570	-0.2612	5.0869	-0.0249	0.0209
USA	DowJones 30	251	1.06E-03	0.00440	0.2308	6.2821	-0.0179	0.0205
USA	S&P 500	250	8.26E-04	0.00455	-0.0243	6.5978	-0.0183	0.0220
USA	Nasdaq	251	1.11E-03	0.00687	-0.5112	6.1731	-0.0255	0.0287
Brazil	Bovespa	248	7.20E-04	0.01303	-1.5747	13.0742	-0.0921	0.0391
Chile	IPSA	248	1.09E-03	0.00619	-0.1246	3.9666	-0.0191	0.0228
China	CSI 300	245	7.41E-04	0.00600	-0.2331	4.3670	-0.0244	0.0179
China	SSE	245	3.53E-04	0.00558	-0.3287	4.8000	-0.0250	0.0182
Colombia	IGBC	243	2.46E-04	0.00625	-0.5826	5.2657	-0.0276	0.0162
Czech Republic	PX	252	6.59E-04	0.00525	-0.2353	4.0755	-0.0176	0.0187
Egypt	EGX 30	244	2.13E-03	0.01227	0.7191	6.2119	-0.0381	0.0594
Greece	Athex	253	1.10E-03	0.01157	-0.3044	4.6478	-0.0415	0.0413
Hungary	Budapest SE	253	1.22E-03	0.00782	-0.1140	5.6012	-0.0254	0.0392
India	Nifty 50	248	8.18E-04	0.00659	-0.4197	4.6855	-0.0273	0.0185
India	BSE Sensex	249	8.01E-04	0.00633	-0.2798	4.2903	-0.0257	0.0175
Indonesia	IDX Composite	240	4.56E-04	0.00676	-0.6217	9.6635	-0.0409	0.0256
Malaysia	KLCI	244	1.96E-04	0.00364	0.1660	3.9486	-0.0113	0.0115
Mexico	IPC	252	1.38E-04	0.00742	-0.9003	9.8457	-0.0468	0.0286
Peru	Lima General	250	1.11E-03	0.00669	0.0212	3.4830	-0.0183	0.0220
Philippines	PSEi	244	6.58E-04	0.00865	-0.2380	4.2911	-0.0292	0.0279
Poland	WIG	251	1.19E-03	0.00760	0.4032	3.5238	-0.0189	0.0273
Qatar	QE 20 Index	248	-8.50E-04	0.00938	-1.7707	18.7009	-0.0754	0.0300
Russia	MICEX	253	2.07E-04	0.00827	-0.0543	3.3711	-0.0253	0.0242
Russia	RTSI	251	7.48E-04	0.01050	-0.5694	7.0801	-0.0566	0.0351
Saudi Arabia	TASI	250	5.89E-04	0.00851	1.1154	9.1039	-0.0262	0.0535
South Africa	JSE	249	6.60E-04	0.00712	-0.1218	3.3873	-0.0235	0.0213
Taiwan	TWII	247	6.72E-04	0.00594	-0.5747	6.3984	-0.0302	0.0231
Thailand	SET	244	5.21E-04	0.00434	-0.1857	5.2244	-0.0171	0.0177
Turkey	BIST 100	254	1.54E-03	0.00960	0.1329	4.7235	-0.0320	0.0407
Un Arab Em	DFM	251	3.81E-04	0.00729	0.5581	4.0359	-0.0176	0.0273
Un Arab Em	Abu Dhabi	251	1.83E-04	0.00698	0.1540	5.1772	-0.0295	0.0259
Argentina	MERVAL	246	2.07E-03	0.01343	-0.2658	4.7290	-0.0494	0.0488
Bahrain	All Share	245	4.57E-04	0.00481	0.9688	8.7882	-0.0178	0.0275
Bulgaria	SOFIX	251	8.85E-04	0.00729	-0.4216	12.6743	-0.0467	0.0390
Croatia	CROBEX	252	-1.55E-04	0.00739	-0.6573	6.9662	-0.0311	0.0229
Cyprus	CYMAIN	250	1.72E-04	0.01229	0.2000	4.4878	-0.0361	0.0537
Estonia	OMXT	254	6.84E-04	0.00449	0.0762	4.4556	-0.0133	0.0196
Kazakhstan	KASE Index	246	1.97E-03	0.00820	-0.1724	3.4053	-0.0288	0.0219
Kuwait	Kuwait 15	249	5.93E-04	0.00780	0.3506	4.3000	-0.0254	0.0298
Latvia	OMXR	251	1.44E-03	0.00823	3.8235	36.2884	-0.0209	0.0804
Lithuania	OMXV	250	7.04E-04	0.00375	-0.1413	4.4677	-0.0124	0.0149
Mauritius	SEMDEX	249	8.05E-04	0.00269	0.3366	5.9271	-0.0116	0.0103
Morocco	MASI	250	6.33E-04	0.00745	0.8390	6.6608	-0.0209	0.0330
Namibia	NSX Overall	249	4.92E-04	0.00972	0.1206	4.1788	-0.0323	0.0327
Oman	MSM 30	247	-3.32E-04	0.00438	0.1873	4.3251	-0.0143	0.0185
Pakistan	KSE 100	251	-1.21E-04	0.01113	-0.7080	5.6065	-0.0476	0.0317
Romania	BET 10	250	5.68E-04	0.00651	-0.5429	9.5517	-0.0390	0.0266
Serbia	BELEX	252	3.57E-04	0.00557	-0.3319	6.3354	-0.0256	0.0202
Sri Lanka	CSE All-Share	240	1.23E-04	0.00378	0.5970	4.0644	-0.0090	0.0153
Tunesia	Tunindex	253	3.95E-04	0.00308	0.3839	3.3156	-0.0070	0.0109
Venezuela	IBC	238	1.61E-02	0.03575	1.1060	6.0132	-0.0827	0.1704
Vietnam	HNX 30	250	9.62E-04	0.00657	-0.2804	3.1174	-0.0180	0.0179
Zambia	All Share	161	1.08E-03	0.00698	-0.0933	6.3659	-0.0226	0.0278

Table 4.2: Countries with equity indices, number of non-zero daily log-returns from 11/03/2016 until 11/02/2017, mean, standard deviation, skewness, kurtosis, minimal and maximal log-return.

Countries	Index	n	Mean	Sd	Skewness	Kurtosis	Min	Max
Australia	ASX 200	1800	7.06E-05	0.00245	0.4388	21.3538	-0.0181	0.0297
Australia	All Ordinaries	1814	6.82E-05	0.00231	0.4833	23.6521	-0.0177	0.0291
Austria	ATX	2242	1.54E-04	0.00257	0.2388	9.5376	-0.0182	0.0191
Belgium	BEL 20	2309	7.37E-05	0.00223	0.8710	20.2231	-0.0126	0.0289
Canada	TSX 60	1995	4.54E-05	0.00194	-0.2382	9.0734	-0.0132	0.0113
Canada	TSX Composite	2007	4.19E-05	0.00179	-0.2498	9.3709	-0.0124	0.0102
EuroStoxx	EuroStoxx 50	2320	6.63E-05	0.00207	0.5640	12.4904	-0.0135	0.0177
Finland	OMXH25	2275	7.55E-05	0.00216	0.1201	12.5739	-0.0159	0.0158
France	CAC 40	2311	9.37E-05	0.00250	1.7853	32.8108	-0.0137	0.0391
Germany	DAX	2283	1.11E-04	0.00236	1.0342	16.4528	-0.0147	0.0256
Hong Kong	Hang Seng	1927	1.15E-04	0.00250	-0.1732	12.1575	-0.0173	0.0205
Ireland	ISEQ Overall	2434	6.97E-05	0.00237	0.7375	12.4769	-0.0140	0.0214
Israel	TA 35	2127	1.60E-05	0.00181	0.4841	11.6591	-0.0125	0.0136
Italy	FTSE MIB	2304	1.42E-04	0.00320	0.5716	12.4431	-0.0208	0.0335
Japan	Topix	1723	1.68E-04	0.00304	2.4663	52.5856	-0.0222	0.0498
Luxembourg	LuxX Index	2270	1.79E-05	0.00387	-0.3749	12.0211	-0.0300	0.0262
Netherlands	AEX	2293	9.52E-05	0.00217	0.3290	14.6740	-0.0148	0.0210
New Zealand	NZX 50 Index	2107	7.83E-05	0.00166	-0.4736	61.1024	-0.0241	0.0264
Norway	OBX Index	2019	1.38E-04	0.00247	-0.2709	9.4210	-0.0167	0.0146
Portugal	PSI 20	2311	7.49E-05	0.00246	0.1126	17.2719	-0.0252	0.0222
Singapore	STI Index	2249	8.35E-05	0.00180	-0.1456	10.6594	-0.0110	0.0123
South Korea	KOSPI	1711	1.47E-04	0.00219	0.1866	14.7022	-0.0157	0.0183
Spain	IBEX 35	2564	6.32E-05	0.00287	-0.1460	28.5718	-0.0401	0.0316
Sweden	OMXS30	2259	7.09E-05	0.00221	0.1992	11.2113	-0.0134	0.0170
Switzerland	SMI	2276	7.89E-05	0.00202	0.6186	12.4761	-0.0123	0.0183
UK	FTSE 100	2269	3.73E-05	0.00203	0.1778	10.6633	-0.0126	0.0163
USA	DowJones 30	2008	1.31E-04	0.00154	1.0947	14.2450	-0.0105	0.0147
USA	S&P 500	2000	1.00E-04	0.00159	0.6406	13.4870	-0.0102	0.0155
USA	Nasdaq	2009	1.35E-04	0.00234	-0.3633	16.4007	-0.0232	0.0193
Brazil	Bovespa	2077	7.46E-05	0.00438	-3.9932	91.6913	-0.0901	0.0252
Chile	IPSA	2070	1.29E-04	0.00281	0.1156	300.5028	-0.0656	0.0668
China	CSI 300	1709	1.06E-04	0.00249	0.1219	7.7060	-0.0120	0.0171
China	SSE	1711	5.06E-05	0.00234	-0.4025	8.5230	-0.0157	0.0117
Colombia	IGBC	1837	3.11E-05	0.00207	-0.1891	8.0009	-0.0134	0.0116
Czech Republic	PX	2008	8.42E-05	0.00196	-0.1772	12.0585	-0.0195	0.0135
Egypt	EGX 30	1200	4.32E-04	0.00500	2.3446	20.7353	-0.0292	0.0450
Greece	Athex	2019	1.35E-04	0.00381	-0.0536	8.0771	-0.0233	0.0253
Hungary	Budapest SE	2279	1.31E-04	0.00235	0.2235	8.1885	-0.0130	0.0182
India	Nifty 50	1734	1.17E-04	0.00234	-0.4861	15.2852	-0.0238	0.0156
India	BSE Sensex	1738	1.14E-04	0.00231	-0.1696	13.8418	-0.0224	0.0162
Indonesia	IDX Composite	1819	6.16E-05	0.00225	-1.1355	45.1226	-0.0299	0.0235
Malaysia	KLCI	1694	2.88E-05	0.00133	-0.5679	13.6636	-0.0117	0.0080
Mexico	IPC	1879	1.20E-05	0.00266	-0.1461	11.9105	-0.0206	0.0217
Peru	Lima General	2043	1.29E-04	0.00194	0.1635	7.4021	-0.0130	0.0119
Philippines	PSEi	1706	9.81E-05	0.00318	0.3536	9.7002	-0.0213	0.0206
Poland	WIG	2259	1.28E-04	0.00235	0.3952	8.8587	-0.0143	0.0184
Qatar	QE 20 Index	1240	-1.71E-04	0.00422	-5.3766	108.2169	-0.0798	0.0267
Russia	MICEX	2277	1.84E-05	0.00275	-0.3768	7.2733	-0.0209	0.0139
Russia	RTSI	2223	8.47E-05	0.00375	-0.5897	15.1628	-0.0434	0.0231
Saudi Arabia	TASI	1303	1.15E-04	0.00341	0.7533	13.0481	-0.0271	0.0268
South Africa	JSE	2230	7.40E-05	0.00235	0.3934	8.5755	-0.0127	0.0154
Taiwan	TWII	1233	1.37E-04	0.00250	0.3247	15.9052	-0.0203	0.0238
Thailand	SET	1699	7.46E-05	0.00178	0.0030	6.7063	-0.0085	0.0097
Turkey	BIST 100	2526	1.54E-04	0.00268	-1.2968	21.8438	-0.0373	0.0174
Un Arab Em	DFM	1003	9.55E-05	0.00360	0.1046	8.4330	-0.0266	0.0202
Un Arab Em	Abu Dhabi	1255	3.66E-05	0.00324	-0.7373	15.2062	-0.0336	0.0214
Argentina	MERVAL	1735	3.03E-04	0.00450	-0.5839	18.7074	-0.0446	0.0325
Bahrain	All Share	885	1.28E-04	0.00273	0.7879	36.2110	-0.0281	0.0315
Bulgaria	SOFIX	1931	1.20E-04	0.00293	1.0336	28.3603	-0.0287	0.0368
Croatia	CROBEX	2000	-2.15E-05	0.00268	-2.5604	50.9294	-0.0439	0.0192
Cyprus	CYMAIN	1683	2.80E-05	0.00710	-0.1935	7.7709	-0.0472	0.0394
Estonia	OMXT	1629	1.05E-04	0.00236	0.4862	13.9078	-0.0197	0.0221
Kazakhstan	KASE Index	1673	2.89E-04	0.00374	0.3373	7.4059	-0.0229	0.0242
Kuwait	Kuwait 15	992	1.52E-04	0.00423	0.5725	6.4445	-0.0143	0.0251
Latvia	OMXR	1421	2.50E-04	0.00390	6.9598	142.2951	-0.0194	0.0818
Lithuania	OMXV	1580	1.11E-04	0.02007	-0.2090	778.6937	-0.5631	0.5605
Mauritius	SEMDEX	998	2.00E-04	0.00133	0.4685	11.6620	-0.0083	0.0087
Morocco	MASI	1738	9.34E-05	0.00276	2.2058	36.8220	-0.0132	0.0421
Namibia	NSX Overall	2221	5.16E-05	0.00403	-0.3037	13.4956	-0.0311	0.0307
Oman	MSM 30	916	-8.97E-05	0.00186	0.0456	7.8146	-0.0103	0.0118
Pakistan	KSE 100	1727	-1.72E-05	0.00389	-0.5270	10.2687	-0.0332	0.0208
Romania	BET 10	2496	5.62E-05	0.00200	-0.5344	19.2760	-0.0186	0.0201
Serbia	BELEX	1409	6.44E-05	0.00337	0.0670	5.6360	-0.0134	0.0164
Sri Lanka	CSE All-Share	1435	2.05E-05	0.00121	0.5534	6.2710	-0.0052	0.0070
Tunesia	Tunindex	1203	8.53E-05	0.00169	0.1193	4.4026	-0.0068	0.0069
Venezuela	IBC	890	4.32E-03	0.01754	0.7130	8.7080	-0.0835	0.1071
Vietnam	HNX 30	1264	1.97E-04	0.00317	0.1264	4.4978	-0.0115	0.0140
Zambia	All Share	470	3.30E-04	0.02537	0.0328	81.6378	-0.2973	0.2986

Table 4.3: Countries with equity indices, number of non-zero hourly log-returns from 11/03/2016 1pm until 11/02/2017 12pm, mean, standard deviation, skewness, kurtosis, minimal and maximal log-return.

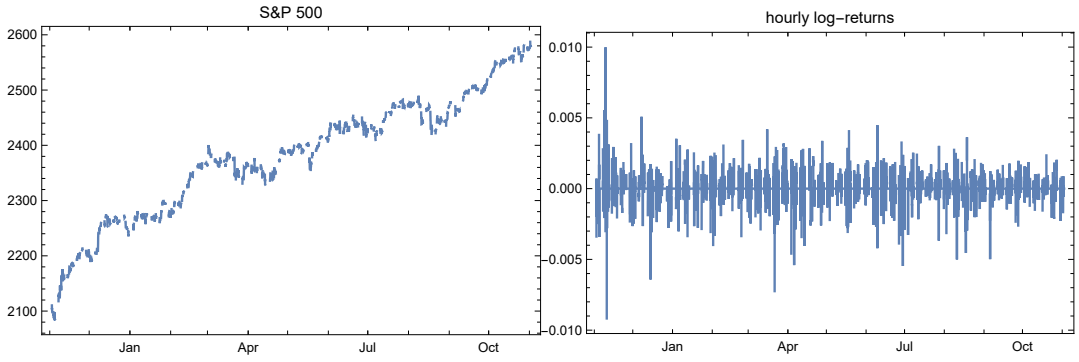

(a) (b)

Figure 4.3: Panel (a) shows the hourly S&P 500 from 11/02/2016 12pm until 11/02/2017 12pm. Panel (b) shows hourly log-returns.

interquartile range are widely dispersed. For some indices, e.g., the Tunisian Tunindex, there occur extreme outliers. Figure 4.5 likewise shows dot plots for hourly returns. The red boxes' share of the full range is smaller than for daily returns, indicating that the tails are heavier.

4.4 Goodness of fit

This section aims to decide which Lévy model is the best fit for daily and intraday returns. We compare the Lévy models $L \in \{N, St, SSt, NIG, V\Gamma, H, GH, M, S_\alpha\}$ presented in Section 4.2. We fit the distributions to the log-returns by (possibly numerically) maximizing the log-likelihood $\ell^L(\theta) = \sum_{i=1}^n \log f^L(x_i;\theta)$, where $\theta = (\theta_1, \ldots, \theta_k)$ is the vector of parameters. Note that k depends on the specific Lévy model L. Let $\hat{\theta}$ denote the ML estimate given the log-returns $x_1, \ldots, x_n$.

We use three different measures of goodness of fit.

- The *Kolmogorov-Smirnov (KS) statistic* (Kolmogorov 1933) compares the empirical distribution function $F_n(x) = \frac{1}{n}\sum_{i=1}^n \mathbb{1}_{(-\infty,x]}(x_i)$ with the distribution function of the fitted Lévy model $F^L(x;\hat{\theta})$ and is given by the maximal deviance

$$KS = \sup_{x\in\mathbb{R}} |F_n(x) - F^L(x;\hat{\theta})|.$$

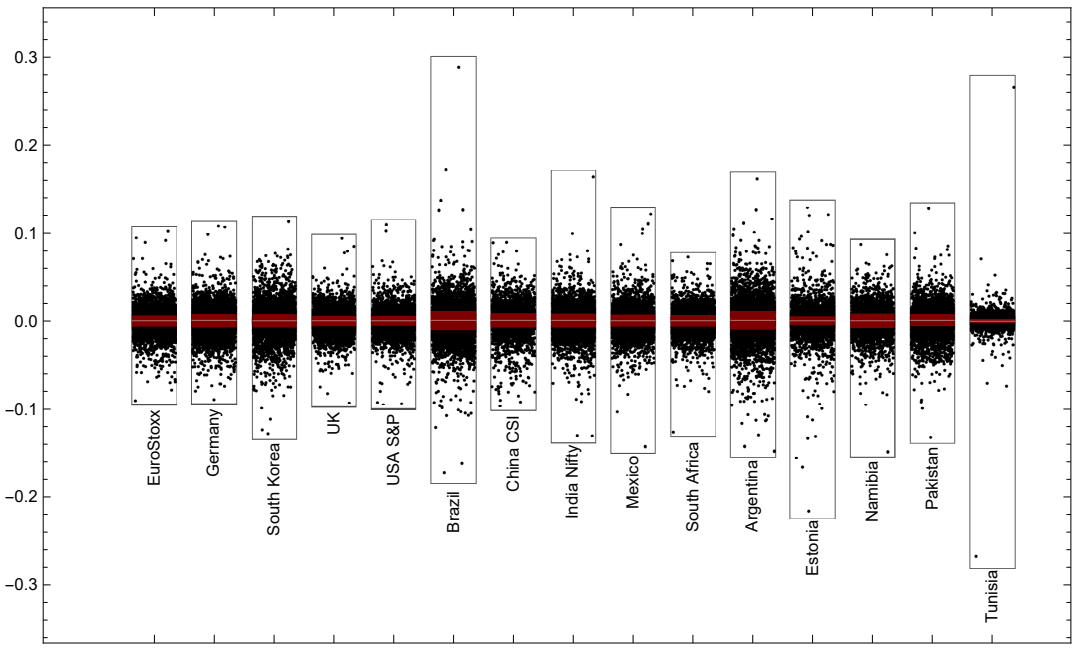

Figure 4.4: Dot plots of daily log-returns for several countries. The red box indicates the interquartile range and the white line within it the median.

- The *Anderson-Darling (AD) statistic* (Anderson & Darling 1954) is defined by

$$\begin{aligned} AD &= n \int_{-\infty}^{\infty} \frac{(F_n(x) - F^L(x;\hat{\theta}))^2}{F^L(x;\hat{\theta})(1 - F^L(x;\hat{\theta}))} \mathrm{d}F^L(x;\hat{\theta}) \\ &= -n - \sum_{i=1}^{n} \frac{2i-1}{n} \left(\log F^L(x_{(i)};\hat{\theta}) + \log \left(1 - F^L(x_{(i)};\hat{\theta}) \right) \right), \end{aligned}$$

  where $x_{(1)} \leq \ldots \leq x_{(n)}$ are the observed ordered data.

- The *Bayesian information criterion (BIC)* (Schwarz 1978) is defined by

$$BIC = k \log(n) - 2\ell^L(\hat{\theta}).$$

For each criterion the model with the smallest statistic is considered to be the best fit among the models investigated. The KS statistic better reflects the deviance between the empirical and the fitted distribution close to the center and the AD statistic better reflects the deviance in the tails (Razali et al. 2011). Generally, the KS and AD statistics do not account for overfitting. However, it is possible that a special or limiting case may have a lower distance due to the nature of the distances and the

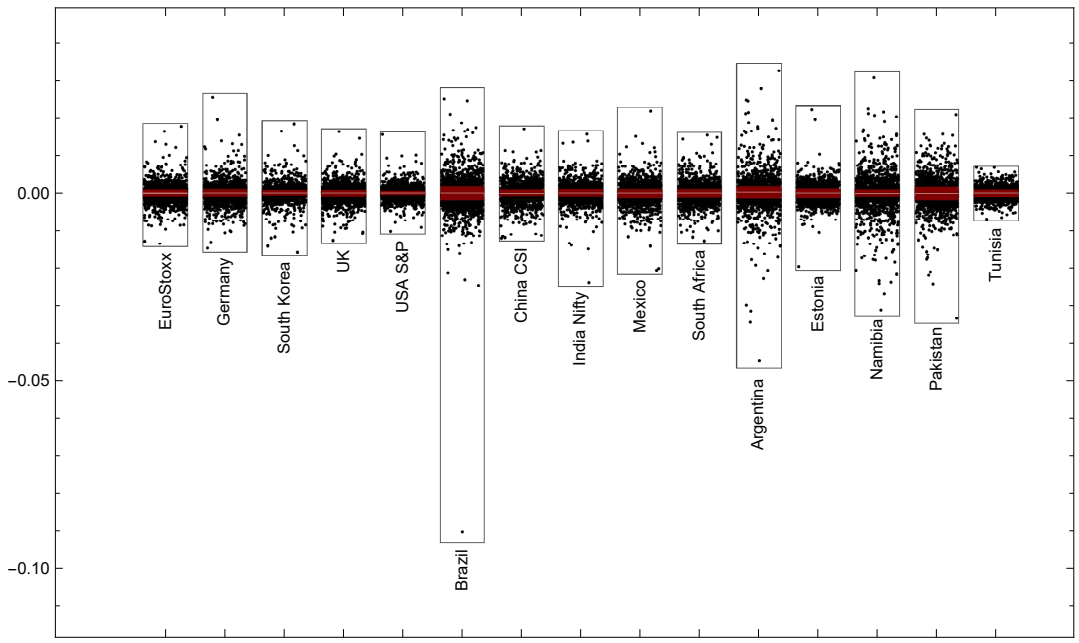

Figure 4.5: Dot plots of hourly log-returns for several countries. The red box indicates the interquartile range and the white line within it the median.

distributions. The BIC statistics adjust the log-likelihood by penalizing models which are too large to avoid overfitting.

In the following, we compare Lévy models to determine which fits best for each index. The decision as to which physical time unit corresponds to $t = 1$ is crucial. This is because models which are not closed under convolution have no closed-form distribution for $t \neq 1$. Thus, if we observe data with time distance unequal to one, estimation is tricky. Of course, it is possible to redefine the meaning of $t = 1$ by making it correspond to the new physical time. However, since in this chapter $t = 1$ always corresponds to one day, there is no problem in ML estimation for daily returns as we basically fit the distributions of Section 4.2 to them.

For hourly returns there also is no problem for the distributions which are closed under convolution, viz. the normal, the variance gamma, the NIG, the Meixner and the stable distributions. We refer the reader to the corresponding subsections for their distributions at time t. We can fit these to hourly data as in the case of daily data. The skew Student t, the hyperbolic and the GH distribution are not closed under convolution. This means that for hourly data there exists no known distribution. Moreover, as yet, there exists no ML estimation routine. Hence we do not fit these Lévy models to hourly data. The Student-Lévy process is a special case because

the Student t distribution is not closed under convolution but we have developed an MCEM estimation routine in Chapter 3. However, this algorithm only works for fixed degree of freedom ν. Thus, we maximize the log-likelihood only for small integer values of ν.

Tables 4.4 – 4.6 report KS, AD and BIC for daily log-returns for the last 20 years. For each country we compare all Lévy models presented here. The minimal statistic is printed in bold to indicate the best fit. The different criteria do not always lead to the same conclusion. This is reasonable, as they focus on different features. In terms of KS (Table 4.4) and AD (Table 4.5) statistics the GH distribution often yields a good fit, due not least to its five parameters. In these cases the NIG distribution often is the second best choice. This applies both to highly developed (USA) as well as less developed (Oman) countries. For certain other indices it is the first choice. Almost all countries have a semi-heavy-tailed (NIG, variance gamma, H, GH, Meixner) distribution as best fit. The heavy-tailed Student t and skew Student t are the first choices only for some exotic markets, e.g., Kuwait, Namibia or Tunisia. Kuwait is the only country for which the symmetric Student t distribution yields the best fit. It is noteworthy that the stable distributions never yield the best fit, probably due to their overly heavy tails. The AD statistic for the stable distribution often is much larger than the minimum. The normal distribution yields a bad fit for all countries.

The BIC favors small models. This makes it attractive since models with many parameters can lead to overfitting. The BIC for daily returns in the long period is minimal in many countries for the NIG and Student t distributions. According to the BIC, the GH distribution leads to overfitting, as also discussed by Prause (1997). If all three criteria suggest the same model, e.g., for Kuwait the Student t distribution, for the USA's Nasdaq the GH distribution and for Finland the Meixner distribution, this model can be assumed to be the best fit and not to be overfitted. If the three criteria suggest different models we may follow the criterion which reflects a certain desired property well. For asset returns, where we are interested in modeling the tails, the AD statistic is very important.

So far we have only investigated which of the models fit best and not whether the fits are qualitatively good. To analyze this, we plot QQ-plots. We discuss one example in more detail (others are available on request). Figure 4.6 plots the empirical quantiles of the German DAX index against the theoretical quantiles, each panel corresponding to one model. Obviously, the normal model yields a bad fit. The symmetric Student model has some difficulty capturing the skewness in the data. Each of the other distributions fits quite well, making it hard to find the best by visual inspection. KS, AD and BIC suggest that the variance gamma model yields the best fit. In fact, there is at least one good fit for almost all other indices.

The entire sampling period is very long (approx. 20 years) and contains various

Country	Index	N	St	SSt	NIG	VΓ	Hyp	GH	Meix	Stable
Australia	ASX 200	0.0589	0.0125	0.0107	**0.0069**	0.0090	0.0079	0.0089	0.0079	0.0174
Australia	All Ordinaries	0.0611	0.0130	0.0106	**0.0077**	0.0090	0.0082	0.0099	0.0083	0.0172
Austria	ATX	0.0813	0.0154	0.0080	0.0090	0.0181	0.0169	**0.0075**	0.0115	0.0114
Belgium	BEL 20	0.0731	0.0168	0.0117	0.0072	0.0123	0.0111	**0.0071**	0.0077	0.0175
Canada	TSX 60	0.0776	0.0155	0.0093	**0.0084**	0.0143	0.0130	0.0090	0.0100	0.0150
Canada	TSX Composite	0.0809	0.0163	0.0080	0.0098	0.0165	0.0139	**0.0075**	0.0111	0.0119
EuroStoxx	EuroStoxx 50	0.0704	0.0135	0.0113	0.0060	0.0097	0.0090	0.0055	**0.0052**	0.0175
Finland	OMXH25	0.0787	0.0156	0.0120	0.0069	0.0131	0.0135	0.0095	**0.0061**	0.0170
France	CAC 40	0.0656	0.0111	0.0086	0.0050	0.0111	0.0082	**0.0050**	0.0064	0.0147
Germany	DAX	0.0671	0.0160	0.0162	0.0107	**0.0055**	0.0058	0.0055	0.0095	0.0235
Hong Kong	Hang Seng	0.0801	0.0165	0.0160	0.0107	0.0109	0.0096	0.0118	**0.0095**	0.0234
Ireland	ISEQ Overall	0.0790	0.0101	0.0072	0.0076	0.0160	0.0155	**0.0055**	0.0088	0.0130
Israel	TA 35	0.0618	0.0125	0.0129	0.0094	0.0093	**0.0082**	0.0084	0.0086	0.0203
Italy	FTSE MIB	0.0668	0.0164	0.0540	0.0093	0.0082	0.0066	**0.0060**	0.0074	0.0224
Japan	Topix	0.0575	0.0131	0.0114	**0.0079**	0.0101	0.0085	0.0110	0.0080	0.0195
Luxembourg	LuxX Index	0.0639	0.0078	0.0063	0.0064	0.0126	0.0112	**0.0062**	0.0076	0.0123
Netherlands	AEX	0.0731	0.0231	0.0104	**0.0064**	0.0112	0.0109	0.0064	0.0066	0.0158
New Zealand	NZX 50 Index	0.0526	0.0163	0.0135	0.0102	0.0106	**0.0084**	0.0130	0.0088	0.0157
Norway	OBX Index	0.0717	0.0134	0.0075	0.0070	0.0147	0.0130	**0.0064**	0.0092	0.0135
Portugal	PSI 20	0.0692	0.0118	0.0108	0.0075	0.0108	0.0092	0.0077	**0.0062**	0.0192
Singapore	STI Index	0.0715	0.0124	0.0109	**0.0058**	0.0111	0.0091	0.0059	0.0069	0.0174
South Korea	KOSPI	0.0919	0.0199	0.0195	0.0124	0.0158	0.0216	**0.0073**	0.0107	0.0230
Spain	IBEX 35	0.0569	0.0143	0.0134	0.0100	0.0078	**0.0072**	0.0091	0.0088	0.0177
Sweden	OMXS30	0.0580	0.0125	0.0121	0.0087	0.0101	0.0091	0.0079	**0.0074**	0.0154
Switzerland	SMI	0.0724	0.0126	0.0087	0.0067	0.0120	0.0117	0.0078	**0.0065**	0.0144
UK	FTSE 100	0.0685	0.0099	0.0086	0.0057	0.0100	0.0093	**0.0052**	0.0074	0.0129
USA	DowJones 30	0.0812	0.0151	0.0156	0.0097	0.0130	0.0105	**0.0085**	0.0086	0.0228
USA	S&P 500	0.0827	0.0170	0.0166	0.0095	0.0122	0.0117	**0.0077**	0.0080	0.0232
USA	Nasdaq	0.0865	0.0233	0.0213	0.0166	0.0126	0.0171	**0.0085**	0.0150	0.0275
Brazil	Bovespa	0.0599	0.0100	**0.0065**	0.0090	0.0130	0.0116	0.0065	0.0106	0.0117
Chile	IPSA	0.0610	0.0084	0.0086	**0.0072**	0.0115	0.0088	0.0081	0.0079	0.0158
China	CSI 300	0.0867	0.0281	0.0269	0.0182	0.0167	0.0206	**0.0158**	0.0191	0.0357
China	SSE	0.0842	0.0185	0.0178	0.0115	0.0144	0.0161	**0.0095**	0.0106	0.0245
Colombia	IGBC	0.0830	0.0137	0.0137	**0.0098**	0.0142	0.0144	0.0130	0.0099	0.0192
Czech Republic	PX	0.0721	0.0127	0.0083	0.0092	0.0153	0.0140	**0.0080**	0.0107	0.0107
Egypt	EGX 30	0.0691	0.0103	0.0079	0.0072	0.0136	0.0125	**0.0072**	0.0082	0.0141
Greece	Athex	0.0711	0.0119	0.0125	0.0076	0.0113	0.0082	**0.0068**	0.0073	0.0189
Hungary	Budapest SE	0.0682	0.0070	0.0063	0.0102	0.0172	0.0157	**0.0062**	0.0124	0.0149
India	Nifty 50	0.0684	0.0111	0.0107	**0.0058**	0.0091	0.0082	0.0073	0.0058	0.0178
India	BSE Sensex	0.0661	0.0120	0.0110	**0.0060**	0.0096	0.0081	0.0065	0.0062	0.0162
Indonesia	IDX Composite	0.0863	0.0119	0.0109	0.0111	0.0185	0.0195	**0.0091**	0.0130	0.0126
Malaysia	KLCI	0.1392	0.0107	0.0103	0.0092	0.0254	0.0341	**0.0081**	0.0113	0.0129
Mexico	IPC	0.0716	0.0110	0.0101	**0.0071**	0.0134	0.0127	0.0075	0.0074	0.0149
Peru	Lima General	0.0927	0.0116	0.0114	**0.0096**	0.0204	0.0209	0.0108	0.0106	0.0131
Philippines	PSEi	0.0711	0.0082	0.0063	0.0097	0.0151	0.0138	**0.0062**	0.0111	0.0111
Poland	WIG	0.0615	0.0126	0.0129	0.0077	0.0090	0.0065	**0.0059**	0.0060	0.0188
Qatar	QE 20 Index	0.2211	0.0139	0.0174	0.0140	0.0378	0.0716	**0.0138**	0.0140	0.0166
Russia	MICEX	0.1090	0.0106	0.0090	0.0116	0.0207	0.0240	**0.0078**	0.0132	0.0150
Russia	RTSI	0.1308	0.0190	0.0192	0.0118	0.0220	0.0323	0.0157	**0.0110**	0.0247
Saudi Arabia	TASI	0.1371	0.0157	0.0123	**0.0090**	0.0287	0.0447	0.0090	0.0097	0.0167
South Africa	JSE	0.0569	0.0124	0.0067	0.0079	0.0112	0.0093	**0.0062**	0.0089	0.0116
Taiwan	TWII	0.0720	0.0164	0.0176	0.0111	0.0108	0.0109	**0.0074**	0.0676	0.0228
Thailand	SET	0.0754	0.0150	0.0154	0.0106	0.0128	0.0125	0.0104	**0.0098**	0.0241
Turkey	BIST 100	0.0735	0.0086	0.0088	0.0065	0.0120	0.0119	**0.0060**	0.0066	0.0151
Un Arab Em	DFM	0.0894	0.0138	0.0134	**0.0100**	0.0199	0.0208	0.0101	0.0107	0.0193
Un Arab Em	Abu Dhabi	0.1056	0.0169	0.0180	0.0112	0.0193	0.0289	**0.0088**	0.0096	0.0226
Argentina	MERVAL	0.0718	0.0114	0.0110	0.0052	0.0111	0.0095	**0.0049**	0.0055	0.0168
Bahrain	All Share	0.0835	0.0162	0.0163	0.0111	0.0103	0.0143	0.0103	**0.0101**	0.0223
Bulgaria	SOFIX	0.1393	0.0092	0.0096	0.0095	0.0302	0.0399	**0.0076**	0.0113	0.0100
Croatia	CROBEX	0.1226	0.0095	0.0092	0.0096	0.0258	0.0341	**0.0091**	0.0113	0.0118
Cyprus	CYMAIN	0.1042	0.0210	0.0200	0.0144	0.0174	0.0300	**0.0101**	0.0140	0.0241
Estonia	OMXT	0.1310	0.0146	0.0138	0.0079	0.0208	0.0374	0.0074	**0.0063**	0.0166
Kazakhstan	KASE Index	0.1625	0.0375	0.0350	0.0333	**0.0237**	0.0549	0.0392	0.0326	0.0354
Kuwait	Kuwait 15	0.0546	**0.0146**	0.0149	0.0164	0.0170	0.0155	0.0148	0.0173	0.0171
Latvia	OMXR	0.1191	0.0083	0.0076	0.0069	0.0224	0.0298	**0.0059**	0.0086	0.0118
Lithuania	OMXV	0.1140	0.0075	0.0088	0.0083	0.0232	0.0270	**0.0070**	0.0109	0.0121
Mauritius	SEMDEX	0.1330	0.0103	**0.0073**	0.0126	0.0284	0.0329	0.0079	0.0152	0.0095
Morocco	MASI	0.0813	0.0122	0.0117	0.0068	0.0120	0.0121	**0.0068**	0.0071	0.0166
Namibia	NSX Overall	0.0577	0.0095	0.0084	**0.0080**	0.0116	0.0100	0.0120	0.0092	0.0154
Oman	MSM 30	0.1805	0.0100	0.0104	0.0101	0.0365	0.0410	**0.0099**	0.0136	0.0138
Pakistan	KSE 100	0.0970	0.0176	0.0152	**0.0113**	0.0227	0.0258	0.0120	0.0114	0.0197
Romania	BET 10	0.0988	0.0106	0.0102	**0.0080**	0.0206	0.0245	0.0083	0.0087	0.0158
Serbia	BELEX	0.1118	0.0099	0.0100	0.0084	0.0209	0.0270	**0.0064**	0.0096	0.0144
Sri Lanka	CSE All-Share	0.1168	0.0243	0.0140	0.0119	0.0242	0.0293	0.0134	**0.0119**	0.0170
Tunesia	Tunindex	0.1642	0.0150	**0.0118**	0.0162	0.0267	0.0283	0.0145	0.0494	0.0143
Venezuela	IBC	0.1329	0.0242	0.0187	0.0142	0.0225	0.0392	**0.0118**	0.0128	0.0214
Vietnam	HNX 30	0.0998	0.0144	0.0144	**0.0097**	0.0212	0.0274	0.0103	0.1071	0.0169
Zambia	All Share	0.1870	0.0539	0.0500	0.0525	0.0285	0.0933	**0.0265**	0.0516	0.0356

Table 4.4: KS distance between the empirical and fitted distributions for daily log-returns, from 01/03/1997 until 11/02/2017.

Country	Index	N	St	SSt	NIG	VΓ	Hyp	GH	Meix	Stable
Australia	ASX 200	43.516	1.760	0.502	**0.416**	0.916	0.656	0.463	0.563	1.657
Australia	All Ordinaries	44.923	2.122	0.488	**0.361**	0.872	0.603	0.385	0.506	1.650
Austria	ATX	71.487	2.795	0.379	0.560	2.436	1.926	**0.307**	0.949	1.060
Belgium	BEL 20	59.925	2.435	1.020	0.314	1.115	0.794	0.311	**0.309**	2.510
Canada	TSX 60	70.282	2.817	0.578	0.453	1.828	1.385	**0.395**	0.728	1.128
Canada	TSX Composite	81.535	3.848	0.512	0.493	2.374	1.826	**0.329**	0.875	0.940
EuroStoxx	EuroStoxx 50	63.128	1.815	1.078	0.234	0.685	0.495	0.175	**0.172**	2.996
Finland	OMXH25	76.874	2.178	1.333	0.292	1.181	1.182	0.498	**0.193**	2.646
France	CAC 40	49.004	1.414	0.618	**0.171**	0.767	0.469	0.180	0.209	2.208
Germany	DAX	50.763	3.561	2.282	1.033	**0.297**	0.351	0.297	0.768	4.842
Hong Kong	Hang Seng	79.722	2.078	1.609	0.663	0.843	0.829	0.673	**0.597**	3.502
Ireland	ISEQ Overall	75.723	1.703	0.173	0.412	2.484	1.966	**0.123**	0.824	0.861
Israel	TA 35	40.764	1.290	1.125	0.473	0.572	0.400	**0.367**	0.388	3.241
Italy	FTSE MIB	47.894	2.330	1.344	0.382	0.323	0.209	**0.164**	0.230	3.406
Japan	Topix	35.508	1.394	0.644	**0.542**	0.853	0.635	0.618	0.629	2.158
Luxembourg	LuxX Index	48.748	0.408	0.214	0.258	1.203	0.821	**0.153**	0.473	1.204
Netherlands	AEX	73.830	3.944	0.676	**0.192**	1.324	1.124	0.197	0.297	1.846
New Zealand	NZX 50 Index	30.797	2.169	0.448	**0.368**	0.669	0.474	0.401	0.465	1.329
Norway	OBX Index	56.761	1.607	0.223	0.308	1.639	1.171	**0.145**	0.594	1.077
Portugal	PSI 20	54.471	1.873	0.944	0.318	0.909	0.604	0.329	**0.312**	3.081
Singapore	STI Index	53.246	1.057	0.644	**0.188**	0.956	0.713	0.193	0.228	2.011
South Korea	KOSPI	97.551	4.250	2.946	1.046	2.109	3.536	**0.305**	0.663	4.150
Spain	IBEX 35	43.842	2.168	1.218	0.471	0.398	**0.305**	0.395	0.367	3.219
Sweden	OMXS30	44.296	1.352	0.811	0.235	0.590	0.380	**0.202**	0.203	2.160
Switzerland	SMI	62.191	1.615	0.496	0.296	1.292	0.950	**0.274**	0.473	1.814
UK	FTSE 100	56.698	1.248	0.591	**0.130**	0.912	0.630	0.137	0.189	1.993
USA	DowJones 30	78.320	2.581	1.788	0.668	0.954	0.800	**0.519**	0.543	3.995
USA	S&P 500	85.227	3.033	1.874	0.624	1.096	1.005	**0.436**	0.480	3.773
USA	Nasdaq	91.106	6.277	4.427	1.977	0.742	2.323	**0.440**	1.424	5.626
Brazil	Bovespa	51.911	0.908	0.334	0.776	1.757	1.203	**0.330**	1.144	0.747
Chile	IPSA	51.484	0.383	0.262	0.385	1.247	0.848	**0.243**	0.628	1.254
China	CSI 300	46.209	2.589	2.414	1.480	1.169	1.603	**1.011**	1.315	3.819
China	SSE	75.902	2.216	1.950	0.837	1.034	1.249	**0.589**	0.698	4.100
Colombia	IGBC	66.175	0.709	0.435	0.394	1.487	1.268	**0.358**	0.622	1.684
Czech Republic	PX	62.759	0.975	0.225	0.614	2.085	1.447	**0.220**	1.030	1.128
Egypt	EGX 30	49.920	0.751	0.544	0.336	1.246	0.873	**0.332**	0.457	2.000
Greece	Athex	57.853	1.608	1.102	0.249	0.698	0.497	0.179	**0.160**	2.849
Hungary	Budapest SE	67.531	0.304	**0.265**	0.770	2.183	1.589	0.267	1.224	1.133
India	Nifty 50	58.594	1.494	0.642	**0.196**	0.794	0.546	0.249	0.260	2.279
India	BSE Sensex	57.263	1.404	0.595	**0.164**	0.856	0.577	0.176	0.226	1.967
Indonesia	IDX Composite	95.961	1.436	0.602	0.398	2.762	2.792	**0.314**	0.671	1.313
Malaysia	KLCI	279.559	0.853	0.694	0.685	7.105	12.418	**0.401**	1.351	1.277
Mexico	IPC	71.177	1.053	0.634	**0.301**	1.460	1.167	0.313	0.450	1.723
Peru	Lima General	107.334	0.381	0.411	0.598	3.805	3.580	**0.323**	1.040	1.308
Philippines	PSEi	70.053	0.520	0.186	0.632	2.428	1.793	**0.185**	1.082	0.721
Poland	WIG	49.279	1.286	0.953	0.275	0.512	0.335	**0.199**	0.214	2.799
Qatar	QE 20 Index	567.411	1.491	1.509	**0.914**	15.135	49.254	0.950	1.292	2.027
Russia	MICEX	153.140	1.138	0.536	0.665	4.680	5.981	**0.368**	1.191	1.411
Russia	RTSI	130.471	1.846	1.289	**0.702**	2.980	6.056	0.855	0.878	2.377
Saudi Arabia	TASI	201.078	2.858	1.285	**0.534**	7.301	17.865	0.556	0.647	2.373
South Africa	JSE	43.017	1.371	0.221	0.422	1.393	0.909	**0.204**	0.698	0.807
Taiwan	TWII	58.654	3.017	2.161	0.747	0.672	0.628	**0.283**	48.096	3.883
Thailand	SET	72.188	1.618	1.514	0.654	0.974	0.900	0.624	**0.598**	3.222
Turkey	BIST 100	73.079	0.441	0.422	0.164	1.464	1.213	**0.146**	0.334	1.734
Un Arab Em	DFM	67.300	0.789	0.741	0.508	2.039	2.338	**0.499**	0.630	1.573
Un Arab Em	Abu Dhabi	114.357	1.851	1.659	0.540	2.640	5.775	**0.375**	0.445	2.867
Argentina	MERVAL	61.402	1.432	0.626	**0.107**	1.105	0.835	0.107	0.157	1.894
Bahrain	All Share	57.749	1.573	1.597	0.722	0.798	1.032	**0.483**	0.596	2.955
Bulgaria	SOFIX	190.920	0.496	0.523	0.436	6.573	12.319	**0.277**	0.813	1.018
Croatia	CROBEX	190.928	0.558	0.513	0.396	8.019	12.800	**0.254**	0.744	1.165
Cyprus	CYMAIN	83.564	2.238	2.161	0.936	1.251	5.242	**0.299**	0.694	2.849
Estonia	OMXT	221.515	1.796	1.714	0.409	5.343	15.900	**0.374**	0.426	2.799
Kazakhstan	KASE Index	271.291	6.059	5.955	4.566	**3.350**	35.930	9.626	4.254	6.131
Kuwait	Kuwait 15	8.526	**0.330**	0.340	0.482	0.726	0.581	0.341	0.573	0.342
Latvia	OMXR	153.699	0.368	0.298	0.325	4.844	7.903	**0.109**	0.772	0.995
Lithuania	OMXV	146.364	0.459	0.441	0.389	4.605	6.545	**0.234**	0.777	1.256
Mauritius	SEMDEX	241.176	1.139	0.446	0.949	8.562	14.469	**0.298**	1.828	0.736
Morocco	MASI	67.482	0.623	0.602	0.224	1.490	1.607	**0.223**	0.301	1.527
Namibia	NSX Overall	29.052	0.274	**0.176**	0.210	0.794	0.522	0.412	0.342	0.890
Oman	MSM 30	424.079	0.534	0.528	0.910	13.598	21.119	**0.453**	1.885	1.427
Pakistan	KSE 100	92.759	3.313	1.893	0.971	3.072	3.714	0.969	**0.924**	3.188
Romania	BET 10	107.736	0.951	0.979	**0.257**	2.520	3.629	0.276	0.314	2.186
Serbia	BELEX	99.618	0.381	0.381	0.181	2.704	3.997	**0.144**	0.379	1.010
Sri Lanka	CSE All-Share	164.830	3.070	1.456	**0.945**	4.776	6.199	0.980	1.251	1.955
Tunesia	Tunindex	335.949	1.971	**1.033**	2.855	7.478	6.883	1.783	31.006	1.274
Venezuela	IBC	210.915	7.605	2.549	0.785	3.806	14.641	**0.544**	0.643	3.134
Vietnam	HNX 30	61.007	1.182	1.105	0.381	1.721	2.988	**0.273**	63.437	1.636
Zambia	All Share	317.758	16.669	14.746	16.887	4.561	67.387	**3.156**	16.412	10.160

Table 4.5: AD distance between the empirical and fitted distributions for daily log-returns, from 01/03/1997 until 11/02/2017.

Country	Index	N	St	SSt	NIG	VΓ	Hyp	GH	Meix	Stable
Australia	ASX 200	-33712	-34490	**-34495**	-34488	-34454	-34464	-34488	-34477	-34448
Australia	All Ordinaries	-34004	-34801	**-34810**	-34804	-34768	-34779	-34803	-34792	-34763
Austria	ATX	-29256	-30348	**-30363**	-30363	-30286	-30302	-30363	-30348	-30310
Belgium	BEL 20	-31557	-32475	-32477	**-32497**	-32459	-32470	-32488	-32493	-32392
Canada	TSX 60	-28525	-29664	**-29673**	-29667	-29597	-29607	-29669	-29652	-29630
Canada	TSX Composite	-32352	-33636	**-33654**	-33650	-33559	-33576	-33652	-33632	-33610
EuroStoxx	EuroStoxx 50	-31051	-32015	-32012	**-32036**	-32009	-32015	-32028	-32035	-31921
Finland	OMXH25	-27102	-28223	-28219	-28256	-28215	-28219	-28248	**-28257**	-28119
France	CAC 40	-29831	-30605	-30603	**-30617**	-30588	-30598	-30608	-30613	-30527
Germany	DAX	-29242	-29975	-29976	-30007	**-30026**	-30025	-30018	-30012	-29887
Hong Kong	Hang Seng	-27582	-28849	-28843	**-28859**	-28826	-28825	-28850	-28852	-28761
Ireland	ISEQ Overall	-30346	-31544	**-31552**	-31550	-31462	-31480	-31551	-31534	-31493
Israel	TA 35	-30324	-30959	-30955	**-30972**	-30964	-30969	-30965	-30972	-30868
Italy	FTSE MIB	-27538	-28243	-28243	-28270	-28264	-28269	-28266	**-28272**	-28151
Japan	Topix	-29242	-29901	**-29902**	-29892	-29866	-29875	-29894	-29882	-29863
Luxembourg	LuxX Index	-27758	**-28612**	-28605	-28599	-28548	-28562	-28599	-28587	-28549
Netherlands	AEX	-29935	-31013	-31048	**-31067**	-31014	-31022	-31059	-31061	-30972
New Zealand	NZX 50 Index	-30046	-30588	**-30599**	-30592	-30569	-30577	-30591	-30584	-30563
Norway	OBX Index	-25137	-26069	**-26076**	-26071	-26009	-26024	-26071	-26058	-26024
Portugal	PSI 20	-31460	-32323	-32327	**-32341**	-32308	-32321	-32333	-32337	-32238
Singapore	STI Index	-27785	-28609	-28604	**-28619**	-28579	-28591	-28611	-28615	-28532
South Korea	KOSPI	-27587	-28812	-28810	-28891	-28882	-28857	**-28909**	-28907	-28694
Spain	IBEX 35	-29246	-29946	-29945	**-29958**	-29949	-29953	-29950	-29956	-29865
Sweden	OMXS30	-28939	-29605	-29600	-29621	-29604	-29612	-29613	**-29621**	-29512
Switzerland	SMI	-31342	-32327	-32329	**-32334**	-32289	-32296	-32329	-32324	-32268
UK	FTSE 100	-31681	-32574	-32571	**-32586**	-32548	-32559	-32578	-32581	-32487
USA	DowJones 30	-31969	-33132	-33129	**-33153**	-33128	-33128	-33145	-33149	-33041
USA	S&P 500	-31339	-32575	-32574	**-32604**	-32573	-32571	-32597	-32602	-32484
USA	Nasdaq	-27061	-28237	-28235	-28314	-28339	-28314	**-28346**	-28329	-28117
Brazil	Bovespa	-25415	**-26401**	-26397	-26364	-26300	-26317	-26388	-26341	-26378
Chile	IPSA	-32478	**-33418**	-33411	-33396	-33342	-33357	-33402	-33380	-33359
China	CSI 300	-15874	-16441	-16439	-16477	**-16500**	-16491	-16492	-16484	-16366
China	SSE	-27189	-28256	-28253	-28293	-28283	-28278	-28292	**-28297**	-28153
Colombia	IGBC	-23353	**-24459**	-24455	-24445	-24384	-24387	-24448	-24430	-24408
Czech Republic	PX	-29852	-31001	**-31001**	-30975	-30891	-30913	-30993	-30952	-30956
Egypt	EGX 30	-25649	**-26481**	-26477	-26480	-26436	-26450	-26474	-26471	-26401
Greece	Athex	-26019	-26881	-26877	-26905	-26881	-26889	-26898	**-26906**	-26782
Hungary	Budapest SE	-27588	**-28856**	-28849	-28815	-28728	-28745	-28841	-28789	-28815
India	Nifty 50	-28555	-29507	-29507	**-29514**	-29479	-29486	-29507	-29506	-29435
India	BSE Sensex	-28542	-29432	-29430	**-29444**	-29413	-29420	-29436	-29439	-29353
Indonesia	IDX Composite	-27671	-29108	-29105	**-29118**	-29022	-29022	-29113	-29107	-29039
Malaysia	KLCI	-29961	**-33573**	-33565	-33547	-33271	-33154	-33563	-33517	-33512
Mexico	IPC	-29715	-30845	-30839	**-30846**	-30787	-30796	-30840	-30837	-30767
Peru	Lima General	-29943	**-31607**	-31600	-31596	-31478	-31472	-31599	-31578	-31535
Philippines	PSEi	-28976	**-30139**	-30133	-30114	-30024	-30046	-30126	-30094	-30084
Poland	WIG	-29926	-30667	-30664	-30687	-30673	-30680	-30680	**-30687**	-30570
Qatar	QE 20 Index	-22476	-30281	-30273	**-30283**	-29781	-29168	-30281	-30261	-30229
Russia	MICEX	-22351	**-24530**	-24525	-24519	-24346	-24318	-24526	-24498	-24471
Russia	RTSI	-15750	**-17622**	-17618	-17622	-17522	-17440	-17618	-17608	-17574
Saudi Arabia	TASI	-28756	-31389	-31393	-31452	-31278	-31108	-31444	**-31452**	-31319
South Africa	JSE	-30917	-31679	**-31683**	-31675	-31623	-31643	-31677	-31662	-31635
Taiwan	TWII	-30025	-30732	-30729	-30788	-30801	**-30803**	-30800	-30099	-30608
Thailand	SET	-27910	-29051	-29042	**-29061**	-29029	-29030	-29052	-29056	-28959
Turkey	BIST 100	-24071	-25227	-25218	**-25228**	-25167	-25174	-25222	-25219	-25144
Un Arab Em	DFM	-18834	-19788	-19781	**-19800**	-19745	-19741	-19792	-19797	-19725
Un Arab Em	Abu Dhabi	-26165	-27755	-27747	-27792	-27722	-27660	-27787	**-27792**	-27672
Argentina	MERVAL	-24692	-25602	-25601	**-25624**	-25582	-25593	-25615	-25621	-25516
Bahrain	All Share	-27380	-28216	-28207	-28236	-28226	-28220	-28233	**-28237**	-28137
Bulgaria	SOFIX	-23168	**-25843**	-25835	-25842	-25622	-25511	-25841	-25827	-25788
Croatia	CROBEX	-27262	-29793	-29785	**-29808**	-29583	-29489	-29803	-29798	-29729
Cyprus	CYMAIN	-14209	-15290	-15283	-15338	-15324	-15262	**-15351**	-15347	-15216
Estonia	OMXT	-28286	-31412	-31405	**-31448**	-31234	-31055	-31440	-31440	-31326
Kazakhstan	KASE Index	-18181	-21793	-21785	-21868	-22102	-21281	**-22125**	-21874	-21735
Kuwait	Kuwait 15	-9328	**-9490**	-9483	-9478	-9464	-9470	-9476	-9473	-9476
Latvia	OMXR	-25002	**-27252**	-27243	-27245	-27060	-26998	-27247	-27228	-27193
Lithuania	OMXV	-27803	**-29932**	-29924	-29925	-29751	-29713	-29926	-29908	-29868
Mauritius	SEMDEX	-37297	**-40627**	-40621	-40603	-40291	-40172	-40621	-40575	-40585
Morocco	MASI	-27289	-28274	-28267	**-28287**	-28238	-28236	-28278	-28284	-28204
Namibia	NSX Overall	-20695	**-21191**	-21185	-21186	-21160	-21169	-21179	-21180	-21138
Oman	MSM 30	-29094	**-35103**	-35095	-35051	-34644	-34429	-35087	-35009	-35043
Pakistan	KSE 100	-28221	-29423	-29427	-29480	-29436	-29428	-29475	**-29485**	-29323
Romania	BET 10	-26985	-28534	-28526	**-28560**	-28475	-28455	-28552	-28557	-28439
Serbia	BELEX	-17957	**-19312**	-19304	-19310	-19199	-19176	-19305	-19300	-19261
Sri Lanka	CSE All-Share	-30574	-32956	-32966	-32967	-32792	-32758	**-32968**	-32948	-32903
Tunesia	Tunindex	-33483	**-38597**	-38589	-38457	-38198	-38165	-38581	-37910	-38586
Venezuela	IBC	-23729	-26343	-26358	**-26421**	-26336	-26126	-26416	-26420	-26295
Vietnam	HNX 30	-14823	-15575	-15567	**-15612**	-15577	-15565	-15611	-14764	-15506
Zambia	All Share	-19269	-23362	-23355	-23441	-23861	-22511	**-23872**	-23456	-23404

Table 4.6: BIC of fitted distributions for daily log-returns, from 01/03/1997 until 11/02/2017.

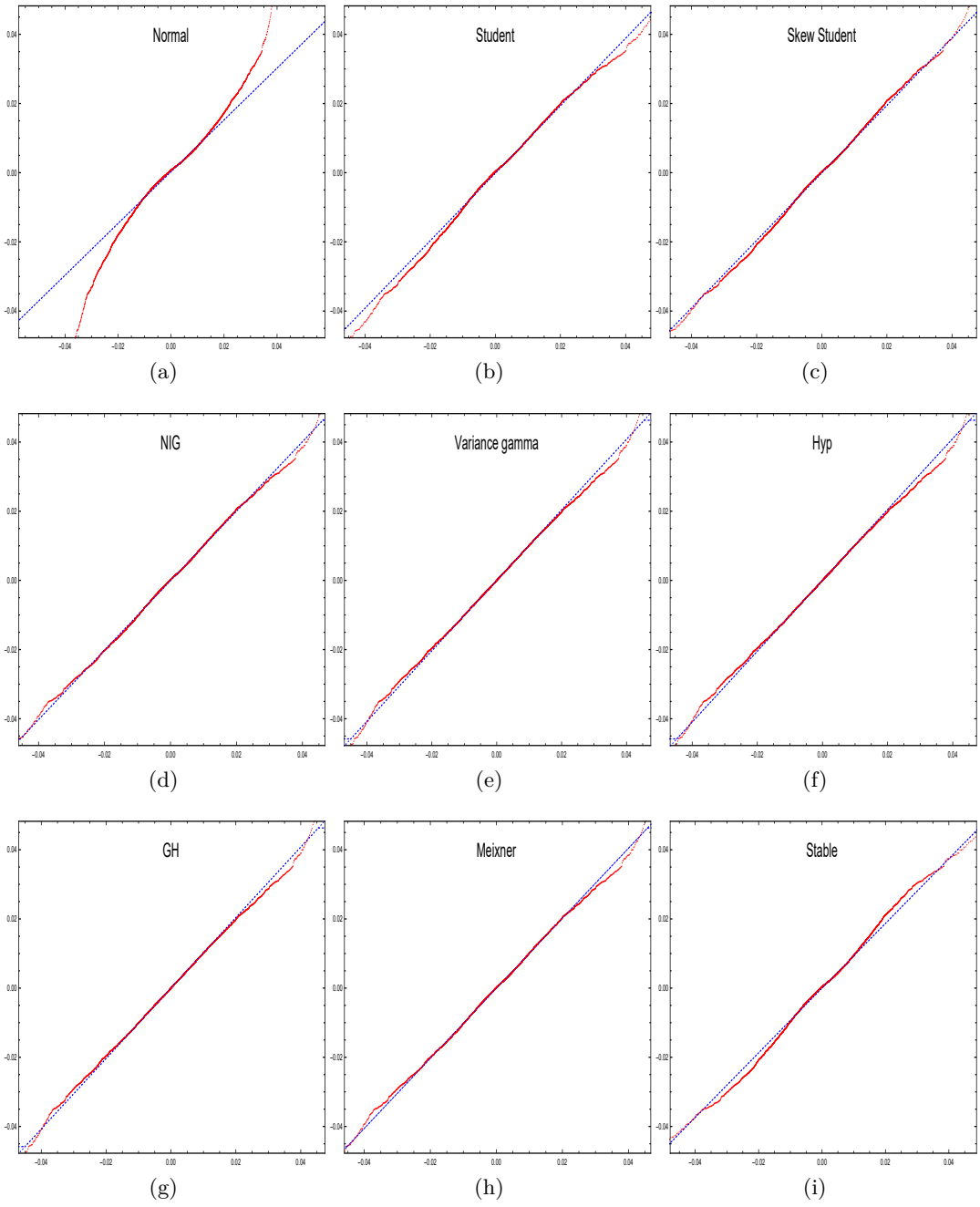

Figure 4.6: QQ-plots of empirical quantiles for daily DAX log-returns from 01/03/1997 until 11/02/2017 versus model distributions.

turbulent phases (e.g., the financial crisis). The i.i.d. assumption for log-returns is unlikely to be valid across the entire period. This implies a violation of the Lévy model. Some authors (e.g., Corlu et al. 2016) have split a long period into several shorter subperiods and investigated which model fits best in each subperiod. For our data, we do not find outstanding differences between the periods. Here, we only consider the last year as an example so as not to overload the discussion, and relegate the subperiod issue to Appendix 4.A. A second reason for only considering the last year is that we only have hourly data for this period. A common time period is needed for investigating time consistency in Section 4.5. Tables 4.7 – 4.9 present the KS, AD and BIC statistics for the last year for daily log-returns. There are some changes in the KS and AD statistics. Obviously, the return series are much shorter at about 250 days. This implies that rare events may not have occurred. Hence, even the normal distribution yields the best fit in some cases. The GH distribution is not as often the first choice as for the entire sample. In most cases, the BIC favors the Student t or the normal distribution. Again, this is also due to the small sample size.

We now turn back to the DAX example. Figure 4.7 shows QQ-plots comparing the empirical with the model distributions. Again, the normal distribution is not a good fit. The other models appear not to be as good as in Figure 4.6 but this is due to the lower sample size and thus the different scaling. The KS and AD statistics recommend the NIG model, the BIC the variance gamma model. The QQ-plots suggest that both yield a reasonable fit.

Table 4.10 summarizes how often each distribution has the lowest KS, AD and BIC statistic among all distributions considered, both for the full and the one-year sample. The GH distribution performs well, especially for the full sample. This is also due to the large sample size and the fact that the GH distribution, with its five parameters, is the most flexible one.

We now turn to the case of hourly data. As already mentioned, we only have data for one year. Nonetheless, the number of hourly log-returns is of a decent size (see Table 4.3). Again, we still consider that $t = 1$ corresponds to one trading day. Thus we now take $t = t_h := 1/(\#\text{trading hours per day})$. This implies that we can only use convolution invariant models because no maximum likelihood estimation routines exist for the others. The only exception is the Student-Lévy process with the routine derived in Chapter 3. Hence, from now on we will be considering six models (normal, Student, NIG, variance gamma, Meixner and stable).

Tables 4.11 – 4.13 present the KS, AD and BIC statistics. Each of the distributions except the normal has an almost equal number of best fits among the indices. Evidently, this does not mean that the distributions are always equally appropriate. For example the Student-Lévy model has an AD distance of 0.3 for the South Korean KOSPI but the variance gamma distribution has 3, more than ten times higher. There are

Code	Index	N	St	SSt	NIG	VΓ	Hyp	GH	Meix	Stable
Australia	ASX 200	0.0495	0.0354	0.0345	0.0339	**0.0334**	0.0336	0.0356	0.0335	0.0416
Australia	All Ordinaries	0.0525	0.0372	0.0355	0.0342	**0.0329**	0.0336	0.0372	0.0335	0.0419
Austria	ATX	0.0465	0.0449	**0.0449**	0.0480	0.0471	0.0480	0.0456	0.0476	0.0507
Belgium	BEL 20	0.0487	0.0297	0.0331	0.0281	**0.0240**	0.0264	0.0245	0.0266	0.0466
Canada	TSX 60	0.0552	0.0521	0.0402	0.0390	**0.0345**	0.0381	0.0372	0.0377	0.0426
Canada	TSX Composite	0.0424	0.0326	0.0298	0.0326	0.0355	0.0335	0.0355	0.0339	**0.0275**
EuroStoxx	EuroStoxx 50	0.0547	**0.0318**	0.0332	0.0335	0.0323	0.0333	0.0330	0.0393	0.0376
Finland	OMXH25	0.0419	0.0329	0.0342	0.0336	0.0317	0.0333	**0.0317**	0.0361	0.0387
France	CAC 40	0.0653	**0.0294**	0.0338	0.0323	0.0303	0.0316	0.0340	0.0312	0.0367
Germany	DAX	0.1028	0.0385	0.0333	**0.0289**	0.0367	0.0399	0.0389	0.0904	0.0355
Hong Kong	Hang Seng	0.0451	**0.0256**	0.0267	0.0275	0.0280	0.0277	0.0279	0.0346	0.0346
Ireland	ISEQ Overall	0.0448	**0.0412**	0.0478	0.0470	0.0460	0.0646	0.0488	0.0463	0.0459
Israel	TA 35	0.0595	0.0365	0.0349	0.0298	0.0277	**0.0267**	0.0277	0.0524	0.0517
Italy	FTSE MIB	0.0878	0.0343	0.0383	0.0344	0.0345	0.0343	0.0344	**0.0338**	0.0487
Japan	Topix	0.0949	0.0379	0.0378	0.0351	0.0311	**0.0270**	0.0378	0.0337	0.0384
Luxembourg	LuxX Index	0.0623	0.0354	0.0337	0.0314	0.0323	**0.0311**	0.0320	0.0503	0.0440
Netherlands	AEX	0.0375	0.0285	0.0299	0.0279	**0.0258**	0.0274	0.0258	0.0270	0.0400
New Zealand	NZX 50 Index	0.0820	0.0315	0.0286	0.0314	0.0403	0.0333	0.0286	0.0333	**0.0274**
Norway	OBX Index	**0.0360**	0.0375	0.0369	0.0431	0.0431	0.0432	0.0392	0.5043	0.0386
Portugal	PSI 20	0.0628	**0.0269**	0.0336	0.0367	0.0413	0.0393	0.0361	0.0384	0.0341
Singapore	STI Index	0.0441	0.0464	0.0457	0.0493	0.0496	0.0494	0.0495	0.0488	**0.0441**
South Korea	KOSPI	0.0686	0.0364	0.0322	**0.0305**	0.0336	0.0322	0.0321	0.0306	0.0400
Spain	IBEX 35	0.0717	0.0313	0.0314	0.0282	0.0276	0.0272	**0.0271**	0.0273	0.0384
Sweden	OMXS30	**0.0405**	0.0447	0.0446	0.0522	0.0523	0.0522	0.0522	0.0522	0.0492
Switzerland	SMI	0.0598	0.0409	0.0443	0.0424	**0.0318**	0.0403	0.0414	0.0544	0.0524
UK	FTSE 100	0.0612	0.0341	**0.0271**	0.0273	0.0284	0.0274	0.0318	0.0272	0.0276
USA	DowJones 30	0.0761	0.0386	0.0388	0.0302	0.0392	0.0327	**0.0299**	0.0328	0.0314
USA	S&P 500	0.1038	0.0444	0.0451	0.0339	0.0494	0.0411	0.0337	**0.0328**	0.0524
USA	Nasdaq	0.0941	0.0475	0.0457	**0.0364**	0.0409	0.0421	0.0412	0.0961	0.0586
Brazil	Bovespa	0.0856	**0.0248**	0.0294	0.0267	0.0262	0.0259	0.0263	0.0255	0.0333
Chile	IPSA	0.0426	**0.0283**	0.0295	0.0293	0.0285	0.0288	0.0296	0.0291	0.0325
China	CSI 300	0.0425	0.0214	0.0226	0.0221	**0.0209**	0.0217	0.0226	0.0217	0.0304
China	SSE	0.0688	0.0613	0.0573	0.0548	**0.0474**	0.0524	0.0476	0.0531	0.0603
Colombia	IGBC	0.0596	0.0441	0.0463	0.0431	**0.0344**	0.0401	0.0461	0.0410	0.0515
Czech Republic	PX	0.0605	0.0307	0.0303	0.0279	0.0278	0.0274	**0.0273**	0.0274	0.0368
Egypt	EGX 30	0.0734	**0.0258**	0.0259	0.0279	0.0323	0.0291	0.0269	0.0284	0.0322
Greece	Athex	0.0851	0.0488	0.0489	0.0416	0.0364	**0.0334**	0.0344	0.0692	0.0553
Hungary	Budapest SE	0.0709	0.0442	0.0387	0.0369	**0.0321**	0.0343	0.0365	0.0354	0.0341
India	Nifty 50	0.0664	0.0416	0.0455	0.0418	**0.0346**	0.0350	0.0375	0.0390	0.0504
India	BSE Sensex	0.0584	0.0429	0.0456	0.0409	0.0441	0.0452	0.0421	**0.0397**	0.0520
Indonesia	IDX Composite	0.0826	0.0279	0.0283	0.0299	0.0329	0.0294	0.0283	0.0304	**0.0278**
Malaysia	KLCI	0.0643	0.0353	**0.0341**	0.0341	0.0388	0.0359	0.0350	0.0560	0.0379
Mexico	IPC	0.0732	0.0312	0.0314	0.0311	0.0346	**0.0301**	0.0312	0.0308	0.0302
Peru	Lima General	0.0402	0.0304	**0.0296**	0.0304	0.0307	0.0307	0.0309	0.0329	0.0392
Philippines	PSEi	0.0595	0.0393	0.0368	0.0329	0.0322	**0.0307**	0.0319	0.0462	0.0397
Poland	WIG	0.0600	0.0388	0.0374	0.0360	0.0363	0.0361	0.0388	**0.0354**	0.0385
Qatar	QE 20 Index	0.1064	0.0354	0.0377	0.0337	0.0363	0.0370	0.0402	**0.0329**	0.0504
Russia	MICEX	0.0402	**0.0298**	0.0302	0.0310	0.0309	0.0311	0.0310	0.0304	0.0385
Russia	RTSI	0.0673	**0.0253**	0.0262	0.0298	0.0341	0.0312	0.0268	0.0312	0.0279
Saudi Arabia	TASI	0.0661	0.0349	**0.0269**	0.0287	0.0285	0.0286	0.0304	0.0289	0.0272
South Africa	JSE	0.0366	0.0261	0.0256	**0.0254**	0.0257	0.0255	0.0257	0.0256	0.0311
Taiwan	TWII	0.0611	0.0403	0.0443	0.0418	**0.0372**	0.0390	0.0401	0.0400	0.0481
Thailand	SET	0.0609	0.0255	0.0242	0.0261	0.0268	0.0254	0.0252	0.0265	**0.0223**
Turkey	BIST 100	0.0537	0.0274	0.0264	0.0271	0.0263	0.0265	0.0268	0.0272	**0.0257**
Un Arab Em	DFM	0.0595	**0.0297**	0.0423	0.0439	0.0470	0.0451	0.0470	0.0448	0.0405
Un Arab Em	Abu Dhabi	0.0630	0.0241	0.0230	**0.0201**	0.0213	0.0222	0.0211	0.0214	0.0275
Argentina	MERVAL	0.0530	0.0324	0.0305	0.0306	**0.0285**	0.0304	0.0311	0.0308	0.0345
Bahrain	All Share	0.1147	0.0302	0.0304	0.0311	0.0423	0.0442	**0.0289**	0.0338	0.0347
Bulgaria	SOFIX	0.0869	0.0337	0.0340	0.0335	0.0380	0.0359	0.0340	**0.0330**	0.0373
Croatia	CROBEX	0.1072	0.0285	0.0312	0.0347	0.0453	0.0470	0.0324	0.0979	**0.0265**
Cyprus	CYMAIN	0.0635	0.0393	0.0385	0.0348	**0.0342**	0.0363	0.0342	0.0744	0.0529
Estonia	OMXT	0.0661	0.0364	0.0365	0.0327	0.0329	**0.0316**	0.0321	0.0318	0.0448
Kazakhstan	KASE Index	**0.0394**	0.0403	0.0452	0.0446	0.0438	0.0445	0.0440	0.0442	0.0439
Kuwait	Kuwait 15	0.0579	0.0263	0.0288	0.0269	**0.0230**	0.0252	0.0238	0.0257	0.0388
Latvia	OMXR	0.1511	0.0322	**0.0273**	0.0324	0.0515	0.0544	0.0273	0.0345	0.0288
Lithuania	OMXV	0.0576	0.0461	0.0427	0.0426	**0.0416**	0.0418	0.0425	0.0423	0.0438
Mauritius	SEMDEX	0.0814	0.0439	0.0355	**0.0323**	0.0348	0.0342	0.0386	0.0868	0.0361
Morocco	MASI	0.1064	0.0287	**0.0260**	0.0289	0.0381	0.0383	0.0296	0.0918	0.0318
Namibia	NSX Overall	0.0667	0.0409	0.0426	0.0418	**0.0367**	0.0392	0.0368	0.0512	0.0448
Oman	MSM 30	0.0494	0.0273	0.0273	0.0250	0.0250	0.0246	0.0249	**0.0244**	0.0382
Pakistan	KSE 100	0.0733	0.0321	0.0350	**0.0305**	0.0385	0.0328	0.0334	0.0311	0.0425
Romania	BET 10	0.0718	0.0455	0.0447	0.0403	0.0362	**0.0353**	0.0459	0.0380	0.0466
Serbia	BELEX	0.0751	0.0275	0.0261	0.0244	0.0274	0.0266	**0.0242**	0.0243	0.0276
Sri Lanka	CSE All-Share	0.0702	0.0508	**0.0367**	0.0387	0.0370	0.0405	0.0375	0.0432	0.0438
Tunesia	Tunindex	0.0550	0.0385	0.0388	0.0382	**0.0347**	0.0379	0.0370	0.0443	0.0370
Venezuela	IBC	0.1469	0.0869	0.0479	0.0442	0.0439	0.0520	0.0401	0.5041	**0.0368**
Vietnam	HNX 30	0.0615	0.0575	0.0582	0.0391	**0.0345**	0.0380	0.0345	0.5048	0.0529
Zambia	All Share	0.1789	0.0988	0.0899	0.0876	0.0782	0.1126	**0.0597**	0.0851	0.0728

Table 4.7: KS distance between the empirical and fitted distributions for daily log-returns, from 11/03/2016 until 11/02/2017.

Country	Index	N	St	SSt	NIG	VΓ	Hyp	GH	Meix	Stable
Australia	ASX 200	0.664	0.354	0.322	0.295	**0.277**	0.286	0.365	0.285	0.360
Australia	All Ordinaries	0.719	0.329	0.285	0.255	**0.234**	0.244	0.329	0.244	0.324
Austria	ATX	0.459	0.433	**0.432**	0.468	0.459	0.467	0.438	0.464	0.470
Belgium	BEL 20	0.788	0.227	0.287	0.245	**0.207**	0.226	0.209	0.228	0.481
Canada	TSX 60	0.906	0.530	0.261	0.244	**0.228**	0.239	0.236	0.237	0.327
Canada	TSX Composite	0.854	0.383	**0.157**	0.158	0.166	0.160	0.166	0.162	0.207
EuroStoxx	EuroStoxx 50	0.792	0.263	0.266	0.229	**0.202**	0.212	0.211	0.569	0.426
Finland	OMXH25	0.365	0.213	0.217	0.209	0.200	0.207	**0.200**	0.257	0.333
France	CAC 40	1.418	0.241	0.188	0.203	0.233	0.214	**0.188**	0.213	0.247
Germany	DAX	3.499	0.606	0.518	**0.371**	0.487	0.491	0.554	3.049	0.584
Hong Kong	Hang Seng	0.628	0.238	0.189	**0.182**	0.190	0.182	0.190	0.303	0.280
Ireland	ISEQ Overall	0.521	**0.284**	0.374	0.379	0.391	1.235	0.381	0.381	0.334
Israel	TA 35	1.144	0.314	0.297	0.220	0.180	**0.179**	0.180	0.791	0.707
Italy	FTSE MIB	1.840	0.315	0.234	0.185	0.212	**0.173**	0.174	0.176	0.419
Japan	Topix	4.049	0.234	0.234	**0.231**	0.325	0.296	0.234	0.246	0.370
Luxembourg	LuxX Index	1.063	0.430	0.293	0.243	0.228	0.228	**0.227**	0.619	0.459
Netherlands	AEX	0.374	0.215	0.227	0.216	0.208	0.214	**0.208**	0.212	0.339
New Zealand	NZX 50 Index	2.955	0.488	0.228	0.259	0.341	0.283	0.228	0.291	**0.171**
Norway	OBX Index	0.433	0.429	0.417	0.426	0.422	0.427	0.411	97.364	**0.392**
Portugal	PSI 20	1.455	0.357	0.300	0.342	0.406	0.369	0.329	0.366	**0.288**
Singapore	STI Index	0.360	0.344	0.345	**0.342**	0.342	0.342	0.342	0.343	0.360
South Korea	KOSPI	1.972	0.334	0.246	0.199	0.183	0.179	**0.179**	0.189	0.274
Spain	IBEX 35	1.331	0.288	0.174	0.149	0.147	0.143	**0.143**	0.144	0.286
Sweden	OMXS30	0.337	0.289	0.289	0.281	0.284	0.282	0.281	0.283	**0.262**
Switzerland	SMI	1.163	0.377	0.381	0.322	0.253	0.382	**0.249**	0.879	0.692
UK	FTSE 100	1.267	0.311	0.187	0.193	0.224	0.203	0.221	0.203	**0.162**
USA	DowJones 30	2.776	0.446	0.453	0.258	0.350	0.295	0.255	0.271	**0.222**
USA	S&P 500	3.633	0.851	0.616	0.492	0.578	0.502	**0.454**	0.464	0.503
USA	Nasdaq	4.029	0.415	0.381	**0.332**	0.449	0.370	0.445	3.747	0.517
Brazil	Bovespa	2.605	0.244	**0.182**	0.228	0.296	0.261	0.243	0.250	0.199
Chile	IPSA	0.538	0.252	0.264	0.275	0.285	0.277	0.267	0.280	**0.240**
China	CSI 300	0.530	**0.132**	0.143	0.144	0.153	0.147	0.143	0.147	0.163
China	SSE	0.905	0.361	0.301	0.293	0.289	0.289	**0.288**	0.290	0.347
Colombia	IGBC	1.368	**0.321**	0.394	0.374	0.362	0.367	0.392	0.368	0.461
Czech Republic	PX	0.772	0.230	0.144	0.133	0.133	**0.131**	0.131	0.131	0.191
Egypt	EGX 30	2.106	0.156	**0.139**	0.160	0.229	0.200	0.144	0.176	0.183
Greece	Athex	1.991	0.396	0.350	0.255	0.176	**0.171**	0.171	1.465	0.519
Hungary	Budapest SE	1.401	0.451	0.273	0.270	0.288	0.273	0.271	0.275	**0.260**
India	Nifty 50	1.212	0.364	0.373	0.353	**0.323**	0.334	0.356	0.344	0.454
India	BSE Sensex	1.096	0.466	0.495	0.444	**0.348**	0.377	0.362	0.416	0.651
Indonesia	IDX Composite	2.794	0.256	0.236	0.302	0.430	0.363	0.237	0.344	**0.168**
Malaysia	KLCI	1.235	0.477	0.367	**0.359**	0.394	0.370	0.364	0.903	0.370
Mexico	IPC	2.115	0.210	0.239	0.260	0.315	0.277	**0.204**	0.276	0.249
Peru	Lima General	0.480	0.270	0.243	0.228	**0.222**	0.225	0.223	0.321	0.440
Philippines	PSEi	1.227	0.261	0.200	0.182	0.177	0.177	**0.176**	0.650	0.235
Poland	WIG	0.816	0.447	0.385	0.380	0.383	0.383	0.393	0.378	**0.363**
Qatar	QE 20 Index	3.507	0.297	0.291	0.274	0.278	**0.266**	0.297	0.279	0.441
Russia	MICEX	0.363	0.260	**0.258**	0.259	0.262	0.259	0.260	0.261	0.336
Russia	RTSI	1.741	0.159	0.139	0.147	0.189	0.166	**0.139**	0.157	0.208
Saudi Arabia	TASI	2.043	0.275	0.183	0.232	0.289	0.259	0.195	0.257	**0.161**
South Africa	JSE	0.216	0.138	**0.123**	0.123	0.125	0.124	0.125	0.124	0.151
Taiwan	TWII	1.220	**0.278**	0.279	0.284	0.294	0.283	0.282	0.285	0.326
Thailand	SET	1.359	0.149	**0.138**	0.158	0.202	0.178	0.145	0.171	0.139
Turkey	BIST 100	0.954	0.158	0.148	0.168	0.199	0.179	0.155	0.180	**0.129**
Un Arab Em	DFM	1.102	**0.444**	0.533	0.550	0.610	0.572	0.611	0.558	0.478
Un Arab Em	Abu Dhabi	1.582	0.172	0.120	**0.108**	0.120	0.113	0.109	0.110	0.166
Argentina	MERVAL	1.049	**0.171**	0.178	0.182	0.201	0.189	0.180	0.187	0.209
Bahrain	All Share	4.924	0.406	0.415	0.195	0.333	0.332	**0.185**	0.216	0.241
Bulgaria	SOFIX	3.787	0.261	**0.250**	0.265	0.431	0.397	0.250	0.282	0.303
Croatia	CROBEX	5.327	0.236	0.257	0.314	0.532	0.557	0.286	4.990	**0.219**
Cyprus	CYMAIN	1.228	0.522	0.493	0.397	**0.287**	0.317	0.288	1.504	0.683
Estonia	OMXT	1.160	0.268	0.270	0.218	0.204	0.202	**0.202**	0.207	0.442
Kazakhstan	KASE Index	0.388	**0.330**	0.390	0.386	0.381	0.386	0.382	0.383	0.373
Kuwait	Kuwait 15	1.069	0.186	0.192	0.175	0.175	**0.171**	0.172	0.171	0.295
Latvia	OMXR	9.803	0.442	**0.124**	0.207	0.533	0.512	0.124	0.271	0.184
Lithuania	OMXV	1.062	0.714	0.629	0.633	0.624	0.626	0.631	0.632	**0.570**
Mauritius	SEMDEX	3.924	0.898	0.379	0.284	0.323	**0.243**	0.361	4.464	0.326
Morocco	MASI	5.046	**0.232**	0.236	0.236	0.418	0.468	0.244	4.458	0.241
Namibia	NSX Overall	1.104	0.267	0.259	0.234	0.239	**0.227**	0.230	0.571	0.341
Oman	MSM 30	0.601	0.172	0.171	0.160	0.157	0.156	0.159	**0.155**	0.275
Pakistan	KSE 100	2.210	**0.294**	0.333	0.361	0.441	0.403	0.342	0.380	0.326
Romania	BET 10	2.414	0.340	0.301	0.324	0.382	0.334	0.302	0.344	**0.224**
Serbia	BELEX	2.163	0.156	0.136	0.109	0.120	0.112	**0.107**	0.107	0.201
Sri Lanka	CSE All-Share	1.663	1.013	0.424	0.346	**0.269**	0.302	0.272	0.670	0.572
Tunesia	Tunindex	0.885	0.602	0.606	0.335	**0.305**	0.332	0.324	0.434	0.369
Venezuela	IBC	10.221	3.874	1.049	0.923	0.753	1.470	0.699	91.944	**0.464**
Vietnam	HNX 30	0.805	0.697	0.711	0.272	0.223	0.258	**0.223**	96.595	0.503
Zambia	All Share	6.785	1.993	1.492	1.742	1.180	2.333	**0.708**	1.690	1.107

Table 4.8: AD distance between the empirical and fitted distributions for daily log-returns, from 11/03/2016 until 11/02/2017.

Country	Index	N	St	SSt	NIG	VΓ	Hyp	GH	Meix	Stable
Australia	ASX 200	-1812	**-1815**	-1810	-1810	-1810	-1810	-1804	-1810	-1811
Australia	All Ordinaries	-1836	**-1841**	-1836	-1835	-1835	-1835	-1830	-1835	-1836
Austria	ATX	**-1695**	-1691	-1685	-1685	-1685	-1685	-1680	-1685	-1686
Belgium	BEL 20	-1864	**-1869**	-1864	-1864	-1864	-1864	-1858	-1864	-1864
Canada	TSX 60	**-1926**	-1926	-1924	-1924	-1925	-1925	-1919	-1925	-1922
Canada	TSX Composite	-1941	**-1942**	-1940	-1940	-1940	-1940	-1935	-1940	-1938
EuroStoxx	EuroStoxx 50	**-1933**	-1932	-1928	-1929	-1929	-1929	-1923	-1926	-1926
Finland	OMXH25	**-1812**	-1808	-1803	-1803	-1803	-1803	-1798	-1803	-1801
France	CAC 40	-1828	**-1847**	-1843	-1842	-1841	-1842	-1838	-1842	-1841
Germany	DAX	-1808	-1832	-1828	-1833	**-1837**	-1836	-1832	-1804	-1819
Hong Kong	Hang Seng	**-1728**	-1727	-1722	-1723	-1723	-1723	-1717	-1722	-1719
Ireland	ISEQ Overall	**-1751**	-1750	-1746	-1746	-1745	-1728	-1741	-1746	-1746
Israel	TA 35	-1857	**-1858**	-1853	-1855	-1856	-1856	-1851	-1849	-1847
Italy	FTSE MIB	-1635	**-1652**	-1648	-1649	-1649	-1649	-1644	-1649	-1643
Japan	Topix	-1660	**-1727**	-1721	-1720	-1717	-1717	-1716	-1718	-1719
Luxembourg	LuxX Index	-1592	**-1593**	-1588	-1589	-1590	-1590	-1585	-1585	-1584
Netherlands	AEX	**-1904**	-1901	-1895	-1895	-1895	-1895	-1890	-1895	-1895
New Zealand	NZX 50 Index	-1916	**-1962**	-1959	-1957	-1952	-1954	-1954	-1956	-1960
Norway	OBX Index	**-1744**	-1738	-1733	-1735	-1735	-1735	-1728	3991	-1733
Portugal	PSI 20	-1781	**-1792**	-1789	-1788	-1786	-1787	-1783	-1788	-1787
Singapore	STI Index	**-1903**	-1898	-1892	-1893	-1893	-1893	-1887	-1893	-1892
South Korea	KOSPI	-1802	**-1821**	-1816	-1817	-1817	-1817	-1812	-1817	-1813
Spain	IBEX 35	-1715	**-1723**	-1720	-1720	-1720	-1720	-1715	-1720	-1717
Sweden	OMXS30	**-1825**	-1821	-1815	-1816	-1816	-1816	-1811	-1816	-1815
Switzerland	SMI	-1850	**-1852**	-1847	-1848	-1850	-1849	-1844	-1843	-1842
UK	FTSE 100	-1887	**-1898**	-1894	-1894	-1893	-1894	-1888	-1894	-1892
USA	DowJones 30	-2001	**-2032**	-2027	-2028	-2026	-2027	-2023	-2028	-2026
USA	S&P 500	-1976	**-2012**	-2008	-2011	-2009	-2010	-2006	-2011	-2005
USA	Nasdaq	-1778	**-1819**	-1814	-1816	-1818	-1818	-1813	-1769	-1809
Brazil	Bovespa	-1439	**-1483**	-1480	-1477	-1474	-1475	-1471	-1476	-1479
Chile	IPSA	-1808	**-1809**	-1804	-1804	-1803	-1803	-1798	-1803	-1802
China	CSI 300	-1802	**-1805**	-1799	-1799	-1799	-1799	-1794	-1799	-1798
China	SSE	-1837	**-1843**	-1838	-1838	-1839	-1838	-1833	-1838	-1836
Colombia	IGBC	-1767	**-1780**	-1775	-1774	-1774	-1774	-1769	-1774	-1773
Czech Republic	PX	-1921	**-1923**	-1919	-1919	-1919	-1919	-1914	-1919	-1916
Egypt	EGX 30	-1445	**-1470**	-1466	-1466	-1464	-1464	-1460	-1465	-1462
Greece	Athex	-1528	**-1542**	-1537	-1540	-1542	-1542	-1536	-1524	-1531
Hungary	Budapest SE	-1726	**-1740**	-1736	-1736	-1735	-1736	-1731	-1736	-1737
India	Nifty 50	-1777	**-1784**	-1780	-1780	-1781	-1780	-1775	-1780	-1777
India	BSE Sensex	-1804	**-1808**	-1803	-1803	-1805	-1804	-1799	-1804	-1800
Indonesia	IDX Composite	-1707	**-1750**	-1744	-1742	-1737	-1739	-1739	-1741	-1745
Malaysia	KLCI	-2038	**-2041**	-2037	-2037	-2037	-2038	-2032	-2031	-2032
Mexico	IPC	-1746	**-1782**	-1777	-1775	-1772	-1773	-1771	-1774	-1777
Peru	Lima General	**-1784**	-1781	-1775	-1776	-1776	-1776	-1770	-1775	-1773
Philippines	PSEi	-1615	**-1622**	-1618	-1619	-1619	-1619	-1614	-1611	-1613
Poland	WIG	**-1727**	-1725	-1723	-1723	-1723	-1723	-1717	-1723	-1721
Qatar	QE 20 Index	-1602	**-1664**	-1659	-1656	-1653	-1654	-1653	-1655	-1657
Russia	MICEX	**-1698**	-1694	-1689	-1689	-1689	-1689	-1683	-1689	-1687
Russia	RTSI	-1565	**-1589**	-1584	-1584	-1582	-1583	-1579	-1583	-1582
Saudi Arabia	TASI	-1664	**-1695**	-1692	-1690	-1687	-1689	-1687	-1689	-1691
South Africa	JSE	**-1746**	-1742	-1737	-1737	-1737	-1737	-1731	-1737	-1736
Taiwan	TWII	-1821	**-1837**	-1833	-1832	-1831	-1831	-1826	-1831	-1833
Thailand	SET	-1952	**-1967**	-1961	-1961	-1960	-1961	-1956	-1961	-1959
Turkey	BIST 100	-1630	**-1639**	-1633	-1633	-1632	-1633	-1628	-1633	-1631
Un Arab Em	DFM	-1748	**-1750**	-1749	-1748	-1747	-1748	-1742	-1748	-1748
Un Arab Em	Abu Dhabi	-1770	**-1786**	-1781	-1781	-1781	-1781	-1776	-1781	-1777
Argentina	MERVAL	-1413	**-1422**	-1417	-1417	-1416	-1417	-1411	-1417	-1414
Bahrain	All Share	-1910	**-1968**	-1962	-1966	-1964	-1963	-1960	-1965	-1962
Bulgaria	SOFIX	-1748	**-1809**	-1804	-1802	-1800	-1800	-1798	-1801	-1804
Croatia	CROBEX	-1749	**-1808**	-1802	-1803	-1798	-1798	-1798	-1742	-1800
Cyprus	CYMAIN	-1480	**-1485**	-1480	-1481	-1483	-1482	-1478	-1469	-1476
Estonia	OMXT	-2015	**-2022**	-2016	-2017	-2018	-2018	-2012	-2018	-2012
Kazakhstan	KASE Index	**-1655**	-1651	-1646	-1646	-1646	-1646	-1640	-1646	-1646
Kuwait	Kuwait 15	-1701	**-1706**	-1702	-1703	-1702	-1703	-1697	-1703	-1699
Latvia	OMXR	-1687	**-1817**	-1816	-1814	-1802	-1803	-1811	-1811	-1813
Lithuania	OMXV	-2074	**-2078**	-2074	-2073	-2072	-2073	-2068	-2073	-2073
Mauritius	SEMDEX	-2230	-2263	-2261	-2265	**-2269**	-2268	-2263	-2215	-2257
Morocco	MASI	-1731	**-1783**	-1778	-1780	-1778	-1777	-1775	-1729	-1773
Namibia	NSX Overall	-1591	**-1596**	-1591	-1592	-1592	-1592	-1586	-1587	-1586
Oman	MSM 30	-1971	**-1974**	-1968	-1968	-1968	-1968	-1963	-1968	-1966
Pakistan	KSE 100	-1536	**-1558**	-1554	-1554	-1553	-1552	-1548	-1553	-1550
Romania	BET 10	-1798	**-1838**	-1832	-1830	-1827	-1827	-1827	-1829	-1834
Serbia	BELEX	-1891	**-1917**	-1912	-1913	-1912	-1912	-1907	-1912	-1908
Sri Lanka	CSE All-Share	-1987	-1988	-1990	-1991	**-1993**	-1992	-1987	-1987	-1987
Tunesia	Tunindex	**-2197**	-2193	-2187	-2192	-2192	-2192	-2187	-2192	-2190
Venezuela	IBC	-900	-974	-979	-990	**-999**	-987	-993	3505	-987
Vietnam	HNX 30	**-1793**	-1788	-1782	-1786	-1786	-1786	-1781	3840	-1783
Zambia	All Share	-1133	-1197	-1192	-1199	**-1222**	-1189	-1213	-1201	-1195

Table 4.9: BIC of fitted distributions for daily log-returns, from 11/03/2016 until 11/02/2017.

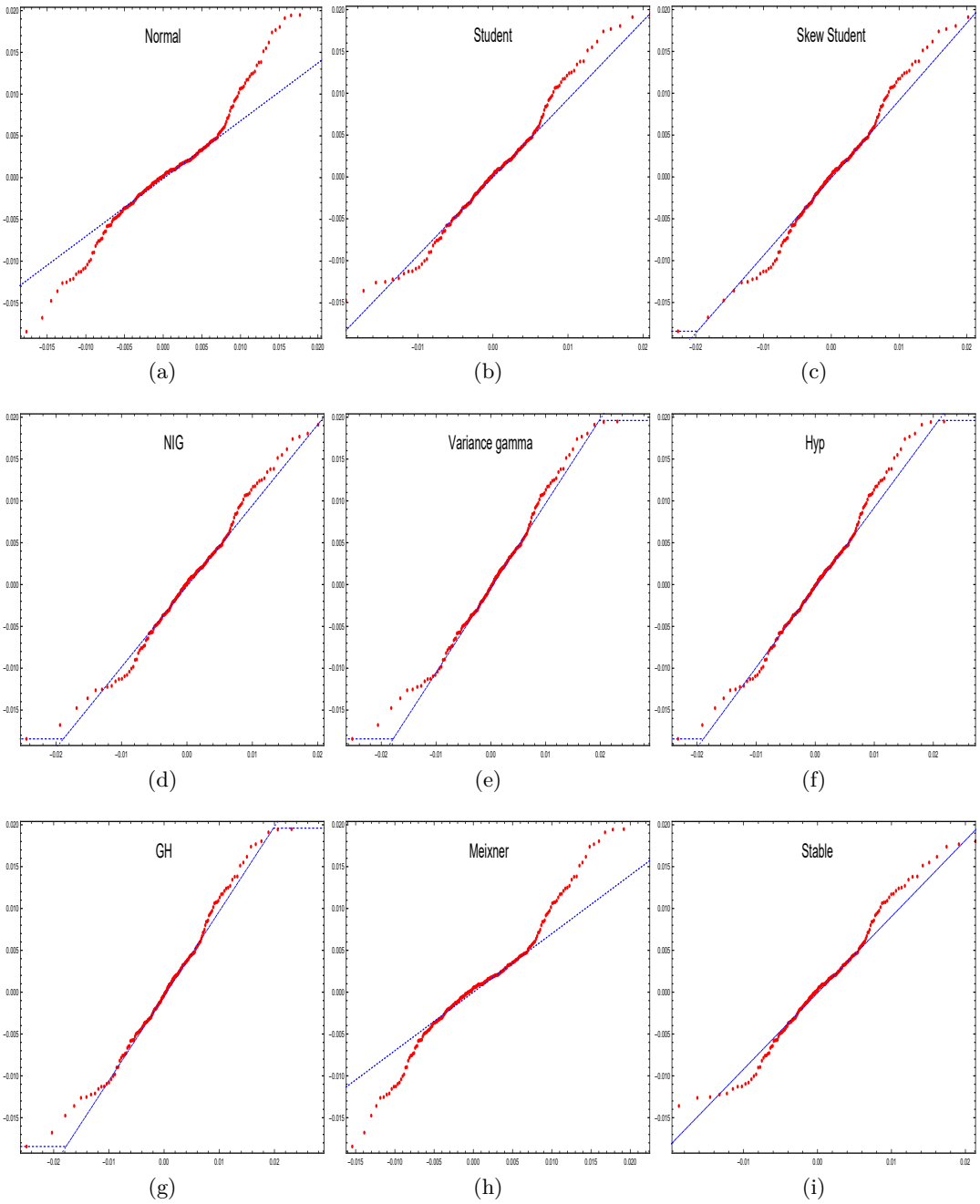

Figure 4.7: QQ-plots of empirical quantiles for daily DAX log-returns from 11/03/2016 until 11/02/2017 versus model distributions.

	N	St	SSt	NIG	VΓ	Hyp	GH	Meix	Stable
KS – daily, full sample	0	1	3	18	2	3	40	11	0
AD – daily, full sample	0	1	3	17	2	1	46	8	0
BIC – daily, full sample	0	20	11	28	2	1	6	10	0
KS – daily, one year	3	11	8	7	19	8	7	7	8
AD – daily, one year	0	9	9	7	11	8	17	1	16
BIC – daily, one year	17	56	0	0	5	0	0	0	0

Table 4.10: Number of lowest statistics per distribution.

examples for which this is the other way round (e.g., the Philippines). Hence, proper model choice is crucial.

Table 4.14 summarizes how often each distribution has the lowest KS, AD and BIC statistic among the models which are closed under convolution (and the Student-Lévy model for which ML estimation is available). For the purposes of comparison, the table also includes numbers for the daily fit. For the full sample, the NIG model most often is appropriate, followed by the Meixner model. For the last year and daily data the variance gamma model most often yields a good fit, while for hourly data there is no obvious "winner".

Figure 4.8 shows QQ-plots for hourly returns for the DAX example against model distributions. The Student model (not the Student t distribution but the distribution of X_t of a Student-Lévy process $\{X_t\}$ with $t = t_h$, using the estimation routine from Chapter 3) and the stable model outperform the other models. KS, AD and BIC favor the Student model. Hence the DAX is a good example of where the daily data is best modeled by a variance gamma or NIG distribution while the hourly data seem to fit well to a Student-Lévy process and therefore a different Lévy model. This means that in this case it is difficult to find a model which fits both hourly and daily returns equally well. We discuss time consistency further in the next section.

4.5 Time consistency

In this section we elaborate on the notion of time consistency which we briefly introduced above. In a nutshell, a model is time consistent if it fits to both daily and intraday data (or other time dimensions). Eberlein & Özkan (2003) introduced the concept and analyzed German stocks with the hyperbolic model. However, we do not use the hyperbolic model because it is not closed under convolution. Eberlein & Özkan (2003) redefined the meaning of $t = 1$ in their paper, which we do not do

Country	Index	N	St	NIG	VΓ	Meix	Stable
Australia	ASX 200	0.1218	0.0149	**0.0146**	0.0329	0.0149	0.0189
Australia	All Ordinaries	0.1236	0.0185	0.0187	0.0301	**0.0183**	0.0207
Austria	ATX	0.0806	0.0127	**0.0116**	0.0186	0.0128	0.0133
Belgium	BEL 20	0.0866	0.0137	**0.0132**	0.0204	0.0154	0.0142
Canada	TSX 60	0.1132	0.0305	0.0232	**0.0200**	0.0218	0.0338
Canada	TSX Composite	0.1132	0.0313	0.0247	**0.0177**	0.0233	0.0322
EuroStoxx	EuroStoxx 50	0.0874	**0.0129**	0.0142	0.0215	0.0167	0.0191
Finland	OMXH25	0.1050	0.0151	0.0183	0.0272	0.0201	**0.0141**
France	CAC 40	0.0934	**0.0094**	0.0127	0.0232	0.0151	0.0164
Germany	DAX	0.1027	**0.0121**	0.0173	0.0305	0.0198	0.0132
Hong Kong	Hang Seng	0.1223	0.0389	0.0382	**0.0328**	0.0377	0.0407
Ireland	ISEQ Overall	0.0747	0.0173	0.0142	0.0218	0.0165	**0.0077**
Israel	TA 35	0.1074	**0.0102**	0.0144	0.0268	0.0156	0.0170
Italy	FTSE MIB	0.0842	**0.0088**	0.0105	0.0145	0.0124	0.0156
Japan	Topix	0.1729	0.0197	0.0168	0.0405	**0.0157**	0.0211
Luxembourg	LuxX Index	0.1399	0.0219	0.0180	0.0303	**0.0172**	0.0203
Netherlands	AEX	0.0966	0.0156	**0.0124**	0.0196	0.0126	0.0179
New Zealand	NZX 50 Index	0.1084	**0.0160**	0.0198	0.0279	0.0216	0.0186
Norway	OBX Index	0.0835	0.0125	0.0144	0.0211	0.0154	**0.0117**
Portugal	PSI 20	0.0881	0.0133	**0.0128**	0.0200	0.0137	0.0147
Singapore	STI Index	0.1079	0.0159	0.0167	0.0307	0.0194	**0.0120**
South Korea	KOSPI	0.1223	**0.0140**	0.0159	0.0302	0.0169	0.0150
Spain	IBEX 35	0.0740	0.0160	**0.0103**	0.0145	0.0117	0.0143
Sweden	OMXS30	0.0902	**0.0098**	0.0108	0.0183	0.0133	0.0142
Switzerland	SMI	0.0872	0.0175	0.0171	0.0242	0.0183	**0.0149**
UK	FTSE 100	0.0859	**0.0087**	0.0108	0.0159	0.0129	0.0114
USA	DowJones 30	0.1167	0.0320	0.0270	0.0314	**0.0258**	0.0341
USA	S&P 500	0.1053	0.0405	0.0370	**0.0190**	0.0359	0.0430
USA	Nasdaq	0.1157	0.0372	0.0309	**0.0291**	0.0302	0.0399
Brazil	Bovespa	0.1021	**0.0125**	0.0129	0.0186	0.0138	0.0151
Chile	IPSA	0.1397	**0.0126**	0.0131	0.0205	0.0162	0.0167
China	CSI 300	0.1293	0.0930	0.0793	**0.0504**	0.0786	0.0739
China	SSE	0.1321	0.0784	0.0696	**0.0501**	0.0687	0.0636
Colombia	IGBC	0.0752	**0.0088**	0.0090	0.0182	0.0094	0.0152
Czech Republic	PX	0.0684	0.0221	0.0159	0.0150	0.0162	**0.0144**
Egypt	EGX 30	0.1860	0.0376	0.0176	0.0489	**0.0136**	0.0217
Greece	Athex	0.0702	0.0123	**0.0110**	0.0141	0.0126	0.0172
Hungary	Budapest SE	0.0731	**0.0106**	0.0109	0.0188	0.0122	0.0171
India	Nifty 50	0.0919	0.0123	**0.0102**	0.0171	0.0118	0.0179
India	BSE Sensex	0.0957	**0.0129**	0.0161	0.0268	0.0177	0.0192
Indonesia	IDX Composite	0.1205	0.0227	**0.0137**	0.0237	0.0148	0.0215
Malaysia	KLCI	0.1009	0.0149	**0.0131**	0.0236	0.0154	0.0220
Mexico	IPC	0.0826	0.0135	0.0106	0.0164	**0.0105**	0.0200
Peru	Lima General	0.0902	0.0276	0.0236	0.0261	**0.0220**	0.0330
Philippines	PSEi	0.1194	0.0423	0.0358	**0.0122**	0.0351	0.0404
Poland	WIG	0.0773	**0.0085**	0.0119	0.0193	0.0142	0.0140
Qatar	QE 20 Index	0.1124	0.0159	0.0169	0.0247	0.0199	**0.0156**
Russia	MICEX	0.0653	0.0133	**0.0108**	0.0145	0.0111	0.0183
Russia	RTSI	0.0694	0.0280	0.0264	0.0395	**0.0258**	0.0273
Saudi Arabia	TASI	0.1116	0.0295	0.0269	0.0309	**0.0262**	0.0312
South Africa	JSE	0.0784	0.0124	**0.0114**	0.0205	0.0135	0.0163
Taiwan	TWII	0.1110	0.0171	0.0172	0.0328	0.0186	**0.0106**
Thailand	SET	0.0656	0.0094	**0.0084**	0.0136	0.0096	0.0158
Turkey	BIST 100	0.0928	0.0218	0.0201	**0.0176**	0.0194	0.0298
Un Arab Em	DFM	0.0665	0.0192	0.0189	0.0198	0.0194	**0.0168**
Un Arab Em	Abu Dhabi	0.0630	0.0167	**0.0133**	0.0161	0.0139	0.0264
Argentina	MERVAL	0.1216	0.0144	0.0112	0.0243	**0.0111**	0.0174
Bahrain	All Share	0.1135	0.0204	0.0187	0.0206	**0.0177**	0.0275
Bulgaria	SOFIX	0.1015	0.0120	**0.0099**	0.0188	0.0120	0.0205
Croatia	CROBEX	0.1191	**0.0103**	0.0112	0.0227	0.0130	0.0213
Cyprus	CYMAIN	0.1039	0.0289	0.0273	0.0633	**0.0272**	0.0347
Estonia	OMXT	0.0573	0.0191	0.0159	**0.0108**	0.0139	0.0298
Kazakhstan	KASE Index	0.0765	0.0266	0.0149	0.0135	**0.0129**	0.0290
Kuwait	Kuwait 15	0.0746	0.0323	0.0239	**0.0199**	0.0216	0.0377
Latvia	OMXR	0.1579	0.0284	0.0184	0.0406	**0.0171**	0.0264
Lithuania	OMXV	0.4093	**0.0176**	0.0476	0.0879	0.0497	0.0240
Mauritius	SEMDEX	0.1276	0.0462	**0.0302**	0.0330	0.5024	0.0329
Morocco	MASI	0.0972	0.0269	0.0215	0.0208	**0.0196**	0.0327
Namibia	NSX Overall	0.1631	0.0501	0.0414	0.0354	0.0412	**0.0282**
Oman	MSM 30	0.1040	0.0782	0.0718	**0.0612**	0.0983	0.0772
Pakistan	KSE 100	0.0816	0.0177	0.0154	0.0149	**0.0144**	0.0212
Romania	BET 10	0.0935	0.0135	0.0134	0.0203	0.0153	**0.0102**
Serbia	BELEX	0.0722	0.0194	**0.0169**	0.0305	0.0813	0.0223
Sri Lanka	CSE All-Share	0.0604	0.0185	0.0144	**0.0138**	0.0144	0.0221
Tunesia	Tunindex	0.0497	0.0240	0.0247	0.0246	**0.0225**	0.0336
Venezuela	IBC	0.1638	0.0728	0.0595	0.0671	0.0551	**0.0427**
Vietnam	HNX 30	0.0380	0.0275	**0.0163**	0.0170	0.0163	0.0169
Zambia	All Share	0.1744	0.1573	0.1420	0.1635	**0.1404**	0.1567

Table 4.11: KS distance between the empirical and fitted distributions for hourly log-returns, from 11/02/2016 1pm until 11/02/2017 12pm.

Country	Index	N	St	NIG	VΓ	Meix	Stable
Australia	ASX 200	63.540	**0.291**	0.380	3.251	0.529	0.507
Australia	All Ordinaries	66.286	**0.383**	0.471	2.797	0.620	0.632
Austria	ATX	34.272	0.364	0.364	1.435	0.571	**0.356**
Belgium	BEL 20	45.905	0.582	0.606	1.775	0.877	**0.410**
Canada	TSX 60	50.918	2.170	1.652	**0.709**	1.427	3.048
Canada	TSX Composite	53.264	2.743	2.013	**0.455**	1.770	3.500
EuroStoxx	EuroStoxx 50	46.016	**0.214**	0.367	1.484	0.571	0.582
Finland	OMXH25	56.098	0.574	0.947	3.309	1.329	**0.458**
France	CAC 40	54.462	**0.191**	0.401	1.772	0.635	0.485
Germany	DAX	56.900	**0.351**	0.679	2.771	0.988	0.392
Hong Kong	Hang Seng	72.237	2.579	2.181	2.686	**2.030**	3.121
Ireland	ISEQ Overall	37.529	0.892	0.835	1.991	1.175	**0.188**
Israel	TA 35	50.562	**0.300**	0.412	2.007	0.610	0.590
Italy	FTSE MIB	36.691	**0.218**	0.274	1.113	0.368	0.817
Japan	Topix	118.466	0.568	0.369	6.272	**0.346**	0.824
Luxembourg	LuxX Index	97.834	1.780	1.195	3.203	**1.044**	1.730
Netherlands	AEX	53.426	**0.249**	0.348	1.743	0.547	0.713
New Zealand	NZX 50 Index	59.536	**0.556**	0.962	2.445	1.377	0.612
Norway	OBX Index	34.518	0.436	0.734	2.167	1.050	**0.220**
Portugal	PSI 20	44.022	**0.491**	0.511	1.579	0.735	0.746
Singapore	STI Index	60.301	0.531	0.864	3.582	1.210	**0.374**
South Korea	KOSPI	62.350	**0.302**	0.355	3.070	0.505	0.427
Spain	IBEX 35	36.154	1.189	**0.405**	0.970	0.610	0.810
Sweden	OMXS30	42.643	**0.211**	0.353	1.584	0.574	0.553
Switzerland	SMI	41.136	**0.343**	0.545	1.788	0.812	0.482
UK	FTSE 100	41.781	**0.155**	0.273	1.545	0.483	0.419
USA	DowJones 30	65.320	2.468	1.598	1.714	**1.413**	2.987
USA	S&P 500	55.878	3.258	2.732	**0.690**	2.502	4.401
USA	Nasdaq	66.541	2.260	1.797	2.498	**1.690**	3.103
Brazil	Bovespa	51.275	**0.357**	0.415	1.347	0.588	0.732
Chile	IPSA	108.909	0.650	0.763	2.854	1.228	**0.563**
China	CSI 300	48.564	12.544	12.353	**3.181**	12.229	11.734
China	SSE	50.734	10.206	10.164	**4.085**	10.021	9.883
Colombia	IGBC	23.708	0.160	**0.128**	0.726	0.170	0.675
Czech Republic	PX	24.528	1.377	0.469	0.948	0.618	**0.382**
Egypt	EGX 30	77.160	3.858	0.343	4.078	**0.203**	0.931
Greece	Athex	21.915	0.394	**0.284**	0.689	0.370	0.764
Hungary	Budapest SE	28.272	0.332	**0.262**	0.917	0.352	0.665
India	Nifty 50	34.837	**0.131**	0.169	1.109	0.290	0.474
India	BSE Sensex	35.134	0.400	**0.269**	1.498	0.371	0.568
Indonesia	IDX Composite	66.925	1.897	**0.613**	1.653	0.759	0.828
Malaysia	KLCI	41.523	0.496	**0.361**	1.404	0.443	0.750
Mexico	IPC	32.563	0.274	**0.170**	0.616	0.202	0.823
Peru	Lima General	33.246	2.022	1.401	**0.808**	1.156	3.404
Philippines	PSEi	49.089	3.876	2.963	**0.384**	2.724	4.061
Poland	WIG	31.645	0.339	**0.238**	1.090	0.388	0.544
Qatar	QE 20 Index	37.261	0.283	0.632	1.298	0.915	**0.211**
Russia	MICEX	18.465	0.777	**0.244**	0.576	0.282	0.973
Russia	RTSI	27.283	0.927	**0.571**	1.585	0.698	0.975
Saudi Arabia	TASI	35.007	0.537	**0.468**	1.518	0.530	0.801
South Africa	JSE	32.425	**0.312**	0.418	1.410	0.603	0.469
Taiwan	TWII	36.355	0.364	0.433	2.093	0.561	**0.290**
Thailand	SET	18.106	**0.139**	0.151	0.523	0.215	0.424
Turkey	BIST 100	41.677	1.747	1.441	**0.966**	1.249	3.453
Un Arab Em	DFM	8.296	0.577	0.311	0.525	0.375	**0.299**
Un Arab Em	Abu Dhabi	10.154	0.386	**0.255**	0.370	0.300	0.651
Argentina	MERVAL	64.605	0.398	**0.178**	1.826	0.199	0.806
Bahrain	All Share	25.626	0.390	**0.280**	0.628	0.306	0.738
Bulgaria	SOFIX	48.991	0.486	**0.319**	1.009	0.477	0.903
Croatia	CROBEX	72.540	**0.318**	0.443	1.685	0.691	1.016
Cyprus	CYMAIN	36.140	1.787	1.323	3.674	**1.162**	2.454
Estonia	OMXT	12.615	0.943	0.527	**0.414**	0.508	1.302
Kazakhstan	KASE Index	20.729	2.338	0.574	**0.270**	0.430	1.459
Kuwait	Kuwait 15	7.892	1.157	0.776	**0.441**	0.682	1.935
Latvia	OMXR	82.066	1.674	0.775	1.967	**0.682**	1.739
Lithuania	OMXV	504.101	0.796	9.581	31.016	10.398	**0.734**
Mauritius	SEMDEX	35.630	2.887	1.154	1.322	385.546	**1.099**
Morocco	MASI	42.008	1.143	0.633	0.564	**0.540**	1.928
Namibia	NSX Overall	130.738	9.478	8.215	**3.014**	8.229	5.003
Oman	MSM 30	19.998	4.438	**4.259**	4.270	20.962	4.929
Pakistan	KSE 100	28.955	0.343	0.268	0.581	**0.263**	1.003
Romania	BET 10	55.507	0.472	0.755	2.433	1.178	**0.314**
Serbia	BELEX	15.247	0.813	**0.479**	0.936	17.100	0.977
Sri Lanka	CSE All-Share	8.382	0.824	**0.186**	0.307	0.210	0.626
Tunesia	Tunindex	4.920	0.911	0.719	**0.643**	0.688	1.178
Venezuela	IBC	47.998	9.908	5.242	3.412	4.299	**2.829**
Vietnam	HNX 30	3.692	1.255	**0.275**	0.376	0.309	0.326
Zambia	All Share	24.919	17.366	15.469	18.966	**15.315**	17.453

Table 4.12: AD distance between the empirical and fitted distributions for hourly log-returns, from 11/02/2016 1pm until 11/02/2017 12pm.

Country	Index	N	St	NIG	VΓ	Meix	Stable
Australia	ASX 200	-16517	**-17391**	-17383	-17337	-17379	-17358
Australia	All Ordinaries	-16857	**-17773**	-17765	-17732	-17761	-17740
Austria	ATX	-20372	**-20902**	-20892	-20850	-20886	-20870
Belgium	BEL 20	-21628	**-22360**	-22343	-22290	-22332	-22339
Canada	TSX 60	-19244	-19900	-19915	**-19949**	-19924	-19821
Canada	TSX Composite	-19689	-20375	-20393	**-20446**	-20403	-20294
EuroStoxx	EuroStoxx 50	-22077	**-22779**	-22766	-22718	-22758	-22745
Finland	OMXH25	-21449	**-22276**	-22260	-22174	-22250	-22251
France	CAC 40	-21111	**-21964**	-21948	-21887	-21938	-21931
Germany	DAX	-21131	**-21973**	-21957	-21884	-21947	-21944
Hong Kong	Hang Seng	-17613	-18552	-18565	**-18649**	-18571	-18493
Ireland	ISEQ Overall	-22508	**-23121**	-23106	-23051	-23093	-23111
Israel	TA 35	-20813	**-21542**	-21534	-21478	-21529	-21505
Italy	FTSE MIB	-19915	**-20473**	-20466	-20436	-20461	-20426
Japan	Topix	-15072	-16637	-16643	-16521	**-16643**	-16604
Luxembourg	LuxX Index	-18766	-20006	-20027	-19979	**-20036**	-19944
Netherlands	AEX	-21611	**-22416**	-22404	-22347	-22396	-22379
New Zealand	NZX 50 Index	-20975	**-22012**	-21980	-21911	-21958	-22008
Norway	OBX Index	-18507	**-19034**	-19019	-18963	-19011	-19014
Portugal	PSI 20	-21187	**-21866**	-21851	-21798	-21839	-21839
Singapore	STI Index	-22029	**-22869**	-22857	-22766	-22849	-22840
South Korea	KOSPI	-16087	**-16926**	-16920	-16831	-16917	-16894
Spain	IBEX 35	-22726	-23420	-23413	-23368	-23398	**-23424**
Sweden	OMXS30	-21207	**-21872**	-21859	-21804	-21851	-21840
Switzerland	SMI	-21764	**-22412**	-22397	-22340	-22387	-22385
UK	FTSE 100	-21676	**-22317**	-22305	-22253	-22298	-22283
USA	DowJones 30	-20302	-21168	-21184	**-21215**	-21189	-21100
USA	S&P 500	-20081	-20829	-20842	**-20929**	-20848	-20752
USA	Nasdaq	-18630	-19550	-19556	**-19597**	-19559	-19489
Brazil	Bovespa	-16649	**-17535**	-17517	-17467	-17507	-17502
Chile	IPSA	-18436	-20238	-20192	-20097	-20161	**-20238**
China	CSI 300	-15629	-16148	-16185	**-16529**	-16201	-16080
China	SSE	-15867	-16446	-16476	**-16714**	-16490	-16372
Colombia	IGBC	-17471	**-17826**	-17822	-17800	-17820	-17784
Czech Republic	PX	-19323	**-19737**	-19733	-19705	-19726	-19731
Egypt	EGX 30	-9297	-10209	-10239	-10172	**-10243**	-10198
Greece	Athex	-16746	**-17103**	-17097	-17076	-17093	-17077
Hungary	Budapest SE	-21115	**-21546**	-21542	-21519	-21539	-21505
India	Nifty 50	-16069	**-16612**	-16602	-16561	-16596	-16579
India	BSE Sensex	-16157	**-16684**	-16677	-16637	-16673	-16648
Indonesia	IDX Composite	-17001	**-18024**	-18015	-17949	-18005	-18006
Malaysia	KLCI	-17612	**-18222**	-18215	-18174	-18211	-18189
Mexico	IPC	-16943	**-17442**	-17436	-17416	-17434	-17399
Peru	Lima General	-19709	-20129	-20141	**-20196**	-20150	-20049
Philippines	PSEi	-14761	-15373	-15396	**-15495**	-15407	-15304
Poland	WIG	-20917	**-21402**	-21397	-21365	-21392	-21366
Qatar	QE 20 Index	-10029	**-10698**	-10672	-10626	-10657	-10697
Russia	MICEX	-20378	-20659	**-20670**	-20655	-20668	-20631
Russia	RTSI	-18509	**-18990**	-18984	-18955	-18976	-18971
Saudi Arabia	TASI	-11094	-11576	-11574	**-11584**	-11573	-11545
South Africa	JSE	-20656	**-21150**	-21142	-21102	-21136	-21116
Taiwan	TWII	-11261	**-11749**	-11742	-11688	-11740	-11726
Thailand	SET	-16678	**-16947**	-16942	-16930	-16940	-16913
Turkey	BIST 100	-22726	-23377	-23377	**-23382**	-23379	-23299
Un Arab Em	DFM	-8429	**-8566**	-8561	-8551	-8558	-8555
Un Arab Em	Abu Dhabi	-10811	**-11023**	-11013	-11000	-11008	-11013
Argentina	MERVAL	-13817	**-14723**	-14721	-14670	-14719	-14682
Bahrain	All Share	-7926	**-8323**	-8315	-8295	-8311	-8300
Bulgaria	SOFIX	-17035	**-17789**	-17775	-17733	-17765	-17765
Croatia	CROBEX	-17991	**-19136**	-19116	-19043	-19102	-19108
Cyprus	CYMAIN	-11862	-12312	-12322	-12310	**-12329**	-12245
Estonia	OMXT	-15073	**-15316**	-15313	-15308	-15308	-15312
Kazakhstan	KASE Index	-13940	-14210	-14222	**-14229**	-14226	-14177
Kuwait	Kuwait 15	-8014	-8115	-8115	**-8124**	-8117	-8090
Latvia	OMXR	-11720	-12906	**-12911**	-12878	-12908	-12865
Lithuania	OMXV	-7854	-15768	-15566	-14836	-15563	**-15796**
Mauritius	SEMDEX	-10379	-10826	**-10844**	-10832	20553	-10816
Morocco	MASI	-15537	-16171	**-16171**	-16169	-16171	-16121
Namibia	NSX Overall	-18172	-19856	-19908	**-20073**	-19921	-19856
Oman	MSM 30	-8908	-9119	-9131	**-9411**	-8882	-9076
Pakistan	KSE 100	-14254	**-14679**	-14675	-14670	-14675	-14634
Romania	BET 10	-23934	**-24835**	-24812	-24734	-24795	-24820
Serbia	BELEX	-12031	-12219	**-12220**	-12218	-11996	-12179
Sri Lanka	CSE All-Share	-15182	-15305	**-15313**	-15307	-15312	-15296
Tunesia	Tunindex	-11934	-11978	-11983	**-11987**	-11984	-11960
Venezuela	IBC	-4658	-5168	-5220	**-5285**	-5233	-5203
Vietnam	HNX 30	-10943	-10975	**-10990**	-10987	-10990	-10974
Zambia	All Share	-2109	-2397	-2375	-2416	-2362	**-2458**

Table 4.13: BIC of fitted distributions for hourly log-returns, from 11/02/2016 1pm until 11/02/2017 12pm.

	N	St	NIG	VΓ	Meix	Stable
KS – daily, full sample	0	9	37	7	23	2
AD – daily, full sample	0	6	42	6	21	3
BIC – daily, full sample	0	24	36	6	12	0
KS – daily, one year	3	15	10	26	12	12
AD – daily, one year	0	13	16	22	7	20
BIC – daily, one year	17	56	0	5	0	0
KS – hourly, one year	0	17	18	13	18	12
AD – hourly, one year	0	19	20	13	11	15
BIC – hourly, one year	0	45	7	18	4	4

Table 4.14: Number of lowest statistics per distribution among models which are closed under convolution and Student model.

here because this causes comparison issues (see below). Figueroa-López et al. (2011) focused on the variance gamma and the NIG distributions and explored in simulations how the estimation error evolves with an increasing sampling frequency for a given Lévy path. They found that if the frequency is too high, e.g., just a few minutes, microstructure effects inhibit time consistency. Apart from these two works, the topic has received little attention in the literature. However, the idea one well-performing model for both hourly and daily data is appealing, e.g., for pricing path-dependent options.

We here focus on establishing which model is more time consistent. Eberlein & Özkan (2003) defined two sorts of time consistency between daily and intraday returns, which we adopt. *Downward convolution* means that we fit a distribution $F^L_{t=1}(x;\hat{\theta}_d)$ to daily data, where L denotes a Lévy model and $\hat{\theta}_d$ is the ML estimate for daily data. We then compare the implied distribution at time $t = t_h$, $F^L_{t=t_h}(x;\hat{\theta}_d)$, with the empirical distribution of the hourly returns $F_{n,h}(x)$. We compute the distance between $F^L_{t=t_h}(x;\hat{\theta}_d)$ and $F_{n,h}(x)$. If the distance is close to the distance between $F^L_{t=t_h}(x;\hat{\theta}_h)$ and $F_{n,h}(x)$, we say that the model is downwardly time consistent. On the other hand, *upward convolution* means that we fit a distribution $F^L_{t=t_h}(x;\hat{\theta}_h)$ to hourly returns, where $\hat{\theta}_h$ is the corresponding ML estimate for hourly data. Then we compare the implied distribution at time $t = 1$, $F^L_{t=1}(x;\hat{\theta}_h)$, with the empirical distribution of daily returns $F_{n,d}(x)$ and compute the distance between $F^L_{t=1}(x;\hat{\theta}_h)$ and $F_{n,d}(x)$. A model is upwardly time consistent if this distance is close to the distance between $F^L_{t=1}(x;\hat{\theta}_d)$ and $F_{n,d}(x)$ of the direct fit. Here is the reason why we do not redefine the meaning of t for the models which are not closed under convolution.

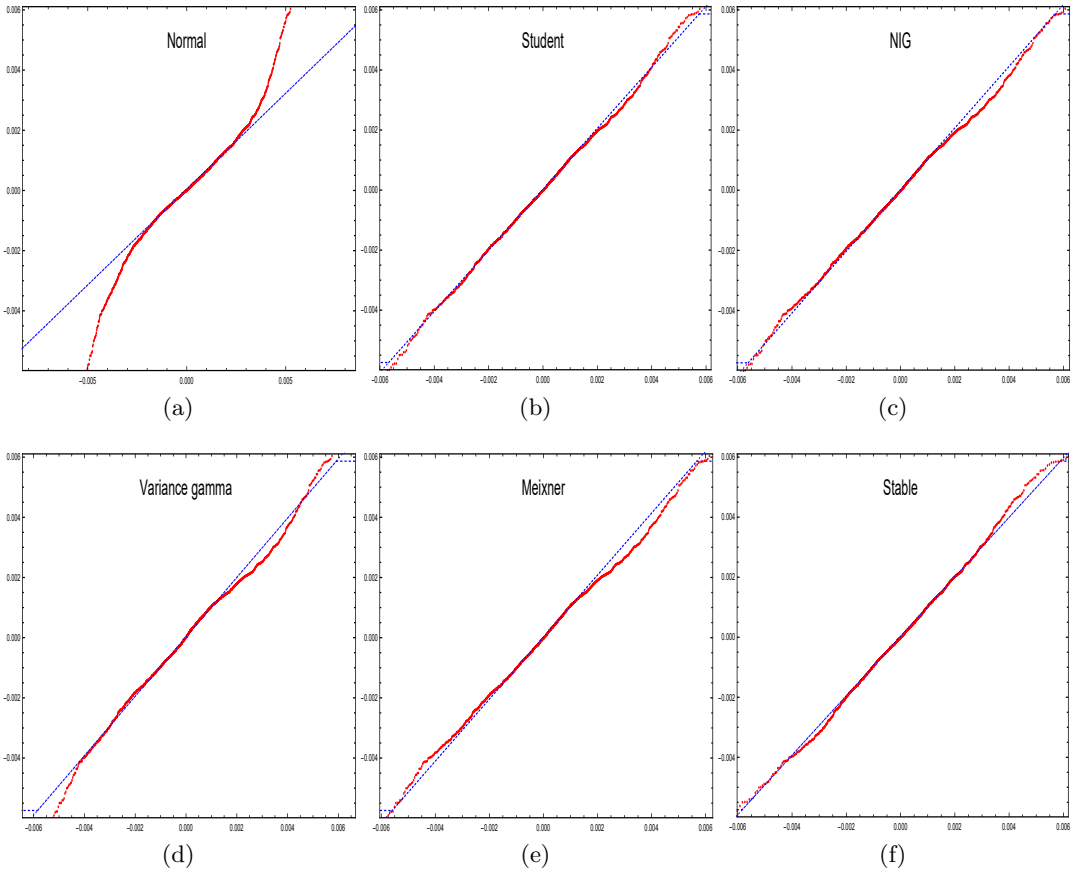

Figure 4.8: QQ-plots of empirical quantiles for daily DAX log-returns from 11/02/2016 1pm until 11/02/2017 12pm versus model distributions.

The upward convolution would then not be comparable since it would not be from the same distributional class.

We start with downward convolution. The number of trading hours per day varies for each index. It may be that the number of hours is not an integer, e.g., 8.75 hours (for the DAX). In such cases we round up to full hours and use an adjusted t_h. The reason for this is that Eberlein & Özkan (2003) found that the distance for downward convolution is minimal for a t which is slightly smaller than the actual physical time. We find that this is also true for our data but omit a detailed discussion.

Tables 4.15 and 4.16 present the KS and AD distances between $F^L_{t=t_h}(x;\hat{\theta}_d)$ and $F_{n,h}(x)$. Table 4.17 presents the BIC of the model $F^L_{t=t_h}(x;\hat{\theta}_d)$ using hourly data. We observe that the downwardly convoluted variance gamma model is a poor fit in many

cases. For example, while it was the best fit (in terms of AD) for the daily returns of the EuroStoxx (cf. Table 4.8) the downward convolution is the worst fit for hourly returns. The implied distribution of the Student-Lévy model is the best fit in the most cases, followed by the stable model. Even the Gaussian model sometimes has the lowest distance. This leads us to conclude that in these cases downward time consistency is not given, as the Gaussian model is a poor fit.

It is also important to check whether the downward convolution can compete with the ML fit to hourly returns. We compare, e.g., for AD, Table 4.12 (ML fit) with Table 4.16 (downward convolution). The distances for the downward convolution are in most cases vastly greater, indicating poor downward consistency. Only a few indices can compete with the ML fit, e.g., the South Korean KOSPI's 0.31 (downward convolution) with 0.302 (ML) in the Student-Lévy model. To summarize, downward time consistency is generally not given.

We return to the DAX example from Section 4.4. Figure 4.9 shows QQ-plots comparing the downward convolution with the empirical quantiles. It is very obvious that the normal, the Student, the NIG, the variance gamma and the Meixner model do not fit. The stable distribution looks promising at first glance. However, it underestimates the left tail. The AD distance is 24.64 for the stable downward convolution while it is 0.392 for the hourly ML fit. We also see this if we compare panel (f) of Figure 4.9 with Figure 4.8 (f).

Of course, it is reasonable for the downward convolution distances to be higher than those of the ML fit, even if the underlying Lévy model is true. It is of interest to study what proportion of these high distances is due to the specific market data and which to model estimation difficulties. To address this issue we generate 1,000 sample paths from the Lévy models with parameters estimated from daily returns. We then compute the sample mean of the KS, AD and BIC. For example, we use the fitted stable distribution of the DAX for daily returns to generate 1,000 paths of the stable log-return process with an hourly frequency. The downward convolution has an average AD distance to the simulated paths of 7.47 compared with the real world AD distance of 24.64. This suggests that the time inconsistency is also caused by some violations of the model. We only outlined this issue here, since a rigorous discussion would require numerous simulations for each index and each model, which is beyond the scope of this chapter.

Next, we turn to upward time consistency. Although downward time consistency is interesting in itself, upward time consistency is more relevant in practice. A model fitted to hourly data should be useful in explaining daily behavior. In order to address this, we fit Lévy models to hourly returns and use the upward convolution as a model for daily returns. Tables 4.18 – 4.20 report the KS, AD and BIC statistics. There is, again, no obvious first choice, as the Student, the NIG and the variance gamma

Country	Index	N	St	NIG	VΓ	Meix	Stable
Australia	ASX 200	0.12497	0.05445	0.03505	0.07995	**0.02620**	0.09998
Australia	All Ordinaries	0.12846	0.05497	0.03424	0.09343	**0.03200**	0.09917
Austria	ATX	0.08497	0.04674	0.04168	**0.03605**	0.03882	0.07413
Belgium	BEL 20	0.07374	**0.02922**	0.05880	0.14934	0.07342	0.06282
Canada	TSX 60	0.09831	**0.04588**	0.09062	0.16219	0.09572	0.09035
Canada	TSX Composite	0.10716	**0.04920**	0.08910	0.15529	0.09612	0.10371
EuroStoxx	EuroStoxx 50	0.06712	**0.02594**	0.05446	0.11870	0.07253	0.06107
Finland	OMXH25	0.10810	0.05551	**0.04138**	0.05144	0.06630	0.10779
France	CAC 40	0.07219	0.04975	0.08388	0.17289	0.09647	**0.04001**
Germany	DAX	0.09308	0.09884	0.12933	0.26462	0.12055	**0.06473**
Hong Kong	Hang Seng	0.12469	**0.06713**	0.08723	0.12920	0.11159	0.11445
Ireland	ISEQ Overall	0.08835	**0.02523**	0.04527	0.07039	0.04595	0.07306
Israel	TA 35	0.10146	**0.02922**	0.05883	0.15939	0.05126	0.07512
Italy	FTSE MIB	0.08684	0.05680	0.09309	0.20226	0.10688	**0.03696**
Japan	Topix	0.17476	0.04189	**0.02658**	0.17113	0.02865	0.09422
Luxembourg	LuxX Index	0.12858	0.05881	**0.05610**	0.14446	0.10481	0.11463
Netherlands	AEX	0.07550	0.01805	**0.01709**	0.06408	0.02232	0.06821
New Zealand	NZX 50 Index	0.12670	**0.03825**	0.07961	0.19580	0.09193	0.05279
Norway	OBX Index	0.09572	**0.07488**	0.11292	0.11658	0.51224	0.09061
Portugal	PSI 20	0.08808	**0.05077**	0.07853	0.15352	0.08971	0.05706
Singapore	STI Index	0.10540	**0.07807**	0.08575	0.07889	0.09182	0.10540
South Korea	KOSPI	0.12788	**0.01308**	0.04842	0.16940	0.06208	0.06411
Spain	IBEX 35	0.05968	0.06878	0.10753	0.19191	0.12200	**0.03756**
Sweden	OMXS30	0.08425	**0.04323**	0.05479	0.04912	0.05248	0.08259
Switzerland	SMI	0.08932	**0.03178**	0.06788	0.19229	0.06995	0.07142
UK	FTSE 100	0.07158	0.04707	0.08499	0.16205	0.09725	**0.02684**
USA	DowJones 30	0.11892	**0.04011**	0.05863	0.16202	0.06976	0.05143
USA	S&P 500	0.10601	**0.05997**	0.09733	0.18486	0.10727	0.07151
USA	Nasdaq	0.12080	**0.05537**	0.08120	0.26870	0.14014	0.05765
Brazil	Bovespa	0.10041	0.06527	0.09567	0.20019	0.10896	**0.04740**
Chile	IPSA	0.08171	**0.01776**	0.02919	0.08381	0.03756	0.04461
China	CSI 300	0.12654	0.11318	0.11345	**0.10600**	0.11110	0.12603
China	SSE	0.12259	**0.08382**	0.09624	0.16035	0.09663	0.10454
Colombia	IGBC	0.07495	0.05088	0.07444	0.16961	0.08577	**0.03690**
Czech Republic	PX	0.05651	0.05251	0.08835	0.15840	0.10168	**0.04589**
Egypt	EGX 30	0.19601	0.12408	0.09628	0.13184	**0.08916**	0.13786
Greece	Athex	0.08219	0.05886	0.09522	0.20691	0.06882	**0.02735**
Hungary	Budapest SE	0.09419	**0.03678**	0.07325	0.16431	0.08704	0.06007
India	Nifty 50	0.10353	**0.01423**	0.04455	0.13874	0.05632	0.07221
India	BSE Sensex	0.10244	**0.02596**	0.04344	0.15040	0.05455	0.08272
Indonesia	IDX Composite	0.13212	**0.04368**	0.06664	0.17563	0.07762	0.05091
Malaysia	KLCI	0.10600	**0.02565**	0.03413	0.10140	0.07602	0.06391
Mexico	IPC	0.07905	0.05958	0.08254	0.15838	0.09527	**0.02527**
Peru	Lima General	0.12008	0.07425	0.05231	**0.02758**	0.08115	0.11823
Philippines	PSEi	0.12228	**0.07744**	0.09156	0.19118	0.11587	0.10342
Poland	WIG	0.09185	**0.02418**	0.05874	0.08713	0.05814	0.07264
Qatar	QE 20 Index	0.11094	0.04755	0.07594	0.14209	0.08680	**0.02740**
Russia	MICEX	0.06500	0.01726	**0.01416**	0.04401	0.01664	0.06122
Russia	RTSI	0.05589	0.09293	0.11084	0.19897	0.11981	**0.03301**
Saudi Arabia	TASI	0.12918	**0.03288**	0.05099	0.11381	0.05427	0.06772
South Africa	JSE	0.07991	0.03384	0.03809	0.05078	**0.03270**	0.07775
Taiwan	TWII	0.12382	0.04284	**0.03968**	0.11682	0.04510	0.09217
Thailand	SET	0.04756	0.07129	0.09414	0.14423	0.10284	**0.03509**
Turkey	BIST 100	0.11487	**0.02527**	0.04366	0.12660	0.05167	0.06940
Un Arab Em	DFM	0.06865	**0.02001**	0.04115	0.05454	0.04120	0.04817
Un Arab Em	Abu Dhabi	0.05490	0.06752	0.08590	0.15254	0.09535	**0.03726**
Argentina	MERVAL	0.14251	0.05912	0.04451	0.10399	**0.03410**	0.11055
Bahrain	All Share	0.08982	0.06675	0.08907	0.17875	0.09682	**0.05574**
Bulgaria	SOFIX	0.07649	0.10287	0.13172	0.25261	0.14189	**0.05486**
Croatia	CROBEX	0.11380	0.08174	0.10491	0.21971	0.12858	**0.04664**
Cyprus	CYMAIN	**0.06279**	0.10045	0.11321	0.22277	0.08267	0.08481
Estonia	OMXT	**0.03454**	0.09360	0.11036	0.14353	0.11848	0.06373
Kazakhstan	KASE Index	0.05717	**0.05037**	0.06538	0.07266	0.06706	0.06322
Kuwait	Kuwait 15	0.06202	0.04967	0.05902	0.07620	0.06625	**0.03667**
Latvia	OMXR	0.13276	0.07482	0.08775	0.17393	0.09411	**0.05089**
Lithuania	OMXV	**0.03767**	0.06633	0.07433	0.11434	0.08233	0.05039
Mauritius	SEMDEX	0.13017	0.05249	**0.04559**	0.13975	0.13573	0.04616
Morocco	MASI	0.08709	0.10004	0.11924	0.23512	0.12157	**0.07945**
Namibia	NSX Overall	0.14064	0.07491	**0.06149**	0.10085	0.11621	0.12011
Oman	MSM 30	0.12297	0.09780	0.09504	**0.07410**	0.09367	0.10721
Pakistan	KSE 100	0.09646	**0.03762**	0.06107	0.15968	0.07114	0.04344
Romania	BET 10	0.09952	0.06792	0.10493	0.22698	0.11857	**0.02325**
Serbia	BELEX	**0.06278**	0.15538	0.17457	0.20660	0.18165	0.11460
Sri Lanka	CSE All-Share	0.10140	**0.03533**	0.07158	0.15814	0.10469	0.08021
Tunesia	Tunindex	**0.03536**	0.05849	0.06954	0.08682	0.07388	0.05262
Venezuela	IBC	0.15442	0.12768	0.12504	0.22650	0.50928	**0.11604**
Vietnam	HNX 30	**0.02450**	0.04152	0.07187	0.10249	0.51170	0.03226
Zambia	All Share	**0.28998**	0.30074	0.30359	0.30358	0.30280	0.29862

Table 4.15: KS distance between the empirical distribution for hourly log-returns and the downward convoluted fitted distribution for daily log-returns.

Country	Index	N	St	NIG	VΓ	Meix	Stable
Australia	ASX 200	66.91	12.28	5.59	11.17	**3.24**	42.46
Australia	All Ordinaries	71.90	12.41	5.33	15.21	**3.19**	43.80
Austria	ATX	38.36	9.68	9.12	**5.83**	7.66	31.34
Belgium	BEL 20	33.99	**3.80**	14.34	92.24	23.68	19.81
Canada	TSX 60	38.55	**5.73**	17.33	53.17	21.29	28.75
Canada	TSX Composite	47.67	**6.61**	15.66	42.14	18.25	34.40
EuroStoxx	EuroStoxx 50	30.43	**3.33**	11.21	68.29	19.77	16.43
Finland	OMXH25	59.72	12.53	**6.41**	8.38	18.27	55.79
France	CAC 40	33.56	16.02	34.58	140.94	46.24	**5.93**
Germany	DAX	49.43	55.48	101.86	407.61	88.59	**24.64**
Hong Kong	Hang Seng	74.78	19.49	**17.08**	21.17	41.66	58.34
Ireland	ISEQ Overall	51.09	**2.92**	10.61	16.21	10.62	31.37
Israel	TA 35	44.69	**1.99**	13.29	117.27	10.92	23.74
Italy	FTSE MIB	38.88	18.95	46.55	225.57	61.79	**5.03**
Japan	Topix	123.27	4.04	**1.22**	93.23	2.44	32.82
Luxembourg	LuxX Index	81.85	10.67	**8.89**	48.55	37.28	51.40
Netherlands	AEX	33.81	1.06	**0.81**	15.53	2.02	22.42
New Zealand	NZX 50 Index	86.81	**4.88**	22.68	113.83	31.61	8.79
Norway	OBX Index	47.22	**28.79**	54.44	58.08	781.13	38.94
Portugal	PSI 20	44.51	**9.37**	22.39	83.35	29.82	11.41
Singapore	STI Index	57.86	30.06	33.68	**29.29**	39.06	57.86
South Korea	KOSPI	67.61	**0.31**	4.97	80.74	9.00	10.37
Spain	IBEX 35	24.70	30.54	60.71	206.78	80.43	**7.63**
Sweden	OMXS30	36.71	**7.40**	10.19	10.36	9.78	28.92
Switzerland	SMI	42.78	**2.55**	15.53	189.24	18.98	21.72
UK	FTSE 100	30.44	14.78	33.08	107.26	43.11	**5.61**
USA	DowJones 30	67.54	**7.72**	15.36	97.40	20.50	9.46
USA	S&P 500	57.65	**18.39**	40.27	166.40	48.34	21.27
USA	Nasdaq	74.18	14.33	33.23	243.31	163.14	**7.55**
Brazil	Bovespa	48.93	17.01	37.38	167.93	50.04	**6.87**
Chile	IPSA	30.60	**0.84**	3.53	26.24	6.34	7.62
China	CSI 300	39.66	17.47	16.30	17.59	**15.80**	28.32
China	SSE	39.84	**14.38**	15.52	47.91	16.86	24.80
Colombia	IGBC	24.01	12.53	25.93	120.81	35.81	**4.32**
Czech Republic	PX	16.69	10.44	26.81	79.52	35.67	**6.41**
Egypt	EGX 30	85.35	25.53	15.64	18.16	**13.94**	39.08
Greece	Athex	33.34	16.87	45.05	182.18	17.19	**1.96**
Hungary	Budapest SE	49.08	**4.39**	19.73	99.45	28.86	12.30
India	Nifty 50	45.18	**0.50**	3.57	60.45	6.45	16.98
India	BSE Sensex	40.68	**1.33**	3.11	71.64	6.23	22.20
Indonesia	IDX Composite	79.92	**5.36**	13.26	86.34	18.53	6.60
Malaysia	KLCI	46.74	**1.52**	2.03	18.97	25.06	12.65
Mexico	IPC	30.50	17.25	33.94	113.65	43.05	**3.89**
Peru	Lima General	71.79	22.64	13.16	**4.27**	29.15	68.47
Philippines	PSEi	52.65	**8.31**	12.20	62.16	30.46	23.35
Poland	WIG	45.89	**3.20**	11.73	18.13	11.06	25.88
Qatar	QE 20 Index	36.19	4.58	14.44	53.63	19.16	**1.34**
Russia	MICEX	18.59	**0.52**	0.56	6.87	0.81	16.74
Russia	RTSI	16.70	47.94	79.00	197.47	94.18	**9.24**
Saudi Arabia	TASI	49.96	1.97	**1.71**	12.93	1.98	12.80
South Africa	JSE	33.77	4.84	4.69	5.37	**3.96**	28.97
Taiwan	TWII	43.83	3.98	3.48	17.95	**3.03**	21.14
Thailand	SET	10.72	24.56	37.70	84.75	44.55	**8.34**
Turkey	BIST 100	70.92	**1.97**	6.96	71.90	11.76	16.45
Un Arab Em	DFM	9.04	**0.56**	2.05	3.60	2.19	3.28
Un Arab Em	Abu Dhabi	7.15	12.27	21.56	51.17	26.12	**4.59**
Argentina	MERVAL	89.23	12.24	5.76	22.18	**3.56**	42.78
Bahrain	All Share	15.26	12.30	18.32	49.00	20.90	**8.61**
Bulgaria	SOFIX	27.70	58.80	94.90	275.01	109.60	**19.65**
Croatia	CROBEX	65.56	35.58	61.49	222.76	148.18	**14.22**
Cyprus	CYMAIN	56.15	73.96	98.53	219.48	448.04	**55.23**
Estonia	OMXT	**12.84**	48.90	64.88	101.13	72.59	25.23
Kazakhstan	KASE Index	12.31	**9.15**	13.25	14.00	13.37	14.40
Kuwait	Kuwait 15	5.05	5.84	7.19	13.33	8.52	**3.62**
Latvia	OMXR	56.68	20.09	30.14	93.35	35.67	**13.12**
Lithuania	OMXV	59.00	20.15	27.67	43.93	30.99	**13.67**
Mauritius	SEMDEX	36.95	3.19	**2.27**	30.44	41.28	3.06
Morocco	MASI	**34.38**	54.20	78.56	228.26	69.03	35.46
Namibia	NSX Overall	94.66	21.63	**14.09**	39.92	39.30	53.19
Oman	MSM 30	33.35	13.69	10.85	**6.11**	9.53	24.09
Pakistan	KSE 100	41.01	4.63	12.33	95.22	17.43	**4.01**
Romania	BET 10	63.15	25.25	58.90	269.00	75.92	**2.52**
Serbia	BELEX	**32.06**	105.45	125.42	172.83	133.05	79.76
Sri Lanka	CSE All-Share	38.78	**4.24**	9.45	38.53	29.93	19.59
Tunesia	Tunindex	**7.87**	12.34	20.42	25.72	25.97	13.47
Venezuela	IBC	41.27	25.99	**25.52**	77.81	344.07	34.76
Vietnam	HNX 30	**4.60**	7.00	17.29	31.05	488.96	6.79
Zambia	All Share	1350.28	**288.20**	335.58	378.14	347.45	292.81

Table 4.16: AD distance between the empirical distribution for hourly log-returns and the downward convoluted fitted distribution for daily log-returns.

Country	Index	N	St	NIG	VΓ	Meix	Stable
Australia	ASX 200	-16516	-17297	-17347	-17123	**-17363**	-16965
Australia	All Ordinaries	-16854	-17682	-17733	-17448	**-17746**	-17346
Austria	ATX	-20370	-20827	-20821	**-20830**	-20830	-20513
Belgium	BEL 20	-21611	**-22341**	-22251	-21334	-22172	-21874
Canada	TSX 60	-19211	**-19856**	-19793	-19462	-19788	-19295
Canada	TSX Composite	-19684	**-20334**	-20293	-20049	-20294	-19773
EuroStoxx	EuroStoxx 50	-22022	**-22760**	-22699	-22043	-22489	-22276
Finland	OMXH25	-21448	-22183	**-22223**	-22070	-22112	-21611
France	CAC 40	-21055	**-21870**	-21731	-20546	-21641	-21831
Germany	DAX	-21120	-21622	-21296	-18465	-16665	**-21794**
Hong Kong	Hang Seng	-17613	-18402	**-18440**	-18335	-18195	-17940
Ireland	ISEQ Overall	-22492	**-23111**	-23044	-22942	-23034	-22755
Israel	TA 35	-20809	**-21533**	-21442	-20243	-21415	-21268
Italy	FTSE MIB	-19914	-20344	-20137	-18319	-20020	**-20375**
Japan	Topix	-15070	-16608	**-16638**	-15386	-16629	-16280
Luxembourg	LuxX Index	-18735	-19909	**-19977**	-19452	-19623	-19383
Netherlands	AEX	-21536	-22391	**-22391**	-22195	-22381	-21913
New Zealand	NZX 50 Index	-20934	**-21962**	-21799	-20615	-21712	-21961
Norway	OBX Index	-18490	**-18798**	-18174	-18104	27637	-18624
Portugal	PSI 20	-21187	**-21805**	-21695	-20930	-21627	-21736
Singapore	STI Index	-22028	**-22585**	-22525	-22560	-22443	-22013
South Korea	KOSPI	-16083	**-16926**	-16886	-15881	-16853	-16793
Spain	IBEX 35	-22697	-23235	-23004	-21486	-22847	**-23348**
Sweden	OMXS30	-21202	**-21800**	-21764	-21750	-21764	-21436
Switzerland	SMI	-21764	**-22395**	-22277	-20478	-22222	-22184
UK	FTSE 100	-21654	**-22228**	-22093	-21235	-22015	-22217
USA	DowJones 30	-20301	**-21143**	-21101	-20184	-21066	-21020
USA	S&P 500	-20081	**-20747**	-20621	-19396	-20568	-20616
USA	Nasdaq	-18625	**-19479**	-19355	-17347	-17383	-19444
Brazil	Bovespa	-16648	-17423	-17261	-15827	-17157	**-17431**
Chile	IPSA	-17941	**-20240**	-20174	-19806	-20126	-20182
China	CSI 300	-15595	-16092	-16140	**-16342**	-16169	-15859
China	SSE	-15827	-16402	-16435	-16262	**-16450**	-16176
Colombia	IGBC	-17471	**-17744**	-17636	-16584	-17558	-17739
Czech Republic	PX	-19309	**-19687**	-19559	-18955	-19486	-19659
Egypt	EGX 30	-9278	-10053	-10137	-9961	**-10156**	-9871
Greece	Athex	-16728	-16975	-16752	-15322	-16952	**-17069**
Hungary	Budapest SE	-21070	**-21508**	-21383	-20364	-21304	-21399
India	Nifty 50	-16056	**-16609**	-16572	-15798	-16540	-16447
India	BSE Sensex	-16153	**-16680**	-16654	-15769	-16622	-16466
Indonesia	IDX Composite	-16989	**-17997**	-17912	-16975	-17861	-17959
Malaysia	KLCI	-17609	**-18215**	-18205	-17912	-17977	-18090
Mexico	IPC	-16942	-17336	-17209	-16306	-17139	**-17349**
Peru	Lima General	-19568	-19995	-20060	**-20140**	-19952	-19605
Philippines	PSEi	-14759	-15346	**-15347**	-14843	-15129	-15136
Poland	WIG	-20895	**-21386**	-21321	-21211	-21323	-21054
Qatar	QE 20 Index	-10029	-10663	-10558	-10034	-10510	**-10689**
Russia	MICEX	-20378	**-20674**	-20666	-20568	-20663	-20459
Russia	RTSI	-18485	-18701	-18470	-17163	-18354	**-18903**
Saudi Arabia	TASI	-11066	**-11566**	-11566	-11340	-11560	-11444
South Africa	JSE	-20655	**-21114**	-21108	-21071	-21113	-20735
Taiwan	TWII	-11253	**-11726**	-11725	-11439	-11725	-11534
Thailand	SET	-16654	-16798	-16699	-16166	-16646	**-16849**
Turkey	BIST 100	-22658	**-23364**	-23308	-22412	-23260	-23226
Un Arab Em	DFM	-8429	**-8566**	-8546	-8525	-8544	-8439
Un Arab Em	Abu Dhabi	-10807	-10942	-10859	-10508	-10818	**-10981**
Argentina	MERVAL	-13771	-14643	-14687	-14294	**-14699**	-14351
Bahrain	All Share	-7893	**-8252**	-8203	-7807	-8181	-8248
Bulgaria	SOFIX	-16965	-17448	-17196	-15533	-17089	**-17631**
Croatia	CROBEX	-17988	-18907	-18705	-16960	-9725	**-19020**
Cyprus	CYMAIN	-10694	**-11902**	-11805	-10784	32467	-11764
Estonia	OMXT	-14823	-15048	-14940	-14576	-14885	**-15142**
Kazakhstan	KASE Index	-13804	**-14148**	-14092	-14088	-14094	-13883
Kuwait	Kuwait 15	-7999	**-8086**	-8076	-8019	-8068	-8069
Latvia	OMXR	-11649	**-12807**	-12747	-11994	-12707	-12759
Lithuania	OMXV	300166	-15645	-14734	-13952	-14366	**-15673**
Mauritius	SEMDEX	-10378	-10824	**-10836**	-10437	-10278	-10794
Morocco	MASI	-15528	-15848	-15682	-14207	-8954	**-15911**
Namibia	NSX Overall	-17920	-19671	**-19821**	-19579	-19411	-19142
Oman	MSM 30	-8863	-9051	-9073	**-9191**	-9088	-8944
Pakistan	KSE 100	-14235	**-14645**	-14577	-13668	-14532	-14607
Romania	BET 10	-23930	-24666	-24396	-22217	-24261	**-24789**
Serbia	BELEX	-11450	-11655	-11543	-11085	-11497	**-11707**
Sri Lanka	CSE All-Share	-15044	**-15275**	-15235	-14852	-15120	-15183
Tunesia	Tunindex	-11820	**-11915**	-11821	-11809	-11527	-11775
Venezuela	IBC	-4637	-5109	**-5140**	-4610	11619	-5026
Vietnam	HNX 30	-10862	**-10949**	-10857	-10770	17068	-10828
Zambia	All Share	20514	**-1041**	-955	-725	-920	-1006

Table 4.17: BIC for hourly log-returns using the downward convoluted fitted distribution for daily log-returns.

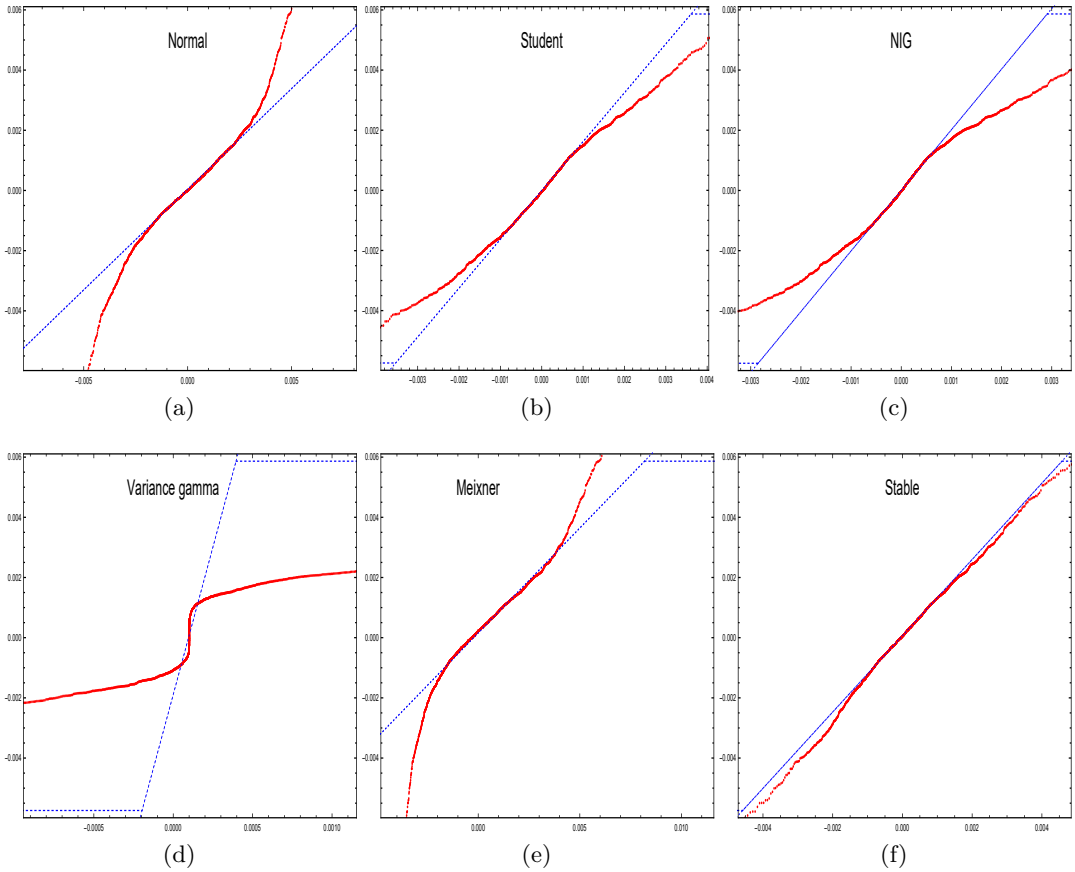

Figure 4.9: QQ-plots of empirical quantiles for hourly DAX returns versus downward convoluted model distribution fitted to daily returns.

models have comparable numbers of best fits. Comparing, for instance, the upward convolution ADs (Table 4.19) with the daily ML fit ADs (Table 4.12) we see that, with some exceptions, the former are not vastly higher than the latter. For example, for the Japanese Topix the direct daily fit has an AD of 0.231 and the upward convolution one of 0.297. This often implies an appropriate fit.

Figure 4.10 shows QQ-plots for the DAX example, comparing the upwardly convoluted distribution with the empirical distribution of daily returns. At first sight none of the distributions seems to be a good fit. Again, this is also due to the low sample size of daily returns in one year. It is useful to compare this figure with Figure 4.7, the direct fit to daily returns. This reveals that the Student t fit is more or less appropriate. The AD distance also favors the Student model.

Country	Index	N	St	NIG	VΓ	Meix	Stable
Australia	ASX 200	0.0471	0.0510	0.0466	0.0524	0.0442	**0.0382**
Australia	All Ordinaries	0.0498	0.0524	0.0477	0.0657	0.0456	**0.0387**
Austria	ATX	**0.0450**	0.0592	0.0520	0.0548	0.0509	0.0468
Belgium	BEL 20	0.0579	0.0515	0.0455	**0.0451**	0.0464	0.0507
Canada	TSX 60	0.0586	0.0548	0.0618	**0.0540**	0.0621	0.0842
Canada	TSX Composite	0.0501	**0.0408**	0.0458	0.0428	0.0467	0.0751
EuroStoxx	EuroStoxx 50	0.0716	**0.0441**	0.0528	0.0529	0.0545	0.0471
Finland	OMXH25	0.0394	0.0468	0.0384	0.0424	0.0357	**0.0305**
France	CAC 40	0.0828	**0.0509**	0.0596	0.0610	0.0612	0.0612
Germany	DAX	0.1111	**0.0752**	0.0872	0.0860	0.0898	0.0756
Hong Kong	Hang Seng	**0.0415**	0.0537	0.0510	0.0600	0.0498	0.0654
Ireland	ISEQ Overall	**0.0338**	0.0437	0.0426	0.0422	0.0416	0.0562
Israel	TA 35	0.0665	0.0648	0.0468	**0.0434**	0.0484	0.0691
Italy	FTSE MIB	0.0840	**0.0590**	0.0681	0.0694	0.0694	0.0637
Japan	Topix	0.0875	0.0462	**0.0294**	0.0540	0.0315	0.0466
Luxembourg	LuxX Index	0.0796	0.0542	0.0497	0.0495	**0.0491**	0.0935
Netherlands	AEX	0.0576	**0.0365**	0.0382	0.0378	0.0398	0.0514
New Zealand	NZX 50 Index	0.0667	**0.0428**	0.0570	0.0609	0.0558	0.0481
Norway	OBX Index	**0.0529**	0.0665	0.0671	0.0708	0.0655	0.0583
Portugal	PSI 20	0.0609	0.0518	0.0412	**0.0386**	0.0426	0.0485
Singapore	STI Index	**0.0441**	0.0547	0.0538	0.0538	0.0528	0.0512
South Korea	KOSPI	0.0629	**0.0349**	0.0423	0.0433	0.0441	0.0487
Spain	IBEX 35	0.0802	0.0715	0.0664	0.0661	0.0673	**0.0572**
Sweden	OMXS30	**0.0403**	0.0437	0.0424	0.0427	0.0424	0.0428
Switzerland	SMI	0.0575	0.0445	0.0415	**0.0413**	0.0431	0.0491
UK	FTSE 100	0.0755	**0.0553**	0.0576	0.0570	0.0593	0.0669
USA	DowJones 30	0.0743	0.0746	0.0519	0.0541	**0.0508**	0.0920
USA	S&P 500	0.1008	**0.0832**	0.0832	0.0852	0.0834	0.0983
USA	Nasdaq	0.0903	0.0712	**0.0617**	0.0722	0.0636	0.0753
Brazil	Bovespa	0.0886	**0.0543**	0.0602	0.0604	0.0618	0.0678
Chile	IPSA	0.1102	0.0388	0.0334	**0.0320**	0.0347	0.0366
China	CSI 300	0.0638	0.0641	0.0386	0.0904	**0.0325**	0.1253
China	SSE	0.0690	**0.0634**	0.0716	0.0765	0.0714	0.1282
Colombia	IGBC	0.0573	0.0525	0.0476	**0.0461**	0.0481	0.0514
Czech Republic	PX	0.0698	0.0863	0.0618	0.0606	0.0623	**0.0539**
Egypt	EGX 30	**0.0541**	0.1600	0.0911	0.1079	0.0813	0.1004
Greece	Athex	0.0796	0.0720	0.0726	0.0727	0.0733	**0.0701**
Hungary	Budapest SE	0.0555	0.0473	**0.0439**	0.0441	0.0445	0.0601
India	Nifty 50	0.0598	0.0456	0.0455	0.0471	0.0466	**0.0447**
India	BSE Sensex	0.0534	0.0546	0.0417	0.0427	**0.0405**	0.0425
Indonesia	IDX Composite	0.0725	0.0724	0.0351	**0.0269**	0.0321	0.0430
Malaysia	KLCI	0.0581	**0.0338**	0.0416	0.0432	0.0404	0.0522
Mexico	IPC	0.0779	**0.0502**	0.0579	0.0580	0.0592	0.0674
Peru	Lima General	0.0581	0.0739	0.0682	0.0650	0.0692	**0.0471**
Philippines	PSEi	**0.0566**	0.0936	0.0658	0.0797	0.0632	0.0714
Poland	WIG	0.0468	0.0415	0.0394	0.0420	0.0387	**0.0287**
Qatar	QE 20 Index	0.1078	0.0450	0.0567	0.0603	0.0600	**0.0420**
Russia	MICEX	0.0414	0.0408	0.0313	**0.0311**	0.0318	0.0396
Russia	RTSI	0.0817	0.0752	0.0649	**0.0647**	0.0659	0.0715
Saudi Arabia	TASI	0.0571	0.0558	0.0430	0.0430	**0.0425**	0.0433
South Africa	JSE	0.0347	0.0405	0.0304	0.0302	**0.0290**	0.0403
Taiwan	TWII	0.0485	0.0562	0.0469	0.0490	0.0441	**0.0435**
Thailand	SET	0.0781	**0.0638**	0.0647	0.0650	0.0656	0.0710
Turkey	BIST 100	**0.0259**	0.0406	0.0356	0.0344	0.0351	0.0526
Un Arab Em	DFM	0.0573	**0.0277**	0.0373	0.0377	0.0384	0.0402
Un Arab Em	Abu Dhabi	0.0705	0.0554	**0.0537**	0.0547	0.0546	0.0552
Argentina	MERVAL	0.0389	0.0624	0.0515	0.0563	0.0488	**0.0386**
Bahrain	All Share	0.1430	**0.0747**	0.0908	0.0992	0.0939	0.0829
Bulgaria	SOFIX	0.1061	0.0901	0.0803	0.0841	0.0827	**0.0751**
Croatia	CROBEX	0.1137	0.0608	0.0698	0.0721	0.0739	**0.0597**
Cyprus	CYMAIN	0.1613	0.1512	0.1449	0.1485	**0.1442**	0.1717
Estonia	OMXT	0.1217	0.1195	**0.1090**	0.1092	0.1093	0.1095
Kazakhstan	KASE Index	0.0742	0.1002	0.0709	**0.0677**	0.0700	0.0763
Kuwait	Kuwait 15	0.0737	0.0577	**0.0525**	0.0562	0.0533	0.0550
Latvia	OMXR	0.1759	**0.0936**	0.0996	0.1137	0.1043	0.0974
Lithuania	OMXV	0.4288	0.1178	0.2176	0.2356	0.2262	**0.1112**
Mauritius	SEMDEX	0.0788	0.0588	**0.0401**	0.0429	0.5012	0.0523
Morocco	MASI	0.1201	**0.0860**	0.0903	0.0956	0.0920	0.0914
Namibia	NSX Overall	0.0967	0.0587	0.0529	0.0766	**0.0499**	0.1429
Oman	MSM 30	**0.0465**	0.0582	0.0673	0.0711	0.0471	0.0591
Pakistan	KSE 100	0.0610	**0.0418**	0.0429	0.0456	0.0438	0.0470
Romania	BET 10	0.0650	0.0490	0.0469	0.0488	**0.0464**	0.0538
Serbia	BELEX	0.1548	0.1537	0.1464	0.1439	0.1536	**0.1433**
Sri Lanka	CSE All-Share	0.0817	**0.0784**	0.0887	0.0897	0.0887	0.0839
Tunesia	Tunindex	0.0924	**0.0798**	0.0841	0.0869	0.0848	0.0860
Venezuela	IBC	0.2114	0.1510	**0.0897**	0.1595	0.1056	0.1342
Vietnam	HNX 30	0.0797	0.0821	**0.0734**	0.0736	0.0737	0.0768
Zambia	All Share	0.3741	0.3451	0.3529	0.4811	0.3544	**0.3409**

Table 4.18: AD distance between the empirical distribution for daily log-returns and the upward convoluted fitted distribution for hourly log-returns.

Country	Index	N	St	NIG	VΓ	Meix	Stable
Australia	ASX 200	0.570	0.661	0.575	0.705	**0.496**	0.796
Australia	All Ordinaries	0.565	0.714	0.617	1.320	**0.528**	0.748
Austria	ATX	**0.455**	0.838	0.676	0.787	0.641	0.827
Belgium	BEL 20	1.435	0.619	0.510	**0.487**	0.566	1.059
Canada	TSX 60	1.798	1.436	1.186	**0.902**	1.099	4.008
Canada	TSX Composite	1.189	0.749	0.707	**0.603**	0.661	3.301
EuroStoxx	EuroStoxx 50	2.011	**0.765**	0.865	0.777	0.943	1.818
Finland	OMXH25	0.322	0.533	0.366	0.661	**0.314**	0.551
France	CAC 40	3.227	1.241	1.310	**1.177**	1.433	2.335
Germany	DAX	4.167	**2.097**	2.387	2.436	2.549	3.001
Hong Kong	Hang Seng	0.560	0.672	0.459	1.018	**0.448**	1.682
Ireland	ISEQ Overall	0.449	**0.447**	0.704	0.919	0.663	0.550
Israel	TA 35	1.404	0.923	**0.510**	0.611	0.573	1.448
Italy	FTSE MIB	1.686	**0.863**	0.871	0.989	0.930	1.573
Japan	Topix	3.593	0.846	**0.297**	1.169	0.324	1.411
Luxembourg	LuxX Index	1.953	1.114	0.805	**0.648**	0.708	5.034
Netherlands	AEX	1.737	0.540	0.619	**0.467**	0.685	1.720
New Zealand	NZX 50 Index	1.678	1.004	1.161	1.677	1.135	**0.581**
Norway	OBX Index	**0.805**	1.671	1.596	1.952	1.477	1.278
Portugal	PSI 20	1.401	1.007	**0.683**	0.716	0.713	0.922
Singapore	STI Index	**0.378**	0.681	0.566	0.754	0.496	1.074
South Korea	KOSPI	1.593	**0.333**	0.355	0.680	0.400	0.817
Spain	IBEX 35	2.272	1.638	1.040	**1.027**	1.096	1.182
Sweden	OMXS30	0.457	0.440	0.341	0.375	**0.324**	0.820
Switzerland	SMI	1.100	**0.468**	0.530	0.692	0.569	0.733
UK	FTSE 100	2.251	**0.999**	1.121	1.021	1.207	2.155
USA	DowJones 30	2.592	1.685	**0.778**	1.147	0.792	3.380
USA	S&P 500	3.481	2.053	1.771	1.978	**1.762**	4.222
USA	Nasdaq	3.524	**1.151**	1.325	1.948	1.438	2.661
Brazil	Bovespa	2.829	**0.687**	0.855	0.902	0.924	1.571
Chile	IPSA	6.950	0.366	0.318	**0.296**	0.382	0.482
China	CSI 300	1.692	2.304	1.019	2.855	**0.660**	9.969
China	SSE	2.289	2.112	1.280	1.514	**0.997**	9.001
Colombia	IGBC	1.325	0.919	0.746	**0.745**	0.777	1.615
Czech Republic	PX	1.362	1.904	0.846	**0.787**	0.867	1.133
Egypt	EGX 30	**1.241**	10.228	2.521	4.926	2.084	2.731
Greece	Athex	1.486	0.844	0.955	1.095	1.003	**0.810**
Hungary	Budapest SE	0.954	**0.632**	0.790	0.966	0.808	1.099
India	Nifty 50	0.874	0.733	0.608	0.889	0.607	**0.522**
India	BSE Sensex	0.909	0.951	**0.589**	0.826	0.591	0.724
Indonesia	IDX Composite	1.892	1.865	**0.335**	0.599	0.364	0.620
Malaysia	KLCI	1.068	**0.491**	0.551	0.878	0.565	0.997
Mexico	IPC	2.370	1.131	1.131	**1.093**	1.190	2.236
Peru	Lima General	2.311	1.925	2.243	2.215	2.500	**0.736**
Philippines	PSEi	1.018	2.244	0.698	1.208	**0.630**	3.198
Poland	WIG	0.819	0.689	0.738	1.035	0.759	**0.433**
Qatar	QE 20 Index	3.657	0.500	0.532	0.680	0.602	**0.391**
Russia	MICEX	0.367	0.666	**0.264**	0.286	0.269	0.625
Russia	RTSI	2.972	2.287	1.698	**1.679**	1.765	2.367
Saudi Arabia	TASI	0.992	0.684	0.497	0.617	**0.485**	0.541
South Africa	JSE	0.197	0.387	0.207	0.279	**0.192**	0.790
Taiwan	TWII	0.748	0.878	0.595	0.809	**0.524**	0.678
Thailand	SET	2.640	1.842	1.675	**1.669**	1.728	2.511
Turkey	BIST 100	0.565	**0.397**	0.552	0.806	0.622	1.043
Un Arab Em	DFM	1.039	**0.465**	0.500	0.585	0.523	0.500
Un Arab Em	Abu Dhabi	2.133	1.013	1.004	1.063	1.054	**0.957**
Argentina	MERVAL	**0.645**	1.520	1.100	1.889	1.014	0.729
Bahrain	All Share	8.034	**2.416**	2.725	3.299	2.948	2.698
Bulgaria	SOFIX	7.162	4.055	3.679	**3.566**	3.892	4.301
Croatia	CROBEX	5.966	**1.692**	1.907	2.235	2.189	1.906
Cyprus	CYMAIN	14.626	12.544	12.029	12.146	**11.889**	16.539
Estonia	OMXT	6.384	5.361	**4.555**	4.618	4.610	4.634
Kazakhstan	KASE Index	2.777	3.624	2.108	**1.986**	2.067	3.547
Kuwait	Kuwait 15	2.162	1.241	**1.076**	1.174	1.084	1.352
Latvia	OMXR	13.809	3.986	**3.743**	4.364	4.054	5.638
Lithuania	OMXV	81.970	4.930	23.646	26.310	25.707	**4.452**
Mauritius	SEMDEX	3.730	1.188	**0.410**	0.846	96.189	1.278
Morocco	MASI	6.153	**3.191**	3.237	3.560	3.357	4.441
Namibia	NSX Overall	5.235	2.327	1.822	2.491	**1.334**	13.580
Oman	MSM 30	1.155	**1.013**	1.891	1.481	1.094	1.046
Pakistan	KSE 100	1.458	**0.497**	0.616	0.812	0.675	0.861
Romania	BET 10	1.930	**0.629**	0.676	0.687	0.769	1.123
Serbia	BELEX	13.341	11.556	**11.340**	11.437	13.727	13.025
Sri Lanka	CSE All-Share	4.159	**2.610**	3.963	4.324	4.038	2.633
Tunesia	Tunindex	3.744	3.683	**3.085**	3.240	3.110	3.646
Venezuela	IBC	16.122	6.252	**4.210**	9.704	5.025	9.791
Vietnam	HNX 30	2.636	3.275	2.245	**2.244**	2.257	2.738
Zambia	All Share	46.539	40.667	41.779	53.236	41.952	**40.005**

Table 4.19: AD distance between the empirical distribution for daily log-returns and the upward convoluted fitted distribution for hourly log-returns.

Country	Index	N	St	NIG	VΓ	Meix	Stable
Australia	ASX 200	**-1811**	-1811	-1808	-1806	-1808	-1788
Australia	All Ordinaries	-1835	**-1837**	-1833	-1828	-1834	-1814
Austria	ATX	**-1695**	-1689	-1684	-1683	-1684	-1669
Belgium	BEL 20	-1862	**-1867**	-1861	-1859	-1860	-1850
Canada	TSX 60	**-1923**	-1915	-1915	-1917	-1916	-1875
Canada	TSX Composite	**-1940**	-1936	-1934	-1936	-1935	-1895
EuroStoxx	EuroStoxx 50	-1928	**-1929**	-1924	-1925	-1924	-1907
Finland	OMXH25	**-1812**	-1806	-1802	-1799	-1802	-1785
France	CAC 40	-1823	**-1841**	-1833	-1830	-1832	-1822
Germany	DAX	-1807	**-1823**	-1816	-1810	-1814	-1805
Hong Kong	Hang Seng	**-1728**	-1717	-1718	-1719	-1720	-1686
Ireland	ISEQ Overall	**-1749**	-1749	-1741	-1738	-1741	-1734
Israel	TA 35	**-1857**	-1856	-1853	-1851	-1853	-1836
Italy	FTSE MIB	-1635	**-1648**	-1640	-1634	-1639	-1633
Japan	Topix	-1659	**-1720**	-1719	-1692	-1717	-1699
Luxembourg	LuxX Index	**-1589**	-1583	-1583	-1587	-1586	-1534
Netherlands	AEX	-1896	**-1897**	-1892	-1894	-1892	-1872
New Zealand	NZX 50 Index	-1911	-1952	-1938	-1917	-1934	**-1955**
Norway	OBX Index	**-1741**	-1730	-1726	-1725	-1727	-1710
Portugal	PSI 20	-1781	**-1789**	-1781	-1777	-1780	-1777
Singapore	STI Index	**-1903**	-1893	-1890	-1890	-1891	-1866
South Korea	KOSPI	-1801	**-1821**	-1815	-1803	-1814	-1803
Spain	IBEX 35	-1712	**-1715**	-1711	-1709	-1710	-1708
Sweden	OMXS30	**-1825**	-1819	-1815	-1815	-1815	-1797
Switzerland	SMI	-1850	**-1851**	-1845	-1842	-1845	-1836
UK	FTSE 100	-1884	**-1894**	-1887	-1884	-1886	-1876
USA	DowJones 30	-2001	**-2028**	-2024	-2013	-2022	-1999
USA	S&P 500	-1976	**-2004**	-1999	-1990	-1997	-1977
USA	Nasdaq	-1777	**-1814**	-1807	-1791	-1804	-1792
Brazil	Bovespa	-1439	**-1477**	-1465	-1454	-1462	-1467
Chile	IPSA	-1769	**-1809**	-1803	-1802	-1802	-1797
China	CSI 300	**-1797**	-1785	-1789	-1785	-1794	-1697
China	SSE	**-1832**	-1825	-1829	-1829	-1832	-1750
Colombia	IGBC	-1767	**-1776**	-1769	-1765	-1767	-1761
Czech Republic	PX	**-1919**	-1918	-1913	-1912	-1913	-1905
Egypt	EGX 30	-1441	-1439	-1449	-1437	**-1451**	-1431
Greece	Athex	-1526	**-1538**	-1528	-1523	-1527	-1529
Hungary	Budapest SE	-1721	**-1738**	-1727	-1720	-1725	-1728
India	Nifty 50	-1775	**-1782**	-1776	-1769	-1776	-1769
India	BSE Sensex	-1804	**-1807**	-1801	-1796	-1801	-1790
Indonesia	IDX Composite	-1706	**-1745**	-1734	-1714	-1730	-1739
Malaysia	KLCI	-2038	**-2041**	-2036	-2031	-2036	-2023
Mexico	IPC	-1746	**-1775**	-1765	-1758	-1763	-1761
Peru	Lima General	-1762	**-1772**	-1764	-1761	-1761	-1756
Philippines	PSEi	**-1615**	-1613	-1614	-1614	-1615	-1579
Poland	WIG	**-1725**	-1723	-1718	-1715	-1718	-1708
Qatar	QE 20 Index	-1602	**-1658**	-1647	-1633	-1643	-1656
Russia	MICEX	**-1698**	-1691	-1689	-1688	-1689	-1678
Russia	RTSI	-1562	**-1575**	-1569	-1566	-1568	-1568
Saudi Arabia	TASI	-1658	**-1694**	-1688	-1679	-1686	-1680
South Africa	JSE	**-1746**	-1740	-1736	-1735	-1736	-1721
Taiwan	TWII	-1820	**-1834**	-1829	-1821	-1829	-1817
Thailand	SET	-1949	**-1956**	-1950	-1948	-1949	-1943
Turkey	BIST 100	-1621	**-1636**	-1626	-1618	-1623	-1623
Un Arab Em	DFM	-1748	**-1750**	-1747	-1745	-1746	-1741
Un Arab Em	Abu Dhabi	-1769	**-1780**	-1772	-1769	-1771	-1773
Argentina	MERVAL	-1405	**-1414**	-1411	-1397	-1411	-1397
Bahrain	All Share	-1903	**-1954**	-1947	-1937	-1945	-1946
Bulgaria	SOFIX	-1740	**-1784**	-1773	-1765	-1769	-1777
Croatia	CROBEX	-1748	**-1795**	-1783	-1764	-1779	-1790
Cyprus	CYMAIN	-1390	-1398	-1397	-1398	**-1399**	-1355
Estonia	OMXT	-1988	**-1990**	-1990	-1989	-1989	-1987
Kazakhstan	KASE Index	**-1640**	-1632	-1630	-1632	-1631	-1611
Kuwait	Kuwait 15	-1697	**-1701**	-1697	-1696	-1697	-1692
Latvia	OMXR	-1677	**-1795**	-1789	-1769	-1784	-1772
Lithuania	OMXV	-996	**-2047**	-1879	-1878	-1859	-2042
Mauritius	SEMDEX	-2230	-2263	**-2264**	-2255	5488	-2249
Morocco	MASI	-1729	**-1761**	-1754	-1744	-1752	-1747
Namibia	NSX Overall	-1570	-1571	-1573	**-1580**	-1580	-1465
Oman	MSM 30	-1956	**-1963**	-1958	-1959	-1948	-1942
Pakistan	KSE 100	-1533	**-1556**	-1547	-1539	-1544	-1544
Romania	BET 10	-1797	**-1831**	-1818	-1806	-1814	-1826
Serbia	BELEX	-1829	**-1840**	-1835	-1834	-1816	-1820
Sri Lanka	CSE All-Share	-1955	**-1979**	-1963	-1957	-1961	-1972
Tunesia	Tunindex	**-2179**	-2169	-2171	-2170	-2171	-2163
Venezuela	IBC	-892	-948	-968	-941	**-970**	-927
Vietnam	HNX 30	**-1780**	-1765	-1770	-1771	-1770	-1762
Zambia	All Share	-651	-762	-737	-694	-734	**-768**

Table 4.20: BIC for daily log-returns using the upward convoluted fitted distribution for hourly log-returns.

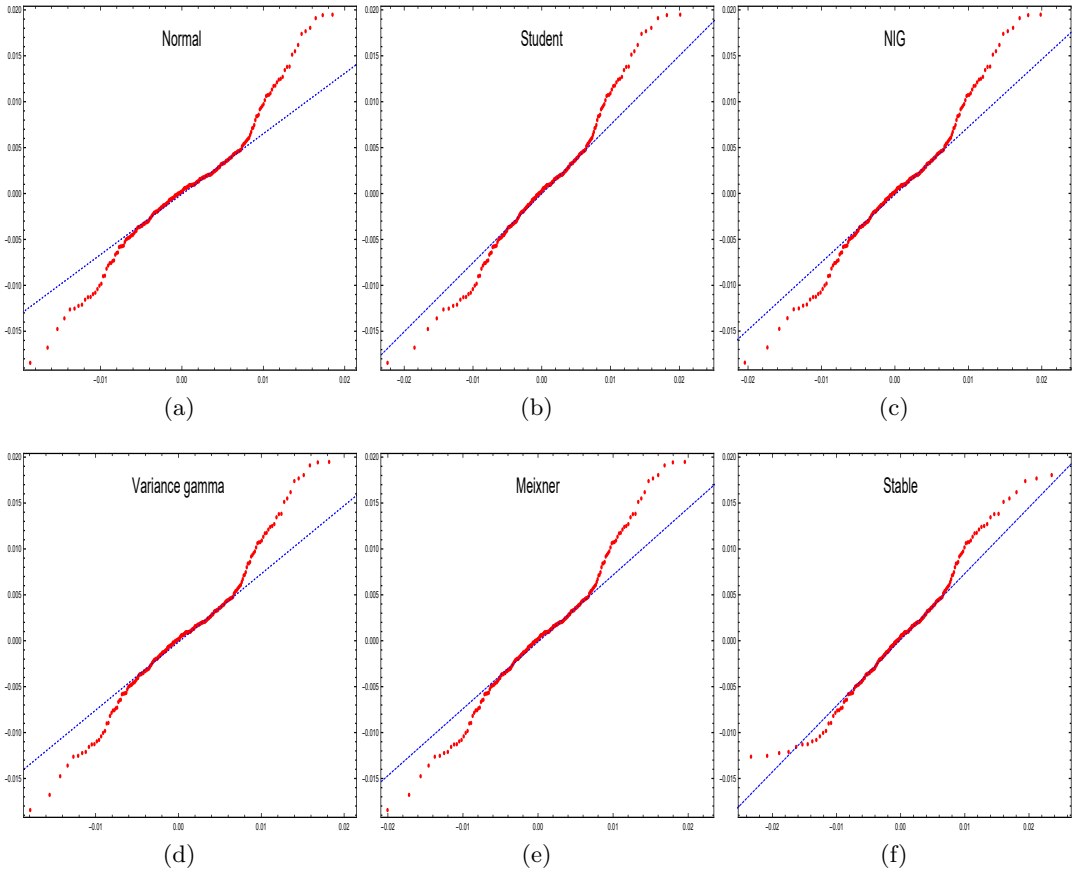

Figure 4.10: QQ-plots of empirical quantiles for daily DAX returns versus upward convoluted model distribution fitted to hourly returns.

Table 4.10 reports the number of minimal KS, AD and BIC statistics among the models considered for the downward and upward convolutions. The Student-Lévy process and the stable process are ranked first and second in terms of downward time consistency. The Student-Lévy upward convolution is most often well suited to the daily data.

4.6 Conclusion

This chapter provides a comprehensive comparison of Lévy models for equity index returns, including both traditional and exotic markets. We analyze three samples, namely daily returns over an almost twenty-year horizon, daily returns for the final

	N	St	NIG	VΓ	Meix	Stable
KS – downward	7	32	8	4	5	22
AD – downward	5	29	9	4	7	24
BIC – downward	0	43	9	4	5	17
KS – upward	10	22	9	11	9	17
AD – upward	5	20	14	16	14	9
BIC – upward	22	49	1	1	3	2

Table 4.21: Number of lowest statistics for downward and upward time consistency per model.

year, and hourly returns for this same last year. We find that the GH distribution yields a very good and flexible fit for the long period. However, it may lead to overfitting. Another drawback is that the GH distribution is not closed under convolution, making it hardly accessible for hourly data. Other models, such as the NIG and the variance gamma models, which also fit very well, overcome this issue. For the last year, there is no unique most appropriate model anymore. This is also due to the small sample size. However, in a long sample period the parameters may change over time. This could be modeled using stochastic volatility approaches (in fact, all parameters could be modeled stochastically). We here restrict ourselves to the basic Lévy models. More involved models may fit better to empirical data but are less useful for the purposes of comparison.

We investigate hourly intraday returns for the assets. We find that the Student and the stable models often fit these well because of their heavy tails. As a second contribution we also analyze whether daily and intraday returns fit to the same underlying Lévy model. We here distinguish between downward and upward time consistency. Downward consistency is more difficult to identify as hourly data has to fit to the downwardly convoluted model when fitted to daily data. The Student-Lévy process most frequently has the lowest downward time consistency distances. On the other hand, the variance gamma and the NIG processes are less useful in this regard. Moreover, in contrast to the best fit for daily returns (Section 4.4), where the second best choice is little worse, some models, e.g., the variance gamma model for the DAX, fail to provide any time consistent fit. This makes clear that a well-fitting model for daily data may be a very poor fit for hourly data. Upward time consistency is less problematic. Models for hourly data may be carried over to daily data.

We use three different criteria. The KS distance and the AD distance often prefer the same model. The BIC tends to favor the Student model with its three parameters. Unfortunately, we could not identify a pattern as to which model is the most useful

for a given index. Developed, emerging and frontier markets can all be modeled well by the same class of distributions.

Future research may study models not closed under convolution for hourly data, as soon as ML estimation becomes feasible. Additionally, a higher frequency may be considered provided data is available. Further extensions of models could include, e.g., tempered versions (Rachev et al. 2011).

4.A Additional return fits

We perform some additional comparisons as to which model in Chapter 4 fits best to daily log-returns. Like Corlu et al. (2016), we split the whole sampling period into several subperiods to decide which model yields the best fit in each subperiod. Table 4.22 reports the number of minimal KS, AD and BIC for each model. Note that for the early periods some indices were not available on Thomson Reuters Eikon and have to be excluded. At the macroscopic level we do not see tremendous differences for different periods. The temporal position apparently is not as important as the length of the period. If we compare Table 4.22 with Table 4.7 on page 121, we see, e.g., that the GH model is favored more often for the full sampling period while less often for the one year sample.

Subperiod	Criterion	N	St	SSt	NIG	VΓ	Hyp	GH	Meix	Stable
1997-2001	KS	0	7	5	12	10	10	9	3	7
	AD	0	6	10	2	8	3	25	3	6
	BIC	0	46	1	5	5	1	0	3	2
2002-2005	KS	0	4	8	9	10	5	19	11	7
	AD	0	3	5	10	8	6	28	6	7
	BIC	0	34	3	9	9	3	2	10	3
2006-2009	KS	0	4	7	16	4	6	22	14	4
	AD	0	1	5	11	2	3	39	10	6
	BIC	0	31	0	19	6	4	1	15	0
2010-2013	KS	0	7	6	18	7	10	18	9	3
	AD	0	1	4	14	11	9	25	9	5
	BIC	0	41	3	2	13	3	0	14	2
2014-2017	KS	0	3	5	12	7	12	17	14	8
	AD	0	7	8	13	9	6	26	5	4
	BIC	0	47	2	9	7	6	1	6	0

Table 4.22: Number of lowest statistics for each subperiod per model.

5 Conclusion

In this thesis we developed simulation and estimation techniques for the Student-Lévy process, both of which are more theoretical and largely of computational interest. Chapter 4, on the other hand, discusses an application and provides evidence that the Student-Lévy process can be a useful tool in finance.

In future, we will continue to investigate in both the theoretical and empirical directions. Since the Student-Lévy process is part of the generalized hyperbolic Lévy process family, the next step will be to further examine local asymptotic normality in this class of Lévy processes. First of all, a full parameter LAN theorem, including the parameter ν for the Student-Lévy process, is of interest. This may, as pointed out in Chapter 3, not be easy to achieve as the likelihood function of the inverse gamma subordinator has no closed form. However, the methods of the proofs in Chapter 3 should prove useful for, for example, the hyperbolic Lévy process.

From the empirical point of view, it is interesting to investigate which Lévy model is most useful (and in which cases) for option pricing and the impact of the availability of high-frequency data. This is of particular interest for path-dependent options. Note that the moment-generating function of the Student-Lévy process is infinite, which makes a direct option price formula unavailable. Truncation, capping or tempering, as in Cassidy et al. (2010), may be used to derive an option price formula for a modified Student-Lévy process. Monte Carlo option pricing (Hilber et al. 2009) is an alternative.

This thesis was based on Monte Carlo methods. Of course there have been rapid and wide-reaching developments in this field, which may help to improve the approaches used in this thesis. (Randomized) Quasi-Monte Carlo methods are the next step.

Bibliography

Aas, K. & Haff, I. H. (2006), 'The Generalized Hyperbolic Skew Student's t-distribution', *Journal of Financial Econometrics* **4**(2), 275–309.
URL: *https://academic.oup.com/jfec/article/4/2/275/788320*

Aït-Sahalia, Y. & Jacod, J. (2008), 'Fisher's Information for Discretely Sampled Lévy Processes', *Econometrica* **76**(4), 727–761.
URL: *https://onlinelibrary.wiley.com/doi/full/10.1111/j.1468-0262.2008.00858.x*

Anderson, T. W. & Darling, D. A. (1954), 'A Test of Goodness of Fit', *Journal of the American Statistical Association* **49**(268), 765–769.
URL: *https://www.tandfonline.com/doi/abs/10.1080/01621459.1954.10501232*

Aparicio, F. M. & Estrada, J. (2001), 'Empirical distributions of stock returns: European securities markets, 1990-95', *The European Journal of Finance* **7**(1), 1–21.
URL: *https://www.tandfonline.com/doi/abs/10.1080/13518470121786*

Asmussen, S. & Rosiński, J. (2001), 'Approximations of small jumps of Lévy processes with a view towards simulation', *Journal of Applied Probability* **38**(2), 482–493.
URL: *http://dx.doi.org/10.1239/jap/996986757*

Azzalini, A. & Capitanio, A. (2003), 'Distributions generated by perturbation of symmetry with emphasis on a multivariate skew t-distribution', *Journal of the Royal Statistical Society: Series B (Statistical Methodology)* **65**(2), 367–389.
URL: *https://rss.onlinelibrary.wiley.com/doi/full/10.1111/1467-9868.00391*

Bachelier, L. (1900), Théorie de la spéculation, PhD thesis, Annales Scientifiques de l'École Normale Supérieure.
URL: *http://archive.numdam.org/article/ASENS_1900_3_17___21_0.pdf*

Barndorff-Nielsen, O. E. (1977), 'Exponentially decreasing distributions for the logarithm of particle size', *Proceedings of the Royal Society of London A: Mathematical, Physical and Engineering Sciences* **353**(1674), 401–419.
URL: *http://rspa.royalsocietypublishing.org/content/353/1674/401*

Barndorff-Nielsen, O. E. (1997), 'Normal inverse gaussian distributions and stochastic volatility modelling', *Scandinavian Journal of Statistics* **24**(1), 1–13.
URL: *https://onlinelibrary.wiley.com/doi/abs/10.1111/1467-9469.00045*

Barndorff-Nielsen, O. E. & Shephard, N. (2001), 'Non-Gaussian Ornstein–Uhlenbeck-based models and some of their uses in financial economics', *Journal of the Royal Statistical Society: Series B (Statistical Methodology)* **63**(2), 167–241.
URL: *https://rss.onlinelibrary.wiley.com/doi/abs/10.1111/1467-9868.00282*

Barndorff-Nielsen, O. & Halgreen, C. (1977), 'Infinite Divisibility of the Hyperbolic and generalized Inverse Gaussian Distributions', *Zeitschrift für Wahrscheinlichkeitstheorie und Verwandte Gebiete* **38**(4), 309–311.
URL: *http://dx.doi.org/10.1007/BF00533162*

Barth, A. & Stein, A. (2016), 'Approximation and simulation of infinite-dimensional Lévy processes', *Stochastics and Partial Differential Equations: Analysis and Computations* pp. 1–49.
URL: *https://link.springer.com/article/10.1007/s40072-017-0109-2*

Berg, C. & Vignat, C. (2008), 'On some results of Cufaro Petroni about Student t-processes', *Journal of Physics A: Mathematical and Theoretical* **41**(26), 265004.
URL: *http://stacks.iop.org/1751-8121/41/i=26/a=265004*

Black, F. & Scholes, M. (1973), 'The Pricing of Options and Corporate Liabilities', *Journal of Political Economy* **81**(3), 637–654.
URL: *https://www.journals.uchicago.edu/doi/abs/10.1086/260062*

Blattberg, R. C. & Gonedes, N. J. (1974), 'A Comparison of the Stable and Student Distributions as Statistical Models for Stock Prices', *The Journal of Business* **47**(2), 244–280.
URL: *https://www.worldscientific.com/doi/abs/10.1142/9789814287067_0003*

Bondesson, L. (1982), 'On simulation from infinitely divisible distributions', *Advances in Applied Probability* **14**(4), 855–869.
URL: *https://www.cambridge.org/core/article/on-simulation-from-infinitely-divisible-distributions/5C994F0918C55A4103087A580083FFD6*

Bouchaud, J.-P. & Potters, M. (2003), *Theory of financial risk and derivative pricing: from statistical physics to risk management*, Cambridge University Press, Cambridge.
URL: *https://books.google.de/books?id=neT6jVyMtlIC*

Breymann, W. & Lüthi, D. (2013), 'ghyp: A package on generalized hyperbolic distributions', *Manual for R Package ghyp* .
URL: *https://pdfs.semanticscholar.org/6081/ee4e27094b6547e1d2c70e941ab9fb954ef7.pdf*

Cassidy, D. T. (2011), 'Describing n-day returns with Student's t-distributions', *Physica A: Statistical Mechanics and its Applications* **390**(15), 2794 – 2802.
URL: *http://www.sciencedirect.com/science/article/pii/S0378437111002329*

Cassidy, D. T., Hamp, M. J. & Ouyed, R. (2010), 'Pricing European options with a log Student's t-distribution: A Gosset formula', *Physica A: Statistical Mechanics and its Applications* **389**(24), 5736 – 5748.
URL: *http://www.sciencedirect.com/science/article/pii/S0378437110007405*

Cohen, S. & Rosiński, J. (2007), 'Gaussian Approximation of Multivariate Lévy Processes with Applications to Simulation of Tempered Stable Processes', *Bernoulli* **13**(1), 195–210.
URL: *http://dx.doi.org/10.3150/07-BEJ6011*

Corlu, C. G. & Corlu, A. (2015), 'Modelling exchange rate returns: which flexible distribution to use?', *Quantitative Finance* **15**(11), 1851–1864.
URL: *https://www.tandfonline.com/doi/abs/10.1080/14697688.2014.942231*

Corlu, C. G., Meterelliyoz, M. & Tinic, M. (2016), 'Empirical distributions of daily equity index returns: A comparison', *Expert Systems with Applications* **54**, 170–192.
URL: *https://www.sciencedirect.com/science/article/pii/S095741741600052X*

Cufaro Petroni, N. (2007), 'Mixtures in nonstable Lévy processes', *Journal of Physics A: Mathematical and Theoretical* **40**(10), 2227.
URL: *http://stacks.iop.org/1751-8121/40/i=10/a=001*

Cufaro Petroni, N., De Martino, S., De Siena, S. & Illuminati, F. (2005), 'Lévy-Student distributions for halos in accelerator beams', *Phys. Rev. E* **72**(6), 066502.
URL: *http://link.aps.org/doi/10.1103/PhysRevE.72.066502*

Dempster, A. P., Laird, N. M. & Rubin, D. B. (1977), 'Maximum likelihood from incomplete data via the EM algorithm', *Journal of the Royal Statistical Society. Series B (Methodological)* **39**(1), 1–38.
URL: *http://www.jstor.org/stable/2984875*

Derflinger, G., Hörmann, W. & Leydold, J. (2010), 'Random variate generation by numerical inversion when only the density is known', *ACM Trans. Model. Comput. Simul.* **20**(4), 18:1–18:25.
URL: *http://doi.acm.org/10.1145/1842722.1842723*

Devroye, L. (1981), 'On the computer generation of random variables with a given characteristic function', *Computers and Mathematics with Applications* **7**(6), 547 – 552.
URL: *http://www.sciencedirect.com/science/article/pii/0898122181900389*

Doob, J. (2012), *Measure Theory*, Graduate Texts in Mathematics, Springer, New York.
URL: *https://books.google.de/books?id=H0PhBwAAQBAJ*

Eberlein, E., Keller, U. et al. (1995), 'Hyperbolic distributions in finance', *Bernoulli* **1**(3), 281–299.
URL: *https://projecteuclid.org/euclid.bj/1193667819*

Eberlein, E. & Özkan, F. (2003), 'Time consistency of lévy models', *Quantitative Finance* **3**(1), 40–50.
URL: *https://www.tandfonline.com/doi/abs/10.1088/1469-7688/3/1/304*

Eberlein, E. & Prause, K. (2002), The Generalized Hyperbolic Model: Financial Derivatives and Risk Measures, *in* H. Geman, D. Madan, S. R. Pliska & T. Vorst, eds, 'Mathematical Finance — Bachelier Congress 2000: Selected Papers from the First World Congress of the Bachelier Finance Society, Paris, June 29–July 1, 2000', Springer Finance, Berlin, Heidelberg, pp. 245–267.
URL: *https://doi.org/10.1007/978-3-662-12429-1_12*

Eberlein, E. & v. Hammerstein, E. A. (2004), Generalized Hyperbolic and Inverse Gaussian Distributions: Limiting Cases and Approximation of Processes, *in* R. C. Dalang, M. Dozzi & F. Russo, eds, 'Seminar on Stochastic Analysis, Random Fields and Applications IV', Birkhäuser, Basel, pp. 221–264.
URL: *https://link.springer.com/chapter/10.1007/978-3-0348-7943-9_15*

Ferguson, T. S. & Klass, M. J. (1972), 'A Representation of Independent Increment Processes without Gaussian Components', *The Annals of Mathematical Statistics* **43**(5), 1634–1643.
URL: *http://dx.doi.org/10.1214/aoms/1177692395*

Figueroa-López, J. E., Lancette, S., Lee, K. & Mi, Y. (2011), Estimation of NIG and VG models for high frequency financial data, *in* F. Viens, M. Mariani & I. Florescu, eds, 'Handbook of modeling high-frequency data in finance', Vol. 4, John Wiley & Sons, Inc., Hoboken, New Jersey, pp. 3–26.
URL: *https://books.google.de/books?id=mk63AFFUhXYC*

Gil-Pelaez, J. (1951), 'Note on the inversion theorem', *Biometrika* **38**(3-4), 481–482.
URL: *http://biomet.oxfordjournals.org/content/38/3-4/481.short*

Girón, F. & del Castillo, C. (2001), 'A note on the convolution of inverted-gamma distributions with applications to the Behrens-Fisher distribution', *RACSAM. Revista de la Real Academia de Ciencias Exactas, Físicas y Naturales. Serie A: Matemáticas* **95**(1), 39–44.
URL: *http://www.rac.es/ficheros/doc/00043.pdf*

Göncü, A., Karahan, M. O. & Kuzubaş, T. U. (2016), 'A comparative goodness-of-fit analysis of distributions of some Lévy processes and Heston model to stock index returns', *The North American Journal of Economics and Finance* **36**, 69–83.
URL: *https://www.sciencedirect.com/science/article/pii/S1062940815001266*

Gray, J. B. & French, D. W. (1990), 'Empirical comparisons of distributional models for stock index returns', *Journal of Business Finance & Accounting* **17**(3), 451–459.
URL: *https://onlinelibrary.wiley.com/doi/abs/10.1111/j.1468-5957.1990.tb01197.x*

Grigelionis, B. (2012), *Student's t-Distribution and Related Stochastic Processes*, SpringerBriefs in Statistics, Springer, Berlin, Heidelberg.
URL: *https://books.google.de/books?id=eC72q491I6sC*

Grosswald, E. (1976), 'The Student t-distribution of any degree of freedom is infinitely divisible', *Zeitschrift für Wahrscheinlichkeitstheorie und Verwandte Gebiete* **36**(2), 103–109.
URL: *http://dx.doi.org/10.1007/BF00533993*

Grothe, O. & Schmidt, R. (2010), 'Scaling of Lévy-Student processes ', *Physica A: Statistical Mechanics and its Applications* **389**(7), 1455 – 1463.
URL: *http://www.sciencedirect.com/science/article/pii/S037843710900973X*

Guo, B.-N., Qi, F., Zhao, J.-L. & Luo, Q.-M. (2015), 'Sharp Inequalities for Polygamma Functions', *Mathematica Slovaca* **65**(1), 103–120.
URL: *https://www.degruyter.com/view/j/ms.2015.65.issue-1/ms-2015-0010/ms-2015-0010.xml*

Haas, G. N. (1969), Statistical inferences for the Cauchy distribution based on maximum likelihood estimators, PhD thesis, University of Missouri–Rolla.
URL: *http://scholarsmine.mst.edu/doctoral_dissertations/2274/*

Heyde, C. C. & Leonenko, N. N. (2005), 'Student processes', *Advances in Applied Probability* **37**(2), 342–365.
URL: *http://dx.doi.org/10.1239/aap/1118858629*

Hilber, N., Reich, N., Schwab, C. & Winter, C. (2009), 'Numerical methods for Lévy processes', *Finance and Stochastics* **13**(4), 471–500.
URL: *http://dx.doi.org/10.1007/s00780-009-0100-5*

Hörmann, W., Leydold, J. & Derflinger, G. (2004), *Automatic Nonuniform Random Variate Generation*, Statistics and Computing, Springer, Berlin, Heildelberg.
URL: *https://books.google.de/books?id=vjOJySM27PIC*

Hubalek, F. (2005), 'On the simulation from the marginal distribution of a Student t and generalized hyperbolic Lévy process', *Working paper* .
URL: *https://pdfs.semanticscholar.org/4368/3935c410951d8145211a3d79148151cb07d8.pdf*

Imai, J. & Kawai, R. (2011), 'On finite truncation of infinite shot noise series representation of tempered stable laws', *Physica A: Statistical Mechanics and its Applications* **390**(23), 4411 – 4425.
URL: *http://www.sciencedirect.com/science/article/pii/S0378437111005759*

Imai, J. & Kawai, R. (2013), 'Numerical inverse Lévy measure method for infinite shot noise series representation', *Journal of Computational and Applied Mathematics* **253**, 264–283.
URL: *http://dx.doi.org/10.1016/j.cam.2013.04.003*

Ivanenko, D., Kulik, A. & Masuda, H. (2015), 'Uniform LAN property of locally stable Lévy process observed at high frequency', *Latin American Journal of Probability and Mathematical Statistics* **12**(2), 835–862.
URL: *http://alea.impa.br/articles/v12/12-32.pdf*

Kawai, R. (2013), On Singularity of Fisher Information Matrix for Stochastic Processes Under High Frequency Sampling, *in* A. Cangiani, R. L. Davidchack, E. Georgoulis, A. N. Gorban, J. Levesley & M. V. Tretyakov, eds, 'Numerical Mathematics and Advanced Applications 2011', Springer, Berlin, Heidelberg, pp. 841–849.
URL: *https://doi.org/10.1007/978-3-642-33134-3_87*

Kawai, R. (2015), 'On the likelihood function of small time variance Gamma Lévy processes', *Statistics* **49**(1), 63–83.
URL: *http://dx.doi.org/10.1080/02331888.2014.918980*

Kawai, R. & Masuda, H. (2011), 'On the local asymptotic behavior of the likelihood function for Meixner Lévy processes under high-frequency sampling', *Statistics & Probability Letters* **81**(4), 460 – 469.
URL: *http://www.sciencedirect.com/science/article/pii/S0167715210003512*

Kawai, R. & Masuda, H. (2013), 'Local asymptotic normality for normal inverse Gaussian Lévy processes with high-frequency sampling', *ESAIM: Probability and Statistics* **17**, 13–32.
URL: *https://doi.org/10.1051/ps/2011101*

Kolmogorov, A. N. (1933), 'Sulla Determinazione Empirica di una Legge di Distribuzione', *Giornale dell'Istituto Italiano degli Attuari* **4**, 83–91.

Lange, K. L., Little, R. J. & Taylor, J. M. (1989), 'Robust Statistical Modeling Using the t Distribution', *Journal of the American Statistical Association* **84**(408), 881–

896.
URL: *https://amstat.tandfonline.com/doi/abs/10.1080/01621459.1989.10478852*

Le Cam, L. (1960), 'Locally asymptotic normal families of distribution.', *University of California Publications in Statistics* **3**, 37–98.

Le Cam, L. & Lo Yang, G. (1990), Locally asymptotically normal families, *in* 'Asymptotics in Statistics: Some Basic Concepts', Springer, New York, pp. 52–98.
URL: *https://doi.org/10.1007/978-1-4684-0377-0_5*

Levine, R. A. & Casella, G. (2001), 'Implementations of the Monte Carlo EM algorithm', *Journal of Computational and Graphical Statistics* **10**(3), 422–439.
URL: *https://www.tandfonline.com/doi/abs/10.1198/106186001317115045*

Lévy, P. (1948), *Processus stochastiques et mouvement Brownien: suivi d'une note de M. Loève*, Monographies des probabilités, Paris.
URL: *https://books.google.de/books?id=tzM7AQAAIAAJ*

Little, R. & Rubin, D. (2014), *Statistical Analysis with Missing Data*, Wiley Series in Probability and Statistics, Wiley, Hoboken, New Jersey.
URL: *https://books.google.de/books?id=AyVeBAAAQBAJ*

Liu, C. & Rubin, D. B. (1994), 'The ECME algorithm: a simple extension of EM and ECM with faster monotone convergence', *Biometrika* **81**(4), 633–648.
URL: *https://academic.oup.com/biomet/article/81/4/633/224325*

Liu, C. & Rubin, D. B. (1995), 'ML estimation of the t distribution using EM and its extensions, ECM and ECME', *Statistica Sinica* **5**(1), 19–39.
URL: *http://www.jstor.org/stable/24305551*

Madan, D. B. & Seneta, E. (1990), 'The Variance Gamma (VG) Model for Share Market Returns', *The Journal of Business* **63**(4), 511–524.
URL: *http://www.jstor.org/stable/2353303*

Mandelbrot, B. (1961), 'Stable Paretian Random Functions and the Multiplicative Variation of Income', *Econometrica* **29**(4), 517–543.
URL: *http://www.jstor.org/stable/1911802*

Mandelbrot, B. (1967), 'The Variation of Some Other Speculative Prices', *The Journal of Business* **40**(4), 393–413.
URL: *http://www.jstor.org/stable/2351623*

Masuda, H. (2009*a*), 'Joint Estimation of Discretely Observed Stable Lévy Processes with Symmetric Lévy Density', *Journal of the Japan Statistical Society* **39**(1), 49–75.
URL: *https://www.jstage.jst.go.jp/article/jjss/39/1/39_1_49/_article/-char/ja/*

Masuda, H. (2009*b*), 'Notes on estimating inverse-Gaussian and gamma subordinators under high-frequency sampling', *Annals of the Institute of Statistical Mathematics* **61**(1), 181–195.
URL: *https://doi.org/10.1007/s10463-007-0131-7*

Masuda, H. (2015), Parametric Estimation of Lévy Processes, *in* 'Lévy Matters IV: Estimation for Discretely Observed Lévy Processes', Springer International Publishing, Cham, pp. 179–286.
URL: *https://doi.org/10.1007/978-3-319-12373-8_3*

McLachlan, G. & Krishnan, T. (2007), *The EM Algorithm and Extensions*, Wiley Series in Probability and Statistics, Wiley.
URL: *https://books.google.de/books?hl=en&lr=&id=NBawzaWoWa8C*

Nadarajah, S., Afuecheta, E. & Chan, S. (2015), 'A note on "Modelling exchange rate returns: Which flexible distribution to use?"', *Quantitative Finance* **15**(11), 1777–1785.
URL: *https://www.tandfonline.com/doi/abs/10.1080/14697688.2015.1032997*

Nadarajah, S. & Kotz, S. (2008), 'Estimation Methods for the Multivariate t Distribution', *Acta Applicandae Mathematicae* **102**(1), 99–118.
URL: *https://link.springer.com/article/10.1007/s10440-008-9212-8*

Nelder, J. A. & Mead, R. (1965), 'A Simplex Method for Function Minimization', *The Computer Journal* **7**(4), 308–313.
URL: *https://academic.oup.com/comjnl/article/7/4/308/354237*

Nolan, J. P. (2001), Maximum Likelihood Estimation and Diagnostics for Stable Distributions, *in* O. E. Barndorff-Nielsen, S. I. Resnick & T. Mikosch, eds, 'Lévy Processes: Theory and Applications', Birkhäuser, Boston, MA, pp. 379–400.
URL: *https://doi.org/10.1007/978-1-4612-0197-7_17*

Nolan, J. P. (2018), *Stable Distributions - Models for Heavy Tailed Data*, Birkhauser, Boston. In progress, Chapter 1 online.
URL: *http://fs2.american.edu/jpnolan/www/stable/stable.html*

Olver, F., of Standards, N. I., (U.S.), T., Lozier, D., Boisvert, R. & Clark, C. (2010), *NIST Handbook of Mathematical Functions Hardback and CD-ROM*, Cambridge University Press, New York.
URL: *https://books.google.de/books?id=3I15Ph1Qf38C*

Omey, E., Gulck, S. & Vesilo, R. (2017), 'Semi-heavy tails', *Working Paper* .
URL: *https://www.researchgate.net/publication/319153506_Semi-heavy_tails*

Peiró, A. (1994), 'The distribution of stock returns: international evidence', *Applied Financial Economics* **4**(6), 431–439.
URL: *https://www.tandfonline.com/doi/abs/10.1080/758518675*

Piessens, R. & Branders, M. (1974), 'A Note on the Optimal Addition of Abscissas to Quadrature Formulas of Gauss and Lobatto Type', *Mathematics of Computation* **28**(125), 135–139.
URL: *http://www.jstor.org/stable/2005820*

Praetz, P. D. (1972), 'The Distribution of Share Price Changes', *The Journal of Business* **45**(1), 49–55.
URL: *http://www.jstor.org/stable/2351598*

Prause, K. (1997), 'Modelling financial data using generalized hyperbolic distributions', *FDM Preprint, Universität Freiburg* **48**.
URL: *http://citeseerx.ist.psu.edu/viewdoc/download?doi=10.1.1.416.1199&rep=rep1&type=pdf*

Rachev, S., Kim, Y., Bianchi, M. & Fabozzi, F. (2011), *Financial Models with Levy Processes and Volatility Clustering*, Frank J. Fabozzi Series, Wiley.
URL: *https://books.google.de/books?id=XKvUUrcS_twC*

Raible, S. (2000), Lévy Processes in Finance: Theory, Numerics, and Empirical Facts, PhD thesis, Universität Freiburg.
URL: *https://www.freidok.uni-freiburg.de/fedora/objects/freidok:51/datastreams/FILE1/content*

Razali, N. M., Wah, Y. B. et al. (2011), 'Power comparisons of Shapiro-Wilk, Kolmogorov-Smirnov, Lilliefors and Anderson-Sarling tests', *Journal of Statistical Modeling and Analytics* **2**(1), 21–33.
URL: *https://www.researchgate.net/publication/267205556*

Rosiński, J. (1990), 'On Series Representations of Infinitely Divisible Random Vectors', *The Annals of Probability* **18**(1), 405–430.
URL: *http://dx.doi.org/10.1214/aop/1176990956*

Rosiński, J. (2001), Series representations of Lévy processes from the perspective of point processes, *in* O. E. Barndorff-Nielsen, S. I. Resnick & T. Mikosch, eds, 'Lévy Processes: Theory and Applications', Birkhäuser, Boston, pp. 401–415.
URL: *https://doi.org/10.1007/978-1-4612-0197-7_18*

Rubin, D. B. (1983), Iteratively reweighted least squares, *in* S. Kotz, C. Read, N. Balakrishnan, B. Vidakovic & N. Johnson, eds, 'Encyclopedia of Statistical Sciences', Wiley, Hoboken, New Jersey.
URL: *http://onlinelibrary.wiley.com/doi/10.1002/0471667196.ess1296.pub2/abstract*

Sato, K.-i. (1999), *Lévy Processes and Infinitely Divisible Distributions*, Cambridge Studies in Advanced Mathematics, Cambridge University Press, Cambridge.
URL: *https://books.google.de/books?id=tbZPLquJjSoC*

Schafheitlin, P. (1906), 'Die Lage der Nullstellen der Besselschen Funktionen zweiter Art', *Sitzungsberichte Berliner Math. Gesellschaft* **5**, 82–93.

Schoutens, W. (2001), 'Meixner Processes in Finance', *Eurandom Report 2001-002* .
URL: *https://www.eurandom.tue.nl/reports/2001/002-report.pdf*

Schoutens, W. & Teugels, J. L. (1998), 'Lévy processes, polynomials and martingales', *Stochastic Models* **14**(1-2), 335–349.
URL: *https://www.tandfonline.com/doi/abs/10.1080/15326349808807475*

Schwarz, G. (1978), 'Estimating the Dimension of a Model', *The Annals of Statistics* **6**(2), 461–464.
URL: *https://projecteuclid.org/euclid.aos/1176344136*

Student (1908), 'The Probable Error of a Mean', *Biometrika* **6**(1), 1–25.
URL: *http://www.jstor.org/stable/2331554*

Tankov, P. & Cont, R. (2015), *Financial Modelling with Jump Processes, Second Edition*, Chapman and Hall/CRC Financial Mathematics Series, Taylor & Francis, London.
URL: *https://books.google.de/books?id=-fZtKgAACAAJ*

Todorov, V. & Tauchen, G. (2006), 'Simulation Methods for Lévy-Driven Continuous-Time Autoregressive Moving Average (CARMA) Stochastic Volatility Models', *Journal of Business & Economic Statistics* **24**(4), 455–469.
URL: *http://dx.doi.org/10.1198/073500106000000260*

v. Hammerstein, E. A. (2010), Generalized hyperbolic distributions: Theory and applications to CDO pricing, PhD thesis, Universität Freiburg.
URL: *https://d-nb.info/1010445391/34*

Walker, J. (1996), *Fast Fourier Transforms, Second Edition*, Chapman and Hall/CRC Financial Mathematics Series, Taylor & Francis, Boca Raton, Florida.
URL: *https://books.google.de/books?id=cOA-vwKIffkC*

Watson, G. (1995), *A Treatise on the Theory of Bessel Functions*, Cambridge Mathematical Library, Cambridge University Press, New York.
URL: *https://books.google.de/books?id=Mlk3FrNoEVoC*

Wei, G. C. & Tanner, M. A. (1990), 'A Monte Carlo Implementation of the EM Algorithm and the Poor Man's Data Augmentation Algorithms', *Journal of the*

American Statistical Association **85**(411), 699–704.
URL: *https://www.tandfonline.com/doi/abs/10.1080/01621459.1990.10474930*

Eidesstattliche Erklärung

Hiermit versichere ich diese Arbeit selbstständig verfasst zu haben und dabei keine anderen als die angegebenen Quellen und Hilfsmittel benutzt habe. Zitate wurden an den entsprechenden Stellen in der Arbeit kenntlich gemacht.

Essen, 18.07.2018

Till Massing

Affidavit

Herewith I confirm that I have written this thesis solely and did not use any other references or assistance than stated. Citations are indicated at the corresponding passages in the text.

Essen, 18.07.2018

Till Massing